

**Signatures of Higher Functions of Brain Dynamics
in Electroencephalogram: A Nonlinear Analysis**

**Pravitha Ramanand
International School of Photonics
Cochin University of Science and Technology
Kochi 682022 India**

Ph. D. Thesis submitted to Cochin University of Science and
Technology for
the award of the Degree of Doctor of Philosophy.

June 2003

Signatures of Higher Functions of Brain Dynamics in Electroencephalogram: A Nonlinear Analysis
Ph. D. thesis in the field of Neuro-Technology

Author

Pravitha Ramanand
Research Fellow, International School of Photonics
Cochin University of Science and Technology, Kochi – 682 022, India.
pravitha@cusat.ac.in

Research Advisor

Dr V P N Nampoori
Professor, International School of Photonics
Cochin University of Science and Technology, Kochi - 682 022, India.
vpnnampoori@cusat.ac.in

Cover Design - Dr. V. P. N. Nampoori

An artist's interpretation of the topological manifolds in the brain. The structures depict the temporal evolution of the iso-structures of the motion generating function evaluated as part of this work.

G 8575

**International School of Photonics, Cochin University of Science and Technology,
Kochi – 682 022, India.
www.photonics.cusat.edu**

June 2003

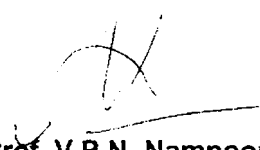


**International School of Photonics
Cochin University of Science and Technology
Cochin - 682 022, India**

CERTIFICATE

Certified that the work presented in this thesis entitled **“SIGNATURES OF HIGHER FUNCTIONS OF BRAIN DYNAMICS IN ELECTROENCEPHALOGRAM: A NONLINEAR ANALYSIS”** based on the bonafide research work done by Ms. Pravitha Ramanand is an authentic record of research work done by her under my guidance in the International School of Photonics, Cochin University of Science and Technology, Cochin 682 022 and has not been included in any other thesis submitted previously for the award of any degree.

Kochi – 22
Date: 15 June 2003

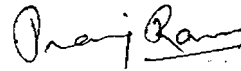

Prof. V.P.N. Nampoory
(Supervising Guide)
International School of Photonics
CUSAT.

DECLARATION

I hereby declare that the present work entitled "**SIGNATURES OF HIGHER FUNCTIONS OF BRAIN DYNAMICS IN ELECTROENCEPHALOGRAM: A NONLINEAR ANALYSIS**" which will be submitted is based on the original work done by me under the guidance of Prof. V.P.N.Nampoori, International School of Photonics, Cochin University of Science and Technology, has not been included in any other thesis submitted previously for the award of any degree.

Kochi – 22

Date: 15 June 2003



Pravitha Ramanand

Acknowledgement

Writing this thesis has been both an invigorating as well as humbling experience. Even as a sense of accomplishment arises with each completed section in which a body of work is presented, it also evokes memories of the times when it was done and the many people with whom one has interacted at the time and who've contributed to make it a thing of some import. It is in such moments that gratitude and joy fill the heart and it becomes a pleasure to travel down memory lane and acknowledge the unforgettable people who are a part of this work.

It is a great pleasure to express my heartfelt gratitude to Prof. V. P. N. Nampoore, my research advisor who has been a constant source of encouragement and support throughout the course of my research. His keen intellect, enthusiasm, and receptiveness to new ideas have impressed me greatly and I have drawn a lot from his unending store of knowledge and resource. I have found in Sir a wholesome personality of many talents and accomplishments with a totally unassuming and humble attitude. It has been a wonderful opportunity to associate with him during the first major scientific endeavour of my life and it is an experience that will remain cherished.

I have been highly fortunate to be one of the final links in the string of Prof. R. Pratap's students. An emeritus professor at CUSAT after superannuation from Physical Research Laboratory, Ahmedabad, Prof. Pratap is the nucleus of the Brain Dynamics Group at ISP. An authority on statistical mechanics, his dedication to Physics and single minded objective of unraveling the dynamics in the mystery of the brain using techniques from Physics, struck awe and inspired confidence in me from the day of my first meeting with him. Over the years, the awe in me has given way to deep love and respect for Pratap Sir and I have tried to emulate Sir's almost supermanly go-getting attitude, perseverance and eye for detail in professional matters. Pratap Sir's patience with my infinite follies during this period and his affection for me in letting me openly voice my doubts, ideas, opinions and frustrations to him have filled in a much lacked grandfatherly figure in my life. Saying "Thank You" to Sir will only be trifling the special bond that we share. An old Malayalam saying goes, "the tiniest pebble at the foot of the jasmine vale emanates perfume after a while". I have been lucky in being chosen a tiny pebble.

I would also like to express my sincere thanks to Prof. C. P. Girjavallabhan who always showed a deep interest in my work. His comments, critiques and suggestions have helped considerably in the progress of my research.

The Director, Prof. V M Nandakumaran and Prof. P Radhakrishnan, Faculty, ISP have always been encouraging and I thank them for all the help received during my research years. I am thankful to Mr. Basheer, ISP for all the help he has rendered.

I am grateful to the administrative staff at ISP during the period from 1999 to 2003 who were extremely helpful in tiding me over many official hassles. The library staff of ISP as well as the Dept. of Physics is also thanked profusely for their assistance. I am happy to acknowledge CSIR (New Delhi) for Research Fellowship in the form of JRF and SRF during the period of my work.

Dr. K.T. Damodaran and Dr. M.R. Radhakrishna, Faculty and Mr. Arts K. P., research student, Dept. of Marine Geology and Geophysics, CUSAT were of tremendous help in acquainting me with the software to do the isocontour plots that have been included in this thesis. The faculty of the Dept. of Statistics and Dr. Anandakuttan of the School of Management Studies, CUSAT are thanked for their help with the statistical software package used in this work.

Ms. Rekha Mathew, my colleague and friend has spent days on end working for the conversion of typed pages into the final format of this thesis. The front cover illustration is a result of hours of meticulous work on the part of Mr. Jijo P. U. and Mr. Rajesh M. It is a rare pleasure to acknowledge such selfless acts.

I owe a lot to Dr. P. Indic, presently Postdoctoral Fellow at Harvard University, who got me going with the programming techniques essential for this work. His innate skill at troubleshooting glitches that are a daily feature of any researcher's work life and the deep rooted conviction he had at the efficacy of the nonlinear research methods have enthused me a great deal. He has been a wonderful listener to my research woes and his suggestions and advice have been time tested to be the best in most situations.

It was in late 2001 that our group's collaboration with Dr. R. Sreenivasan, Faculty in the Department of Human Biology, University of Cape Town was established and it has grown in leaps and bounds ever since. I have benefited a lot in my research from the dense array EEG data, Dr. Sreenivasan shipped to us as well as from his constant tips and suggestions to particular problems we

worked on together using the cognitive task data. Even as I thank him for all the help received, I hope that the academic fellowship that we have forged will continue in the years to come.

Despite being the odd (wo)man out in the group pursuing Photonics related research, my peers, colleagues and juniors at ISP have been highly accommodating and supportive of my research interests through these years. My seniors, Dr. Achamma Kurien, Dr. Nibu A. George, Dr. Shelly John, Dr. Jayan Thomas, Ms. Bindu V., Mr. Pramod Gopinath, Mr. Binoy Paul and Mr. K. P. Unnikrishnan among several others have imparted bits of wisdom, at times inadvertently, regarding the do's and don'ts in a research. It has been both challenging and exciting to grow up with them as well as my batchmates, Mr. S. Thomas Lee, Mr. P. Suresh Kumar, Ms. K. Geetha and Mr. Sajan D. George from being a naïve, fresher right out of postgraduate school to a seasoned research fellow. Our sandwich researchers, Mr. Aneeshkumar B. and Mr. R. Prasanth have been very considerate to me from being ever ready with sound advice and tips for various academic matters to sending journal papers electronically whenever requested. My colleagues of later years, Sr. Ritty Nedumapara, Ms. Santhi A., Ms. Dilna S., Ms. Sreeja S., Mr. Jijo P.U., Mr. Abraham V.S., Mr. Rajesh M., Mr. Vinu Namboodiri, Mr. Rajesh S and Mr. Manu Punnen John have been of immense help at many junctures in the completion of this work. The various batches of M.Tech & M. Phil. students of ISP have also been assistance on several occasions. A formal "Thank you" to all these people will get shouted down before the ink dries on this paper. I would rather let them know in all sincerity, my appreciation for their presence and efforts to ease the strain in the course of my work both on academic and sometimes on personal fronts. The experience of working with and sharing sometime with all these wonderful people has been enriching and will be ever cherished.

I am also obliged to Dr. A. Deepthy, Young Scientist Fellow at ISP and Dr. Madhu Menon, Amrita Institute of Medical Sciences (AIMS), Cochin for their help with the ongoing research collaboration of our group with the Neurology Department at AIMS. Dr. Somasundaram has been instrumental in our building the collaborative research venture with AIMS. I am also grateful to Mr. P. M Radhakrishnan, CAD/CAM Lab, CUSAT who has been of service in getting many illustrations done during the course of this work. I also acknowledge Mr. Gireesh D. who helped with the xeroxing and Ms. Minu Joy, research fellow in Dept. of

Physics for providing me with the LaTeX package during the course of this work. I also express my heartfelt thanks to the research fellows and students in the departments of Physics and Applied Chemistry who have been of inordinate help during various junctures over these years.

Despite research being hard work it has been a time filled with fun and frolic too. Jyotsna Ravi, my roommate in room no. 7, Athulya Hostel has been an integral part of my life from whom I have imbibed the spirit of seeing the funny side of things and keeping everything light. Both Thomas Lee and she have been special people with whom I've shared my research years and who've always stood by me. I am indebted to people like Iswarya Mathew, Kochuthressia S., Radhika T., Anisha T.K., Lekshmi S., Santhi A, Rekha Mathew, Roshni R.S. and Sreedevi Menon, Vrinda S., Sr. Ritty, Jasmin C., Lekshmi V. and the scores of other friends in the hostel especially the badminton pals in the period from 1999 to 2003 who have selflessly indulged my eccentricities and flattered me beyond words by their support and approval of my many escapades and interests that have got me into many a scrape. I am also glad to have long distance friends, Rajani in particular who have kept me buoyed up by regular mails, cards and expensive phone calls. Their joy in my moments of triumph as well as care and concern in times of tension and strain during the past three years have done wonders in keeping me afloat. At the end of a long journey it feels great to thank all these people for their wonderful comradeship.

Mrs. Ammini Pratap's gracious hospitality and kindness with which she welcomed me to their home in Pettah will remain sketched in my mind.

I cherish the love, support, encouragement and patience showered on me by my parents and brother through all these years. And, finally....

**saroasya cāham hṛdi sanniviṣṭho
mattah smṛtir jñānam apohanaṁ ca**

-- Bhagavad Gita 15.15

(I am the indwelling monitor in the heart of all beings, from Me arises consciousness, wisdom and forgetfulness.)

Pravitha Ramanand

List of Publications

In International Journals

R. Pravitha, V.P.N. Nampoori and R. Sreenivasan (2003) Complexity of Dense Array EEG Reflected in Single and Multiscale Sample Entropy Analysis, *Medical and Biological Engineering and Computing*. (Communicated)

R. Pravitha, R. Sreenivasan and V. P. N. Nampoori (2002) Gender Difference Reflected in a Complexity Analysis of Dense Array EEG Signal, *Complexity International*. (Communicated)

R. Pravitha and V.P.N. Nampoori (2002) Coordination in the Dynamics of the Brain as Inferred from EEG Analysis, *International Journal of Neuroscience*, **112**: 10, 1245 - 1262.

R. Pravitha, P. Indic and V. P. N. Nampoori (2002) Dynamical Aspects of Coupled Rossler Systems: Effects of Noise, *Physics Letters A*, **294**: 1, 37-46.

Direct link to this article: [http://dx.doi.org/10.1016/S0375-9601\(01\)00817-9](http://dx.doi.org/10.1016/S0375-9601(01)00817-9)

R. Pravitha, P. Indic, V. P. N. Nampoori and R. Pratap (2001) Effect of time scales on the unfolding of neural attractors, *International Journal of Neuroscience*, **111**, 175-186.

In Seminars and Conferences

Pravitha Ramanand, V.P.N. Nampoori and R.Sreenivasan, *Effect of fatigue on mental co-ordination: A time series study*. Accepted for poster presentation at Modeling, Signal Processing and Control Conference at SPIE's Smart Structures and Materials and NDE for Health Monitoring and Diagnostics, San Diego, March 2003.

Pravitha Ramanand, V.P.N. Nampoori and R.Sreenivasan, *Cortical interactions during various conditions as inferred from EEG analysis*. Presented at the national conference on Recent Advances in Nonlinear Studies 2002 held at the Indian Institute of Science, Bangalore in August, 2002.

Pravitha Ramanand, P. Indic, V.P.N. Nampoori and R. Pratap, *Unfolding of Neural Attractors: A Time Scales Viewpoint*. Presented at "National Seminar on Chaos & Fractals: Theory & Applications" held at Rajagiri School of Engineering and Technology, Cochin in January, 2002.

Pravitha Ramanand and R. Pratap. *Attractor Potential from Electroencephalogram*. Accepted at the International Conference on Complex systems, hosted by NECSI, New England held in June, 2000 at Nashua, USA. Available at: www.interjournal.org. Manuscript No. 358.

Rekha Mathew, **Pravitha Ramanand**, V.P.N. Nampoori and R.Sreenivasan, *Dynamical complexity due to physical exertion in a mental task state: A time series study*, Accepted at Modeling, Signal Processing and Control Conference at SPIE's Smart Structures and Materials and NDE for Health Monitoring and Diagnostics, San Diego, March 2003.

“Almost by instinct I turned myself later towards problems of increasing complexity, perhaps in the belief that I could find there a junction in physical science on one hand and in biology and human science on the other. Many things that are attributed to biological wiring are not produced by selfish, determinist genes, but rather by social interactions under nonequilibrium conditions. The research, in addition, gave me confirmation of the supposition that even human behaviour, with all its complexity, would eventually be susceptible of a mathematical formulation. In this way the dichotomy of the ‘two cultures’ could be and should be removed.”

--- Ilya Prigogine

CONTENTS

PREFACE

1	GENERAL INTRODUCTION	1
1.1	Brain as a complex system	6
1.2	Nonlinearity in the Neural System	9
1.3	Analysing Physiological Time series	13
1.4	Nonlinear Brain analysis	15
1.5	Organization of the thesis	16
2	NONLINEAR SYSTEMS: A THEORETICAL APPROACH	21
2.1	Nonlinear systems: Terminology and definitions	22
2.2	Cauchy-Lipschitz condition	25
2.3	Conservative vs. Dissipative systems	27
2.4	Stability of equilibrium points	28
2.5	Linear stability analysis	29
2.5.1	Limit Cycles	35
2.6	Poincare Map	36
2.7	Lyapunov's Theorems of stability	38
2.8	Chaotic dynamics	40
2.9	Bifurcations in dynamical systems	42
2.10	Dimension and Entropy measures	44
2.11	Lyapunov exponents	48
2.12	Stochastic resonance	50
2.13	Conclusion	52
3	CURRENT TECHNIQUES IN TIME SERIES ANALYSIS- AN OVERVIEW	53
	PART I - Time Series Analysis of Complex Systems	
3.1	Dynamical systems and signals	54
3.2	Linear methods of signal analysis	55
3.3	Nonlinear time series analysis	58
	TECHNIQUES IN NONLINEAR TIME SERIES ANALYSIS OF SIGNALS	
3.4	Reconstruction of Phase space	65
3.4.1	Embedding theorems	68
3.5	Choice of embedding dimension	70

3.6	Selection of optimal time lag	76
3.7	Invariant parameters of dynamics	81
3.7.1	Density estimation	82
3.7.2	Generalized Dimensions	83
3.7.3	The Grassberger- Procaccia (G-P) algorithm for estimation of D_2	87
3.7.4	Nonstationarity in Real-life Signals	89
3.7.5	Modifications to the G-P algorithm	92
3.7.6	Generalized Entropies	94
3.7.7	Lyapunov Exponents	97
3.8	Testing for Nonlinearity in the System	99
PART II: Electroencephalogram - A Time Varying Nonlinear Signal		
3.9	The electroencephalogram (EEG)	102
3.10	Neuroimaging techniques	104
3.11	Classification of brain waves	112
3.12	Data collection and pre -processing	115
3.12.1	Recording the EEG	115
3.12.2	Electrode placement configurations	116
3.13	Is the Brain chaotic?	120
3.14	On the threshold of the Big step	124
4	DYNAMICAL ASPECTS OF COUPLED OSCILLATORS: A TIME SERIES ANALYSIS	125
4.1	Model dynamics using time series	127
4.2	Method of analysis	130
4.3	The Uni-directionally coupled systems	134
4.4	The Bi-directional coupling scenario	137
4.5	Noise in the coupled system: Effect on Synchronization	141
4.6	Conclusion of the model system analysis	148
5	TIME SCALES AND THE UNFOLDING OF NEURAL ATTRACTORS	153
5.1	Time scales in the neural system	154
5.2	Unfolding of neural attractors: a time scales viewpoint	163
5.2.1	Method of analysis	165
5.2.2	Data Specifications	167
5.3	Analysis of the time scale effect	168
5.3.1	Normal eyes closed condition	168

5.3.2	Pathological condition of epilepsy	172
5.4	Conclusion	174
6	EEG COMPLEXITY AS A TOOL TO PROBE NEURAL DYNAMICS	179
6.1	Complexity measures for time series data	182
6.2	Approximate entropy as a Complexity measure	186
6.3	Gender difference reflected in EEG complexity analysis	189
6.3.1	Experimental details	190
6.3.2	Complexity analysis	192
6.3.3	Discussions on the observations of the gender based study	202
6.4	Complexity analysis of various brain states	204
6.4.1	Sample Entropy: Quantification of regularity of experimental data	206
6.4.2	Classification of data	211
6.4.3	Complexity analysis using SampEn	211
6.5	Conclusion of the complexity approach to EEG analysis	224
7	SYNCHRONISATION PHENOMENON IN COGNITIVE PROCESSES	227
7.1	Theoretical background on synchronization	231
7.1.1	Entrainment of a periodic oscillator	227
7.1.2	Noisy oscillators	235
7.1.3	Chaotic oscillators	239
7.2	Towards Data Analysis: Quantifying strength of synchronization	241
7.3	Application of phase synchronization to normal and pathological EEG signals	244
7.3.1	No-Task passive states	244
7.3.2	Epileptic condition	256
7.4	Phase synchrony to study effect of fatigue on mental tasks	262
7.4.1	Detecting the directionality of coupling from phase	264
7.4.2	Data acquisition and classification	266
7.4.3	Phase synchrony and directional coupling analysis	268
7.5	Concluding remarks	276
8	NEURAL MODELS	279
8.1	Modeling the brain	280
8.2	Artificial neural networks and models of neocortex	282
8.3	Maps in the Brian	289

8.4	Formulation of nonequilibrium statistical mechanics	293
8.4.1	Schematics of SVD	295
8.4.2	Eigen function representation	296
8.4.3	Inverse scattering calculation	297
8.5	Map construction	298
8.5.1	Topological manifolds	302
8.6	Conclusion	307
9	CONCLUSIONS AND THEMES FOR FUTURE RESEARCH	309

BIBLIOGRAPHY

PREFACE

Advancement of human knowledge finds expression in recent times through new vistas of research that finely blend various disciplines to explore lesser known realities in science and technology. A prime example of one such field is that of Neurotechnology which is an amalgamation of neuroscience, physics, biomedical engineering and computational methods. In this, the human brain, which is probably the most complex system in nature, is explored by the application of ideas from physics and mathematics by judicious use of algorithms. Progress in computational capability, wider scope of applications of nonlinear dynamics and chaos in complex systems has enhanced the growth of Neurodynamics.

It is being increasingly realised that among all the various parts of the human anatomy, the human brain is perhaps the least understood- constitutionally and functionally. The most complex, sophisticated, and powerful information-processing device known, the exploration of the brain functioning was earlier restricted to learning the activation of single neurons and then extending it to include larger populations. This line of research led to the charting of emotion centres and thereby establishing a localized effect in the capacity to think, analyse problems and so on. But the idea of collective effects in any cognitive process is now widely accepted and a complete understanding of the mechanism of the brain functioning would be possible by bridging the gap between the clinical studies and theoretical methods derived from other sciences. In the modern era, the investigation of the human brain was mainly conducted with invasive techniques such as surgery, sensing using internal probes/electrodes etc. However with the advancement of imaging technology, methods such as CT scan, Positron Emission Tomography (PET) and Magnetic Resonance Imaging (MRI) have gained a lot of

importance in the detection and diagnosis of brain disorders at the structural and functional levels. However these methods that detect the distribution of metabolic activity associated with some suitably tagged molecules such as water, oxygen etc. in the case of Positron Emission Tomography (PET) or the directional blood flow in the case of Magnetic Resonance Imaging (MRI) have response time scales of the order of 30-40 seconds and hence any transient activity arising in a time scale shorter than these will go undetected. The recording of brain electrical activity in the form of Electroencephalogram introduced by Hans Berger in the late 1920s' has been in use for sometime now as a first tool to detect abnormal patterns in the electric activity in human brain. Yet in the last two decades of the past century, application of the principles of nonlinear dynamics and chaos to this signal have proved beyond doubt the potential of this signal as a carrier of information regarding the dynamics of the brain.

The EEG is a recording of the electric potential generated within the cortex by the firings of neurons, which are integrated in a complex fashion and conducted to the surface. It can be detected by placing electrodes on the scalp surface and the EEG signal continuously recorded at regular time interval forms the time series signal that can be analysed and studied. Application of time series analysis algorithms in conjunction with surrogate data testing has proved the nonlinear nature of the EEG signal and on the basis of this has been ushered in the new era of computational neuroscience / neuroinformatics that aims at unravelling the complex structure-function relationships of the brain at all levels from molecule to behaviour in an integrative effort of many scientific disciplines.

In this thesis we attempt a comprehensive study of the EEG signal by application of these newly introduced methods of nonlinear dynamics and deterministic chaos to characterize the dynamics of the brain state under a given condition. The main thrust of the thesis is on computing parameters that throw light on the actual dynamics of this highly complex, nonlinear and stochastic system in which feedback and feed forward

processes are operative. The brain is an open system in constant interaction with the external world and moreover it has been proved by Gould et. al. (1999) that the neuronal number is itself not conserved but that there is a constant generation of neurons in the brain even as older ones decay. This is a relevant observation in the sense that a control of such neurons will be useful in controlling the onset of degeneration of the brain. Hence the system at hand is a nonequilibrium and non-Marcovian one.

This work looks into the information content of the EEG signal and its relevance in understanding the brain dynamics from the nonlinear dynamics point of view. The EEG signal from the various electrode locations is considered as a time series and the method of time delay embedding is made use of in most algorithms to compute certain 'invariant' parameters of the attractor in the pseudo phase space. The nonstationary nature of the bio-signal is also taken into account and a theory that derives the relevant timescales of the various significant processes that was earlier proposed is further developed in this work with emphasis on understanding pathological conditions in contrast to 'normal' healthy state. Thus the work is an attempt to develop these new techniques to the level of a clinical tool that will find application in actual diagnosis and treatment of brain disorders.

1 *General Introduction*

The motion of the whole is the sum of the motions of all parts; and therefore in a body double in quantity, with equal velocity, the motion is double; with twice the velocity, it is quadrupled.

--- Sir Issac Newton, Principia Definition II.

'The whole is more than the sum of its parts' in complex systems.

--- John H. Holland in Hidden Order.

Determinism is the philosophical belief that every event or action is the inevitable result of preceding events or actions. Thus, in principle at least, every event or action can be completely predicted in advance if we know the previous states. Determinism became incorporated into modern science around 1500 A.D. with the establishment of the idea that cause-and-effect rules completely govern all motion and structure on the material level. According to the deterministic model of science, the universe unfolds in time like the working of a perfect machine, without a shred of randomness or deviation from the predetermined laws.

The person most closely associated with the establishment of determinism at the core of modern science is Sir Issac Newton whose three laws of motion completely define determinism. This is because they imply that anything that happens at any future time is completely determined by what happens now, and that everything now was completely determined by what happened at any time in the past. Newton's laws were so successful that for several centuries after his discovery, the science of physics consisted largely of demonstrating how his laws could account for the observed motion of nearly any imaginable physical process. This chain of cause-effect resulted in the development of linear dynamics and dynamics being described in linear vector space.

Yet this success story was a mere shadow of the things to come. The world of nature from weather to the prediction of earthquakes remained outside the grasp of the linearized view inherent in classical dynamics. One of the fundamental principles of experimental science is that no real measurement is infinitely precise, but instead must necessarily include a degree of uncertainty in the value. In dynamics, the presence of uncertainty in any real measurement means that in studying any system, the initial conditions cannot be specified to infinite accuracy. It is important to remember that the uncertainty in the dynamical outcome does not arise from any randomness in the equations of motion--since they are completely deterministic--but rather from the lack of accuracy in stating the initial conditions. This imprecision in the specification of initial conditions gives rise to inaccuracy in predicting the state of the system at a later stage. Further the existence of dynamical instability indicated that the system is no longer governed by linear dynamical equations but there exists the so-called 'nonlinear' effects, which are not specified by the linear evolution equations.

This was explicitly stated around 1900, by physicist Henri Poincaré. In his seminal work, 'Les méthodes nouvelles de la mécanique céleste' (1892), Poincaré gave his vision of what would be later known as classical nonlinear dynamics. What puzzled Poincaré in this study of the mathematical equations, which described the motion of planets around the sun, was that certain astronomical systems did not seem to obey the rule that shrinking the initial conditions always shrank the final prediction in a corresponding way. These peculiarities were first observed when he considered dynamics of systems consisting of three or more bodies with interactions between all of them. For these types of systems, Poincaré showed that a very tiny imprecision in the initial conditions would grow in time at an enormous rate. Poincaré mathematically proved that this "blowing up" of tiny uncertainties in the initial conditions into enormous uncertainties in the final predictions remained even if the initial uncertainties were shrunk by smallest imaginable size. The gist of Poincaré's mathematical analysis was a proof that for these 'complex systems', the only way to obtain predictions with any degree of accuracy at all would entail specifying the initial conditions to absolute precision as also the equations for more than two bodies get nonlinearly coupled so much so new mathematical techniques are necessary to develop dynamics with predictive capability.

Without attempting a comprehensive review on the development of nonlinear dynamics, we nevertheless present a peep into the history of the theory highlighting the work of only very few of the many illustrious contributors who together made it the theory that covers all fields of knowledge from the physical sciences, biology, social sciences to even arts and humanities. The time of Poincaré's findings [1878-1900] overlapped with those of Lyapunov [1893] who gave the basis of the theory of motion

stability. From the definitions of two classes of functions known as the Lyapunov functions of the first and the second kind, he could solve the stability problem in critical cases, those for which the linear approximation does not permit a stability conclusion in any small neighbourhood of a steady state (Mira, 1997).

The re-emergence of Poincaré's work occurred with the phenomenal discoveries made in 1963, by the meteorologist Edward Lorenz in his mathematical model for weather prediction (Lorenz, 1963). Specifically Lorenz studied a primitive model of how an air current would rise and fall while being heated by the sun. The simple set of equations in his model gave rise to varying dynamical scenarios as the parameters as well as the initial conditions varied until at certain values, the output was apparently random looking despite being governed by deterministic laws. This was probably the first advocated phenomenon of chaotic evolution, which was earlier thought of as a mathematical oddity. In the decades since then, physicists have come to discover that irregular, complex behaviour chaotic or otherwise is much more widespread, and may even be the norm in the universe. Lorenz's initial work was followed up by many researchers and results started accumulating leading to the establishment of a full-fledged field of Nonlinear Dynamics with Chaos Theory as a subsidiary to it (Ruelle & Takens, 1971; Newhouse et. al., 1978; Mandelbrot, 1985). The concept of nonlinear dynamics centered round the idea of a phase space for a dynamical system in which the system evolution in time was observed, monitored and studied. Most of the systems in the real world being dissipative in nature, their evolution after some transient period was found to be restricted on a geometrical object known as the 'attractor' in phase space. The problem now got reduced to studying the behaviour of trajectories on the attractor by various measures relating to

their static and dynamic distributions. Following the work of Lorenz (1963), Ruelle and Takens in 1971 introduced the abstract concept of a 'strange' attractor in the context of onset of chaos in turbulent fluids, which was to pioneer a new course in the understanding of complex systems. Several years later, May found an example of chaos in the iterative map (logistic map) that was used to study population dynamics in biology (May, 1976). Feigenbaum (1978) discovered that there are certain universal routes, which systems will take in transitioning from regular to irregular motion. This discovery provided the link between chaos and its transitioning phase. All these theoretical formulations were tested by experimental scientists in widely ranging fields such as fluids, mechanical systems (D'Humieres et. al., 1982), chemical reactions (Coffman et. al., 1986; Richetti et. al., 1987) and electronic circuits (Matsumoto et. al., 1987a). By 1980, the widespread interest in chaos, fractals, oscillators and their applications had taken a firm root for this emerging field of dynamics. The resurgence in the study of nonlinear dynamics over the past couple of decades or so may be primarily attributed to a dramatic increase in the available computing power. Secondly, the realization that seemingly simple physical systems whose dynamics is governed by deceptively simple systems of equations give rise to beautiful and complex patterns and phenomena. Furthermore, the methodology developed in the study of simple dynamical systems are common across a broad range of scientific disciplines mostly in physics, chemistry and biology and as it is now emerging, even in social sciences and economics (*Chaos and Society*, 1995; Guastello, 1995; *Chaos Theory in the Social Sciences: Foundations and Applications*, 1995).

1.1 Brain as a Complex System

For centuries, philosophers and scientists puzzled over the workings of the brain. Even today although some of the mystery shrouding this wonder *machine* has been lifted, there still remain questions regarding the complex nature of its functioning. The questions of how this organ accomplishes the coordination of everything from the trifles of routine activity to the profound thoughts, intelligence and creativity that are the hallmarks of human genius are still being debated. Recent advances in technology providing instruments such as the CT scanner, Positron Emission Tomography (PET) and more recently Magnetic Resonance Imaging (MRI) scanner have made it feasible to create pictures of the brain during various mental functions as well as in the pathologic conditions. The effort in understanding the brain functioning has at its heart the idea of getting a grip on various spontaneous and little understood mental maladies such as epilepsy, Alzheimer's disease, schizophrenia, depression, derangement and so on.

Brain research has come a long way from the views of Descartes, the seventeenth century French philosopher who was perhaps the pioneer in unraveling the link between the brain and the mind. He concentrated on the behaviour of circuits connecting sensory receptors of the nervous system to the physical world or broadly with the phenomenon of reflex action. In Descartes's view, physical processes were measurable and thus amenable to scientific laws but the subjective processes were immaterial and not measurable. The physical world was totally delineated from the mental world and they interacted only weakly in one part of the world. The dawn of scientific understanding of the nature of electrical activity in the brain may be said to have occurred with the publication of the book *Reflexes of the Brain* by the founder of the Russian school of Reflexology, I. M. Sechenov in 1863. In

this, he generalized from his many observations that all sensory input would stimulate motor activity automatically unless prevented from doing so by the central mental processes of the brain. The decades following the work of Sechenov saw the realization of the brain as possessing a complex structure made up of millions of discrete units called *neurons* that are interconnected to each other by branches, which form channels of information transfer in the brain. By the early 1900s understanding of the brain processes had progressed to an extent that Charles Sherrington, a renowned British physiologist proposed reflex activity as due to a very complicated neuronal organization in the brain rather than the simpler principles of reflexes accepted till then. In another 49 years time, in 1943 there appeared the book *The Organization of Behaviour: A Neuropsychological Theory* by Donald O. Hebb (1964), which proved an exciting integration of mental and brain processes. At the core of his theories was the concept of 'cell assemblies', which still remains an integral idea in theories of the brain function. Hebb thought that any frequently repeated stimulation would lead to the development of a structure consisting of neurons capable of acting as a closed system. The neurons in a cell assembly were able to act together because of changes in the connections called synapses between them. During the learning process, as cells develop into an assembly; these connections become stronger so that even a weak signal from one neuron would suffice to activate the next one and so on. As a result, the 'firing' of a single cell in the assembly causes all the other cells to fire as well. Such a notion of a 'Hebbian synapse' is central to much of modern neuroscience and the growth of the science through the decades following Hebb saw the development of two streams of research. One is concerned with the description of mental processes in terms of component operations that can be precisely specified.

For eg. a visual image is not created as a whole, but rather is formed over time by an orderly set of operations that includes, for instance, placing the parts of images in their proper relation and scanning the content for specific features. The measurement of these operations has been the task of *cognitive science* for the past 30 years. The second branch called *neuroscience* is the study combining many formerly disparate approaches to understanding the basic principles that underlie the construction of the nervous system. These two branches have been integrated by the technological development of imaging and present research is on a holistic approach in understanding the brain and mind. The crux of the problem lies in learning how mental images are formed, how networks of nerve cells develop and how brain regions interact in specified patterns for accomplishing various actions and finally applying the results to understand what goes wrong with these networks in cases of different mental illnesses (Posner & Raichle, 1994).

The brain is probably the most complex system known to us whose mechanisms are the least understood. About 10^{11} neurons and their interconnections ($\sim 10^3$) defy any form of analysis about its functions. It is thus a complex system, stochastic in nature and with feedback-feedforward processes operative. The dynamical complexities of cellular processes in the brain ranging over timescales from 10^{-3} seconds to several days are of a nature that when interwoven give continuity to conscious experience and produce exquisite abilities unique to human brain such as thinking and creativity (Kuffler et. al., 1984). Emboldened by the recent developments in nonlinear dynamics and physics of complex systems, neuroscience looks towards this paradigm for understanding brain functions. It is generally felt that the nonlinear approach may not only help to understand emergent properties of brain such as perception, cognition and states of consciousness

but also provide solutions to some perplexing neuropsychiatric problems such as epilepsy, schizophrenia, mental depression, response to therapies etc. Applications of nonlinear dynamics till date in neuroscience have resulted in a novel and qualitative change in the outlook on the investigations of the brain and its functions.

1.2 Nonlinearity in the Neural System

The evidence for the existence of nonlinearity in the behaviour and evolution of systems abound in the living world. With special reference to the nervous system, a review of the experimental evidence of the nonlinear nature embedded in the various levels of organization from the single cell level to the large cell assemblies is summarized in this section.

A very simple structure in the living world that exhibits prominent nonlinearity is the neuron. It has a prominent place in research since despite not being governed by very complicated laws; neurons produce highly complex patterns of behaviour. A neuron is a single cell consisting of a cell body and a single axon. The cell receives signals from other cells through dendrites, which are connected to the cell body but the output signal is transmitted only through the single axon. One of the most investigated of these structures is the giant axon of the squid *Doryteuthis bleekeri*, which is known for the rapid transmission of action potentials in the form of neuronal firings. In 1952, Hodgkin and Huxley presented their well-known model through four simultaneous, first order differential equations describing the time course and voltage dependence of the membrane ionic currents flowing through the giant axon of the squid. This model involves three voltage dependent gating variables, the Sodium (Na) - Potassium (K) activation variables and the sodium inactivation variable and a fourth variable involving

the membrane potential. The two noteworthy points in this pioneering study are (i) the irregular behavior of the axon is not due to a noise component in the membrane but results from a nonlinear, coupled deterministic system and (ii) for the giant axon of the squid, there exists a powerful model that is able to generate all the types of oscillations known from experimental observations of the axon. Besides, the specific routes from regular to chaotic behavior could be traced with this model. But it was argued that the oscillations were induced experimentally on the biological specimen in a non-natural solution and hence whether such irregular oscillations could exist in naturally occurring physiological system. In 1987, Matsumoto and his co-workers demonstrated that chaotic oscillations can be generated by applying periodic trains of current pulses to the silent axon immersed in normal seawater. On measuring the correlation dimension, a typical dynamical invariant at two different points along the axon (30-40 mm apart) they found that chaos is stably propagated (D_2 : 3.2-3.4). This observation suggested that chaos could be relevant in neural information processing and established the occurrence of chaotic behaviour in axons and neurons in general under normal conditions (Matsumoto et. al., 1987b).

The first evidence for chaotic behaviour in cell membranes was provided by Hayashi et al. (1982), who could induce irregular oscillations using sinusoidal stimulation to the neuronal membrane. Studies on the giant neurons of the squid were conducted mainly on two categories (i) silent neurons that need a medium to oscillate and (ii) pacemaker neurons which spontaneously show periodic activity in artificial seawater. Both have been shown to produce irregular activation depending on the stimulation provided. In the second category, the pacemaker neuron of the mollusc *O. verruculatum* immersed in artificial seawater exhibited spontaneous chaotic

bursting activity both in the interspike interval as well as in membrane potential when stimulated by a small direct current of about 0.3nA (Hayashi & Ishiyuka, 1987).

Yet another condition under which chaotic activity can be observed is based on chemical induction. Neurons of the pond snail *L. stagnalis* exhibit irregular, chaotic oscillations in the presence of cocaine. These examples indicate that different types of cells under various electrical and chemical stimulants, exhibit phase locking patterns as well as irregular, chaotic or chaotic-like oscillations. The observations of spontaneous chaotic activity clearly support the hypothesis that single cells are capable of exhibiting a variety of behaviour due to their strong nonlinearity.

In the investigations on the presence of nonlinear dynamics in cell assemblies, the work of Rapp and his co-workers may be cited. Correlation dimension analyses of the inter-spike intervals in the precentral and post central gyri of anaesthetized squirrel monkeys gave low values varying from 2.2 to 7 (Rapp et. al., 1985). This report suggested the occurrence of low dimensional chaos in the spontaneous activity of some simian cortical neurons. Later work by Mpitsos and associates on the generation of motor patterns in the mollusc *Pleurobranchaea californica* threw up evidence for low dimensional chaos such as quickly decreasing auto correlation function, fractional dimension, positive Lyapunov exponent etc. (Mpitsos et. al, 1988). But, the limited data as well as brief temporal duration and variability of biological actions made it difficult to justify strong claims on chaos. In the following work on a simple neuronal network comprising of a single input and output units and four hidden units, Mpitsos and co-workers could demonstrate the ability of the network to distinguish between various chaotic signals, generated from Logistic map, Rossler equation etc. The answer to whether a

chaotically coded message in one brain region was understood by other regions was surmised from this result. The neural message is not composed of a signal overlapped by noise but lies in the inherent irregularity itself.

The olfactory bulb is a model neuropil with the same cell types and chemical neuromodulators as the neocortex. Due to its simplicity and knowledge about the electro genesis in it, the study of nonlinear structure in the physiological brain signal, the Electroencephalogram (EEG), is expected to be easier to interpret by this model neuropil than the neocortex. Freeman and his coworkers (1988) investigated the perceptive events in the olfactory system of the conscious rabbit and on the basis of this, developed a mathematical model of the bulb that uses nonlinear, coupled ordinary differential equations. In order to associate these findings with the processes in the neocortex itself, they studied the visual system of the monkey (Freeman, 1986 & 1995; Freeman et. al., 1988). Based on this model, four types of activity were analysed – the first of a silent system which occurs under deep anesthesia, second during normal background activity in the absence of a significant input, thirdly during the reaction of the system to a learned odour and finally that during an epileptic seizure. From among the various interesting findings in their study, some of the significant results are noted here. The researchers concluded that the dynamical process in the olfactory system of a motivated rabbit is characterized in the absence of any significant odour by a spatially and temporally un-patterned chaotic state. Learning of a new odour and its subsequent recognition are related to a process involving a change in the nonlinear dynamics of the system. The study of specific cortical structures such as the auditory cortex, the hippocampus etc. were conducted on cats using implanted electrodes.

Dimension analysis indicated the presence of various attractors with fractional correlation dimension (Roschke & Basar, 1988).

With such varied yet strongly supportive evidence of the presence of nonlinearity and even low dimensional chaos at times, pouring in from various biological systems, the human EEG signal also came to be viewed through the looking glass of nonlinear dynamics. While early studies were mainly demonstrational in nature, in the long run, structured analysis of the signal was carried out using qualitative as well as quantitative techniques. A detailed survey of literature in the dynamical analysis of EEG signal by application of different measures and methods is cited all along this thesis and hence is not included at this stage. Rather we make an attempt to seek the need for such an approach and the salient features inherent in such studies.

1.3 Analyzing Physiological Time Series

Earlier, whenever study of time series from biological systems was undertaken, the statistical techniques usually made use of failed to detect patterns embedded in the irregular looking data. It was suggested that this was probably a result of examining the time series in terms of static rather than dynamic behaviour i.e. the usual techniques do not take into account the nonlinear behaviour. Traditional methods of signal processing used the Fourier, wavelet or other techniques to decompose the signal into its component frequencies; thus reflecting a limited amount of information. In contrast the nonlinear dynamics approach postulates that a time series may be seen to contain the effect of all other variables involved in the dynamics of the system. The theoretical aspect of this formulation is based on a variety of mathematical theorems of which the Taken's theorem is the most significant one (Takens, 1981). According to this formulation, it is given that complex

dynamical systems such as the human nervous system have an enormous number of interrelated dependent variables that cannot be directly measured. If any single variable can be measured with sufficient accuracy at a given rate for a sufficient length of time, then it is possible to make quantitatively meaningful inferences about the dynamic structure of the system from the behaviour of that single variable. The advantage of the nonlinear dynamic theory is the ability to project the dynamics of a system onto a static phase space diagram. In physiology, since the system's variables are not all identified, the phase space must be reconstructed from the observed time series. This is followed by the possibility of looking for an attractor in the reconstructed space and subsequently its characterization using various topological as well as dynamical parameters.

A useful time series analysis requires idealized conditions of infinitely long, noise free data sets. But data from living systems are irreproducible even in a statistical sense. *A living being can never be brought back to a given state.* Besides, changes in its being as well as environment cause variations during measurements thus giving rise to nonstationarity. These various factors affecting the time series impress their own time scale(s) on the series. This could be an explanation for the occurrence of nonstationarity. In addition to nonstationarity is the problem of noise contamination. Noise can be introduced through the measurement device or through the transmission of the signal from the source to the measurement device and also due to the perturbations from the environment.

The advantage of nonlinear dynamical analysis lies in its supplying new tools for studying dynamics and signal classification. Traditional methods for data analysis, as mentioned above characterize a state by averaged quantities like means, variances, autocorrelations, and so on, which are

successful in dominantly linear systems. On the other hand, nonlinear analysis tries to get hold of properties of the underlying complex dynamics. In most cases, the nonlinear methods which allow for a characterization of data by a whole set of quantities such as divergence rates, predictability etc. provide new insights not revealed by the usual linear techniques. Apart from signal classification, a detailed dynamical analysis can help to detect physiological mechanisms and to design, affirm or reject simplified or realistic models for certain processes and disorders. However the application of nonlinear methods to physiological data is yet not fully explored. It is known that physiological systems contain complex structures and also that nonlinearities and time delays in feedback loops abound in them and finally that both the understanding and diagnostics of disorders is related to dynamical properties of the system. These singular features make nonlinear analysis of the geometry and dynamics of such systems worth a challenge.

1.4 Nonlinear Brain Analysis

The complex dynamic behaviour of the brain is reflected in the EEG, which is a recording of a large number of neuronal membrane potentials over distant regions of the brain. EEG is a phenomenon of integrated brain metabolic process, containing signatures of activities in the underlying brain structures particularly in the cerebral brain cortex. The success in the application of principles of nonlinear dynamics to EEG analysis is apparent in the multitude of research publications cited all through this thesis. Despite this, there is a need to be cognizant of the pitfalls and drawbacks that are inherent in this approach as well.

One of the difficulties lies in not being able to confirm whether the experimental data in hand conforms to the assumptions made in applying the

principles of analysis. A basic assumption usually made is regarding stationarity of the signal, which is almost impossible to observe in signals from biological and physiological systems for any considerable stretch of time. The next question of debate is whether EEG is simply noise or in fact a deterministic chaos. Such conflict remains unresolved to an extent even as researchers ask better questions pertaining to the information gained. Whether or not the EEG is low dimensional or chaotic is an interesting question but, may not be ultimately as important as whether the tools of nonlinear dynamical analysis are useful in the characterization of brain states or the prediction of seizure onset. The focus has shifted away from proving the existence or otherwise of chaos or low dimensionality of the system and toward the characterization of dynamical difference between states as a tool for better understanding of the underlying system.

1.5 Organization of the Thesis

The thesis covers the research work in 9 chapters. The first chapter introduces the human brain as the potential nonlinear system under study. The historical development of the science of nonlinear analysis is surveyed and the validation of the brain as a complex, nonlinear system is carried out by citing theoretical as well as experimental findings supporting this. The salient features of the application of nonlinear methods to physiological data analysis are presented. The chapter finally clarifies the relative merits as well as drawbacks inherent in the adaptation of physical principles to understand the dynamics of biological systems. The second chapter is the description of the theory of nonlinear systems with special emphasis on the current research in systems with nonlinear interactions. Chapter III deals with the actual time series methods as applied to observed irregular/chaotic data. This comprises

of both linear as well as nonlinear methods of signal processing. Besides, the chapter deals in detail with the attractor reconstruction and the theoretical backing provided by the embedding theorems as well as the characterization of the system attractor with invariant parameters such as generalized dimensions, entropies and so on. The last part of chapter III is devoted to understanding the electroencephalogram signal, its recording paradigms, characteristics and nonstationary nature and the literature review on the nonlinear time series findings from the EEG signal.

Chapter IV is based on a dynamical study on coupled oscillators. This part of work is carried out on the model Rössler system as a potential system for modelling the characteristics of the system generating the complex EEG signal. The behaviour of the system under two different coupling scenarios: uni-directional and bi-directional is studied by analyzing the time varying output of the composite system. The dynamical as well as co-ordination effects induced by the coupling in the system are looked into and the significant results are discussed. As an extension to the real world situation, noisy coupling is considered next and the effect of coupling on the dynamics of the system is investigated.

The following chapter heralds the beginning of the studies made on the real time EEG data. In this chapter, the nonstationarity of the EEG is discussed in detail with the derivation of a general time scale based on the most important processes occurring in the neural system. The idea is extended to look into the effect of time scales on the unfolding of neural attractors. For this pilot study, the bioelectric signal from the brain, recorded from normal subjects as well patients suffering from the pathological condition of epilepsy are considered. The distinctness in the behaviour of the

signal from the two groups is discussed in detail and its implications on the dynamics are analyzed.

Chapter VI comprises the complexity studies conducted on the EEG signal. In this case the base line state is the normal, eyes closed condition and the complexity variations of the EEG signal with the change of state from passive to a mental task state are monitored. In addition the cortical regions that exhibit these changes as well as their relevance in the brain functioning during the particular states are described. The studies are carried out by computing the nonlinear statistic of Approximate Entropy and its variant, Sample Entropy that characterise the sequential irregularity in the time trace of a signal. The studies are validated using appropriate statistical tests carried out on the computed parameters for a population of subjects. Yet another direction undertaken is to look at the multiscale analysis of the complexity measure and the results obtained give insight into the inherent randomness of the underlying system.

The next chapter deals with the functional coordination existing in the cortical domain. In order to study the coupling between brain regions, we make use of a bi-variate measure based on the signals ensuing from two brain locations. The measure is based on the instantaneous phase of the signal and the strength of interaction is represented by an index of synchronization computed from the relative phase difference. We make a detailed study of the temporal variations in this index during passive conditions of eyes closed and eyes open as also during the abnormal brain experience of epileptic seizure. The interactive nature during mental task conditions is also looked into and finally we apply the idea of directional coupling. With this measure we probe the nature of cortical coupling as to whether there is any coupling present and if so whether it is unidirectional

one or whether the two regions interact mutually with each other during specific task states.

Chapter VIII is an overview of the existing neural models and a theoretical formulation to the idea of topological manifolds inferred from the EEG signal. This theory has its foundation in the nonequilibrium statistical mechanics and a general equation of motion for the system is proposed. An inverse scattering technique is applied to evaluate a motion generating potential and the map of the same in time gives rise to manifolds. The final chapter will summarize the results in the thesis as well as present some general conclusions regarding the dynamical aspects of the systems in the light of the new findings. An outline of projects that can be undertaken in the wake of the present work will also be sketched.

Nonlinear analysis of the brain is still far from maturity and the uses of nonlinear techniques discussed in this review should be considered exploratory. These are however essential and must be pursued if eventually a body of techniques is to evolve to study signals from the brain. Despite the pitfalls encountered occasionally, nonlinear analysis of the EEG remains largely successful. It holds promise in turning the EEG into a true "window on the mind" as hoped by Hans Berger when he first observed electrical activity in the brain seventy-five years ago.

Nonlinear Systems: A Theoretical Approach

It may happen that small differences in the initial conditions produce very great ones in the final phenomena. A small error in the former will produce an enormous error in the latter. Prediction becomes impossible.

--- Henri Poincaré

Nonlinear systems are the norm in nature. Yet study of natural systems was carried out for a long time within the framework of linear or Newtonian dynamics. This approach led to many results and generalizations on systems that could not in any way be matched with the real phenomenon. Nonlinearity in a system simply means that state of a system depends in a complex manner on the measured values at an earlier time or it becomes increasingly difficult to predict the state of the system from that inferred from an earlier occasion. Of late a need for a new approach to complex systems became imperative and this resulted in the development of a new revolutionary

pathway commonly known as chaotic dynamics. Chaotic dynamics is truly dynamic (no pun intended) in the sense that it occurs in all fields of science- Physics, Chemistry, Biology as well as in the fields of social sciences. In such systems, while the evolution occurs in a *deterministic* way, the output from the system is totally irregular and *random* thereby defying the predictive capability. It was observed early in research that whenever deterministic chaos occurs, it is accompanied by nonlinearity.

It was the French mathematician, Henri Poincaré who was the pioneer in the analysis of systems with in-built nonlinearity. Poincaré's work on periodic solutions of ordinary differential equations constitute the foundation of the most part of the results obtained until now. Poincaré's theory included the idea of bifurcations as well as the qualitative study of solutions to generalize to dissipative three-dimensional dynamical systems or conservative four-dimensional systems ones, via a reduction to the map of a surface onto itself. Poincaré was also the first to put in evidence a kind of analogy between fixed points of a 2-dimensional map and the equilibrium points of an autonomous differential equation of the same dimension. This was done by defining behaviours of type node, focus and saddle points. The introduction of the pathbreaking ideas of stability of fixed points, limit cycles and Poincaré sections formed a solid foundation for building the theory of Nonlinear dynamics.

2.1 Nonlinear Systems- Terminology and Definitions

Any nonlinear system, which can be expressed by a set of mathematical equations, includes two types of variables - **dynamic** and **static**. Dynamic variables are the quantities, which change with time whereas the static

variables often referred to as the **control** or **system parameters**, remain constant until changed by an outside force. When studying a nonlinear system, the control parameters are often changed to learn how the behaviour of the system changes in response. The act of changing a control parameter to change the system behaviour is known as **perturbation**.

A **dynamical system** may be defined as a deterministic mathematical relation for the evolution of a system in time. **State space** or **phase space**, is the space of the dynamic variables and might in some cases include their derivatives. A point in the state space specifies the state of the system at a given instant and hence is referred to as the **system point**. As the system evolves with time, the state or the system point moves from point to point in the state space, thus defining a **trajectory**. A trajectory therefore displays the history of the states of the system. As in classical statistical mechanics, a collection of several trajectories with different initial conditions is called a **phase portrait** for the system, which is a graphical representation of the global behaviour of the system. In nonlinear dynamical theory, the number of **degrees of freedom** is usually defined as the number of dynamic variables needed to specify the dynamical state of the system, or equivalently as the number of independent initial conditions that are needed to specify the system.

Dynamical systems may in general be divided into three types (Parker & Chua, 1987).

(a) Autonomous dynamical system: An N^{th} order autonomous dynamical system is defined by the state equation:

$$\begin{aligned}
 \frac{dx^{(1)}}{dt} &= F_1(x^{(1)}, x^{(2)}, \dots, x^{(N)}) \\
 \frac{dx^{(2)}}{dt} &= F_2(x^{(1)}, x^{(2)}, \dots, x^{(N)}) \\
 &\vdots \\
 \frac{dx^{(N)}}{dt} &= F_N(x^{(1)}, x^{(2)}, \dots, x^{(N)})
 \end{aligned}
 \tag{2.1}$$

This is a dynamical system since for any initial state of the system, $x(0)$, the equations can be solved to obtain the state $x(t)$ at a later time, $t > 0$. $F = (F_1, \dots, F_N)$ is a vector field in the state space, i.e. F_i are functions of $x^{(i)}$ and $p^{(i)}$ are the corresponding vectors of control parameters (if any). The dynamical relations are linear if $F(x)$ is linear. For an autonomous system for which the vector field does not depend on time, the initial time may be taken as $t_0 = 0$. If for example, in the above system, $N=3$; then figure 2.1 represents a path in the evolution of the system. The space spanned by (x_1, x_2, x_3) is the phase or state space of the system. A point in this space at a time t specifies the system completely at that given instant. The path traversed by such a system point in state space as the system evolves in time is referred to as orbit or trajectory.

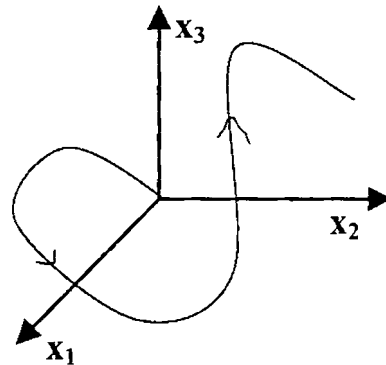


Figure 2.1 The phase space in three-dimensions with the trajectory.

(b) Non-autonomous dynamical system: In this case the system definition is similar to the Eq.(2.1) except that now, $F = F(x,t)$. The vector field depends explicitly on time and unlike the autonomous case the initial time cannot be arbitrarily set to 0. If there exists a $T > 0$ such that $F(x,t) = F(x,t+T)$ for all x and all t , the system is said to be time-periodic with period T . The smallest such T is called the minimal period. In general an N^{th} order time periodic nonautonomous system can be converted to an $(N+1)^{\text{th}}$ order autonomous system by appending an extra state $\theta = \frac{2\pi}{T}$.

(c) Discrete time dynamical systems: In this case the system values are given at equal, discrete, integer valued time. An example of a dynamical system is one that may be written in vector form as:

$$\mathbf{x}_{n+1} = F(\mathbf{x}_n) \tag{2.2}$$

where $n=0,1,2,\dots$ denotes the time variable. \mathbf{x}_n has N components, $x_n = (x_n^{(1)}, x_n^{(2)}, \dots, x_n^{(N)})$. Given an initial condition, \mathbf{x}_0 , a trajectory of the discrete time system can be generated by applying an operator $F(\dots)$ to the previous state, i.e.

$$x_1 = F(x_0), \quad x_2 = F(x_1) = F(F(x_0)), \quad \dots, \quad x_n = F^n(x_1)$$

2.2 Cauchy - Lipschitz Condition

In this context, some inherent mathematical concepts to the development of differential equations theory may be reiterated. While Cauchy's theorem deals with the existence and uniqueness of the solution of a differential equation, the unique determination of solutions by the initial conditions is guaranteed

by the *Cauchy-Lipshitz condition*. Accordingly, for a system of N first order equations as in Eq.(2.1), if $(x_0^{(1)}, x_0^{(2)}, \dots, x_0^{(N)})$ are the given values of the variables; then $F(x^{(1)}, x^{(2)}, \dots, x^{(N)})$ is said to satisfy a Lipschitz condition if there are positive numbers k and δ such that the relation,

$$\left| F(x^{(1)}(0), x^{(2)}(0), \dots, x^{(N)}(0)) - F(x^{(1)}, x^{(2)}, \dots, x^{(N)}) \right| \leq k \sum_{i=1}^N |x^i(0) - x^i| \quad (2.3)$$

holds provided $|x^i(0) - x^i| < \delta$, $i = 1, 2, \dots, N$. If the partial derivatives

$\left(\frac{\partial F}{\partial x^{(i)}} \right)$ exist and are continuous, it can be shown that F satisfies the Lipschitz

condition. It is on the basis of this that the Cauchy-Lipschitz theorem is stated for a system of N first order differential equations. Hence the application of this theorem to a single differential equation of order N involves solving the differential equation for the highest derivative, which is written as,

$$x^{(N)} \equiv \frac{d^N x}{dt^N} = f\left(t, x, \frac{dx}{dt}, \frac{d^2 x}{dt^2}, \dots, \frac{d^{N-1} x}{dt^{N-1}}\right)$$

This is equivalent to the system of N first order differential equations,

$$\dot{x} = x^{(2)}, \ddot{x} = x^{(3)}, \dots \Rightarrow x^{(N)} = f(t, x^{(1)}, x^{(2)}, \dots, x^{(N)})$$

This is a special case covered by the Cauchy-Lipschitz theorem, which states that the solutions of the above system of equations are uniquely determined by the values prescribed for x and its first $(N-1)$ derivatives at $t=t_0$ provided that the function f satisfies a Lipschitz condition. The Cauchy-Lipschitz theorem applied to the autonomous system has a consequence that through

every point of the plane there passes one and only one trajectory. This is the *No-Intersection theorem* as is commonly known in Nonlinear Dynamics literature. The physical content of this theorem is a statement of determinism. Two distinct state space trajectories cannot intersect in a finite period of time. If they do, at the intersection point, the trajectory would have the same values of the state variables and the same values of their time derivatives and yet evolve in *two different ways*; thus violating the Cauchy-Lipschitz theorem (Minorsky, 1969; Ott, 1993).

2.3 Conservative Vs. Dissipative Systems

From a physical point of view, dissipative systems are distinguished from conservative systems by the action of their flow on volume elements in phase space. In conservative systems, the volume of each element remains constant in time while in the case of dissipative systems; it typically shrinks at least in the mean over long time periods. For dissipative systems, the effects of transients associated with initial conditions disappear in time. The trajectory in state space will head for some final attracting region, or regions, which might be a point, curve, area, and so on. Such an object is called the *attractor* for the system, since a number of distinct trajectories will be attracted to this set of points in the state space. The properties of the attractor determine the long-term dynamical behaviour of the system. The set of all initial conditions giving rise to trajectories that approach a given attractor is called the *basin of attraction* for that attractor. If more than one attractor exists for a system with a given set of control parameter values, there will be some initial conditions that lie on the border between the two or more basins of attraction.

2.4 Stability of Equilibrium Points

Linearization of the state space equation provides useful information about the local stability of properties of an equilibrium state. In the context of an autonomous nonlinear dynamical system with equilibrium state \bar{x} , the definitions of stability are as follows:

Def. 1: The equilibrium state \bar{x} is said to be uniformly stable if for any given positive ε , there exists a positive δ such that the condition

$$\|x(0) - \bar{x}\| < \delta \quad \Rightarrow \quad \|x(t) - \bar{x}\| < \varepsilon \quad \text{for all } t > 0.$$

This definition states that a trajectory of the system can be made to stay within a small neighbourhood of the equilibrium state \bar{x} if the initial state $x(0)$ is close to \bar{x} .

Def. 2: The equilibrium state \bar{x} is said to be convergent if there exists a positive δ such that the condition

$$\|x(0) - \bar{x}\| < \delta \quad \Rightarrow \quad x(t) \rightarrow \bar{x} \quad \text{as } t \rightarrow \infty.$$

The second definition means that if the initial state $x(0)$ of a trajectory is close enough to the equilibrium state \bar{x} , then the trajectory described by the state vector $x(t)$ will approach \bar{x} asymptotically.

Def. 3: The equilibrium state \bar{x} is said to be asymptotically stable if it is both stable and convergent.

Def. 4: The equilibrium state \bar{x} is said to be globally asymptotically stable if it is stable and all trajectories of the system converge to \bar{x} as time t approaches infinity.

This definition implies that the system cannot have other equilibrium states and that it requires that every trajectory of the system remains bounded for all time $t > 0$. In other words, global asymptotic stability in a system causes it to ultimately settle down in a stable state for any choice of initial conditions.

2.5 Linear Stability Analysis

Consider a system of N real first-order differential equations,

$$\dot{x} = F(x) \tag{2.4}$$

A few definitions are in order. *Steady state behaviour* refers to the asymptotic behaviour as $t \rightarrow \infty$ and it should be bounded. The difference between a solution and its steady state is called a *transient*. A point y is a *limit set* of x , if for every neighbourhood U of y , the trajectory, say $\phi_t(x)$ enters U as $t \rightarrow \infty$. The set of all limit points of x is called the *limit set* $L(x)$ of x . Limit sets are closed and invariant under ϕ_t . A limit set L is attracting if there exists an open neighbourhood U of L such that $L(x) = L$ for all $x \in U$. The *basin of attraction* $B(L)$ of an attracting set L is defined as the union of all such neighbourhoods U . Every trajectory starting in $B(L)$ tends toward L as $t \rightarrow \infty$. In a stable linear system there is only one limit set. Hence the steady state behaviour is independent of the initial condition. In a typical nonlinear system, there can be several limit sets, each with a different basin of attraction. The initial condition determines in which limit set the system finally settles.

Consider the system in Eq. (2.4). A steady state or fixed point for this system is that point $\mathbf{x} = \mathbf{x}_0$ at which

$$F(\mathbf{x}_0) = 0 \quad (2.5)$$

A trajectory that gets to the fixed point stays there. We are interested in examining the behaviour of trajectories near \mathbf{x}_0 . Hence we set, $\mathbf{x}(t) = \mathbf{x}_0 + \boldsymbol{\eta}(t)$ where the increment $\boldsymbol{\eta}(t)$ is assumed to be small. Substituting this into Eq. (2.4), we expand $F(\mathbf{x})$ to first order in $\boldsymbol{\eta}(t)$,

$$F(\mathbf{x}_0 + t) = F(\mathbf{x}_0) + DF(\mathbf{x}_0) \cdot \boldsymbol{\eta} + O(\boldsymbol{\eta}^2) \quad (2.6)$$

Since \mathbf{x}_0 is a steady state, $F(\mathbf{x}_0) = 0$ and DF denotes the Jacobian matrix of the partial derivatives of F .

Hence,

$$DF(\mathbf{x}) = \begin{bmatrix} \frac{\partial F^{(1)}}{\partial x^{(1)}} & \frac{\partial F^{(1)}}{\partial x^{(2)}} & \frac{\partial F^{(1)}}{\partial x^{(N)}} \\ \frac{\partial F^{(2)}}{\partial x^{(1)}} & \frac{\partial F^{(2)}}{\partial x^{(2)}} & \frac{\partial F^{(2)}}{\partial x^{(N)}} \\ \vdots & \vdots & \vdots \\ \frac{\partial F^{(N)}}{\partial x^{(1)}} & \frac{\partial F^{(N)}}{\partial x^{(2)}} & \dots & \frac{\partial F^{(N)}}{\partial x^{(N)}} \end{bmatrix} \quad (2.7)$$

The equation for the time dependence of the perturbation of \mathbf{x} from the steady state is given by,

$$\frac{d\boldsymbol{\eta}}{dt} = DF(\mathbf{x}_0) \cdot \boldsymbol{\eta} + O(\boldsymbol{\eta}^2) \quad (2.8)$$

The linearized stability problem is obtained by neglecting the terms of order η^2 in Eq. (2.8) and is of the general form,

$$\frac{dy}{dt} = Ay \tag{2.9}$$

where y is a real N-dimensional matrix and A is a real, time dependent NxN matrix. If the determinant of the Jacobian matrix, $\det A$, is unity at all points the system is conservative. If the average of $|\det A| < 1$ then the system is dissipative. If the average of $|\det J| > 1$ then volumes in state space expands with time.

If the solution of Eq. (2.9) is assumed to be of the form, $y(t) = ue^{\lambda t}$, then Eq. (2.9) becomes an eigen value equation,

$$A u = \lambda u \tag{2.10}$$

which has a nontrivial solution for values of λ satisfying the characteristic equation

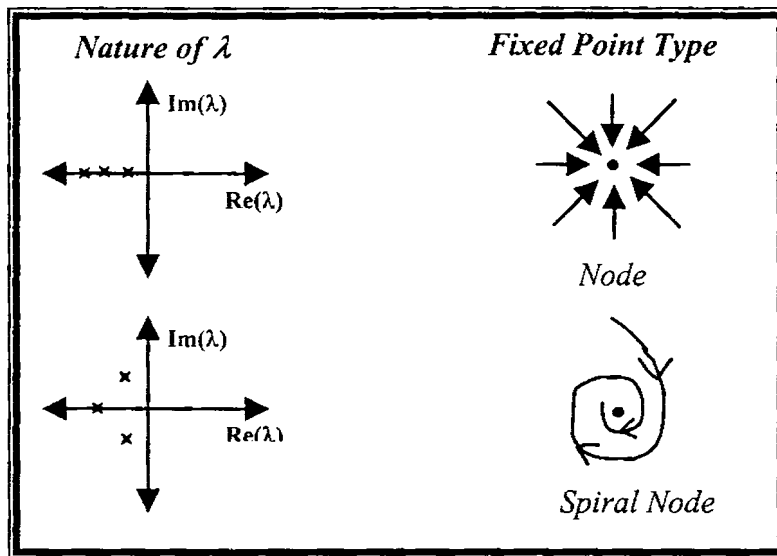
$$|A - \lambda I| = 0 \tag{2.11}$$

where I is an NxN identity matrix. The nature of the fixed points of the system is determined by the roots of the characteristic equation at that fixed point. Hence in general, if $N=3$, the characteristic equation is cubic giving rise to three λ values. In this case therefore three cases may occur: (i) the three characteristic values are real and equal, (ii) the three values are real and unequal and (iii) there is one real characteristic value and the other two are complex conjugates (Ott, 1993; Hilborn, 1994; Minorsky, 1969).

For state spaces with 3 or more dimensions, it is common to specify an Index of the fixed point, which is the number of characteristic values of the fixed point whose real parts are positive.

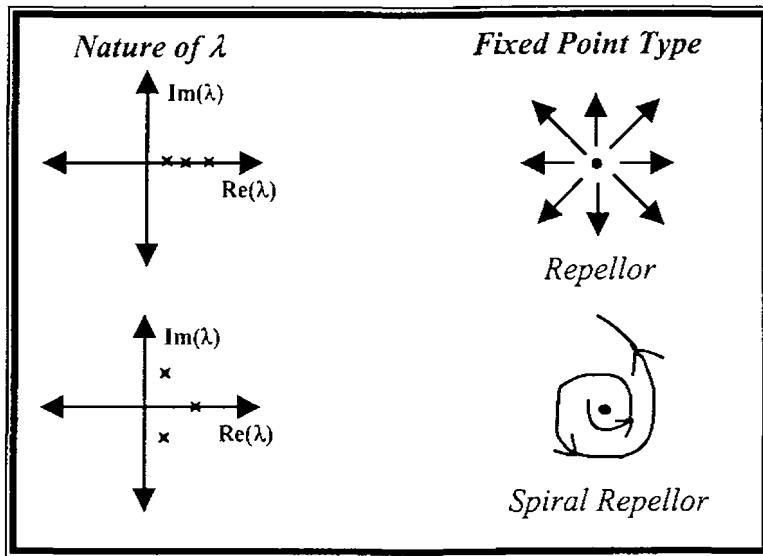
The four basic types of fixed points for a three dimensional space are:

1. Node: All λ s are real and negative. This means all the trajectories in the neighbourhood of the node are attracted to it without any looping around it.
- 1s. Spiral Node: All the λ s have negative real parts but two are complex conjugates. The trajectories spiral around the node on a surface as they approach the node.



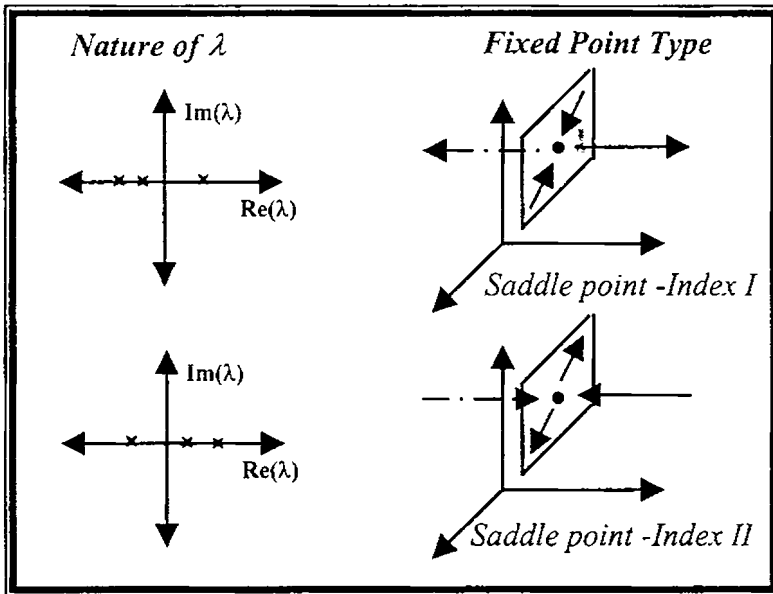
2. Repellor: All λ s have positive real parts causing all the trajectories in the neighbourhood of the fixed point to diverge from it.

2s. Spiral Repellor: All the λ s have positive real parts and two are complex conjugates. The trajectories spiral around the node on a surface as they diverge from the fixed point.



3. Saddle point – index I: All the λ s are real. One is positive while the other two are negative. Trajectories approach the saddle point on a surface (the in-set) and diverge along a curve.

3s. Spiral saddle point- Index I: The two characteristic values with negative real parts form a complex conjugate pair. The trajectories spiral around the saddle point as they approach on the in-set surface.



4. Saddle point – index II: In this case, one λ is real with negative real part and the other two are also real but are positive. Trajectories approach the saddle point on a curve (the in-set) and diverge from it on a surface.

4s. Spiral saddle point- Index II: The two λ s with positive real parts form a complex conjugate pair. Hence the trajectories spiral around the saddle point on a surface (the out-set) as they diverge from the fixed point.

Suppose the Jacobian matrix at an equilibrium point x_0 has d eigenvalues λ_i , $i=1,2,..,d$; then table 2.1 summarizes the type of the equilibrium point x_0 .

Table 2.1: Conditions on the types of equilibrium points

Conditions on $\text{Re}[\lambda]$	Conditions on $\text{Im}[\lambda]$	Equilibrium point type	Stability
$\text{Re}[\lambda_i] < 0 \forall i$	$\text{Im}[\lambda_i] = 0 \forall i$	Node	Stable
$\text{Re}[\lambda_i] < 0 \forall i$	$\text{Im}[\lambda_i] \neq 0$ for some i	Spiral node	Asymptotically stable
$\text{Re}[\lambda_i] > 0 \forall i$	$\text{Im}[\lambda_i] = 0 \forall i$	Repeller	Unstable
$\text{Re}[\lambda_i] > 0 \forall i$	$\text{Im}[\lambda_i] \neq 0$ for some i	Spiral repellor	Asymptotically unstable
$\text{Re}[\lambda_i] > 0$ & $\text{Re}[\lambda_j] < 0$ for some i & j	$\text{Im}[\lambda_k] = 0 \forall k$	Saddle point	Non-stable type 1
$\text{Re}[\lambda_i] > 0$ & $\text{Re}[\lambda_j] < 0$ for some i & j	$\text{Im}[\lambda_k] \neq 0$ for some k	Saddle point	Non-stable type 2

2.5.1 Limit Cycles

Besides the fixed points discussed in the previous section, Poincaré showed that the differential equations representative of a dynamical system in two or higher dimensions can admit special solutions that form closed curves in the

phase plane known as *Limit Cycles*. A limit cycle is a closed trajectory such that no trajectory sufficiently near it is also closed. If all nearby trajectories approach C as $t \rightarrow \infty$ the limit cycle is said to be stable and if C is approached as $t \rightarrow -\infty$; it is unstable. Limit cycles are fundamental in the theory of oscillations of nonlinear, non-conservative systems. A stable limit cycle represents a stable stationary oscillation of a physical system in the same way that a stable singular point represents a stable equilibrium. The presence of limit cycles in two-dimensional phase space is a consequence of the Poincaré-Bendixson theorem, which may be stated in the following manner.

Suppose the long term motion of a state point in a two dimensional state space is limited to some finite size region and suppose that this region R is such that any trajectory within R remains within it. Then a trajectory starting within R, can follow any of the two possibilities.

- (i) *Approach a fixed point as $t \rightarrow \infty$*
- (ii) *Approach a limit cycle as $t \rightarrow \infty$*

The means of studying the stability of the limit cycle is simplified by making use of the Poincaré section. Before proceeding with this discussion, we shall briefly introduce the idea of Poincaré maps.

2.6 Poincaré Map

When studying a continuous nonlinear dynamic system, it is often desirable to reduce it to a discrete time system. The *Poincaré map* is a technique that models a continuous time system as a discrete system. The idea is to choose a specified submanifold of the state space, called the *Poincaré section* in a transverse direction to the flow. In practice, the Poincaré section can be

generated by choosing a Poincaré plane and when a trajectory crosses that plane, the crossing point is recorded. One of the easiest methods for choosing the plane is to set one of the dynamic variables as a constant. The plane should be chosen so that the trajectories cut the surface transversely so that the trajectories do not run parallel to the surface as they pass through.

As the system evolves in time the trajectory repeatedly intersects the Poincaré section. Plotting the points of intersection X_n creates a lower dimensional portrait of the system behaviour. Successive crossing points are determined by integrating the time evolution equations describing the system. This determines a function $F: X_n \rightarrow X_{n+1}$. A detailed knowledge of the function F can prove to be a useful tool in the study of the dynamic system. In general, we write

$$X_{n+1} = F(X_n) \quad F = (F_1, \dots, F_m) \quad (2.12)$$

Hence the analysis of the nature of the attractor reduces to the analysis of the function F and its derivatives. This technique reduces an m -dimensional problem to a $(m-1)$ -dimensional one and also states an iterative relation rather than a differential one. The section simplifies the geometric description of the dynamics by removing one of the state space dimensions. The point of importance is that this simplified geometry contains much of the essential information about system behaviour. The time interval between the two points is roughly the time to go around the attractor once, which is a relatively big jump in time. As such, the location of successive iterates generated by the trajectories on the section is generally unpredictable. Note that finding such a function F is equivalent to solving the original set of equations and that may be impossible in actual practice.

The technique of Poincaré section is applied to study the stability of limit cycles. The limit cycle crosses the section at intervals approximately equal to the time to go round the cycle once. If the point P on the cycle satisfies $P = F(P)$, then a fixed point in a surface of section say ξ_F , is a point of a map F , where $\xi_F = F(\xi_F)$. The nature of a fixed point is determined by the eigenvalues of Jacobian matrix at ξ_F . An eigenvalue of the Jacobian matrix at a fixed point on the Poincaré section is called a *characteristic multiplier* or a *Floquet multiplier*, M . The stability type of a fixed point of a Poincaré map corresponds to the stability type of the underlying equilibrium point. In state space of 3 or more dimensions M can be less than 0 and so the stability criterion is formulated using the absolute value of the multiplier. Hence with 3 dimensions the Floquet matrix will be of order (2×2) giving two characteristic values M_1 and M_2 . The nature of limit cycle is determined according as:

$$|M_1| < 1, |M_2| < 1 \Rightarrow \text{Node in Poincaré section} \Rightarrow \text{Stable limit cycle.}$$

$$|M_1| > 1, |M_2| > 1 \Rightarrow \text{Repellor in Poincaré section} \Rightarrow \text{Unstable limit cycle.}$$

$$|M_1| < 1, |M_2| > 1 \Rightarrow \text{Saddle in Poincaré section} \Rightarrow \text{Saddle cycle.}$$

It is possible that the characteristic multipliers are complex numbers. In graphic terms, the successive Poincaré intersection points associated with complex valued multipliers rotate around the limit cycle intersection point as they approach or diverge from that point.

2.7 Lyapunov's Theorems of Stability

The stability problem can be investigated by applying the direct method of Lyapunov, which makes use of a continuous scalar function of the state vector

called a Lyapunov function. Lyapunov's theorems on stability and asymptotic stability of the state space describing an autonomous nonlinear dynamical system with state vector $x(t)$ and equilibrium state \bar{x} may be stated as follows.

Theorem I: The equilibrium state \bar{x} is stable if in a small neighbourhood of \bar{x} there exists a positive definite function $V(x)$ such that its derivative with respect to time is negative semi-definite in that region.

Theorem II: The equilibrium state \bar{x} is asymptotically stable if in a small neighbourhood of \bar{x} there exists a positive definite function $V(x)$ such that its derivative with respect to time is negative definite in that region.

A scalar function $V(x)$ that satisfies these requirements is called a Lyapunov function for the equilibrium state \bar{x} . The above theorems require $V(x)$ to be a positive definite function. The function $V(x)$ is positive definite in the state space S if, for all x in S , it satisfies the following requirements:

1. The function $V(x)$ has continuous partial derivatives with respect to the elements of state vector x .
2. $V(\bar{x}) = 0$
3. $V(x) > 0$ if $x \neq \bar{x}$

Given that $V(x)$ is a Lyapunov function, then according to Theorem I, equilibrium state \bar{x} is stable if

$$\frac{dV(x)}{dt} \leq 0 \quad \text{for } x \in U - \bar{x}$$

where U is a small neighbourhood around \bar{x} . Furthermore, according to Theorem II, the equilibrium state \bar{x} is asymptotically stable if

$$\frac{dV(x)}{dt} < 0 \quad \text{for } x \in U - \bar{x}$$

The important point to note is that Lyapunov's theorems can be applied without having to solve the state space equation of the system. But the theorems give no indication of how to find a Lyapunov function; it is often a matter of ingenuity and trial and error in each case. The inability to find a suitable Lyapunov function does not however prove instability of the system; i.e. the existence of a Lyapunov function is sufficient but not necessary for stability. The Lyapunov function provides the mathematical basis for the global stability analysis of nonlinear systems. On the other hand, the analysis

based on the eigen values of the Jacobian matrix $\left(\frac{\partial F_i}{\partial x_j} \right)$ furnishes the basis

for the local stability analysis of the system. The global analysis is more powerful than the local stability analysis; every globally stable system is also locally stable but not vice-versa.

2.8 Chaotic Dynamics

The increased interest in nonlinear systems over the past few decades is also due to the discovery of chaos. One of the basic tenets in science is that given the initial conditions and the equations of motion describing a system, deterministic systems are predictable. However chaotic systems belie this idea by the random behaviour they exhibit despite being described by deterministic equations. The application of chaos for understanding complex

and unpredictable behaviour ranges across the spectrum of scientific disciplines.

While there is no generally accepted definition of chaos, it is defined as the behaviour, which is neither an equilibrium point, nor periodic nor quasiperiodic behaviour. Chaotic trajectories are bounded but they are not periodic nor do they have a uniform distribution characteristic of quasiperiodic solutions. A chaotic spectrum is not composed solely of discrete frequencies but has a continuous broadband structure. The noise like spectrum is a hallmark of chaotic systems. The limit set for chaotic behaviour is not a simple geometrical object like a circle or torus, but is related to fractal structures. Another property of chaotic systems is *sensitive dependence on initial conditions*. Given two different initial conditions arbitrarily close to one another, the trajectories emanating from these points diverge at a rate characteristic of the system until, for all practical purposes they are uncorrelated. Hence, no matter how precisely the initial condition is known the long-term behaviour of a chaotic system can never be predicted. This unpredictability is what is meant when chaotic systems are described as 'deterministic systems that exhibit random behaviour'.

The quantitative analysis of chaotic systems rests on the study of the system attractors in the phase space of the system. Attractors may be classified using the concept of dimension. For instance, an equilibrium point is zero-dimensional; a limit cycle is one-dimensional while a torus is two-dimensional. However chaotic attractors are not generally such simple structures but are quite complex and exhibit a fine structure and usually termed 'strange'. They do not have integer dimensions and there are several ways to generalize dimension to the fractional case of which the capacity, information, correlation and Lyapunov dimensions are the most important. An

elaborate description and comparison of these are provided in later chapter on time series techniques to study complex behaviour in nonlinear systems (Ott, 1993; Schuster, 1988).

2.9 Bifurcations in Dynamical Systems

The characteristic values associated with a singular or fixed point depend on the various parameters used to describe the system. As the parameters change, the nature of the characteristic values and hence the character of the fixed point may change. The term 'bifurcation' refers to any sudden change in the dynamics of the system. When a fixed point changes character with change in the parameter values, the behaviour of trajectories in the neighbourhood of that fixed point will change. The classification and understanding of the various possible bifurcations is an important part of the study of nonlinear dynamics.

Bifurcation theory attempts to provide a systematic classification of the sudden changes in the qualitative behaviour of dynamical systems. This may be divided into two parts. The first part of the theory focuses attention on bifurcations that can be linked to the change in stability of either fixed points or limit cycles. These bifurcations are called 'local' because they can be analyzed in terms of the local behaviour of the system near the relevant fixed point or limit cycle. The other part of the theory, deals with bifurcation events that involve larger scale behaviour in state space and hence are called global bifurcations. For both these types, though bifurcation theory attempts to classify the kinds of bifurcations that can occur for dynamic systems as a function of the dimensionality of the state space. This theory is also concerned with the parameter dependence of the bifurcation. In particular,

the number of parameters that must change to 'cause' a bifurcation is called the co-dimension of the bifurcation.

Local bifurcations are those in which fixed points or limit cycles appear, disappear or change their stability. The change in stability is signaled by a change in the real part of one or more of the characteristic exponents associated with that fixed point. As the real part of the characteristic exponents changes from negative to positive, for example, the motion associated with that characteristic direction goes from being stable to being unstable. For a Poincaré map fixed point, this criterion is equivalent to having the absolute value of the characteristic multiplier equal to unity. The central manifold theorem tells that at a local bifurcation, attention need be paid just to those degrees of freedom associated with the characteristic exponents whose real parts are zero.

In order to classify the types of bifurcation, the dynamic equations are usually reduced to a standard form, the normal form in which the bifurcation event occurs when a parameter value μ reaches zero and a fixed point located at $x=0$ has a characteristic exponent with real part zero. Bifurcations are also classified as subtle or supercritical and catastrophic or subcritical. In a subtle bifurcation, the location of the (stable) fixed point changes smoothly with parameter value near the bifurcation point. The Hopf bifurcation is an example of a subtle bifurcation. For a catastrophic bifurcation, the (stable) fixed point suddenly appears (as in a saddle-node bifurcation) or disappears or jumps discontinuously to a new location.

Global bifurcations involve changes in basins of attraction, homoclinic or heteroclinic orbits or other structures that extend over significant regions of state space. With this brief introduction, we consider an example as applied

to one or two-dimensional cases where bifurcation occurs when one control parameter of the system is changed. Since in the general case, a system may have for fixed parameter values, several attractors, in different parts of state space the overall dynamical system is to be considered to understand what happens to trajectories when a bifurcation occurs (Hilborn, 1994; Ott, 1993).

2.10 Dimension and Entropy Measures

A system attractor could be defined to be n -dimensional if in a neighborhood of every point it looks like an open subset of \mathfrak{R}^n . This is how in differential topology the dimension of a manifold is defined. For instance, a fixed point is of 0 dimension, while a limit cycle while locally looks like an interval is one dimensional and a torus is two dimensional. The neighbourhood of any point of a strange attractor however has a fine structure and does not resemble any Euclidean space. Hence strange attractors are not manifolds and do not have integer dimension. There are several ways to generalize dimension to the fractional case, some of which are listed below.

Capacity dimension: The simplest type of dimensional measure, which is also referred to as Fractal dimension. To compute this measure, the attractor in phase space is covered by a regular grid of volume elements (cubes, spheres etc.) of diameter ε . If the attractor is a D -dimensional manifold, the number of volume elements needed to cover it for small ε is given by, $N(\varepsilon) = k\varepsilon^{-D}$ for some constant k . The definition of capacity dimension is obtained from this by taking the ε -limit.

$$D_0 = \lim_{\varepsilon \rightarrow 0} \frac{\ln N(\varepsilon)}{\ln\left(\frac{1}{\varepsilon}\right)} \quad (2.13)$$

For manifolds, D_0 is equal to the dimension of the manifold and is an integer while for objects that are not manifolds it gives a nonintegral value.

Information dimension: While D_0 is a metric concept and does not utilize the information on the time behaviour of the system, information dimension is a probabilistic measure defined in terms of the relative frequency of visitation of a trajectory. This dimension is defined as,

$$D_1 = \lim_{\varepsilon \rightarrow 0} \frac{\ln \left(- \sum_{i=1}^{N(\varepsilon)} p_i \ln p_i \right)}{\ln \left(\frac{1}{\varepsilon} \right)} \tag{2.14}$$

Here, p_i is the relative frequency at which a typical trajectory enters the i^{th} volume element of the covering. $\left(- \sum_{i=1}^{N(\varepsilon)} p_i \ln p_i \right)$ is the amount of information needed to specify the state of the system to accuracy ε if the state is known to be on the attractor. Hence the name information dimension.

Correlation dimension: Yet another probabilistic measure is the correlation dimension defined as

$$D_2 = \lim_{\varepsilon \rightarrow 0} \frac{\ln \sum_{i=1}^{N(\varepsilon)} p_i^2}{\ln \varepsilon} \tag{2.15}$$

An easy way to estimate this dimension is by determination of the correlation function for N points given by,

$$C(\varepsilon) = \lim_{\varepsilon \rightarrow 0} \frac{1}{N^2} \left\{ \text{the number of pairs } x_i \text{ such that } \|x_i - x_j\| < \varepsilon \right\} \tag{2.16}$$

Hence,

$$D_2 = \lim_{\varepsilon \rightarrow 0} \frac{\ln C(\varepsilon)}{\ln \varepsilon} \quad (2.17)$$

With these different measures defined, the natural question is to find out how these are related to each other. Capacity dimension considers the attractor as a static object completely ignoring that it is subject to a dynamical flow. In practical experiments and simulations the attractor is not directly seen, only the trajectories over a finite period are observed. Hence the probabilistic measures are of greater use in practical settings than the capacity dimension. In general, $D_2 \leq D_1 \leq D_0$ since D_2 and D_1 being probabilistic in nature depend on the relative frequency at which each volume element is visited and hence will be equal to D_0 only when these frequencies are all equal.

The dynamical characteristics of the system are studied using the measures of entropy. These measures, which help in understanding how the trajectories evolve in time, are specific of dynamical systems while dimensions can be defined for any fractal measure or point set. In introducing this concept it will be useful to recall the information dimension measure described above. Entropy estimates the average information gained by observing a system's state to a precision ε . In the case of a fixed point or periodic orbit each orbit remains the same in time and thus no new information is gained by observing additional orbits. Or in other words, the uncertainty in the system is almost nil. Thus it becomes easy to predict the outcome of the system under such an evolution. However for a chaotic system, each new orbit contributes to information gain. Hence prediction of the next orbit without observing it becomes very difficult. Such a system is 'creating' information and a suitable measure of the amount of information produced or gained is required.

The Kolmogorov Sinai entropy is such a measure that quantifies the amount of information gained on an average by observing a portion of the system's evolution. It measures the degree of 'chaoticness' of the system and is a long time average rate of information gain of the system. It is inversely proportional to the time interval over which the state of the system can be predicted, given the initial conditions to a precision ε as well as the evolution equations. In order to define this measure, let us consider partitioning the attractor as before into $N(\varepsilon)$ boxes s_1, s_2, \dots, s_N with size ε . If m measurements at regular time intervals are made, these will yield a sequence of boxes visited by the trajectory. Let $P(s_1, s_2, \dots, s_m)$ be the joint probability of finding the trajectory at time τ in box s_1 , at time 2τ in box s_2 and so on. The KS entropy is defined as,

$$K = - \lim_{\tau \rightarrow 0} \lim_{\varepsilon \rightarrow 0} \lim_{m \rightarrow \infty} \times \left[\frac{1}{m\tau} \sum_{s_1 \dots s_m} P(s_1 \dots s_m) \times \ln P(s_1 \dots s_m) \right] \quad (2.18)$$

If K approaches 0, or there is no change in information this means the system is fully predictable. In contrast for a stochastic process, K approaches infinity and it attains in between values depending on the irregular nature for chaotic systems.

The entropies can be generalized to a set of order q Rényi entropies, which are the dynamical counterparts of Rényi dimensions. These are defined as,

$$K_q = - \lim_{\tau \rightarrow 0} \lim_{\varepsilon \rightarrow 0} \lim_{m \rightarrow \infty} \times \left[\frac{1}{m\tau} \frac{1}{q-1} \ln \sum_{s_1 \dots s_m} p^q(s_1 \dots s_m) \right] \quad (2.19)$$

The K entropy in Eq. (2.18) for which $q=2$ in Eq. (2.19) is however the easiest to compute among all the entropies.

2.11 Lyapunov Exponents

The exponential divergence of nearby trajectories is calculated by the *Lyapunov exponent*. It is a measure of the rate of attraction or repulsion. If two nearby trajectories on a chaotic attractor start off with a separation d_0 at time $t = 0$, then the trajectories diverge so that their separation at time t , denoted by $d(t)$ satisfies the expression

$$d(t) = d_0 e^{\lambda t} \quad (2.20)$$

where λ is called the *Lyapunov exponent* for the trajectories.

The Lyapunov exponents provide a coordinate-independent measure of the asymptotic local stability of properties of a trajectory. In a geometric representation, we can imagine a small infinitesimal ball of radius $\varepsilon(0)$ centered on a point $\Phi(0)$ in state space. Under the action of the dynamics the centre of the ball may move, and the ball become distorted. Since the ball is infinitesimal, this distortion is governed by the linear part of the flow. The ball thus remains an ellipsoid. Suppose the principal axes of the ellipsoid at time t are of length $\varepsilon_i(t)$. The spectrum of Lyapunov exponents for the trajectory $\Phi(t)$ is defined as

$$\lambda_i = \lim_{t \rightarrow \infty} \lim_{\varepsilon(0) \rightarrow 0} \frac{1}{t} \log \frac{\varepsilon_i(t)}{\varepsilon(0)} \quad (2.21)$$

The Lyapunov exponents depend on the trajectory $\Phi(t)$. Their values are the same for any state on the same trajectory, but may be different for states on different trajectories. Lyapunov exponents are convenient for

categorizing steady state behaviour. The trajectories of an n -dimensional state space have n Lyapunov exponents. This is often called the *Lyapunov spectrum* and it is conventional to order them according to size. The qualitative features of the asymptotic local stability properties can be summarized by the sign of each Lyapunov exponent; a positive Lyapunov exponent indicating an unstable direction, and a negative exponent indicating a stable direction. If the exponent is positive then the trajectories diverge and the system is chaotic. However, for an attractor, contraction must outweigh expansion and so,

$$\sum_{i=1}^m \lambda_i < 0 \tag{2.22}$$

The geometrical meaning of positive Lyapunov exponents is that there exist directions in which the motion on average is unstable such that nearby trajectories in these directions will diverge from the original orbit. Although the orbit is unstable, its stable directions provide sufficient volume contraction so that the orbit is confined to some bounded region in state space. At least one Lyapunov exponent must be zero for any limit set other than an equilibrium point. To produce a strange attractor the system must be dissipative and hence must have at least one negative Lyapunov exponent. Furthermore, at least one Lyapunov exponent must be zero for any limit set other than an equilibrium point. Also for a chaotic system, at least one Lyapunov exponent must be positive. It follows that a strange attractor must have at least three Lyapunov exponents. Hence, chaos can only occur in third-order autonomous, second-order non-autonomous or higher order continuous time systems.

In four dimensional systems a new type of behaviour can occur known as *hyperchaos* characterized by two positive Lyapunov exponents. There exist relations between the Lyapunov exponents and the dimensional estimates. The information dimension, σ and the positive exponents are related by the Kaplan –Yorke conjecture as,

$$\sigma \leq d_{KY} = j + \frac{\sum_{i=1}^j \lambda_i}{-\lambda_{j+1}} \quad (2.23)$$

where the Lyapunov exponents are assumed to be ordered as $\lambda_1, \lambda_2, \dots, \lambda_N$ and j is the largest integer such that $\lambda_1 > \lambda_2 > \dots > \lambda_j > 0$. The term d_{KY} is sometimes referred to as the Lyapunov Dimension. In terms of the metric entropy on the other hand, Pesin's theorem states that under certain preconditions the sum of the positive exponents is equal to the metric entropy K_1 .

2.12 Stochastic Resonance

Over the last two decades, the phenomenon of stochastic resonance (SR) has continuously attracted considerable attention from the scientific community. The term is given to a strange occurrence that is manifest in nonlinear systems whereby generally feeble input information (such as a weak signal) can be amplified and optimized by the assistance of noise. The phenomenon occurs provided there are three key factors: (i) an energetic activation barrier or, more generally, a form of threshold, (ii) a weak coherent input (such as a periodic signal) and (iii) a source of noise that is inherent in the system, or that adds to the coherent input. It is observed that given these features, the response of the system undergoes resonance-like behavior as a function of

the noise level; hence the name stochastic resonance. The underlying mechanism is fairly simple and robust. As a consequence, stochastic resonance has been observed in a large variety of systems, including bistable ring lasers, semiconductor devices, chemical reactions, and mechanoreceptor cells in the tail fan of a crayfish (Gammaitoni et. al., 1998). In many neural systems, SR has been observed eg., in ion channels (Petracchi et. al., 1994), in neurons (Longtin, et. al., 1991), in animal behavior (Russell et. al., 1999) and eventually in human perception using electroencephalography (Mori & Kai, 2002). Various applications of this phenomenon are being explored, in particular the possibility that stochastic resonance might help enable biological cells to respond to weak 50–60-Hz electromagnetic fields, far below the thermal noise level.

Usually SR is characterized by the existence of a maximum in the signal-to-noise ratio (SNR) vs. noise intensity relation. Another measure for the SR, the amplification, is introduced as a ratio of the magnitudes of ensemble averaged response and the input signal. An alternative is the residence-time probability distribution introduced in yielding a bona-fide resonance of the forced system. In nonlinear regimes, where the amplitude of the signal is sufficiently strong, synchronization-like phenomena can be observed. In such regimes the SNR possesses two maxima: the first maximum corresponds to the strong synchronization between hopping events and periodic force while the second one refers to a decrease of the noise background.

Several recent studies have shown that the higher central nervous system can actually utilize the noise enhanced sensory information; it enhances the human tactile sensation, the human visual perception, or the animal feeding behavior. Whether these functional improvements would be

caused by the enhanced sensory afferents at the receptor level or by the effects of noise in the central nervous system is, however, still unknown (Hidaka et. al., 2000).

2.13 Conclusion

This chapter reviews only a few salient features of the theory of nonlinear oscillations. The newly developed realm of chaotic dynamics, which is being extensively investigated in various fields, has been given some prominence over the other topics. The application of the theoretical aspects in studying the real or simulated data however is a different story altogether, which requires the modification and conversion of the ideas into algorithms that will translate the idea to a computing machine on which the analysis is carried out. The following chapter will present an in-depth view of the techniques that are made use of in applying these theoretical precepts to the time series data that contains all the information regarding the underlying system in a quest to decipher its dynamics.

Current Techniques in Time Series Analysis } *An Overview*

The scientific method is nothing but the normal working of the human mind.

--- Thomas Huxley

The presence of complex data generated in many real life systems posed a puzzling problem to scientists when all known linear methods failed to tame these. The situation was all the more worse since this led to the erroneous classification of such data as 'noisy' totally stochastic in nature without any structure in phase space. However the theory of nonlinear dynamics was applied successfully for the analysis of such random looking observed data. The techniques developed and the algorithms with their relative merits and disadvantages are reviewed here. The second section is concentrated on the description of the EEG signal as a nonlinear scalar time series and the relevant studies carried out which are of import to the aims of this thesis.

Part I: Time Series Analysis of Complex Systems

3.1 Dynamical Systems and Signals

One of the earliest assumptions made in the analysis of signals from physical systems is that a dynamical system in the form of a differential equation or a discrete time evolution rule is responsible for the observations. For continuous time dynamics there is a set of f differential equations for variables $\mathbf{u}(t)=[u_1(t), u_2(t), \dots, u_f(t)]$,

$$\frac{d\mathbf{u}(t)}{dt} = \mathbf{G}(\mathbf{u}(t)) \quad (3.1)$$

where the vector field $\mathbf{G}(\mathbf{u})$ is always taken to be continuous in its variables and also taken to be differentiable as often as needed. When time is discrete, which is the realistic situation when observations are only sampled every τ_s , the evolution is given by a map from vectors in \mathfrak{R}^f to other vectors in \mathfrak{R}^f :

$$\mathbf{u}(n) = \mathbf{u}(t_0 + n\tau_s)$$

$$\mathbf{u}(n+1) = \mathbf{F}(\mathbf{u}(n)) \quad (3.2)$$

The continuous and discrete time views of the dynamics can be connected by approximating the time derivative as,

$$\frac{d\mathbf{u}(t)}{dt} \approx \frac{\mathbf{u}(t_0 + (n+1)\tau_s) - \mathbf{u}(t_0 + n\tau_s)}{\tau_s} \quad (3.3)$$

leading to,

$$\mathbf{F}(\mathbf{u}(n)) = \mathbf{u}(n) + \tau_s \mathbf{G}(\mathbf{u}(n)) \quad (3.4)$$

The vector field $\mathbf{F}(\mathbf{u})$ has parameters that reflect the external settings of forces, frequencies, boundary conditions and physical properties of the system. The dynamical system Eq. (3.2) is generally not volume preserving in f -dimensional space. In evolving from a volume of points $d^f(\mathbf{u}(n))$ to the

volume of points $d^{f+1}(\mathbf{u}(n))$ the volume changes by the determinant of the Jacobian,

$$DF(\mathbf{u}) = \det \left[\frac{\partial F(\mathbf{u})}{\partial \mathbf{u}} \right] \quad (3.5)$$

When this Jacobian is unity, it is usually associated with Hamiltonian evolution in a physical setting and the phase space volume remains constant under the evolution of the system. Generally the Jacobian has a determinant less than unity, which means the volumes in phase space shrink as the system evolves. The physical origin of this volume contraction is dissipation in the system.

3.2 Linear Methods of Signal Analysis

Linear methods interpret all regular structure in a data set such as the dominant frequency and so on. This implies that linear dynamics governs the intrinsic evolution of the system in which small causes lead to small effects. In such a domain, equations of motion can only lead to exponentially growing or periodically oscillating solutions and hence any irregular behaviour of the system is automatically attributed to some random external input to the system. Hence, the simplest system that produces non-periodic signals is a *linear stochastic process*. Hence, a measurement s_n of the state made at a time instant n may be considered to arise from an underlying probability distribution for observing a sequence of values. Linear statistical processing of such a signal derives 'estimates' of meaningful values distinctive of the system based on these measurements. For instance, the mean may be

estimated as $\langle \hat{s} \rangle = \frac{1}{N} \sum_{n=1}^N s_n$ where $\langle \cdot \rangle$ is a time average and N the total

number of measurements in the time series. Based on the underlying

distribution, the mean is $\langle s \rangle_n = \int_{-\infty}^{\infty} ds' s' p(s')$ where $p(s)$ is the probability distribution. Similarly, the variance, the autocorrelation function that gives information about the time ordering of elements etc. may be estimated from the signal.

Instead of describing the statistical properties of a signal in real space, the signal can be represented in its Fourier space. The Fourier transform establishes a one-to-one correspondence between the signals at certain times (time domain) and how certain frequencies contribute to the signal and how the phases of the oscillations are related to the phases of other oscillations (frequency domain). Let s_n , $n=1,2,3,\dots,N$ denote the discrete dataset measured at times $t_n = n\Delta t$ where Δt is the sampling time and is assumed to be uniform. The reciprocals of t_n represent the frequencies and the Nyquist critical frequency $\nu_c = 1/2\Delta t$ plays a pivotal role. If the frequency content of the signal $s(t)$ is limited to frequencies below ν_c , then a result known as the sampling theorem guarantees that the entire information content of $s(t)$ is captured by the finite set of sampled values $\{s_n\}$.

The Fourier transform of a function $s(t)$ is given by

$\tilde{s}(f) = \frac{1}{\sqrt{2\pi}} \int_{-\infty}^{\infty} s(t) e^{i2\pi ft} dt$ and in case of a finite discrete time series by

$\tilde{s}_k = \frac{1}{\sqrt{N}} \sum_{n=1}^N s_n e^{i2\pi kn/N}$. The frequencies are $f_k = \frac{k}{N \Delta t}$ where $k = -N/2, \dots, N/2$

and Δt is the sampling interval. The inverse transformation amounts only to a change in sign and an exchange of f (or respectively t) and t (or respectively n). Both operations are then invertible and are linear. Another useful representation in the frequency domain is using the Power spectrum, which is

the squared modulus of the continuous Fourier transform. It is represented as, $S^{(s)}(f) = |\tilde{s}(f)|^2$.

The Wiener-Khinchin theorem is an important relation, which states that the power spectrum and the auto correlation function are Fourier transforms of each other. The power spectrum is particularly useful for studying the oscillations in the system. There will be sharper or boarder peaks at the dominant frequencies and at their harmonics. Purely periodic or quasi-periodic signals show sharp spectral lines, measurement noise adds a continuous floor to the spectrum. The signal and noise may thus be differentiated. However, the confusion arises in the case of deterministic chaotic signals, which may also have sharp spectral lines, but even in the absence of noise, there will be a continuous part of the spectrum. This is an immediate consequence of the exponentially decaying auto correlation function and without additional information it is impossible to infer from the spectrum whether the continuous part is due to noise superposed on a quasi-periodic signal or to chaoticity. However, its discrete counterpart is not a very suitable quantity for two reasons. Firstly, the finite frequency resolution of the discrete Fourier transforms leads to leakage into adjacent frequency bins. Secondly, its statistical fluctuations are of the same order as $S^{(s)}(f)$ itself. These drawbacks can be remedied either by averaging over adjacent frequency bins or more efficiently by averaging over running windows in the time domain. The inadequacy of such a linear approach to the analysis of observed data from natural systems as well as known chaotic systems prompted the development and growth of alternative methods that came to be grouped under the umbrella of nonlinear time series techniques based on the principles of nonlinear dynamics and deterministic chaos (Kantz & Schreiber, 1997).

3.3 Nonlinear Time Series Analysis

Actual observations of irregular evolution that are observed in complex systems are typically measurement of a single scalar observable at a fixed spatial point. Let this be denoted by $s(t_0 + n\tau_s) \equiv s(n)$ where t_0 is some initial time and τ_s is the sampling time of the instrument used in the experiment. n is an integer and $n\tau_s$ is the instant at which the measurement is effected. In some cases the full structure lies in the observation of a field of quantities

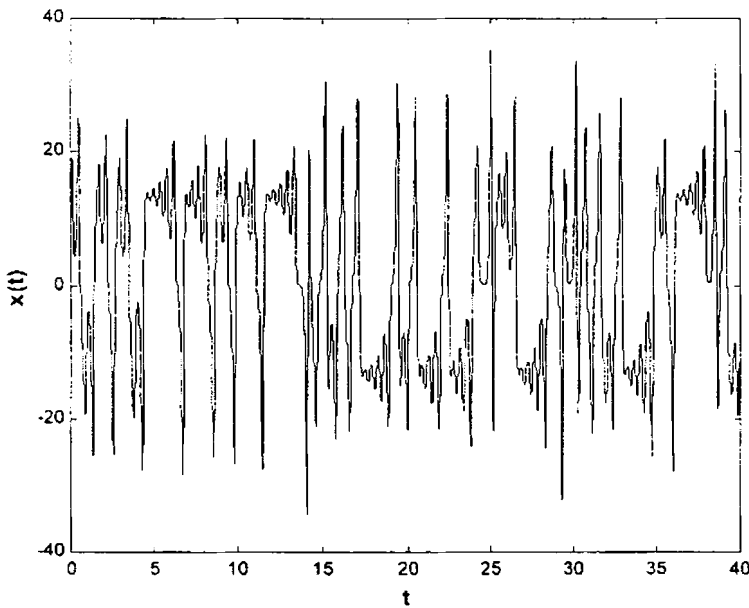


Figure 3.1. Chaotic time series $x(t)$ simulated from the Lorenz system (Lorenz, 1963) using parameter $r=45.92$, $b=4.0$, $\sigma=16.0$

namely $s(\mathbf{x}, t_0 + n\tau_s)$ where $\mathbf{x} = (x, y, z)$ are the spatial coordinates. Consider for example the simulated data from the chaotic Lorenz attractor represented as a time series as in figure 3.1. If this data were observed without knowledge about the underlying system it would merely represent some

variable recorded in equal intervals of time. Hence assuming a linear structure as a first approximation, linear concepts will be applied and in case of their failure; the nonlinear techniques will be resorted to, based on which the system attractor will be reconstructed and characterized. The power spectrum applied to the above data is shown in figure 3.2 and it is evident that the broadband spectrum clearly states the inefficacy of linear methods in analyzing such data.

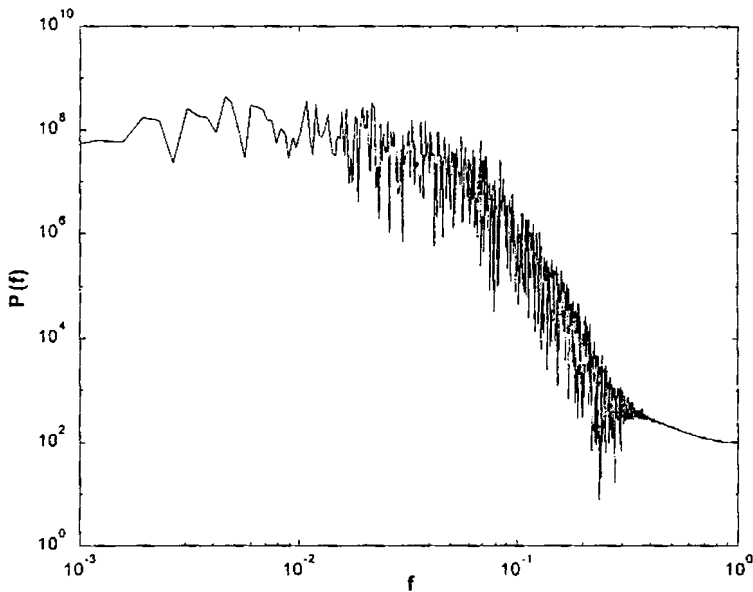


Figure 3.2. *The power spectrum of the $x(t)$ time series generated from the Lorenz equations with the parameters as before.*

As this discussion progresses the actual steps involved in nonlinear signal processing will be introduced leading to better understanding of the analysis of complex data. The tasks encountered in analysis of signals observed from

linear or nonlinear systems are much the same; though the methods followed are substantially different. These are briefly sketched in the sequel.

(a) **Signal separation:** The very first job is to identify the signal of interest in an observation that is possibly contaminated by the environment, by perturbations on the source or by properties¹ of the measuring instrument. In order to carry out the processing, we must establish some difference between the information bearing signal and the interference. In the case of a narrow band signal in a broadband environment, the difference is clear and the Fourier space is the right domain in which to perform the separation. In the case of chaotic signals both the signal and the background are typically broadband and Fourier analysis will not be of much assistance in making the separation. The methods followed in such cases rest on the idea that the signal of interest is chaotic in nature with specific geometric structure in its phase space. In the nonlinear signal separation, three cases may be distinguished:

- ❖ **Known dynamics:** The evolution equations $\mathbf{u}(n+1) = F(\mathbf{u}(n))$ are known and this knowledge can be used to extract the signal satisfying the dynamics from the contaminating signals.
- ❖ **Knowledge of the signal from the system:** This occurs when some signal has been measured from the system of interest at some earlier time and is known to be representative of the system. The earlier signal can be considered as a reference to establish the statistics of evolution on the attractor² and this can be subsequently used for separating the signal from the contaminant.

- ❖ Nothing is known: In this case only a single instance of measuring a signal from the physical source is known. Then the analyst is 'flying blind' and must make models of the signal to establish what part of the observations are deterministic in low dimensional phase space and what part a result of processes in high dimensional state space and thus to be discarded. Though this scenario is more problematic than the other two; it is more often the *realistic* situation.

(b) **Finding the space:** Once the signal is found; the next step is to establish the correct space in which to view the signal. If the source of the signal is a linear physical process, then the natural space in which to view it is the Fourier space. In the case of a nonlinear source, Fourier transformation of the scalar measurements does not lead to any simplification since the processes that give rise to chaotic behaviour are fundamentally multivariate. So the phase space of the system is to be reconstructed as well as possible using the information in $s(n)$. The choice of the vectors of say d -dimension that go into forming this space and how the dimension, d is determined itself become central topics. The answer lies in a combination of dynamical ideas about nonlinear systems and geometrical ideas about how an attractor unfolds using coordinates established on the basis of their information-theoretic content.

(c) **Classification and identification:** With a clean signal and proper phase space in which to work, the next logical step is to understand the physical source of the signal. In the case of linear systems, Fourier analysis leads to characteristic frequencies usually called the resonant frequencies.

These are *invariants* of the dynamics and can be used to classify the physics. Nonlinear systems on the other hand, do not have useful spectral content when operating in a chaotic regime but there are other invariants that are specific in classifying and identifying these sources. These are quantities that are unchanged under various operations on the dynamics or the orbit as well as under small variations in the initial conditions. Some of the invariants are unperturbed under the operation of the dynamics $\mathbf{x} \rightarrow \mathbf{F}(\mathbf{x})$. This ensures that they are unperturbed by initial conditions which is definitely untrue for individual orbits. Some of the invariants are further unchanged under any smooth change of coordinates used to describe the evolution and some, the topological invariants are purely geometric properties of the vector field describing the dynamics. Among these are the various fractal dimensions and the Lyapunov exponents. These latter ones also establish the unpredictability of the nonlinear source. The chaotic motion of a physical system is not unpredictable even with all the instabilities encountered in traversing phase space. The limited predictability of chaos is quantified by the local and global Lyapunov exponents, which can be determined from the measurements themselves. So in one sense chaotic systems allow themselves to be classified and to have their intrinsic predictability established at the same time. Topological invariants together with metric invariants or the other fractal dimensions together provide sufficient discrimination power to allow for the practical separation of observed systems. System identification in nonlinear chaotic systems means establishing a set of invariants and then comparing the observations to a library of invariants of known systems. It may be pointed out that the

invariants mentioned need not form a complete set. They may just be the currently known ones.

- (d) **Modeling:** When all the analysis of the source of measurements has been done, the problem of building of models of physical processes acting at the source may be addressed. Local and global models of how the system evolves in the reconstructed space may be built by working within the coordinate system established by analyzing the signal. In linear systems, the task is relatively easy. The observations $s(n)$ must somehow be linearly related to observations at earlier times and to the driving forces at earlier times. This leads to models of the form:

$$s(n) = \sum_{k=1}^N a_k s(n-k) + \sum_{l=1}^L b_l g(n-l) \quad (3.6)$$

where $\{a_k\}$ and $\{b_l\}$ are to be determined by fits to the data typically using least squares or information-theoretic criterion and $g(n)$ are some deterministic or stochastic forcing terms. Once the coefficients are established, the model equation is used for prediction or as part of a control scheme. From the point of view of dynamical systems, this kind of model consists of simple linear dynamics – the terms involving $\{a_k\}$ - and simple linear averaging over the forcing. The first part of the modeling, which involves the dynamics, is often called autoregressive (AR) and the second the moving average (MA) and the combination is labeled ARMA modeling. This kind of model will always have 0 or negative Lyapunov exponent, zero Kolmogorov-Sinai entropy and will never be chaotic.

Nonlinear modeling of chaotic processes revolves around the idea of a compact geometric attractor on which the observations evolve. Since the

orbit is continually folded back on itself by the dissipative forces of the nonlinear part of the dynamics, we expect to find in the neighbourhood of any orbit point $\mathbf{y}^{(r)}(n)$, $r=1, 2, \dots, N_B$ (r are the number of points) which arrive in the neighbourhood of $\mathbf{y}(n)$ at quite other times than n . Various forms of interpolation function can then be built which account for whole neighbourhoods of phase space and how they evolve from near $\mathbf{y}(n)$ to the whole set of points near $\mathbf{y}(n+1)$. The use of phase space representation in the modeling of the temporal evolution of the physical process is the key innovation in modeling chaotic processes. The implementation of this idea is to build parametrized nonlinear functions $F(\mathbf{x}, \mathbf{a})$ which take $\mathbf{y}(n)$ into $\mathbf{y}(n+1) = F(\mathbf{y}(n), \mathbf{a})$ and then use various criteria to determine \mathbf{a} . Further since one has the notion of local neighbourhoods, one can build up the model of the process neighbourhood by neighbourhood and by piecing together these local models, produce a global nonlinear model that captures much of the structure of the attractor itself. More on modeling relevant to the system under study will be dealt within a later chapter.

- (e) **Signal synthesis:** While the analysis of nonlinear signals is the central theme of interest, another direction being followed is the synthesis of new signals using chaotic models. This mainly concerns engineering problems such as utilization of the signals for communication between distant locations or synchronization of activities at these locations and so on (Abarbanel et. al., 1993; Ott, 1993).

Techniques in nonlinear time series analysis of signals

We shall now describe in detail the techniques employed for handling each of the tasks stated above in signal analysis. This will review the existing methods, their relative merits, demerits and modifications that are incorporated in an attempt to make sense of the information rich though apparently random signal.

3.4 Reconstruction of Phase Space

The key theoretical tool used for quantifying chaos is the notion of a time series of data for the system. As previously stated the actual observations, $s(n)$ are measurements of a single scalar variable at a fixed point. We may denote the signal $s(n)$ as $s(t_0 + n\tau_s)$ where t_0 is the initial time and τ_s the sampling time of the measurements. $s(n)$ could be for eg. a voltage or current in a nonlinear circuit or a density or velocity in a fluid dynamics experiment. It is not obvious that such a set of sampled values of just one variable should be sufficient to capture the features that are needed to describe regarding the system. However it has been shown that if the sampling is carried out at appropriate time intervals, then the phase space can be 'reconstructed' and the essential features of the dynamics can be derived from the time series data.

From the discussion of dynamical systems, it is seen that to establish values for the time derivatives of the measured variable, $s(n)$, we can consider

$$\dot{s}(n) = \left. \frac{ds(t)}{dt} \right|_{t=t_0+n\tau_s} \quad (3.7)$$

Since measurements are made only every τ_s , the approximation to this derivative is,

$$\dot{s}(n) \approx \frac{s(t_0 + (n+1)\tau_s) - s(t_0 + n\tau_s)}{\tau_s} \quad (3.8)$$

With finite τ_s , this is a crude high pass filter for the data and we are producing a poor representation of the time derivative. As we go on to higher order derivatives even poorer representations will be made. However an examination of the formula for the derivative, points out that at each step we are adding to the information already contained in the measurement $s(n)$ at other times lagged by multiples of the observation time step τ_s . Around 1980, two groups - one at the University of California, Packard et. al. (1980) and David Ruelle (1989) - apparently simultaneously and independently introduced the idea of using such *time delay coordinates* to reconstruct the phase space of dynamical systems. This was a generalization of the process first suggested by Poincaré to obtain dynamics from observed data. The main idea is that the derivatives are really not needed to form a coordinate system to capture the structure of orbits in phase space but that lagged coordinates of the form

$$s(n+T) \equiv s(t_0 + (n+T)\tau_s)$$

where T is some integer are sufficient for reconstruction of phase space. Then using various time lags to create a collection of vectors in d dimensions,

$$\mathbf{y}(n) = [s(n), s(n+T), s(n+2T), \dots, s(n+(d-1)T)] \quad (3.9)$$

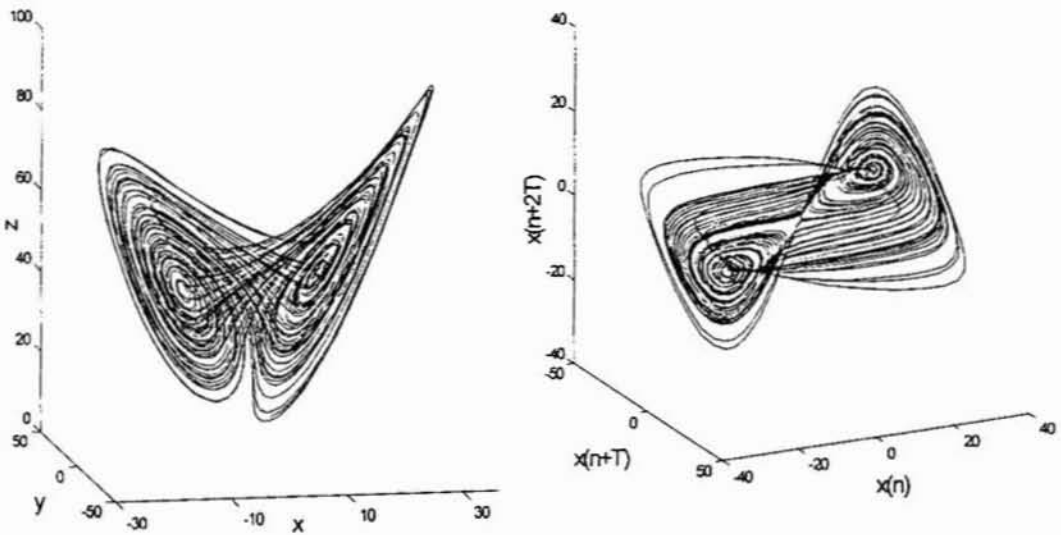


Figure 3.3. The Lorenz attractor in (a) Original phase space (b) reconstructed in time delay coordinates

the required coordinates have been provided. These time lags are used to transform the original time series into a set of vectors in a space of dimension d , which is known as the *Embedding space*. In a nonlinear system, $s(n+jT)$ are some (unknown) nonlinear combination of the actual physical variables that comprise the source of measurements. While the relationship between the physical variables $\mathbf{u}(n)$ and the $s(n+jT)$ is not known, for purposes of creating a phase space, it is not of much significance. This is because any smooth nonlinear change of variables acts as a coordinate basis for the dynamics. The theorems that paved way for such phase space reconstructions are Whitney's and Takens's embedding theorems which are described briefly

below. Figure 3.3 shows the original and reconstructed attractors of the Lorenz system.

3.4.1 Embedding Theorems

A scalar measurement is a projection of the unobserved internal variables of the system onto a real axis. Such a projected, highly distorted data is sufficient to reconstruct a new space of integer dimension in which one can obtain an equivalent projection of the original attractor. This means that the time evolution of a trajectory on the reconstructed space should depend on its current position in the new space and nothing else. Also the Lyapunov exponents, dimensions etc. are invariant only under smooth, nonsingular transformations. Hence to guarantee that the quantities computed for the reconstructed attractor are identical to those in the original state space, we require that the structure of the tangent space i.e. the linearisation of the dynamics at any point in state space is preserved by the reconstruction process. Thus an embedding of a compact smooth manifold \mathcal{A} into \mathbb{R}^d is defined to be a map F which is one-to-one immersion on \mathcal{A} i.e. a one-to-one C^1 map with a Jacobian $DF(x)$ which has full rank everywhere. The crucial point is to show under what conditions the projections due to the scalar measurements and the subsequent reconstruction by delay vectors form an embedding.

The problem with the embedding of scalar data in some \mathbb{R}^m has two aspects. First if the state of a system is uniquely characterized only if D variables are simultaneously specified, then d independent variables ($d \geq D$) are to be constructed from the scalar time series data. Once the variables are known it is also known that the dynamics lives in some D -dimensional manifold. Very often than not, D need not be an integer thereby giving the class of attractors called Strange attractors. Attractors with integral D are

known as regular attractors. Unfortunately this manifold will most probably be curved. The second problem is that since a global representation is needed, one has to find an embedding space for a curved manifold in a Cartesian framework.

The second part of this problem was solved by Whitney in 1936 (Whitney, 1936). He proved that every D - dimensional smooth manifold could be embedded in \mathfrak{R}^{2D+1} and that the set of maps forming an embedding is a dense and open set in the space of C^1 maps. This theory was stated simply based on the idea of a description of a manifold in some local coordinates and the theorem showed that one could embed it globally in \mathfrak{R}^{2D+1} . A generic embedding of a D -dimensional curved manifold in a D -dimensional space will overlap itself in on a set of non-zero measure. If the embedding is done in a space of dimension $(D+1)$ the self-intersection will lie in a subspace of dimension $(D-1)$ and so on such that finally it will be point like in 2D dimensions and in $(2D+1)$ dimensions it will disappear. However since Whitney's theorem is proved only for integer D , it is not of much practical use.

Since the attractor \mathcal{A} is a subset of the state space of the system; this guarantees that the mapping F of the state vector at a certain time to its position at the next instant a sampling interval later is unique. This is of considerable importance in time delay embedding. Since the dynamics can be interpreted as a unique mapping from \mathcal{A} to \mathcal{A} , a time delay embedding is again a time independent map from \mathcal{A} to \mathfrak{R}^d where d is the dimension in which embedding is carried out. Let \mathbf{x}_n be the state vector at time n , s the measurement function and F the map representing the dynamics,

$$\mathbf{x}_{n+1} = F(\mathbf{x}_n)$$

A delay vector is then $(s(\mathbf{x}_n), s(\mathbf{F}(\mathbf{x}_n)), s(\mathbf{F}(\mathbf{F}(\mathbf{x}_n))), \dots)$. Hence it is clear that knowledge of $s(x_{n_i})$ at successive n_i is equivalent to knowing a set of different coordinates at a single moment *if* the map \mathbf{F} couples the different degrees of freedom such that the components of the delay vectors are mutually independent.

Hence the delay reconstruction of only one variable is a peculiar map from \mathcal{A} to \mathfrak{R}^d . Since it mixes dynamics and geometry, the words 'almost every C^1 map' in the generalized Whitney's theorem do not say that every delay map is an embedding. Takens could prove in the time delay embedding theorem (1981) that it is a generic property that a delay map of dimension $d=2D+1$ is an embedding of a compact manifold if the measurement function $s: \mathcal{A} \rightarrow \mathfrak{R}^m$ is C^2 and if either the dynamics or the measurement function is generic in the sense that it couples all degrees of freedom. Sauer et. al. (1991) generalized the theorem calling it the Fractal Delay Embedding Prevalence theorem. Again let D_f be the fractal dimension of the attractor. Then for almost every smooth measurement functions and sampling time, $\tau_s > 0$ the delay map into \mathfrak{R}^d with $d > 2D_f$ is an embedding if there are no periodic orbits of the systems with period τ_s or $2\tau_s$ and only a finite number of periodic orbits with period $p\tau_s$, $p > 2$.

Thus the main result of the embedding theorems is that it is not the dimension D of the underlying state space that is important for the minimal dimension but the fractal dimension D_f of the invariant measure generated by the dynamics in the true state space.

3.5 Choice of Embedding Dimension

The goal of the reconstruction theorem is to provide a Euclidean space \mathfrak{R}^d large enough so that the set of points on the attractor can be unfolded

without ambiguity. If two points of the set lie close to each other in some dimension d they should do so because it is a property of the set of points and not of the small value of d in which the set is viewed. When all the ambiguities in the unfolding of the attractor are resolved, the space \mathfrak{R}^d provides an embedding of the attractor. While the embedding dimension provides a *sufficient* condition from geometrical considerations alone for choosing a dimension large enough i.e. $d_E > 2d_A$ where d_A is the dimension of the attractor; it is not always necessary. For instance in the case of the Lorenz attractor, $d_A = 2.06$ and from the embedding theorem, $d_E \sim 5$. But it is known that the Lorenz attractor is well reconstructed in a space of dimension 3. Hence while working in a dimension that is sufficient to unfold the attractor but greater than necessary; two problems may arise. Firstly, the computational cost while extracting information about the data from \mathfrak{R}^d increases exponentially with d . Also, in the presence of 'noise' or other high-dimensional contamination of the observations, the 'extra' dimensions are not populated by dynamics already captured by a smaller dimension but entirely by the contaminating signal. These realizations have motivated the search for analysis that will identify a 'necessary' embedding dimension from the data itself. Some of these methods are described briefly here.

(a) **Singular value analysis:** If the measurements $\mathbf{y}(n)$ are composed of the signal from the system under study as well as some contamination from other systems, then in the absence of specific information about the contamination, it may be assumed to be rather high dimensional and that it fills more or less uniformly any few dimensional space chosen for consideration. Let the necessary dimension required to unfold the dynamics be denoted as d_N . If we choose $d_E > d_N$, then in a heuristic sense ($d_E - d_N$)

dimensions of space are populated by the contamination alone. This, however is possible if the contamination and signal are additive and this nature is retained for the entire duration. The nonlinearity in the system may interact with noise and result in strange phenomena such as stochastic resonance in which case the additive nature completely breaks down. Under the assumption of the signal and contamination being additive, the sample covariance matrix of the observations $\mathbf{y}(n)$ given by

$$COV = \frac{1}{N} \sum_{n=1}^N [\mathbf{y}(n) - \bar{\mathbf{y}}]^T [\mathbf{y}(n) - \bar{\mathbf{y}}] \quad (3.10)$$

will again in a heuristic sense have d_N eigenvalues arising from the variation of the real signal about its mean and $(d_E - d_N)$ eigenvalues which represent the 'noise'. If the contamination is high enough, the extra dimensions may be thought of as being filled uniformly by noise and so the $(d_E - d_N)$ eigenvalues representing the power in these extra dimensions will be nearly equal. Hence by examining the singular values of the covariance matrix a 'noise floor' at which the eigenvalue spectrum turns over and becomes flat (Broomhead & King, 1986) can be identified. From the d_E eigenvalues the one at which the floor is reached may be chosen as d_N . This method though easy to implement is sometimes hard to interpret. It gives a hint as to the active number of degrees of freedom but it can be misleading because it does not distinguish two processes with nearly the same Fourier spectrum (Fraser & Swinney, 1989) or sometimes different noise floors are reached at different numerical levels by computers.

(b) **Saturation of system invariants:** In the case of an attractor properly unfolded by choosing a large enough d_E , any property depending on the distances between points in the phase space becomes independent of the value of the embedding dimension. Thus in principle, the appropriate

necessary embedding dimension d_N can be established by computing such a property for $d_E = 1, 2, \dots$ until no variation with d_E occurs. One of the quantities made use of in such cases is the generalized correlation sum, $C_q(R)$. This quantity will be discussed in detail in a later section. $C_q(R)$ is evaluated as a function of the embedding dimension d_E and determine when the slope of its logarithm as a function of $\log(R)$ where R is a length scale becomes independent of d_E . While this is a popular method, it does not give any new information regarding the pertinent question posed by the embedding theorem, which is: when is the attractor unfolded by the chosen set of time delay coordinates?

(c) **Method of false nearest neighbours:** This method attempts to determine directly from the data at which embedding dimension one has eliminated the crossings of an orbit with itself which had risen by virtue of having projected the attractor into a too low dimensional space. For this, we determine when points in dimension d are neighbours of each other. This aspect is examined by increasing the value of d from 1, 2 ... till no false neighbours exist and hence from geometrical considerations alone we can arrive at a value $d_E = d_N$, the optimal value for the embedding dimension of the system at hand. The implementation of this technique follows a report by Kennel et. al. (1992) and is briefly portrayed here.

In dimension d , each vector represented as

$$y(n) = [s(n), s(n+T), s(n+2T), \dots, s(n+(d-1)T)] \quad (3.11)$$

has a nearest neighbour $y^{NN}(n)$ with nearness in the sense of the Euclidean distance, $R_d(n)^2$ in dimension d . In the next higher dimension, $(d+1)$ the distance between the nearest neighbours is changed due to the $(d+1)^{st}$ coordinates to

$$R_{d+1}^2(n) = R_d^2(n) + \left[s(n+dT) - s^{NN}(n+dT) \right]^2 \quad (3.12)$$

If $R_{d+1}(n)$ is large, it can be presumed by going from d to $(d+1)$, the two points have been 'projected' away from each other. A threshold size R_T is chosen to decide whether the neighbours are false. The closest neighbours at time instant $n = t_0 + n \tau_s$ are regarded to be false if

$$\left[\frac{R_{d+1}^2(n) - R_d^2(n)}{R_d^2(n)} \right]^{1/2} = \frac{|s(n+dT) - s^{NN}(n+dT)|}{R_d(n)} > R_T \quad (3.13)$$

holds. Usually in the range $10 \leq R_T \leq 50$, the number of false neighbours identified by this criterion is a constant. In the case of a limited data set in which all points have near neighbours that do not move apart as the dimension is increased, a second criterion is considered. As it happens, the fact that points are nearest neighbours does not mean they are close on a distance scale set by the approximate size R_A of the attractor. If the nearest neighbour to $\mathbf{y}(n)$ is not close, so that $R_d(k) \sim R_A$, then $R_{d+1}(k) \sim 2R_A$. This means that distant but near neighbours will be stretched to the extremities of the attractor when unfolded from each other. Hence the second criterion is that if

$$\frac{R_{d+1}(n)}{R_A} \geq 2$$

then $\mathbf{y}(n)$ and its nearest neighbour are regarded false. As a measure of R_A one may use the rms value of the observations. Application of this method to the Lorenz model yields a sufficient embedding dimension of $d_E=3$ and this is indicated in figure 3.4.

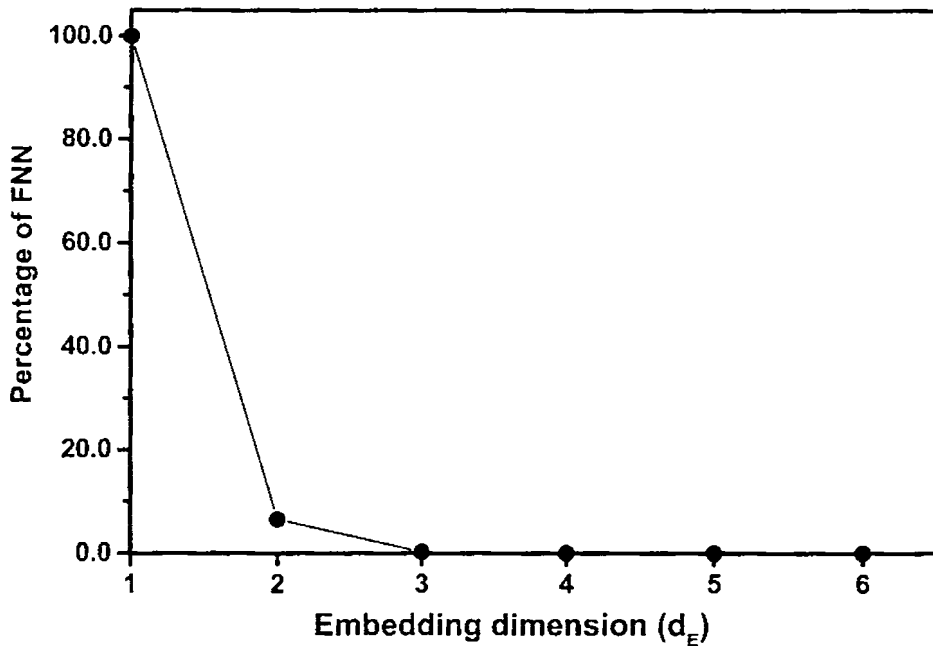


Figure 3.4 The false nearest neighbour (FNN) method applied to the Lorenz model data to determine a suitable embedding dimension, d_E .

This criterion is also useful in finding a suitable embedding dimension for a signal corrupted by noise. This method is robust against contamination from signals from other high or low dimensional dynamical systems. In either case, when the percentage of false neighbours falls to below 1%, that embedding dimension can be chosen as d_N .

(d) **True Vector fields:** Another geometrical approach to determining the embedding dimension for the observed time series data is to examine the uniqueness of the vector field responsible for the dynamics (Kaplan & Glass, 1992). If the dynamics is given by the autonomous rule $\dot{x} = F(x)$ and if $F(x)$ is smooth i.e. differentiable to any order then the tangents to the evolution of

the system are smooth and uniquely given throughout the space. If the dimension chosen, d_E is too low the vector fields in any location will often not be unique as they overlap one another due to projection from a larger embedding space. As one increases the d_E the frequency of overlap will fall to 0 and the vector field will have been unfolded. If the dynamics is very high dimensional then the vector field will not be unfolded until this high dimension is reached. In order to test the deviation of the vector field from what would be expected from a random noise, the statistic

$$\left[\frac{(V_j)^2 - (R_{n_j}^d)^2}{1 - (R_{n_j}^d)^2} \right] V_j$$

is considered. The vectors V_j are average directions of the line segments from entry to exit of the trajectory as it passes through box number j . $R_{n_j}^d$ is the known average displacement per step for a random walk in dimension d after n_j steps. This quantity will be averaged over all boxes.

If the data set is drawn from a random walk the statistic will be 0 and if it is effectively random by being a high dimensional, deterministic system viewed in too low a dimension, it will be small. For a low dimensional system viewed in a large enough dimension this will be near unity. The test works well even with contaminated data. This method is quite similar to that of false neighbours. Both are geometric and attempt to unfold a property of attractors from its overlap on the observation axis to its unambiguous state in an appropriately high dimensional state space.

3.6 Selection of Optimal Time Lag

In the time delay embedding of the single variable s of the system, the vectors of the m dimensional reconstructed state space are as in Eq. 3.9. In

this, T the time delay between successive elements in the delay vectors is not a subject of embedding theorem. Hence from a mathematical point of view, the choice of T is arbitrary since the data are assumed to have infinite precision. However in specific applications the choice of T is important. If the choice of T is too small, then the coordinates $s(n+jT)$ and $s(n+(j+1)T)$ are so close to each other in numerical value that it is not possible to distinguish them from each other. All the points then accumulate around the bisectrix of the embedding space. This is called redundancy by Casdagli et. al. (1991) and Gibson et. al. (1992). If T is very large on the other hand, the different coordinates may be almost uncorrelated so that the projection of an orbit on the attractor is onto two totally unrelated directions. Thus even if the underlying 'true' attractor is simple; the reconstructed attractor may become very complicated. Since the time lag has no relevance in the mathematical framework, there exists no rigorous way of determining its optimal value.

Many methods have been suggested in the literature to yield optimal results. But the different methods yield optimal results for only selected systems and perform just as average for others. In a particular application therefore one should try to optimize the performance by a variation of T . One of the criteria for the choice of time lag applies a geometrical argument. The attractor should be unfolded i.e. the extension of the attractor in all space dimensions should be roughly the same. Statistics such as the fill factor (Buzug & Pfister, 1992) or displacement from diagonal (Rosenstein et. al., 1994) are employed to evaluate this argument quantitatively.

A more popular method of choice uses the autocorrelation function (acf) of the signal. It is useful since it hints about stationarity and typical time scales in the system. Secondly it is related to the shape of the attractor in the reconstructed state. In order to approximate the data by a hyperspace in

higher dimensions, in principle the acf should be 0 at all lags equal to higher than T. The acf of a signal $s(n)$ is given by

$$C_L(T) = \frac{\frac{1}{N} \sum_{n=1}^N (s(n+T) - \bar{s}) - (s(n) - \bar{s})}{\frac{1}{N} \sum_{n=1}^N (s(n) - \bar{s})^2} \quad (3.14)$$

where $\bar{s} = \frac{1}{N} \sum_{n=1}^N s(n)$ is the mean over N points.

Here we look for that value of T at which $C_L(T)$ first passes through 0. However it tells of the independence of the coordinates only in a linear fashion. Also fulfilling the condition that acf be 0 at lag times equal to or greater than T, may drive to the limit of totally uncorrelated elements; which is undesirable. Hence a reasonable thumb rule is to choose the time where the acf decays to (1/e) of the maximum value as the lag in the delay reconstruction.

A reasonable objection to this procedure is that it is based on linear statistics without taking into account nonlinear dynamical correlations. From the context of information theory, the amount of information learnt about a measurement at one time from a measurement taken at another time can be identified. In a general case, let us consider two systems A and B with possible outcomes in making their measurements on them a_i and b_k . The mutual information of two measurements say, a_i and b_k is the amount learned about b_k by measuring a_i and vice-versa. This is defined as,

$$I_{A,B}(a_i, b_k) = \log_2 \left[\frac{P_{A,B}(a_i, b_k)}{P_A(a_i) P_B(b_k)} \right] \quad (3.15)$$

where the probability of observing a out of the set of outcomes for A is $P_A(a)$ and the corresponding quantity for b from B is $P_B(b)$ and the joint probability of the measurement of a and b is $P_{A,B}(a,b)$. The mutual information is symmetric in how much one learns about b_k by measuring a_i . The average mutual information is the average over all possible measurements of $I_{A,B}(a_i, b_k)$,

$$\bar{I}_{A,B}(T) = \sum_{a_i, b_k} P_{A,B}(a_i, b_k) I_{A,B}(a_i, b_k) \tag{3.16}$$

Fraser and Swinney (1986) suggested that one look for the first minimum of the time delayed mutual information. This is the information we already possess about the value of the signal $s(i+\tau)$ if we know $s(i)$. Generalizing Eq.3.15, the average mutual information for time delay τ is,

$$\begin{aligned} \bar{I}(\tau) &= \sum_{i,k} p_{i,k}(\tau) \ln \left[\frac{p_{i,k}(\tau)}{p_i p_k} \right] \\ &= \sum_{i,k} p_{i,k}(\tau) \ln p_{i,k}(\tau) - 2 \sum_i p_i \ln p_i \end{aligned} \tag{3.17}$$

where p_i is the probability that the signal assumes a value in the i^{th} bin of the probability distribution histogram and $p_{i,k}$ is the probability that $s(t)$ is in bin i and $s(t+\tau)$ is in bin k . In the special case $\tau=0$ the joint probabilities $p_{i,k}=p_i \delta_{i,k}$ and Eq. 3.17 yields the Shannon entropy of the data distribution. When τ is large enough, the two measurements $s(t)$ and $s(t+\tau)$ are independent and $p_{i,k}=p_i p_k$ and the mutual information becomes 0. The average mutual information curve for the x variable simulated from the Lorenz set of equations is plotted in figure 3.5.

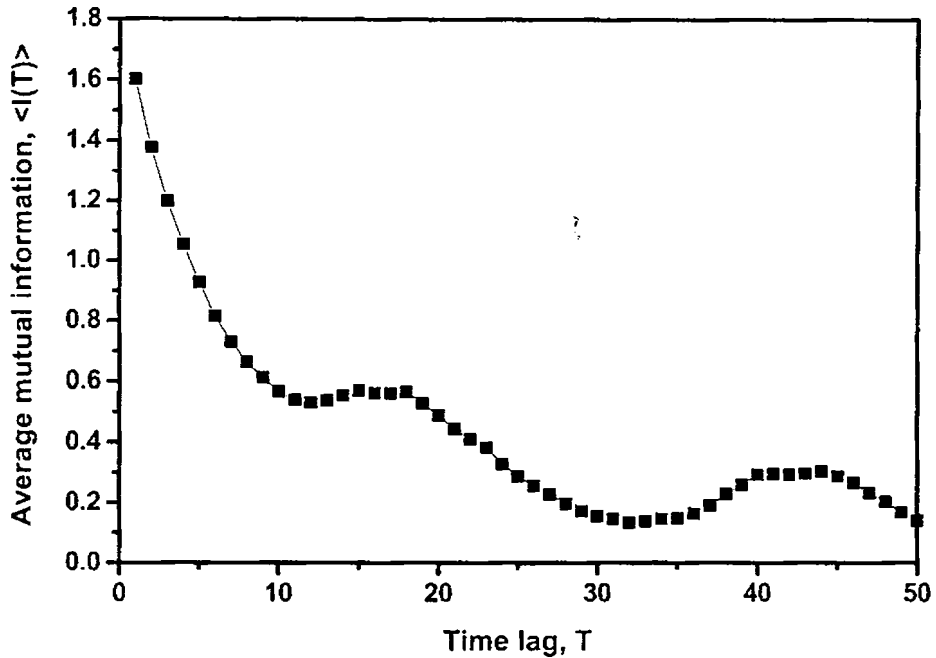


Figure 3.5. The average mutual information curve plotted for varying time lag for the Lorenz data.

The prescription of Fraser and Swinney for the choice of time lag is to choose that T_m where the first minimum of $I(T)$ occurs. The first minimum is the time lag where $s(t+\tau)$ adds maximal information to the knowledge we have from $s(t)$ or where redundancy is the least. In the case where a first minimum does not occur in the $I(T)$ curve, T_m is chosen such that $\frac{I(T_m)}{I(T_0)} \approx \frac{1}{5}$. However in

cases where there is a large difference between the minimum from the mutual information curve and the $(1/e)$ decay of the acf, it is worth optimizing T within that interval. Liebert and Schuster (1989) have examined the first minimum criterion by adding another criterion involving the correlation

integral and concluded that the T_m of the first minimum is also that at which the correlation integral is numerically well established.

3.7 Invariant Parameters of Dynamics

In classifying a physical system from observations, identification of quantities that are unchanged when initial conditions on an orbit are altered or a perturbation is encountered is essential. The relevance of such quantities rests on their invariance under smooth transformations of phase space. Irrespective of the details of their measurement process and reconstruction they will always assume the same values. Although this is strictly true only for ideal, noise-free infinitely long time series, which is not too easily encountered, in practical cases, robust algorithms exist that yield quite reliable results when applied to an approximately noise-free and sufficiently long data sets.

Most quantities are more conveniently defined as averages over the *natural measure* in phase space. This is because of particular interest in invariants, which assume the same value for almost any choice of initial conditions or are *ergodic*. Once the ergodic nature of the natural measure has been established, the averages automatically share this property. A thorough study on the ergodic nature of attractors is given by Eckmann and Ruelle (1985). Since the aim is to look for ergodic invariants, the first requirement is invariance under the action of dynamical equations. Hence in the case of experimental observations from dissipative systems of main interest are stable attractors on which trajectories from a typical initial condition will eventually settle. A possible candidate for the natural measure or invariant distribution that appears to be stable under the influence of errors or noise is the natural density of points in phase space that tells where the orbit has

been and whose integral over a volume of state space counts the number of points in that volume. Its definition in a phase space of dimension d is given by

$$\rho(\mathbf{x}) = \frac{1}{N} \sum_{k=1}^N \delta^d(\mathbf{x} - \mathbf{y}(k)) \quad (3.18)$$

It can be demonstrated that any function, say $g(\mathbf{x})$ when integrated with this density gives $\langle g \rangle$ which is invariant under the dynamics $\mathbf{x} \rightarrow F(\mathbf{x})$; thus qualifying the density of points as a suitable invariant measure on the attractor. The quantities such as $\langle g \rangle$ can be used to identify the system that produces the observations. These are statistical quantities for a deterministic system and are the only quantities that will be the same over any long observation of the same system. Since the orbits will essentially differ everywhere in phase space the issue is to choose a $g(\mathbf{x})$ that will contain some physical meaning regarding the system. Some such invariant quantities that are frequently used in the analysis of complex data are reviewed in this section.

3.7.1 Density Estimation

Before proceeding with the definition of the invariant quantities, some practical issues in the computation of the invariant distribution may be discussed. The invariant measure was defined as the sum of delta functions and is quite convenient in defining other invariant parameters. Any measurement of a tangible variable necessarily imposes a partitioning of phase space. The number of distinct, discrete states observable by any apparatus can be no larger than the inverse of the measurement resolution. In such a discretized space the probability of an element i of the partition is

$$p(x_i) = \frac{\int_{x_i} d^d x \rho(x)}{\sum_i \int_{x_i} d^d x \rho(x)} = \frac{n(x_i)}{\sum_i n(x_i)} \quad (3.19)$$

where $n(x_i)$ is the number of counts in partition element i . The partition-based estimator is a multidimensional histogram and does not provide smooth distributions and suffers from boundary effects. One way of improving upon traditional histograms is to use Kernel density estimators in place of delta functions. Tight Gaussians are a popular choice for the kernel but other functions have also been suggested on the grounds of optimality criteria. The kernel estimators are an alternative to fixed volume techniques for estimating the probabilities. Instead of partitioning the phase space by a uniform grid and counting the number of points within each element, *fixed mass methods* base the estimates on the localized properties of the data set around each individual point. A virtual partitioning is carried out with overlapping elements centered on every point in the data set. The radius of each element $r_{NB}(x)$ is increased until each encloses a pre-specified number of neighbouring points. In this manner a large number of overlapping elements with the same number of points with differing spatial sizes is obtained. The local density or probability is then estimated as a function of the inverse of the bin radius,

$$\rho(x) \propto r_{NB}(x)^{-d_E} \quad (3.20)$$

where d_E is the embedding dimension of the reconstructed space.

3.7.2 Generalized Dimensions

Dissipative dynamical systems possess an asymptotic behaviour, which causes their dynamics to relax onto a small, invariant subset of the full state space called the attractor. The generalized dimensions describe the structure

of such invariant subsets. The attractor dimensions are the most widely studied invariant quantities in the case of complex dynamical systems mainly because chaotic systems particularly were proved to have attractors whose dimensions were fractional as against the integral values of attractors of regular, integrable systems. The geometrically related concept of dimension is how (hyper) volumes scale as a function of a characteristic length parameter, $V \propto L^D$. In real world space, experience tells that planar areas scale quadratically with length i.e. $A \propto L^2$ while volumes scale as cube of the length scale, $V \propto L^3$. Hence in a loose sense we may 'define' the dimension as $D = \frac{\log V}{\log L}$. The simplest technique involved in estimating the dimension

involves partitioning of the d_E dimensional state space with a grid of size ε . The number of elements with atleast one point enclosed is counted and this is taken as an estimate of the dimension at resolution ε . The limit as $\varepsilon \rightarrow 0$ describes the space filling properties of the point set being analyzed. Such a box counting algorithm gives a maximum value D as the embedding dimension d_E . As the minimum-embedding dimension required for unfolding the attractor is achieved, the calculated fractal dimension also saturates at the proper value.

Consider a procedure similar to that used for the box counting method described above. Suppose there are N trajectory points on an attractor. The attractor region is then divided into cells of size ε labeled, $i=1,2,\dots, N(\varepsilon)$. In general, $N \neq N(\varepsilon)$. The number of trajectory points in the i^{th} cell is denoted by N_i and the probability p_i is the relative number of trajectory points in the cell given by $p_i = \frac{N_i}{N}$. The generalized dimensions, D_q are then defined as,

$$D_q = \lim_{\varepsilon \rightarrow 0} \frac{1}{q-1} \frac{\ln \sum_{i=1}^{N(\varepsilon)} p_i^q}{\ln \varepsilon} \tag{3.21}$$

The definition of D_q can be extended to apply to any real value of q . The factor $(q-1)$ in the denominator is included in the denominator so that for $q=0$,

$$D_0 = -\lim_{\varepsilon \rightarrow 0} \frac{\ln N(\varepsilon)}{\ln \varepsilon} \tag{3.22}$$

which is the same as the box-counting or **Capacity dimension**.

As $q \rightarrow \infty$, the largest probability value, p_{max} will dominate the sum and we have, $D_\infty = \lim_{\varepsilon \rightarrow 0} \frac{\ln p_{max}}{\ln \varepsilon}$. At the other extreme as $q \rightarrow -\infty$, the

smallest probability value p_{min} will dominate and so, $D_{-\infty} = \lim_{\varepsilon \rightarrow 0} \frac{\ln p_{min}}{\ln \varepsilon}$. Hence

D_∞ is associated with the most densely occupied region of the attractor while $D_{-\infty}$ is associated with the most rarefied region. It is also observed that $D_{-\infty} \geq D_\infty$ and in general $D_q \geq D_{q'}$ for $q \leq q'$.

For $q=1$, the **Information dimension** is defined as

$$D_1 = \lim_{\varepsilon \rightarrow 0} \frac{\sum_i p_i \ln p_i}{\ln \varepsilon}$$

This can be derived from Eq.3.22, by setting the limit $q \rightarrow 1$ followed by application of L'Hôspital's rule to the result to obtain the final form of the D_1 as given above. This is a measure of how quickly the information required for the specification of the state to precision ε grows with decreasing ε . The presence of $(p \ln p)$ in the definition of this measure is suggestive of the Shannon information term. While the measure D_0 is based

on the bulk of how many partition elements are non-empty; D_1 is calculated from a bulk in which each partition contributes proportional to the number of points it encloses. So bulk in D_0 is simply volume while in the case of D_1 bulk is equivalent to mass. The next one is the popular **Correlation dimension**,

defined as $D_2 = \lim_{\epsilon \rightarrow 0} \frac{-\log \sum p_i p_j}{\log \epsilon}$. The numerator constitutes a two-point

correlation function that gives the probability of finding two random points within a given partition element.

An alternative derivation for the generalized dimensions from a time series follows the generalized sum defined as

$$C_q(r) = \sum_{j=1}^N p_j p_j^{q-1} = \frac{1}{N} \sum_{j=1}^N \left[\frac{1}{N-1} \sum_{k=j+1}^N \Theta(r - |x_j - x_k|) \right]^{q-1} \quad (3.23)$$

where Θ is the Heaviside function given as, $\Theta(x) = 0; x \leq 0$
 $= 1; x > 0$

Setting $q=2$ in the above equation leads to the more popular form of D_2 as

$$D_2 = \lim_{r \rightarrow 0} \frac{\ln C_2(r)}{\ln r} \quad (3.24)$$

Hence the generalized dimensions in terms of the generalized sum is:

$$D_q = \lim_{r \rightarrow 0} \frac{1}{q-1} \frac{\ln C_q(r)}{\ln r} \quad (3.25)$$

In practice, almost all calculations of D_q from experimental data use the generalized correlation sum rather than the crude box-counting method.

Usually, $\frac{1}{q-1} \ln C_q(r)$ is plotted as a function of $\ln r$ and a scaling region is

sought whose slope is taken as the estimate of the generalized dimension, D_q .

3.7.3 The Grassberger-Procaccia (G-P) algorithm for Estimation of D_2

The popularity of the correlation dimension as the quantity most estimated from complex data generated in experimental conditions from fields ranging from fluid dynamics to physiology to meteorology was after Grassberger and Procaccia introduced their famous algorithm (1983a,b) for its computation. The application of box counting algorithm to real data for evaluation of the capacity dimension is fraught with difficulties. The number of computations required for the box-counting procedure increases exponentially with the state space dimension. Moreover this scheme requires the partitioning of state space with boxes and locating the trajectory points within the boxes which is a time consuming process.

In order to circumvent all these drawbacks and define a useful measure characterizing the attractor, Grassberger and Procaccia introduced the Correlation Dimension, D_2 . Though introduced in the previous section, we shall go through the steps of the G-P algorithm and arrive at the definition of this dimensional measure. This algorithm has the added advantage that it uses trajectory points directly without going for a partitioning of the state space.

We let the trajectory evolve for a long time and collect N points on it. For each point i on the trajectory the number of neighbours lying within a distance r of the point is determined after excluding the point i itself. Let this number be $N_i(r)$. Then the relative number of points lying within a distance r

of the point i is given by,
$$p_i(r) = \frac{2}{N-1} \sum_{\substack{j=1 \\ i \neq j}}^N \Theta(r - |x_i - x_j|).$$

The correlation sum is given by

$$C(r) = \frac{2}{N(N-1)} \sum_{i=1}^N \sum_{j=i+1}^N \Theta \left(r - |x_i - x_j| \right) \quad (3.26)$$

The sum in the above equation counts the pairs (x_i, x_j) whose distance is smaller than r in the limit of infinite data i.e. $N \rightarrow \infty$ and for small r , $C(r)$ scales like a power law, $C(r) \propto r^{D_2}$. Hence the correlation dimension is defined as

$$D_2 = \lim_{r \rightarrow 0} \lim_{N \rightarrow \infty} \frac{\log C(r)}{\log r} \quad (3.27)$$

Although the G-P algorithm does provide a quantifier for the self-similar geometry of the distribution underlying the data, its direct implementation to experimental data has many pitfalls. The algorithm assumes the presence of an infinitely long noise free stationary data set in the computation (Theiler, 1986), which is practically impossible to achieve. The number of data points sets an upper limit on the computed D_2 value. D_2 evaluation is also affected by the presence of noise- either 'real' noise in the experimental data or round-off error in numerical calculation and the choice of scaling region in the $\log C(r) - \log r$ plot (Theiler, 1990). It is hence important to test any computational scheme with standard data sets of known properties (Rapp, 1990). Noise tends to make the slope of the log-log plot larger for small values of r while the finite number of data points tends to make it smaller (Theiler 1986, 1991). Osborne and Provenzale (1989) reported certain controversial results that affected the place of honour enjoyed by correlation dimension as a robust marker of chaotic systems. In the last mentioned paper, time series generated by coloured stochastic processes also exhibited finite values of correlation dimension just like low

Table 6.1 The ApEn evaluated for the data from model equations using varying r and N compared with the reported values.

Model	Parameter	Mean	Std. Dev.	r	ApEn(2,r,N) (Reported*)			ApEn(2,r,N) (Evaluated)		
					N=300	N=1000	N=2000	N=300	N=1000	N=2000
Logistic	3.5	0.647	0.210	0.025	0	0	0	0	0	0
				0.05	0	0	0	0	0	
	3.6	0.646	0.211	0.025	0.229	0.229	0.230	0.2267	0.229	0.228
				0.05	0.205	0.206	0.204	0.202	0.205	0.204
	3.8	0.643	0.246	0.025	0.425	0.429	0.445	0.424	0.428	0.45
				0.05	0.424	0.427	0.442	0.424	0.43	0.45
Henon	0.8	0.352	0.622	0.05	0.337	0.385	0.394	0.37	0.385	0.393
				0.1	0.357	0.376	0.386	0.358	0.378	0.382
	1.0	0.254	0.723	0.05	0.386	0.449	0.459	0.387	0.449	0.47
				0.1	0.478	0.483	0.486	0.48	0.482	0.188

* Values as in Pincus, 1991.

dimensional chaotic systems. This contradicted the fact that stochastic data are of infinite dimensions. This effect was later attributed to temporal correlations in the data that caused pairs of points measured within a short time span to be close in phase space as well and thus introduced a bias in the correlation sum estimation. It was generally accepted after this that the correlation dimension just as other methods in science is applicable only when certain conditions are fulfilled and should be made use of judiciously. This is closely related to the possibility of the signal being nonstationary in nature and since this is the case with most experimentally observed data as in the case of biological systems; methods other than the original G-P algorithm were devised to lead to more meaningful estimates of the correlation integral in 'real' data. Before proceeding to the modified algorithms, a brief description of the nonstationary phenomenon in data may be in order.

3.7.4 Nonstationarity in Real-life Signals

Most of the nonlinear analysis tools require the time series under study to be dynamically stationary. This is because for any measurement to be useful in describing some property of the system under study, it should be reproducible. This is possible provided the system satisfies any one of the two generally known definitions of stationarity. The weak form of stationarity requires that all parameters of the studied system remain fixed and constant during the measurement period. However in most cases, direct access to the system producing the signal is not available and hence the constancy of the parameters cannot be established. A second concept of stationarity may thus be formulated based on the data itself. A signal is called *stationary* if all transition probabilities from one state to another are independent of time *within the observation period* i.e. when calculated from data. This includes the

constancy of the relevant parameters and also requires that phenomena belonging to the dynamics be contained in the time series sufficiently frequently so that probabilities and other rules can be inferred properly.

In practical situations, nonstationary time series are very common, the origins of which may be steeped either in the slow drift of the system's parameters during the measurement period arising⁷ due to the presence of multiple or overlapping time scales in the underlying dynamics or the changeable influence of the environment. Most of the methods developed to detect nonstationarity have at the core an indirect measurement of the dependence of statistics on time. The first step is the estimation of a certain parameter using different parts of a sequence. If the observed variations are found to be significant, i.e. outside the expected statistical fluctuations; the time series is regarded as nonstationary. The temporal correlations in the measured data, giving rise to spurious scaling of the correlation sum $C(r)$ with r may be thought of as a kind of nonstationarity of the measurement. The largely successful technique adopted in dealing with such data is the space-time separation plots of Provenzale et. al. (1992). This method is useful in not only detecting temporal correlations but also arriving at an optimal correlation time. A plot of the number of pairs of points as a function of the spatial distance as well as the time elapsed between measurements will saturate after a certain time point in the case of low dimensional complex systems. In the case of infinite dimensional systems, the saturation feature is absent indicating the futility of correlation dimension determination of such a data set. A modified formula for the correlation sum proposed by Theiler (1987) taking into account the temporal effects by excluding the pairs of vectors before saturation sets in gives

$$C_m(r) = \frac{2}{(N - n_{\min})(N - n_{\min} - 1)} \sum_{i=1}^N \sum_{j=i+n_{\min}}^N \Theta(r - |x_i - x_j|) \quad (3.28)$$

where $n_{\min} = \frac{t_{\min}}{T_s}$ and t_{\min} is the time point at which saturation of pairs of vectors occurs in the space-time separation plot and T_s is the sampling time of the signal.

An early method to test for stationarity is provided by the method of recurrence plots due to Eckmann, Kamphorst & Ruelle (1987). A different approach to detect nonstationarity is based on the similarity between parts of the time series themselves rather than the similarity of the parameters derived from the time series by local averages. In particular, the (nonlinear) cross prediction error i.e. the predictability of one segment using another as a database is evaluated. This concept is useful if the nonstationarity is given by changes of the shape of the attractor while dynamical invariants remain effectively unchanged (Scrieber, 1997). A test for stationarity of a time series that combines a test for the time independence of the probability distribution and a test based on the time independence of the power spectra was proposed by Witt, Kurths and Pikovsky (1998). An alternative, successful procedure based on the time distribution information deduced from geometrical structure of the reconstructed attractor in phase space was introduced by Yu et. al. (1999). Their work introduced a cross-time index and its distribution between different data segments and computed distributions of auto and cross time index using all near neighbours for a specified neighbourhood size say, ϵ in phase space. This nearest neighbour approach also smoothes out statistical fluctuations and reduces the probability to falsely reject the null hypothesis of the series being nonstationarity.

3.7.5 Modifications to the G-P Algorithm

Two important alternative measures suggested in place of the traditional D_2 computation are the Pointwise dimension, D_{2i} (PWD2) and point correlation dimension, PD2. The pointwise dimension takes into consideration only one reference point instead of all $i=1,2,\dots$ on the attractor (Farmer, Ott & Yorke, 1983). Based on the correlation sum itself, this is a measure of how fast the number of neighbouring points around the reference points increases as the distance r is increased. In the case of point sets where the pointwise dimension is independent of the reference point i , the correlation dimension D_2 will be the same as the computed D_{2i} . It has also been cited that with an adequate data length in the case of a model system the D_{2i} smoothly converges to the correlation dimension (Mitra & Skinner, 1993). The convergence occurs because the estimated dimension based on several orbits around the attractor i.e. D_{2i} , must be approximately the same as that based on data containing many more orbits as in the D_2 evaluation.

Point D_2 correlation dimension (PD2) was introduced by Skinner and associates (1990) as a variant of the PWD2 and unlike the G-P algorithm does not make use of all the vector difference lengths. Neither does it use all vector differences relative to a fixed reference vector as in the Farmer algorithm (Farmer, Ott & Yorke, 1983) for PWD2. This algorithm finds stationary epochs within the data of the same type as the one in which the reference vector is located, then tests and rejects those for which linear scaling and convergence are not satisfied. This is a marked improvement over accepting every reference vector as valid which leads to erroneous conclusion of certain vector differences for which the scaling relationship that defines dimension does not hold. The model for PD₂ is $C(n, r, n_{ref}^*) \sim r^{D_2}$

3

where n^*_{ref} is an acceptable reference vector showing scaling within its own subspecies i.e. (i) linear in the $\log C(n, r, n^*_{ref})$ versus $\log r$ plot and (ii) convergent in the slope versus embedding dimension plot. Because each n^*_{ref} has a new coordinate that could be of any value, the PD2 values are independent of each other and this justifies using the mean PD2 values over a stationary sub epoch as the best estimate of correlation dimension.

The uncertainty in the correlation dimension estimate due to nonstationarity may be eliminated by using small data sets covering small time segments. The Havstad and Ehlers algorithm (1989) proposes the division of the observed time series into windows that may be overlapping or nonoverlapping. The next step is the estimation of D2 in each of these by a method differing slightly from the original GPA. This allows the dimension estimate as a function of time.

As described in an earlier section the scalar time series, $s(i)$ is embedded in a phase space by the method of delays according as $\mathbf{Y} = \{s(i), s(i+T), s(i+2T), \dots, s(i+(d-1)T)\}$ where T is the time delay and d the chosen embedding dimension. The data set for dimension estimation consists of N vectors and M reference vectors ($M < N$). In this case though, instead of calculating the number of pairs of vectors within a radius r , the radius is predetermined and the distance from a reference vector to each of N vectors within r are noted. From this number of vectors j within a predetermined r , the correlation dimension is calculated as

$$D_c(d) = \frac{\ln j}{\langle \ln r \rangle} \tag{3.29}$$

where $\langle \rangle$ denotes the average. Euclidean norm is used to calculate the distance between the vectors. To avoid prominent distortion of slope in $\ln(j)$

and $\langle \ln r \rangle$ a certain minimum number of vectors are skipped on either side of the reference vector. Thus a reliable estimation of dimension is obtained by careful choice of intervals between vectors and between reference and neighbouring vectors so that the vectors are adequately independent, by proper choice of time lag and by averaging $\ln (r)$.

The algorithms discussed so far attempt to minimize the errors in dimension estimation due to nonstationarity but do not incorporate the notion of nonstationary process as such. The proponents of PD2 claim that their algorithm is superior to others, yet; there is no definition of a nonstationary process included. Some of the vectors in the correlation integral estimation, which do not give similar scaling as the surrounding vectors of reference vector, are rejected. Whether this rejection is valid when the process involves a large class of overlapping time scales is not mentioned. The method proposed by Havstad and Ehlers has been employed in this work as it considers the dynamics within a window and considers at least in some sense the time scales involved in the dynamics within that window. Further, it has been found that it gives more reliable estimation of D2 especially for high dimension signals like those of EEG.

3.7.6 Generalized Entropies

The measures of dimension specify the static qualities of the attractor without regard for the temporal evolution. The dynamical characteristics i.e. the evolution of the system studies the nature of evolution of the trajectories in phase space. This information is contained in the generalized entropies and the spectrum of Lyapunov exponents that study the manner of temporal evolution of the system trajectories. Entropy is actually a measure of the average information gained on observing the state of the system with a

certain precision. This interpretation follows from Information theory developed in the 1940s mainly by Shannon, Rényi and Kolmogorov. In the case of a fixed point or periodic cycle of a dynamical system for instance, each orbit remains the same and hence no new information is created and this implies that no uncertainty exists in the evolution of such a system. The predictive capability is enhanced even before an observation of the next orbit is made. On the other hand, for irregular chaotic systems, each orbit is entirely new to the observer making the prediction before an observation entirely difficult. Such a system may be thought of as creating information as it evolves in time. In order to quantify the amount of such information created the entropies are resorted to.

The trajectories of nonlinear chaotic systems emerging from nearby, indistinguishable initial conditions diverge exponentially and evolve into distinguishable states after a finite time. This sensitivity to initial conditions causes such systems to continuously generate new information making any long-term prediction impossible. Consider the attractor in the phase space of the system partitioned into $N(\varepsilon)$ elements labeled s_1, s_2, \dots, s_N with size ε . If n successive measurements at regularly spaced time intervals τ are taken for a given trajectory then it will yield a sequence of elements (s_1, s_2, \dots, s_n) as visited by this trajectory. Let $P(s_1, s_2, \dots, s_n)$ be the joint probability of finding the trajectory in s_1 at time τ , in s_2 at time 2τ and so. In correspondence with the case of dimensions, entropy can also be generalized to a set of order q Rényi entropies defined as,

$$K_q = -\lim_{\tau \rightarrow 0} \lim_{\varepsilon \rightarrow 0} \lim_{n \rightarrow \infty} \times \left[\frac{1}{n\tau} \frac{1}{1-q} \ln \sum_{s_1 \dots s_d} p^q(s_1, \dots, s_n) \right] \quad (3.30)$$

The easiest to calculate is the $q=2$, K_2 entropy while the famous Kolmogorov-Sinai entropy is the K_1 entropy (Grassberger & Procaccia, 1983c). The

correlation sum that was introduced earlier is related to the joint probability as,

$$C_q(r) = \sum_{s_1 \dots s_n} p^q(s_1, \dots, s_n) \quad (3.31)$$

The advantages of computing the entropy values numerically are many. It gives a time scale over which prediction is relevant in the system and secondly how the dynamics unfolds. But the difficulty in computation is in the requirement of data set much longer than those required in the case of dimensional or Lyapunov exponent. Hence in the general case, we get,

$$C_q(r, d) \propto r^{D_q} e^{-dTK_q(d)} \quad (3.32)$$

where d is the embedding dimension. As in the case of the dimension computation since the finite length of data set as well as noise in the measurements make the imposition of the limit $r \rightarrow 0$ slightly meaningless, a scaling range is determined in which the results are independent of r . Such a scale independence is evident if a plateau is seen in the plot of the scaling exponents, $D_q(d, r)$. For values of r in the plateau regions, in the dimension plots, the factor r^{D_q} is almost constant. Hence the exponent K_q can be defined as

$$K_q(d, r) = \frac{1}{\tau} \ln \left\{ \frac{C_q(d, r)}{C_q(d+1, r)} \right\} \quad (3.33)$$

For sufficiently large values of d , the value converges to a constant K_q . In practice, the K_2 entropy is the easiest to compute just as the D_2 is, since the correlation sum at $q=2$, is the mean over the number of neighbours and hence yields a meaningful result in any case.

Hence for the K_2 entropy we have,

$$K_2(d, r) = \frac{1}{\tau} \ln \left\{ \frac{C_2(d, r)}{C_2(d+1, r)} \right\} \quad (3.34)$$

which is an estimate of,

$$K_2 \cong \lim_{\substack{d \rightarrow \infty \\ r \rightarrow 0 \\ \tau \rightarrow 0}} K_2(d, r) \quad (3.35)$$

(Kantz & Scheiber, 1997)

3.7.7 Lyapunov Exponents

Dimension estimation, despite being successful is frustrating in the meager quantity of useful information gained for the amount of computational cost expended. The dimensions describe how the sample of points along a system orbit tends to be distributed spatially but there is no information about the dynamic, temporally evolving structure of the system. The Lyapunov exponents on the other hand examine the structure of time ordered points making up the trajectory. The significance of the spectrum of Lyapunov exponents can be understood by considering the effects of the dynamics in a small, fiducial hypervolume in phase space. Arbitrarily complicated dynamics exhibited by chaotic systems can cause the fiducial element to evolve to extremely complex shapes. However for small length scales and short enough time scales, the initial effect of the dynamics is to distort the evolving spheroid into an ellipsoidal shape with some directions being stretched while others are contracted. The primary, major axis of this ellipsoid will correspond to the most unstable direction of the flow and the asymptotic rate of expansion of this axis is what is measured as the largest Lyapunov exponent. If the infinitesimal radius of the initial fiducial volume is $r(0)$ and the length of

the i^{th} principal axis at time is $l_i(t)$ then the i^{th} Lyapunov exponent is defined as:

$$\lambda_i = \lim_{t \rightarrow \infty} \frac{1}{t} \log \frac{l_i(t)}{r(0)} \quad (3.36)$$

By convention, the Lyapunov exponents are ordered so that $\lambda_1 > \lambda_2 > \lambda_3 \dots$. Equivalently the Lyapunov exponent can be seen to measure the rate of growth of fiducial subspaces in the phase space. λ_1 measures how quickly linear distances grow. The two largest principal axes define an area element and the sum ($\lambda_1 + \lambda_2$) determines the rate at which two-dimensional areas grow. In general the behaviour of d -dimensional subspaces is described

by the sum of the first d exponents, $\sum_{j=0}^d \lambda_j$.

Estimation of Lyapunov exponents from time series data was first implemented by Wolf and co-workers (Wolf et. al., 1985). In that algorithm the exponential divergence exhibited by data is already assumed. This yields a finite exponent for stochastic data also where the true exponent is infinite. While Wolf's algorithm only uses a delay reconstruction of phase space, another class of algorithms exist which involves the approximation of the underlying deterministic dynamics. This method as in Sano and Sawada (1985) and Eckmann et. al. (1986) is efficient if the data allows for a good approximation of the dynamics. The better one among all these appears to be the one proposed independently by Rosenstein et. al. (1993) and Kantz (1994) that tests for the exponential divergence of nearby trajectories. This allows a decision on the part of the analyst whether it really makes sense to compute a Lyapunov exponent for a given data set.

3.8 Testing for Nonlinearity in the System

In what appeared to be a total deviation from the expected, Osborne and Provenzale (1989) reported finite D_2 estimates for linear stochastic systems ('coloured noises'). These initial and later instances clarified that the presence of a fractal dimension alone is not sufficient to indicate the presence of a strange attractor and, in fact, may be produced by a filtered stochastic process. Theiler demonstrated the increase of error in dimensional estimation with decrease in sample size and pointed out the necessity of discriminating low dimensional chaotic data from filtered high dimensional noise that if properly filtered exhibits low dimensional characteristics. Hence while for many systems the assumption of nonlinearity leading to apparently random looking behaviour may be correct in principle, it should be shown explicitly that employing nonlinear tools and models is justified and useful from an information point of view.

The method of surrogate data testing (Theiler et. al., 1992; Prichard & Theiler, 1994) introduced to test the nonlinearity in a dynamical system is based on a null hypothesis against which both the data as well as discriminating statistic are tested. While the null hypothesis is to be proved to be inadequate for explaining the data, the discriminating statistic is a number that quantifies some aspect of the time series. Once the null hypothesis is stated, the next step involves generation of the surrogate data from the given time series by using the process assumed in the null hypothesis. This ensemble shares certain properties of the generating system such as the mean, variance and Fourier spectrum but is otherwise random as required by the null hypothesis. The chosen discriminating statistic is calculated for both the original and surrogate data sets and in case of significant difference between the two sets, the null hypothesis is rejected. The hypotheses that

are usually proposed for nonlinear testing may be classified into three: those equivalent to the assumption that the data are (i) identically independently distributed noise (Type 0), (ii) linearly filtered noise (Type I) and (iii) a monotonic nonlinear transformation (Type II). The surrogates to test the type II hypothesis are generated by the Amplitude Adjusted Fourier Transform (AAFT) procedure. It is actually a combination of the unwrapped Fourier transform (FT) and windowed FT (WFT) methods followed in the Type 0 and I surrogates resp. (Theiler et.al., 1992). AAFT may be summarized in a few steps:

- Create a Gaussian time series $y(t)$ which is rank ordered according to the original data set denoted by $x(t)$, say.
- A surrogate, $y'(t)$ of the new time series $y(t)$ is formed by shuffling the phases in the Fourier transform of y .
- The final step involves the rank ordering of the original data $x(t)$ so that it follows $y'(t)$. This time re-ordered series provides a surrogate of the original time series that matches its amplitude distribution.

The note worthy point here is that the series underlying the surrogate data $y(t)$ and $y'(t)$ are Gaussian and have the same Fourier power spectrum. Another more general null hypothesis that allows for nonlinear rescalings as well of a Gaussian linear process was later introduced by Schriber & Schmitz (1996). In order to implement this scheme, apart from generating data that represent typical realizations of a model of a system, the surrogate data should also represent a process yielding identical estimates of the parameters of the process when compared to those obtained from the original data. The choice of the distinguishing statistic is based on the context but mostly either the correlation dimension, Lyapunov exponent or forecasting error is made use of. Others include the correlation integral, moments and cross-moments,

the skewed difference statistic and the Takens's best estimator for correlation dimension (Prichard & Theiler, 1994). The significance of the test is determined based on the computed statistic for the original and surrogate data sets. If Q_D is the statistic computed for the original time series and Q_{H_i} for the i^{th} surrogate generated under the null hypothesis; the measure of

significance is given by, $S = \frac{|Q_D - \mu_H|}{\sigma_H}$ where in μ_H and σ_H denote the

sample mean and standard deviation of the distribution of Q_H . Even though it is strictly non-dimensional, the units of S are called 'sigmas'. This method could successfully distinguish the nonlinearity in several known chaotic time series like that from Mackey-Glass equations and at the same time failed to find nonlinear structure in a linear stochastic system (as required).

Another test based on Local Linear Nonlinear Autoregressive models (LLNAR) could test nonlinearity as well as directedness of interactions between neural groups when applied to local field potentials (LFPs) recorded in the macaque monkey (Freiwald et. al., 1999). A novel measure for nonlinearity in time series from continuous dynamical systems that may be safely assumed to underlie complex real life systems has been proposed that combines discrete parametric modeling with a subsampling approach. This provides more specific information on the time series and reduces the detrimental effects of various well known problems and weak points of surrogate data testing (Galka & Ozaki, 2001). Despite the many pitfalls the method of surrogate data remains a favourite among scientists working in complex systems due to its simplicity as well as implementational ease. Some of the findings in the nonlinearity of the signal of interest, EEG will be presented in section II.

Part II: Electroencephalogram - A Time Varying Nonlinear Signal

3.9 The Electroencephalogram (EEG)

The electroencephalogram (EEG) is a time-varying electrical signal recorded from electrodes attached to the scalp of a subject. Electric activity in the brain produces changes of electric potential on the surface of the scalp. These changes are measured using electrodes pasted on the scalp. The electric activity in the brain is a result of the working of Glia cells and neurons. Glia cells produce slow changes in their resting membrane potentials, while neurons display action potentials and synaptic potentials. All of these contribute to the EEG signal. This composite signal that ensues at the scalp is complex, since it is generated as a superposition of different simultaneously acting dynamical systems. In addition to brain activity, the EEG also reflects activation of the head musculature, eye movements, interference from nearby electric devices, and changing conductivity in the electrodes due to the movements of the subject or physiochemical reactions at the electrode sites. All of these activities that are not directly related to the current cognitive processing of the subject are collectively referred to as *background activity* below.

Since the first electric potentials were recorded by Hans Berger in the late 1920s', the EEG has been employed in many clinical settings for decades to find patterns that correlate to disorders like epilepsy, sleep disorders, tumours, and more recently, schizophrenia. Prior to the implementation of digitized recordings and stochastic analysis based around the fast-fourier transform (FFT) in the 1960's, the EEG was observed on a simple ink-based time-scale. The oscillatory activity of neuronal pools reflected in characteristic EEG rhythms constitutes a mechanism by which the brain can regulate

changes of state in selected neuronal networks to cause a qualitative transition between modes of information processing. The gross frequency characteristics were determined by visual inspection of the EEG patterns and were often correlated with conscious and unconscious states, such as sleep. Following this line of study, EEG has also been made use of to suggest or validate models of cognitive behavior and the dynamics of the brain.

The greatest advantage of EEG over other high technology imaging methods such as PET and MRI is its speed-it can record complex patterns of neural activity occurring within fractions of a second after a stimulus has been administered. Some other merits are also evident: EEG is rather simple in use, cheap and almost does not disturb a subject. The EEG can be recorded near the patient's bed and can be used for long-term monitoring of sleep stages or epilepsy. EEG also is a convenient tool for psychophysiological research when the subject has to perform some behavioral tasks or is out of laboratory. But there is one more, not so evident, but very valuable advantage of EEG studies. In fact, PET and fMRI are based on the measurement of secondary metabolic changes in brain tissue, but not of primary electrically active state of neural system, which transports the signal in the afferent and efferent paths. Further more the time scale of EEG recordings are three or four orders smaller as compared to other imaging methods such as CAT and PET and hence will record features, which are smeared out in the conventional methods. EEG can thus reveal one of main parameters of the neural activity - its nonlinear property, which reflects the essence of neural excitation. Therefore while recording electrical (as well as magnetic) field patterns, the physiologist has access to the actual mechanisms of the brain information processing.

In the present section, after a brief note on the other popular tools of brain imaging such as the CAT, PET and MRI, the analysis of EEG carried out by physicists and mathematicians as a potential tool for studying the brain dynamics will be dealt with. This will include the past as well as current trends in EEG processing that have led to a deeper understanding of the mechanism underlying it.

3.10 Neuroimaging Techniques

Several non- or minimally-invasive neuromonitoring techniques for examining functional brain activity are currently available to the psychiatric researcher and clinician. These methods are often categorized in terms of whether they provide direct or indirect information about brain function. Electroencephalography (EEG) was the first to appear on the scene, followed by other technologies including computed axial tomography (CAT), positron emission tomography (PET), single-positron emission computed tomography (SPECT), magnetoencephalography (MEG) and recently functional magnetic resonance imaging (fMRI). Of these MEG, EEG, and event-triggered EEG (also called event related potentials; ERPs), each of which monitors a direct consequence of brain electromagnetic activity belong to the direct category. In particular, EEG and ERP record the electrical fields generated by neuronal activity, while MEG records the magnetic fields induced by such activity. PET, SPECT and fMRI, on the other hand, are indirect methods in that they generally monitor haemodynamic changes consequent to brain electrical activity. PET and SPECT brain imaging operate by monitoring the decay of blood-borne radioactive isotopes as they pass through the brain. FMRI, in contrast, detects changes in the local concentration of deoxyhaemoglobin via its effect on imposed magnetic fields. While each of these techniques has its

own distinct advantages, at present the direct methods tend to have limited spatial resolution, whereas the indirect methods can only detect neuronal activity after it has been filtered by a complex and poorly understood neurovascular coupling function. The latest in this genre is the noninvasive near IR imaging technique that depends on diffuse optical effects and is an upcoming technique for neuroimaging. A brief review of the salient features of some of these techniques is added below.

(a) X-ray Computed Tomography (X-ray CT)

The early 1970s' saw the introduction of a remarkable imaging technique known as the x-ray CT. This technique takes advantage of the fact that when a highly focussed beam of x-rays is passed through the body, the beam is affected in a predictable manner by the relative density of the tissue through which it passes. Because the organs within the body, including the brain differ in density, it is possible to visualize the body's organs in their living state. Unlike conventional x-rays, which produce pictures of the "shadows" cast by body structures of different density, CT scanning uses x-rays in a much different way. In CT of the head, numerous x-ray beams are passed through the skull and brain at different angles, and special sensors measure the amount of radiation absorbed by different tissues (and lesions such as a tumor). The scanner revolves around the patient, who is lying still, emitting and recording x-ray beams from as many as a thousand points on the circle. A special computer program then uses the differences in x-ray absorption to form cross-sectional images, or 'slices', of the head and brain. These slices are called tomograms, hence the name 'computed tomography'. What was really unique in the development of X-ray CT was the employment of clever computing and mathematical techniques to process the vast amount of

information necessary to create actual images. The impact of X-ray CT was incredible in the way it eliminated the need for various radiological examinations that were often unpleasant and hazardous for the subjects and that were frequently difficult for physicians to interpret. In addition, it provoked the research into new ways of imaging the body using the same basic mathematical and computer strategies of image reconstruction.

CT of the head is now widely available and is performed in a relatively short time and at a reasonable cost - especially when compared to other sophisticated methods such as the magnetic resonance imaging (MRI). Compared to MR imaging, the precise details of soft tissue (including some deep parts of the brain) are less visible on CT scans.

(b) Positron Emission Tomography (PET) and Single-Positron Emission Computed Tomography (SPECT)

PET has become a tool for medical diagnosis especially for dynamic studies of human metabolism and for brain activation. Widespread interest and acceleration in PET technology was due to the development of reconstruction algorithms associated with x-ray CT and improvements in nuclear detector technologies. PET has a million-fold sensitivity advantage over other techniques used to study regional metabolism and neuro-receptor activity in the brain and other body tissues. In contrast, magnetic resonance has exquisite resolution for anatomic studies and for flow or angiographic studies. Also, magnetic resonance spectroscopy has the unique attribute of evaluating chemical composition of tissue but in the millimolar range rather than the nanomolar range. Since the nanomolar range is the concentration range of

most receptor proteins in the body, positron emission tomography is ideal for this type of imaging.

PET imaging begins with the injection of a metabolically active tracer—a biological molecule that carries with it a positron-emitting isotope (for example, ^{11}C , ^{13}N , ^{15}O , or ^{18}F). Within minutes, the isotope accumulates in an area of the body for which the molecule has an affinity. The radioactive nuclei then decay by positron emission. The emitted positron collides with a free electron usually within less than 1 mm from the point of emission. The interaction of the two subatomic particles results in a conversion of matter to energy in the form of two gamma rays. These high-energy gamma rays emerge from the collision point in opposite directions, and are detected by an array of detectors, which surround the patient. When the two photons are recorded simultaneously by a pair of detectors, the collision that gave rise to them must have occurred somewhere along the line connecting the detectors. After 500,000 or more annihilation events are detected, the distribution of the positron-emitting tracer is calculated by tomographic reconstruction procedures. PET then reconstructs a two-dimensional image. Three-dimensional reconstructions can also be done using 2D projections from multiple angles.

Generally, SPECT tracers are more limited than PET tracers in the kinds of brain activity they can monitor. SPECT tracers also deteriorate more slowly than many PET tracers, which means that SPECT studies require longer test and retest periods than PET studies do. However, because SPECT tracers are longer lasting, they do not require an onsite cyclotron to produce them. While PET is more versatile than SPECT and produces more detailed images with a higher degree of resolution, particularly of deeper brain structures,

SPECT is much less expensive than PET and can address many of the same research questions that PET can.

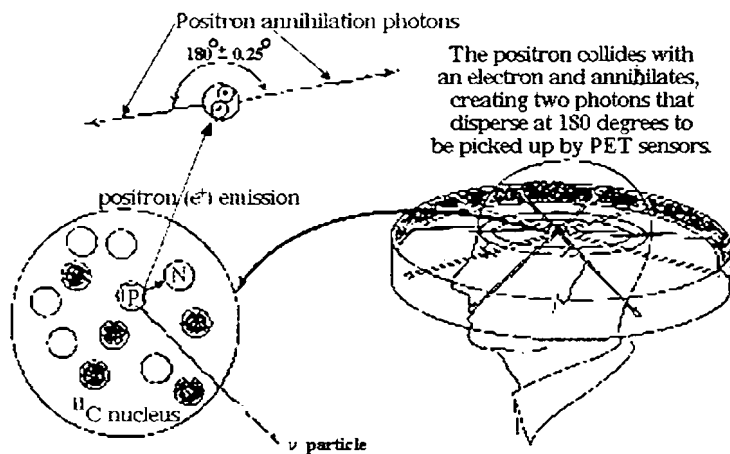


Figure 3.6. A schematic of the PET imaging technique

The major clinical applications of PET have been in cancer detection of the brain, breast, heart, lung and colorectal tumors. Another application is the evaluation of coronary artery disease by imaging the metabolism of heart muscle. Applications to the study of epilepsy, brain tumors, stroke and Alzheimer's disease have occupied the interest of neurologists for nearly 20 years. A major attribute of PET is its ability to show activity of neuroreceptors such as the dopamine, serotonin and noradrenergic receptor systems. The concentrations of neurochemical sites in the body are generally too low (eg. μM) for MRI and MRS studies. In drug abuse research, PET scans are being used to identify the brain sites where drugs and naturally occurring neurotransmitters act, to show how quickly drugs reach and activate a neural receptor, and to determine how long drugs occupy these receptors and how

long they take to leave the brain. PET is also being used to show brain changes following chronic drug abuse, during withdrawal from drugs, and while the research volunteer is experiencing drug craving.

(c) Magnetic Resonance Imaging (MRI) and Functional MRI (fMRI)

Another imaging method, magnetic resonance imaging (MRI), was developed in the 1980s. Most elements have at least one reasonably abundant isotope whose nucleus is magnetic. In biological materials, the magnetic nuclei of ^1H , ^{13}C , ^{23}Na , etc. are all abundant. The hydrogen nucleus (a single proton) is abundant in the body due to the high water content of non-bony tissues. When the body is immersed in a static magnetic field protons become aligned with the magnetic field than against the static field. A rapidly alternating magnetic field at an appropriate resonant frequency in the radio frequency (RF) range, applied by a coil near the subject or specimen in the static magnetic field, changes the orientation of the nuclear spins relative to the direction of the static field. These changes are accompanied by the absorption of energy by nuclei which undergo the transition from a lower energy state to a higher one. When the alternating field is turned off, the nuclei return to the equilibrium state, emitting energy at the same frequency as was previously absorbed. Because the amount of oxygen found in blood affects its magnetic properties, MRI detects regions with changes in levels of blood oxygenation due to activity-related changes in blood flow. MRI can provide both anatomical and functional information helping researchers accurately determine which brain regions are active in each task. Functional MRI (fMRI) relies on the magnetic properties of blood to enable scientists to see images of blood flow in the brain as it is occurring.

An fMRI scan can produce images of brain activity as fast as every second. Scientists can also determine with greater precision when brain regions become active and how long they remain active. An fMRI scan can also produce high-quality images that can pinpoint exactly which areas of the brain are being activated. In summary, fMRI provides superior image clarity of activity deep in the brain with high spatial resolution. It is relatively slow since it is based on the blood-flow response, which takes about 450 milliseconds. To date, however, PET retains the significant advantage of being able to identify which brain receptors are being activated by neurotransmitters, abused drugs, and potential treatment compounds.

(d) Noninvasive near IR Imaging

The discovery that useful information could be obtained from thick tissue samples, including brain-using light applied to and detected from the scalp (Jobsis 1977) spurred the development of diffuse optics as a technique for human brain monitoring. The technique goes variously by the names of near-infrared spectroscopy (NIRS), diffuse optical tomography (or topography; DOT) and/or near-infrared imaging (NIRI). All the techniques are based on the general concept of detecting light scattered by the scalp and analyzing the absorption spectra of light absorbing molecules (chromophores) present in tissue to interpret the detected light (Strangman et. al., 2002). A comparison

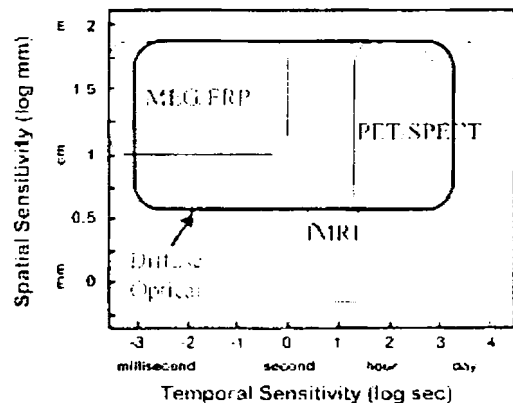


Figure 3.1. A comparative look at the sensitivities of the various brain imaging techniques.

is reproduced in the above figure 3.7 adapted from the above mentioned reference. It is evident that while MEG and ERPs exhibit stronger temporal sensitivity these are relatively weak in terms of spatial sensitivity. In contrast, fMRI, PET and SPECT are stronger in spatial sensitivity but possess weaker temporal resolution. Diffuse optical techniques in comparison provide excellent temporal sensitivity as well as reasonable spatial sensitivity. When multiple colours of light are used, moreover, spectroscopic information about the sampled tissue also becomes available, thereby affording the promise of quantifying the concentrations of the various haemoglobin species—oxyhaemoglobin, deoxy-haemoglobin, and the sum of these (total haemoglobin, which is proportional to blood volume). Thus, diffuse optical techniques simultaneously combine both indirect and direct methods of neuronal activity monitoring which are complementary sources of information about brain function.

Besides the advantages obvious in the above figure, the optical approach has various other merits. In particular, the instrumentation—which is completely noninvasive can be made portable, unobtrusive, low-cost, low power and robust to motion artifacts. One of the first clinical applications of diffuse optical techniques for functional brain monitoring was the investigation of fetal, neonatal and infant cerebral oxygenation and functional activation. This population was of interest because other neuroimaging methods were (and are) not feasible given the high activity level of such subjects. Relatively few psychiatric applications of diffuse optical techniques have thus far been reported. Hock and colleagues have examined Alzheimer's patients during verbal fluency and other cognitive tasks, (Hock et. al., 1997). In addition to cognitive studies, evaluations of the haemodynamic response have also been completed during deep brain stimulation in Parkinson's patients (Sakatani et.

al., 1999), during induced seizures in patients with intractable epilepsy (Watanabe et. al., 2000) and during magnetic brain stimulation for the treatment of depression (Eschweiler et. al., 2000).

3.11 Classification of Brain Waves

EEG in general exhibits a broadband structure but a common classification of waves based on frequency is popular in neuroscience among clinicians, technicians as well as scientists.

Reading an EEG involves interpreting the wave forms on the basis of frequency to a large extent and depending on the morphology to a lesser extent. According to the frequency classification, EEG waves are mainly of four types as in figure

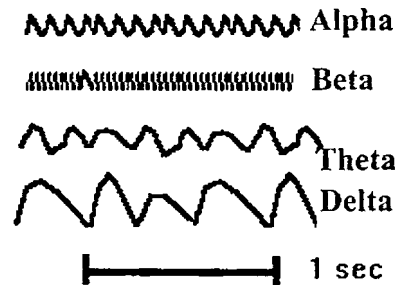


Figure 3.8. *A pictorial representation of the major types of EEG waves classified according to frequency range.*

3.8. A brief description of these 4 classes is given below:

- **Delta waves:** Frequency range – Less than 4 Hz. These are large amplitude waves, which occur in deep sleep and are associated with some abnormal processes and are said to reflect the unconscious mind. Delta waves are found in infants upto about one year of age and are present in stages 3 and 4 of sleep. These waves produce immobile, lethargic and less attentive states. Delta activity is usually most prominent frontally in adults and posteriorly in children.
- **Theta waves:** Frequency range- 4 Hz to 8Hz. Theta is also classed in the 'slow' category and occurs in connection with creativity, emotions,

intuition and is associated with the subconscious mind. While theta waves are abnormal in awake adults, they are perfectly normal in children upto 13 years of age and in sleep. It is usually regional in spread, may involve many lobes, and can be lateralized or diffuse.

- **Alpha waves:** Frequency range – 7.5 Hz to 13 Hz. With amplitude of about 50 μ V, Alpha is a common state for the brain and occurs whenever a person is alert (it is a marker for alertness and sleep), but not actively processing information. Alpha has been linked to extroversion (introverts show less), creativity (creative subjects show alpha when listening and coming to a solution for creative problems), and mental work. They are strongest over the occipital (back of the head) cortex and also over frontal cortex.
- **Beta waves:** Frequency range – above 12 Hz. These are low amplitude or 'fast' waves and are found during the waking state as well as when the brain is working as in some calculation or thinking process. It reflects desynchronized active brain tissue. It is usually seen on both sides of the cortex in symmetrical distribution and is most evident frontally. It may be absent or reduced in areas of cortical damage. Low Beta activity (12-15 Hz) is localized by side and by lobe and represents a relaxed yet alert state; midrange Beta (15-18 Hz) is localized over several areas often associated with thinking and finally, high Beta (above 18 Hz) corresponds to a strongly localized activity leading to agitated mental activity such as planning, math calculation etc.
- **Gamma waves:** Frequency range- 36 Hz-44 Hz. This is the only frequency group distributed over every part of the brain. It is hypothesized and in some cases validated that the 40 Hz activity in the

brain consolidates the required areas for simultaneous processing whenever the brain needs to access information from multiple regions. A good memory is associated with well-regulated and efficient 40Hz activity, whereas a 40Hz deficiency creates learning disabilities.

The next major classification of the observed waves in the EEG is based on morphology. Certain waves have typical forms irrespective of frequency and are readily identified by their shape; in other instances pairs or groups of waves have characteristic forms. Single waves that are specially formed include spikes or sharp waves. Their peculiarity is that they rise rapidly to a point and then fall off quickly to a base that is narrower when compared to the amplitude. Spikes are narrow with high amplitudes giving them a narrow and high form and a sharp top. A sharp wave on the other hand is broader than a spike but has the same significance. It is a hallmark of seizure activity and implies multiple synchronous firing or activity (of dendrites). Sharp waves are thought to represent the discharge as seen from some distance away while spikes are recorded from close to the focus.

Among the waveforms some have specificity due to morphology. The most important among these is the Spike -Wave pattern that consists of a spike, which is probably generated in the cortex, and a large amplitude slow wave (usually delta), thought to originate from thalamic structures, occurring recurrently. These occur synchronously and symmetrically in the generalized epilepsies or focally in the partial ones. In the generalized types of spike and wave, true absence (*petit mal*) is characterized by 3 Hz spike-wave, while slow spike-wave occurs more usually with brain injury and the Lennox-Gastaut syndrome. Other wave groups include polyspike and wave of greater than 3 Hz in which each slow wave is accompanied by two or more spikes and

is often associated with myoclonic seizures; periodic lateralised epileptiform discharges (PLEDS); triphasic waves; burst suppression etc. a discussion on EEG waves will be incomplete if the normal variants are left unmentioned. These are several waves or patterns of waves, which are unusual in appearance, yet are not significant for abnormality or disease. Amongst the more common ones are mu rhythm, psychomotor variant, lambda waves, POSTS, spindles, vertex waves and K Complexes amongst others.

3.12 Data Collection and Preprocessing

3.12.1 Recording the EEG

Any recording system for the EEG requires the following components:

- *Electrodes* -- Attached to the scalp of the subject.
- *Amplifiers* -- The amplitude of the input signals from the electrodes is usually in the range 10-100 μ V and high input impedance differential amplifiers are used to boost this level.
- *Filters* -- The EEG signal is often filtered before recording. High-pass, low-pass and notch filters are all used in this context. However the filtering aimed at removing the contaminants in the data could take out some of the nonlinear component in the data. Hence the filter settings should be chosen carefully.
- *Recording unit* -- Used to keep a permanent record of the EEG signal. Originally the EEG was recorded on paper but digital recording is becoming more usual.

The recorded signals making up the EEG are the potential differences between pairs of electrodes. There are two recording approaches used:

- *Referential* -- The potential difference is measured between an active scalp electrode and an inactive reference electrode elsewhere on the

subject. The reference electrode is often placed on the ear. This location picks up some temporal brain activity so cannot be considered truly inactive; however other sites, e.g., chin or nose, suffer from electrocardiogram (ECG) contamination.

- Bipolar -- The potential difference is measured between two active electrodes. The exact pairing (including polarity) used must be recorded, often by a system of arrows on a diagram of the electrode placements.

Unfortunately the recording of brain activity is easily disturbed. Any signal activity that does not arise from the brain is considered to be a recording artifact. There are many possible causes of artifact including muscle activity (e.g., scalp muscles or eye motion), mains electricity interference and electrode movement (Spehlmann, 1986).

3.12.2 Electrode Placement Configurations

In order to perform consistent testing for electroencephalographic (EEG) recordings, a system was developed which would describe the locations for electrodes on the human skull. A great deal of research was conducted in the creation of the system. Important features that needed to be considered in the development include:

- ✧ A standard format for measured sites
- ✧ The use of common terminology
- ✧ Anatomically correct locations

As a result of the joint effort of neurological societies worldwide, a standardised electrode placement scheme known as the 'International 10-20 system' was established, allowing the comparison of different EEG data derived from different subjects. This universal arrangement of electrodes

known as the international ten twenty system, assures reproducible electrode sites with sufficient coverage of all parts of the head as depicted in figure 3.9. The different electrode positions are derived from measurements taken between standard landmarks on the skull. These measurements allow the calculation of a network of lines, which are superimposed across the head. Electrodes are placed where the lines of this mesh intersect. This results in inter-electrode distances of ten and twenty percent of a line's total length.

In this convention, each electrode site has a letter identifying its sub-cranial lobe i.e. 'F_p'-Frontopolar or prefrontal lobe, 'F'-Frontal lobe, 'T'-Temporal lobe, 'C'-Central lobe, 'P'-Parietal lobe, 'O'-Occipital lobe. In addition there is a number or another letter identifying its hemispherical location. The subscript 'Z' (denoting line zero) ensuing any lobe abbreviation refers to an electrode placed along the cerebrum's midline. The use of an even number (2, 4, 6 or 8) represents the right hemisphere, and odd numbers (1, 3, 5 or 7) referring to the left hemisphere. The numbers rise with increasing distance from the midline of the head. The distances are calculated as percentages of typical lengths such as the head circumference etc. Percentages are made use of because the skull varies from subject to subject. An adolescent's may be smaller than an adult's as also traumatic accidents to the skull may have occurred in the subject's history creating an out of proportion condition. The percentage relationship remains the same for the location of the internal brain lobes. Skull dimensions are measured accordingly in centimeters and then site distances or spacings are converted with the 10 and 20% factors. Fifty percent (50%) is used frequently, but is a composite of 10, 20 and 20%. Supplementary electrodes to those typically employed in the 10-20 system have been devised to improve electroencephalographic spatial resolution. This more extensive placement scheme using modified combinatorial

nomenclature (MCN) was developed by the American Clinical Neurophysiology Society and it broadens the 10-20 system by subdividing the existing inter-electrode distances as in the figure 3.10. More detailed explanations on the identification of electrode sites on the scalp are available either in books on biomedical instrumentation or resources on the World Wide Web.

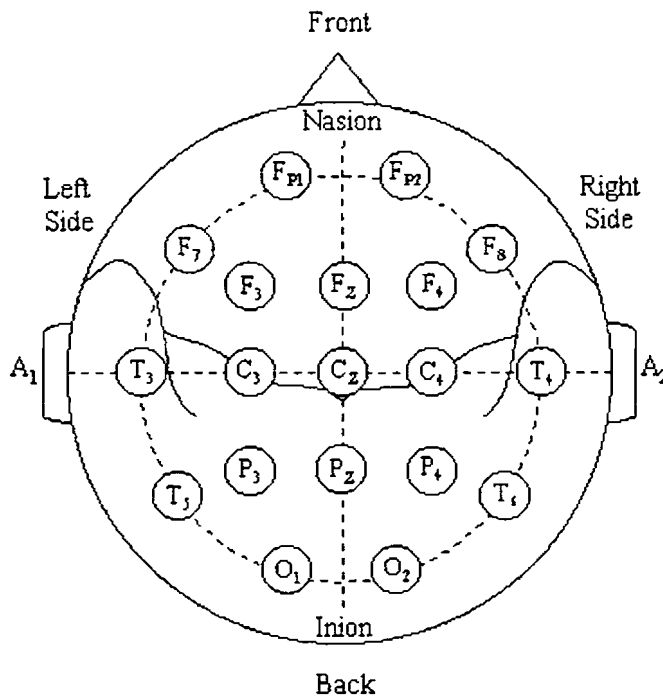


Figure 3.9. A projection of the head on which the standard electrode sites of the international 10-20 system are illustrated. Note that A_1 and A_2 represent sites located on the lobules of each ear.

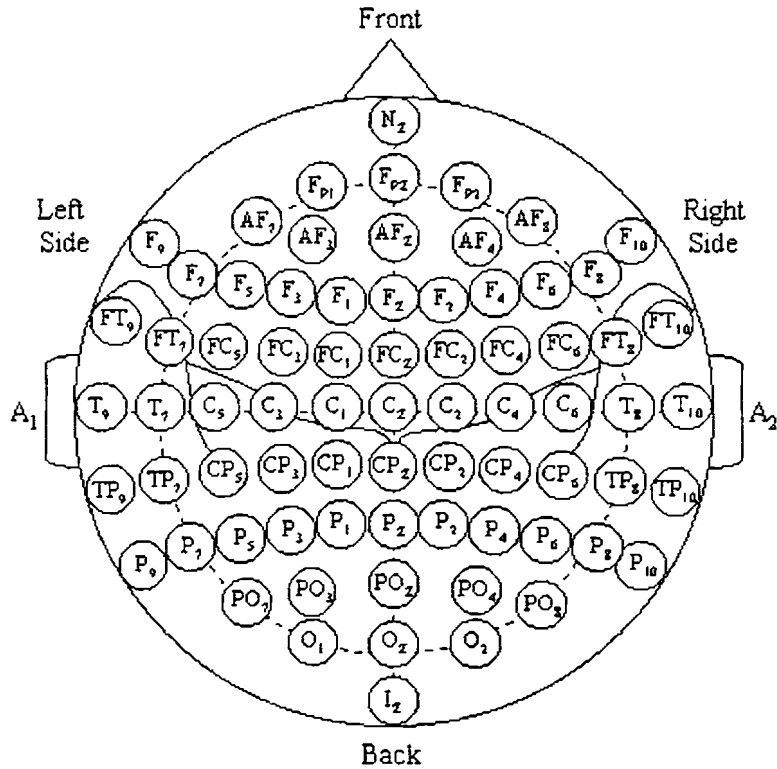


Figure 3.10. An extension of the ten twenty electrode placement scheme using modified combinational nomenclature. Note that four of the standard placement sites, namely 'T₃', 'T₄', 'T₅' and 'T₆', have been renamed 'T₇', 'T₈', 'P₇' and 'P₈' respectively.

In recent times, the limited spatial resolution of the conventional EEG technology has been tackled by introducing high resolution EEG (HR- EEG) (Babiloni et. al., 1997; Edlinger et. al., 1998). A pre-requisite for such methods is adequate sampling of the potential distribution on the scalp surface. The point-spread function of conduction of potential from brain surface to the scalp averages about 2.5 cm (Gevins, 1990). Thus to

adequately cover the surface of the scalp with electrodes having inter-electrode distance in this range, EEG equipment supporting atleast 128-channels is required (Srinivasan et. al., 1998). In accordance with this need, the state-of-the-art technology in EEG recording uses machines with up to 256 electrode positions. The schematic of a 128-electrode Electrical Geodesic™ system marketed by Electrical Geodesics, Inc. is illustrated in figure 3.11.

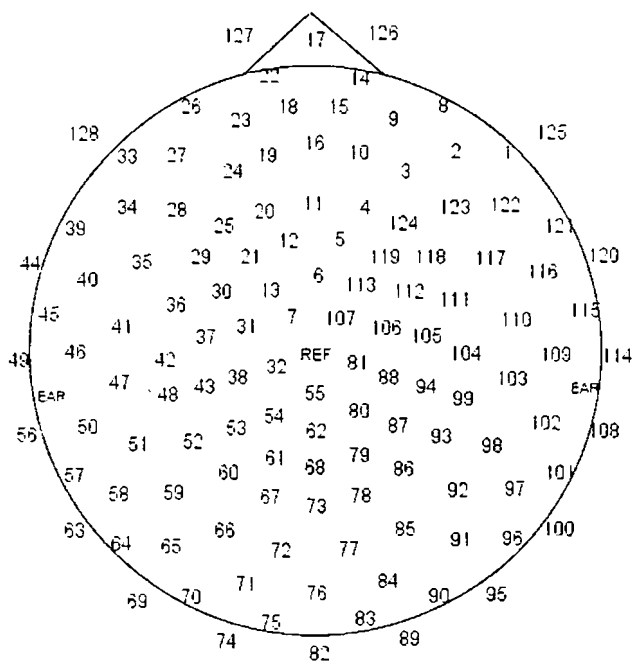


Figure 3.11. Schematic of the 128 electrode Geodesic sensor net of the Electrical Geodesic™ system.

3.13 Is the Brain Chaotic?

Nonlinear dynamics is a fundamentally different approach to the analysis of signals such as the EEG that have been studied since the early quarter of the

past century. This development followed the appearance of abundant evidence that at all levels, the nervous system is rich with complex, nonlinear behaviour. Examples of such behaviour exhibited at the single neuron level, neural ensembles in sensory and motor functions and spatio-temporal modes of activity in large neural assemblies have been cited in an earlier chapter. Deterministic mathematical models of neural system give rise to complex dynamics in the absence of stochastic fluctuations in the variables of the brain, potential to the system. Such dynamics occurs in nonlinear feedback systems possessing time delays and is expected in recurrent inhibition and periodic forcing of neural oscillators. In the recent past, the analysis of the electrophysiological signals such as the EEG and MEG recorded on the scalp as a time series by application of the principles of nonlinear dynamics and deterministic chaos has become a powerful, non-invasive tool in the ongoing exploration into the mysteries of the human brain mechanism.

Babloyantz and co-workers were the pioneers who published results on the dimensionality of human EEG (Babloyantz et. al., 1985). The initial spate of work, which followed in this direction, was mostly demonstrational in nature with data from a few subjects with EEGs' taken from a few isolated sites. Since the early 90's though, research has been on a greater number of subjects and the tasks under study have also grown in number and complexity (Pritchard & Duke, 1992; Lutzenberger et. al., 1992; Birbaumer et. al., 1996). Over the years, sleep data has been extensively studied (Röschke & Aldenhoff, 1992; Ferri et. al., 1998) with particular attention paid to specific sleep stages (Pereda et. al., 1998). Mental task studies are another area of interest with tasks varying from mental arithmetic (Stam et. al., 1996; Micheloyannis et. al., 1998) to verbal processing (Bizas et. al., 1999; Molle et. al., 1999). In most of these studies the global variation of

dimensional complexity over the cortex compared to a passive rest state such as eyes closed condition has been monitored. Of greater clinical advantage are studies on multichannel data recorded on subjects with neuropsychiatric ailments such as epilepsy (Lehnertz & Elger, 1998), schizophrenia (Koukkou et. al., 1993), Alzheimer's disease (Jeong et. al., 1998, 2001; Pritchard et. al., 1994) and Parkinson's disorder (Stam et. al., 1994). All the drawbacks related to dimension estimation such as finite data length, noise contamination, nonstationarity etc. discussed in the previous sections hold in the case of EEG signal processing as well. Nevertheless information regarding the underlying brain state is made available by judicious examination of data by making variance estimations as also inferential statistical comparisons (Rapp, 1993). In one report, the running attractor dimension was evaluated for whole sleep EEG records and the values were found to significantly differ over the sleep stages (Pradhan et. al., 1995). It was also observed that the dimensional value depended critically on the window length. The analysis proved the superiority and implementational ease of such methods over conventional visual scoring of long EEG records. In a study following this, the same group analyzed the behaviour of the dominant Lyapunov exponent during sleep which again characterized transitions indicating the occurrence of different degrees of chaoticity in the states that may be related to various sleep stages (Pradhan & Sadasivan, 1996).

In computing the Kolmogorov entropy and largest Lyapunov exponents, the dynamical evolution of the system is probed. An early study on K_2 entropy during mental arithmetic task undertaken in this group (Lalaja et. al., 1987) could establish the rate of loss of information associated with a mental task carried out several times over. Other studies conducted in pathological cases (Lerner, 1996) have shown the lowering of information

rate associated with a malfunctioning of the neural system in comparison with its normal state. The entropy quantification of spatio-temporal dynamics during mental tasks has also been demonstrated (Pezard et. al., 1996). The Lyapunov exponent, which also characterizes the chaotic nature of the data, has been computed for EEG recorded under various conditions (Röschke et. al., 1993) to be positive. While this is an evidence in support of the supposedly chaotic nature of the system generating the signal, counter examples are also prevalent (Palus, 1996, 1999) that throw doubt on the low dimensional chaotic nature of the complex signal.

The chaos conjecture of EEG is based on a finite correlation dimension and positive Lyapunov exponent (Gallez & Babloyantz, 1991; Albano & Rapp, 1992). The question of whether finite correlation dimension estimates of EEG signals arise from the chaotic nature of the system or are a reflection of its behaviour as linearly correlated noise is still open. Surrogate data testing described in part I of this chapter, was proposed as one way to detect the presence of nonlinearity and low dimensional chaos in experimental time series from physiological systems such as the ECG (electrocardiogram), EEG etc. (Glass, Kaplan & Lewis, 1992; Pritchard, Duke & Kriebel, 1995). The details of the surrogate testing with numerical data has been described in Theiler et. al. (1992). It was observed in that report that one set of EEG did not exhibit nonlinear behaviour; while another did. However invasive studies of electrographic recordings from depth and subdural electrodes in patients with seizures of mesial, temporal origin exhibited statistically significant nonlinearities in prominent cortical areas (Casdagli et. al., 1997). The advocacy of surrogate data testing to distinguish coloured noises from chaotic processes met with a setback in the results reported by Pradhan and Sadasivan (1997). In this paper, they conducted surrogate data testing for

chaotic time series, mixed sine waves, white Gaussian noises, coloured Gaussian noises and EEG with regard to correlation dimension D_2 . Their results clearly indicated that this test alone might not be a sufficient one for distinguishing coloured noises from low dimensional chaos. The test failed for coloured noises of low frequency contents and mixed sine waves- signals, which also have low correlation dimensions. The authors observed that in the case of mixed sine waves, the surrogate testing turned up ambiguous results not differentiating it from chaotic systems and thus in the absence of other measures the test could interpret it as chaotic. Hence they concluded that a limiting or saturating D_2 value with embedding dimension may be considered a prerequisite for identification of chaotic systems. Despite this, the surrogate method is widely applied to establish the nonlinearity in complex signals and in the case of EEG has been used to support its nonlinear nature on various fronts (Kowalik & Elbert, 1995; Rambouts, Keunen & Stam, 1995).

3.14 On the Threshold of the Big Step

The literature reviewed over the past decade and a half abounds with instances of application of methods developed within the framework of nonlinear dynamics to the EEG signal in an attempt to decipher the underlying process in the brain. While the argument relating to the presence of chaos or not in human brain dynamics continues to rage, we attempt a nonlinear analysis of the recorded signal. The nonlinearity present in the microscopic level of the brain i.e. the neurons, gets integrated in a complex manner in its propagation through the system and is evident as nonlinear traces in the EEG. Emboldened by such a finding, we embark on a quest to seek signatures of higher dynamical functions in this complex, stochastic signal using the arsenal of nonlinear dynamics and deterministic chaos.

Dynamical Aspects of Coupled Oscillators: A Time Series Analysis

*Time present and time past
Are both perhaps present in time future,
And time future in time past.
If all time is eternally present
All time is unredeemable.*

--- T.S. Eliot in Burnt Norton.

The knowledge that simple nonlinear systems can have complicated behaviour has prompted the growth of alternative methods of analysis applied to the output of such systems within the framework of nonlinear dynamics (Parker & Chua, 1987). This development occurred due to the breakdown of traditional linear techniques of Fourier transforms, power spectrum analysis and parametric linear modeling in understanding the structures of such systems. At times these methods have even led to erroneous interpretation of the observed behaviour as noise. Against such a backdrop was developed the toolbox of nonlinear time series analysis to suit the physicists or mathematicians in studying the apparently random looking data that exhibits

algorithms for the evaluation of the system invariants as also the significance of each in providing meaningful insights into the dynamics of the system were elaborated in the previous two chapters. Following that discussion, we understand that two of the most widely studied topological parameters are the Correlation Dimension D_2 and the K_2 entropy. The static geometric parameter D_2 refers to the degrees of freedom associated with the system while the entropy provides an intuitive measure of the information that is lost during evolution of the system at a given instant and is hence a dynamic quantity (Ott, 1993). Of late, besides the topological parameters, another set of parameters characterizing the synchronization phenomenon has been found to be of importance [Osipov et. al., 1997; Pikovsky, 1984; Rosenblum, 1996] in the case of coupled systems. Synchronization phenomenon will be dealt with in a later chapter in greater detail. Nevertheless a brief overview is included here. Synchronization may in general be divided into a number of classes. The one in which even while the dynamics in time as represented by the amplitude of the measured signal remains chaotic, the states of the sub-systems of the complex system coincide due to interaction. This is termed as 'complete synchronization' of the chaotic oscillators (Pikovsky, 1984). Another approach is based on the overlap of power spectra of the signals from the interacting systems (Anisichenko et. al., 1992); an alternate recent method is the 'phase synchronization' of chaotic systems which studies the correlation between the phases of individual systems and an eventual phase locking that leads to synchronization between them (Rosenblum, Pikovsky & Kurths, 1996). The complex systems in nature most often exhibit uncorrelated activity in their amplitudes while their phases may be entrained over brief periods of time. For this reason, the phase synchronization is emphasized in this analysis, which applies the technique of nonlinear time series analysis to

a pair of coupled Rossler oscillators in the chaotic regime to study the dynamical behaviour inherent in such a system.

The analysis is carried out in a systematic manner beginning with (a) a unidirectional coupling between the nonlinear units and subsequently moving on to (b) a mutual or bi-directional scenario. The coupled system in the case of uni-directional coupling contains a coupling parameter, g while there is a pair of coupling factors g_1 and g_2 in the mutually coupled closed scenario. The parameter g_1 , which forms the feed forward coupling, may be assumed to be an internal parameter of the system while g_2 the feedback-coupling factor is considered as the control parameter. This scheme is depicted in figure 4.1 (a & b).

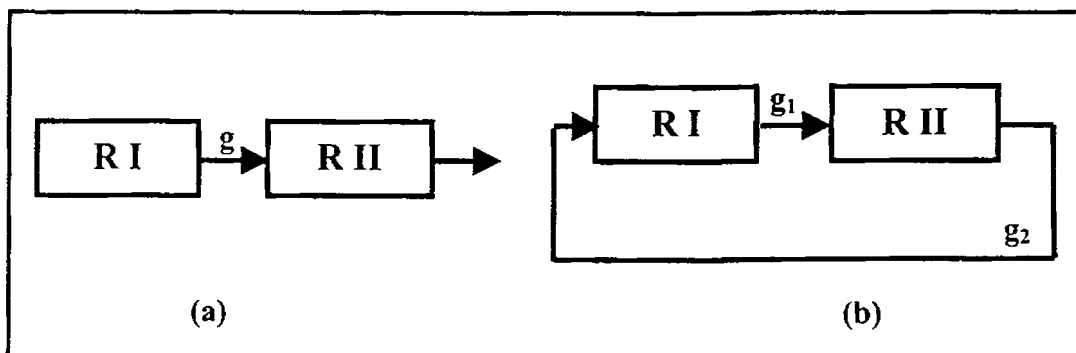


Figure 4.1. Schematic of the coupling modes of the model system considered in the dynamical analysis. In (a) the unidirectional case, the output of the drive is fed at a certain fraction to the response while the bi-directional case (b) has each of the units coupling their output to the other at a specified rate.

In the parameter space of coupling factors the system dynamics is studied by evaluating the correlation dimension, D_2 and K_2 entropy. The synchronization existing between the subsystems may be interpreted as the measure of the coordination present in the system. The phase synchronization phenomenon

exhibited by the system is studied in detail and the empirical relation that may hold between the parameters that characterize the dynamical and interactive behaviour of the coupled system with respect to the coupling parameters is inferred.

Noise is an inevitable reality in natural systems. It can be inherently present in the dynamics or appear extraneously as a result of the measuring process or even due to the external environment (Kantz & Schrieber, 1997). Hence we incorporate the effect of noise in this case by adding it to the coupling factor as an additive term thus making the coupling fuzzy in nature rather than rigid as represented by a constant factor. Noise of various types at varying levels is added in the couplings and as a final objective; the effect of noise in the coupled system with regard to the synchronization phenomenon is investigated.

4.2 Method of Analysis

The Rössler model (Rössler, 1976) is based on abstract chemical kinetics. The dynamics of chemical reactions can display the same kind of periodic and chaotic behaviour that appears in other sciences but the transition from order to chaos is easier to study as the conditions of the experiments can be readily controlled. The system under consideration is the coupled Rossler system (Parlitz et. al., 1996a) described by the flow equations

$$\begin{aligned}
 \alpha \dot{x}_i &= a + x_i(y_i - \mu) \\
 \alpha \dot{y}_i &= -x_i - \omega_i z_i \\
 \alpha \dot{z}_i &= \omega_i y_i + b z_i + g_j(z_j - z_i)
 \end{aligned}$$

where

$$\begin{aligned}
 i, j &= 1, 2; i \neq j \\
 \omega_i &= 1, i = 1 \\
 \omega_i &= 1.1, i = 2 \\
 \alpha &= 0.013, a = 0.2, b = 0.412; \mu = 5.7
 \end{aligned}
 \tag{4.1}$$

The Rossler model follows the period doubling route to chaos and the above stated nonlinear set of equations exhibit chaotic behaviour for the choice of parameters made in this study. The coupled Rossler systems exist as independent systems in the chaotic regime in the uncoupled state. The system attractor in the 3-dimensional phase space spanned by (x, y, z) is represented in figure 4.2 for completeness sake.

The coupled systems are simulated numerically and the invariants are reliably computed by application of algorithms developed and standardized on model data sets. In the initial case of unidirectional coupling, only the feed forward coupling is present and the systems form a drive-response set and hence we have $g_2=0$ and $g_1=g$ as the sole coupling factor. While considering bi-directional coupling, both the coupling parameters come into play. The equations are integrated by the fourth order Runge-Kutta method with a step of 0.0005. The variables y_1 and y_2 are generated as time series from the first and second systems for varying values of coupling parameters g_i . It is well known that any single parameter in a coupled (nonlinear) set of equations ($i=1$ or $i=2$) as in Eq. 4.1, would represent the entire characteristics of the whole system (Abarbanel et. al., 1993). The choice of y_1 and y_2 for the two distinctly different oscillations is made on the basis of this fundamental result.

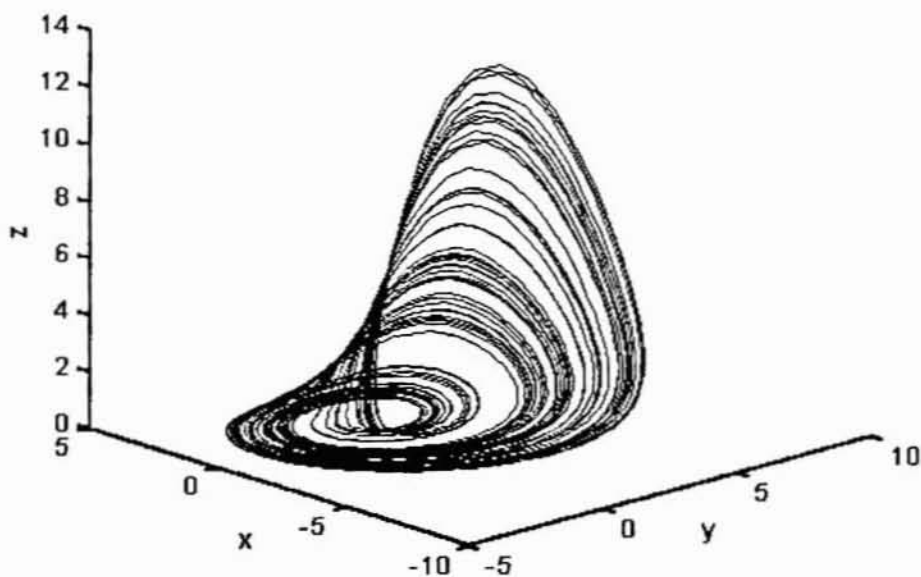


Figure 4.2. *The Rossler oscillator attractor in its phase space spanned by the 3 variables x, y, z .*

For convenience, we use the parlance of unidirectionally coupled systems and name system I as the drive and system II as the response bearing in mind that in the study of the bi-directional case, the two systems are mutually coupled and each acts as a response to the drive from the other. The coupling between the systems introduces nonstationarity in the dynamics and this is reflected in the variation of the typical time scales estimated from the time series of the outputs. The generated time series after removal of transients are subjected to a time delay embedding (Abarbanel et. al., 1993) and the D_2 , K_2 parameters of the systems are determined by adopting the Grassberger-Procaccia algorithm (Grassberger & Procaccia, 1983a,b) The coordinative effect between the individual units due to coupling is investigated

by quantifying the synchronization existing between them. The details of this will be described in a later chapter with special emphasis on experimental data as obtained from the brain in particular. Nevertheless to maintain lucidity of narration the essentials of the theory are mentioned here.

Phase synchronization in the system may be defined as the appearance of phase locking of interacting units even in the absence of apparent amplitude entrainment (Roseblum, Pikovsky & Kurths, 1996). The definition of the phase of a chaotic system remains an ambiguous concept to date and many definitions exist which are followed in accordance with the context. As is common with complex observed data (Roseblum, Pikovsky & Kurths, 1996), an analytic signal concept is made use of in this case and the composite signal is taken as,

$$\psi(t) = s(t) + i \tilde{s}(t) \tag{4.2}$$

where $s(t)$ is the actual signal and $\tilde{s}(t)$ is the Hilbert transform of $s(t)$ given as,

$$\tilde{s}(t) = P.V. \frac{1}{\pi} \int_0^{\infty} \frac{s(\tau)}{t - \tau} d\tau \tag{4.3}$$

Based on this, the phase is defined as

$$\phi(t) = \arctan \left(\frac{\tilde{s}(t)}{s(t)} \right) \tag{4.4}$$

A pair of chaotic systems (i,j) are said to be phase locked in the ratio $n:m$ if at any instant,

$$\left| n\phi_i(t) - m\phi_j(t) \right| < \varepsilon \tag{4.5}$$

ε being a small arbitrary constant. The simplest 1:1 case of phase synchronization is investigated by considering the relative phase distribution of a pair of corresponding variables of the system. The phase synchronization index is defined as

$$S_p = \frac{S_{max} - S}{S_{max}} \quad (4.6)$$

where

$$S = - \sum_{i=1}^{N_b} p_i \ln p_i \quad (4.7)$$

in which $p_i = \frac{N_i}{N}$ is the probability of occupancy of the i^{th} bin with N_i as the number of points in it, N the total number of points and N_b is the total number of bins. Hence we may write, $S_{max} = \ln N_b$ as the normalizing factor (Tass et. al., 1998).

4.3 The Uni-directionally Coupled System

Two independent Rossler oscillators are coupled so that there is a drive provided from the first to the second system through a coupling as described in Eq.(4.1). The strength of coupling is represented by the coupling constant g , which is scanned through a range of values and the corresponding system behaviour in terms of the invariant parameters, D_2 , K_2 and S_p is studied. In determining the parameters as mentioned in the previous section, a time delay embedding technique is adopted and used in the Grassberger- Procaccia algorithm. In the time delay embedding undertaken here the singular value decomposition (SVD) method is followed and the corresponding eigen value

spectrum is as shown in figure 4.3. The average mutual information criterion (Fraser & Swinney, 1986), a nonlinear counterpart of the autocorrelation function is used in the choice of the appropriate time delay and is found to hold in each case of coupling. A modified version of the Grassberger - Procaccia algorithm modified to suit small data sets (Havstad & Ehlers, 1989)

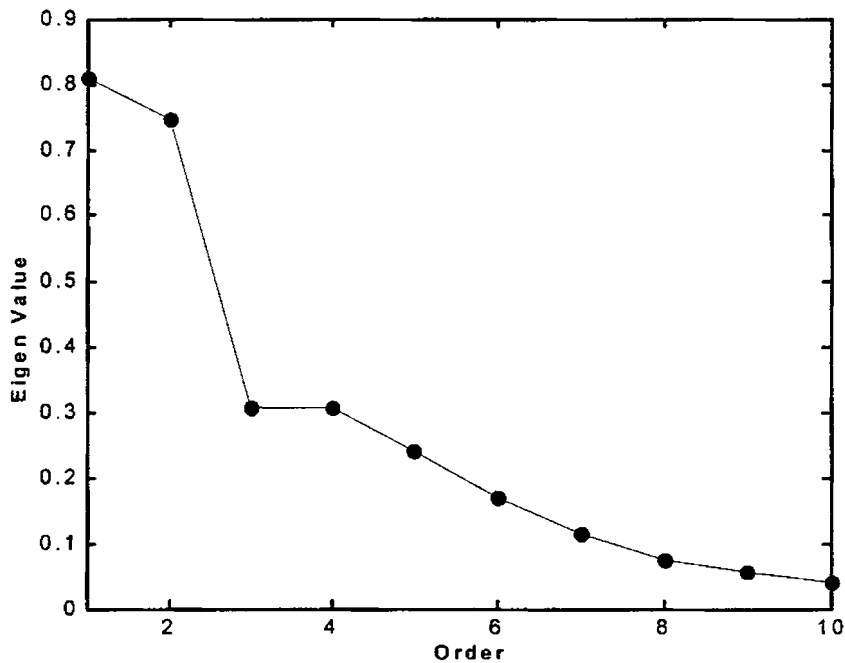


Figure 4.3. The eigen value spectrum evaluated using SVD in the time series from one of the units in the coupled case to choose an optimal embedding dimension.

is employed for the determination of D_2 and K_2 for the systems. The synchronization aspect of the coupled system is investigated and is quantified by a phase synchronization index, S_p as defined in Eq. 4.6.

The correlation dimension for the independent Rossler system is determined to be 1.93 by the use of the algorithm mentioned. This is in general agreement with the value determined earlier (Schmid & Dunki, 1996) as 1.89 and the small discrepancy in the estimated and reported values of D_2 arise from the finite length of the data set used in the evaluation of D_2 . Figure 4.4 gives the variations in correlation dimension, K_2 entropy and phase synchronization factor for the different coupling values.

The D_2 for the drive system remains at a fixed value while that for the response varies as a consequence of the coupling between the two systems. For values of low feedback, $g < 0.5$, D_2 for the response system varies almost randomly but beyond a critical feedback value D_2 for the drive and response systems appear to coincide. A close look at the plot of S_p vs. g reveals that this phenomenon occurs at the value of g where the subsystems begin to synchronize. Thus D_2 , K_2 and S_p for the response system coincide with those of the drive asymptotically with respect to g . It is also interesting to observe that the asymptotic coincidence of these parameters for the drive and response occur more or less at the same g value of ~ 0.5 . This establishes the underlying fact that synchronization between the systems translated into attractor space, is a convergence between the individual attractors of the subsystems with regard to these invariants.

The entropy, K_2 exhibits a random variation in the response system initially but beyond a certain coupling it becomes identical with the K_2 value of the drive system. This phenomenon seems to suggest that flow of information from the coupled systems occurs in an identical manner. The asymptotic behaviour of the static and dynamic parameters implies the system parameters take on finite and definite character as the coupling parameters increase. Such a case usually does not occur in biological systems and thus

simulating biological systems using nonlinear oscillators is beset with such limitations.

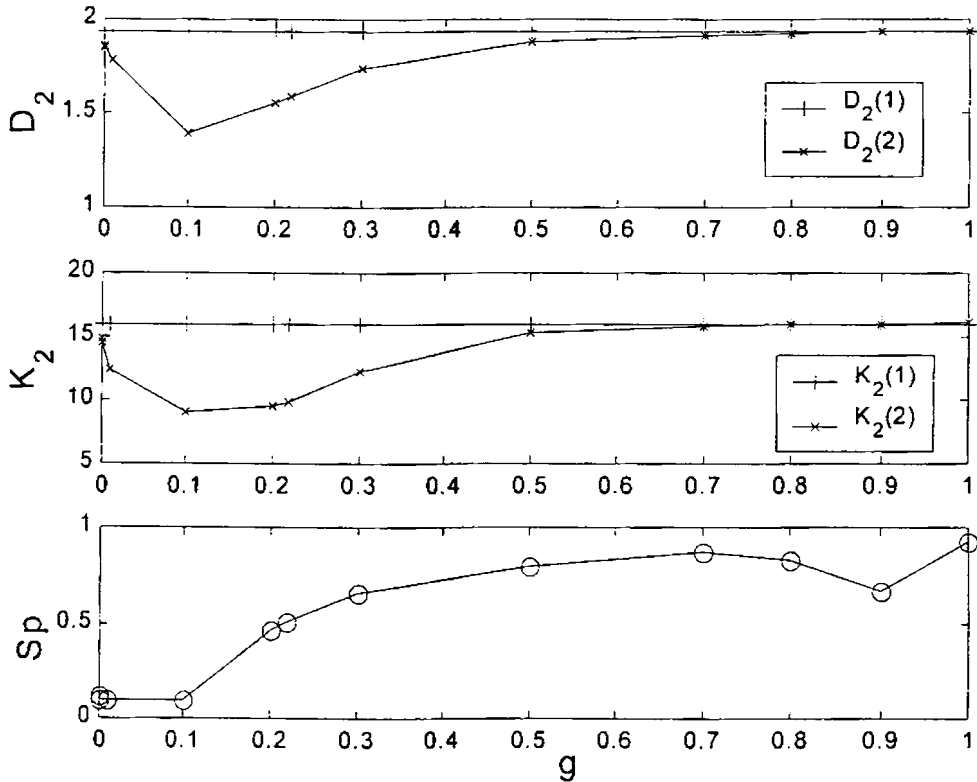


Figure 4.4. The variations in D_2 , K_2 and S_p with the coupling factor g for a unidirectionally coupled Rossler system. 1 refers to the drive system and 2 to the response.

4.4 The Bi-directional Coupling Scenario

In the system dynamics of a pair of bi-directionally coupled oscillators as in figure 4.1 (b), the coupling parameter g_1 is kept fixed while the feedback factor g_2 is scanned through a range of values corresponding to very weak

feedback from the response to the drive to that giving complete feedback i.e. $g_2 \sim 0.1\% - 100\%$. The whole procedure is repeated after raising g_1 to the next higher order of magnitude. The system behaviour in the parameter space of (g_1, g_2) with g_1 varying from 0.0001 to 1 is studied by analyzing the variations in D_2 , K_2 and S_p of the subsystems. The two systems are embedded in their respective phase spaces and the topological parameters corresponding to each of the systems are determined in these spaces. In general, once the systems are synchronized, any one of these spaces effectively acts as the phase space for the coupled system (Abarbanel, 1996). However, in this case, we are focusing on studying the evolution of the subsystems in an independent manner, under the effect of coupling. Hence, with an embedding dimension of 5, each of the subsystems is embedded in the space of lagged coordinates and D_2 and K_2 are evaluated.

Figures 4.5(a-e) depict the variations in D_2 , K_2 of the constituent systems as well as changes in S_p of the composite system as g_2 is varied from 0 to 1 for fixed values of g_1 . In 4.5(a),(b),...(e); the g_1 value increases steadily from 0.0001 to 1. However, there is great deal of parallelism in the behaviour beyond a threshold g_2 value of 0.5. The phase synchronization index, S_p becomes saturated to a value around 0.9 and the saturation starts for $g_2 \sim 0.5$. This implies that the systems get synchronized almost perfectly beyond $g_2 \sim 0.5$. Further, it may be noticed that as the value of forward coupling g_1 is steadily increased to higher orders of magnitude, the parallelism between the constituent systems sets in at earlier values of threshold feedback coupling. This effect is noticeable when compared with the unidirectional case as well in which synchronization is decided by a single coupling factor. This is the cause for the delay in the onset of synchronization

Fig 4.5(a) $g_1=0.0001$

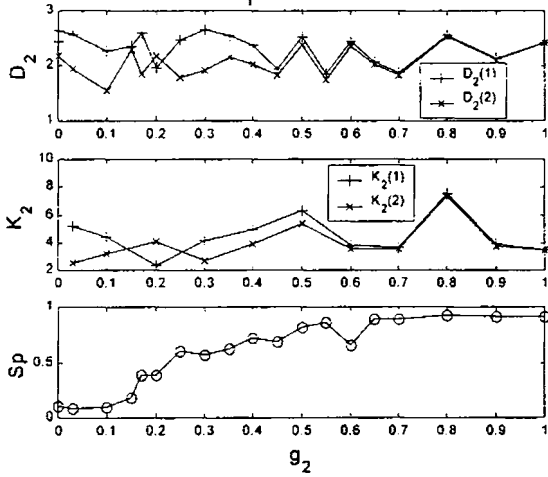


Fig 4.5 (b) $g_1=0.001$

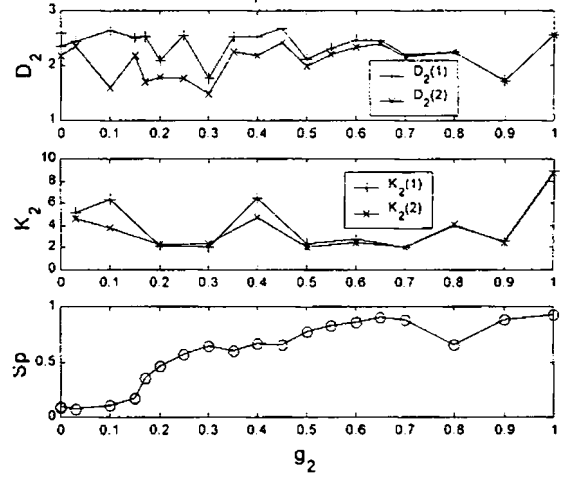


Fig 4.5(c) $g_1=0.01$

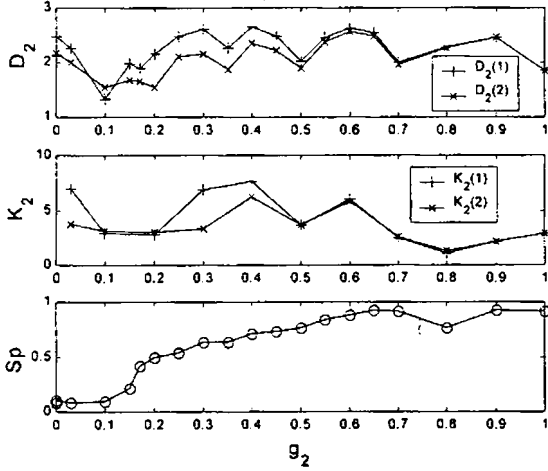
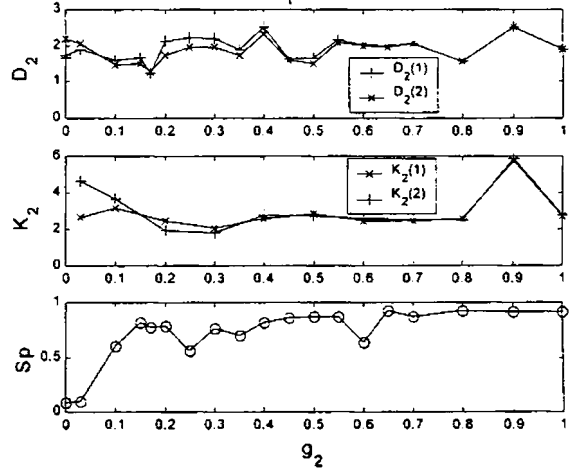


Fig 4.5(d) $g_1=0.1$



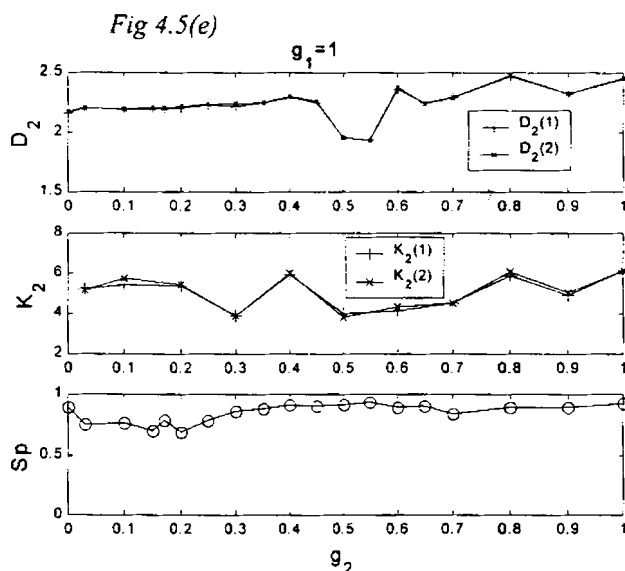


Figure 4.5 The plots exhibiting variations in D_2 , K_2 and S_p with the feedback fraction, g_2 for a mutually coupled system with gradually increasing feed forward coupling, g_1 . In (a) $g_1=0.0001$, (b) $g_1=0.001$, (c) $g_1=0.01$, (d) $g_1=0.1$ and (e) $g_1=1$.

in the unidirectional case. Moreover, once synchronization is achieved the information loss seems to be identical for both systems. Hence, the crucial factor in a mutually coupled set of Rossler oscillators, the synchronization, is the feed forward coupling percentage and the onset of the synchronization phenomenon occurs at an earlier feedback coupling as the feed forward parameter is increased. The individuality of the attractors is increasingly lost as this parameter is steadily increased. The lower values of D_2 imply that the coupling in effect brings down the number of independent variables required to modulate the dynamics of the system. In the attractor space, the variation in D_2 may be pictured as an 'expansion' or 'shrinkage' of the original attractor as the control parameters vary. In general, weak coupling tends to lower the

dimensionality of the system. The point of interest is that for the case with $g_1 \sim 0.001$, the value of $S_p \sim 0.6-0.7$ sets in when g_2 is in the interval $0.3 \leq g_2 \leq 0.4$. The parallelism in D_2 and K_2 values of the drive and response sets in only about $g_2 \geq 0.6$. This also corresponds to the region of strong phase synchronization as indicated by high S_p value $\sim 0.8-0.9$. At a higher $g_1 = 0.1$, $S_p \sim 0.8$ at $g_2 = 0.4$ beyond which the variations in the correlation dimension and entropy for the two systems follow identical variations. Thus the coincidence of the topological parameters for the coupled oscillators as well as strong phase entrainment between them sets in simultaneously at critical values of the coupling parameters. While phase synchronization by itself does not imply coincidence of topological parameters at sufficient values of coupling, strong phase synchronization is followed by an identical behaviour of the D_2 and K_2 parameters of the coupled subsystems.

4.5 Noise in the Coupled System: Effect on Synchronization

The study to this stage has been concentrated on deriving the dynamical aspects of a coupled Rossler system in its characteristic coupling parameter space depending on whether it is a uni directionally or mutually coupled system. Taking into account the fuzzy nature of coupling factors, we incorporate noise at specified levels into the coupling. The effects on the behaviour caused by the randomness due to the presence of noise in the system are analyzed. In this study, noise at a pre-determined level, represented by k is introduced into the system in the form of an additive term to the coupling factor g in the unidirectional case. The effective coupling in such a situation is $(g+kr_n)$ wherein r_n is the noise added to the system at a percentage level k . An identical noise factor is added to the feedback coupling, g_2 for the mutually coupled system. The analysis is extended to

include three types of noise-(a) normally distributed noise (Nml.), (b) uniformly distributed noise of mean 0 (Unif. 0.) and as a special case, (c) uniformly distributed noise of finite mean (Unif.). The system response in each case as contained in the synchronization is studied.

The normally distributed noise with zero mean and unit variance when introduced into the coupled system is found not to affect the behaviour to any great extent. A comparison between the noise free system and that with noise introduced, can be achieved by arbitrarily choosing a threshold of phase synchronization at $S_p=0.5$. With this criterion, we may say phase synchronization sets in at the coupling factor g at which S_p tends to 0.5 in the unidirectional case. Translating to the bi-directional scenario, synchronization

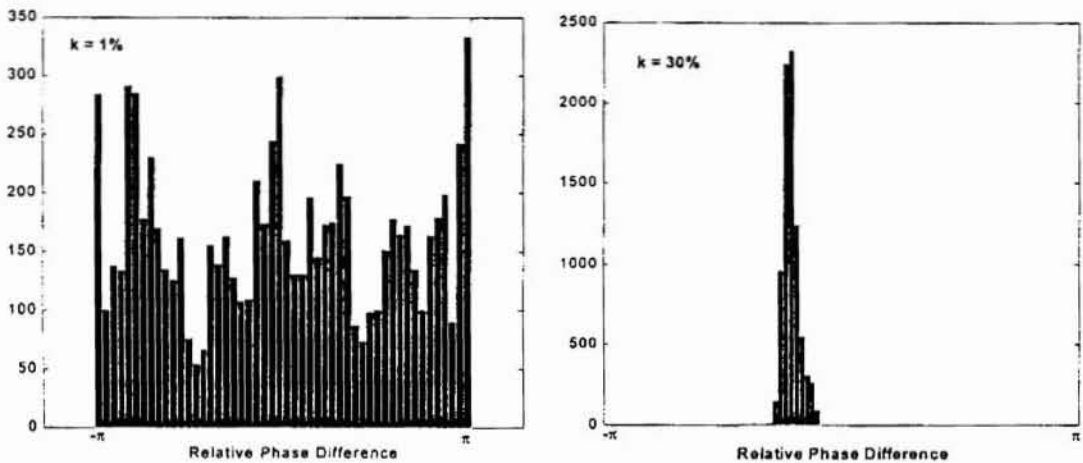


Figure 4.6. The distribution of the relative phase difference in the weakly coupled system with $g_1=0.0001$ and $g_2=0.001$. The additive noise of finite mean is added to a level of (a) 1% and (b) 30%.

is stated to occur at that value of feedback coupling g_2 for a specified g_1 at which S_p reaches a value of 0.5. Moreover, in the evaluation of phase synchronization, we have taken into account the random phase slips that may be introduced by the strong noise added to the system. We determine the distribution of the relative phase as in (Shafer et. al., 1999, Rosenblum et. al., 1998) and find that in cases where there is no phase entrainment between the systems the distribution is flat while phase entrainment gives rise to a unimodal distribution. Figure 4.6 exhibits plots of the relative phase distribution in the bi-directionally coupled system at a noise level of 1% that produces no apparent phase entrainment at low coupling parameters as compared to that at a high noise level of 30% that gives rise to significant phase entrainment even when the systems are very weakly coupled.

With a noise level of $k = 70\%$, normally distributed noise causes the uni-directionally coupled systems to synchronize around $g=0.25$ which is the g value at which the noise free system synchronizes as well. At lower values of coupling, the noise does not cause any significant change in the system behaviour. Identical behaviour is observed in the presence of uniformly distributed noise with zero mean. Figure 4.7 gives the plot of S_p vs. g for the uni-directional system with the three different types of noise mentioned above added at the constant level of $k = 70\%$. The plot reveals the interesting phenomenon of synchronization at low coupling values in the system induced when uniformly distributed noise of finite mean is added to it. It is observed that $S_p \sim 0.65$ occurs between the drive and response systems even when the coupling between them is as low as 0.001. However, once the systems synchronize, i.e. S_p beyond 0.5, the noise seems to play no significant part in the system dynamics. The behaviour exhibited by the system in the absence and presence of noise beyond the onset of synchronization is almost identical.

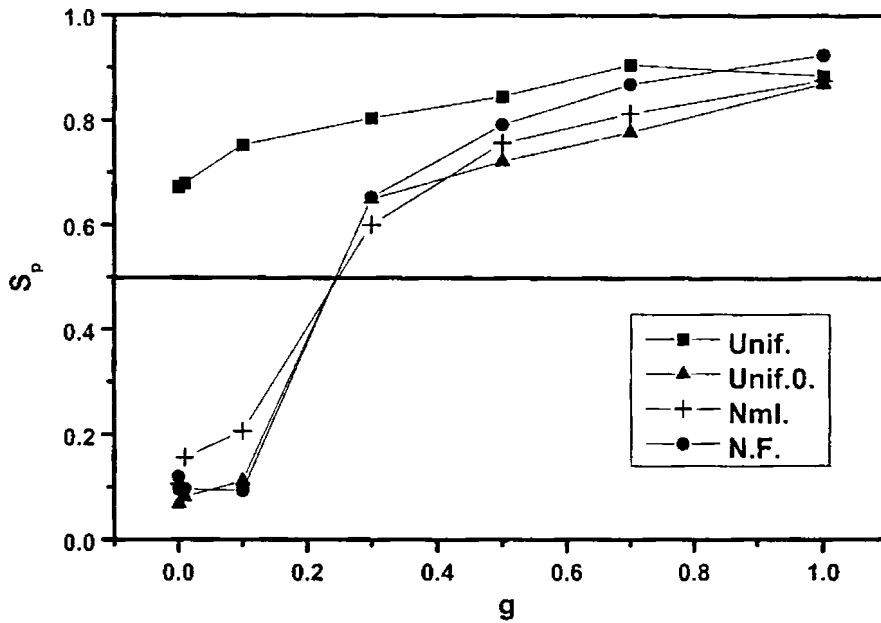


Figure 4.7. The synchronization index, S_p versus coupling, g for the uni directionally coupled system with various types of additive noise in the coupling. The noise level, k is 70% in each case. In the figure, N.F. refers to noise free case, Unif. to additive uniform noise of finite mean, Unif.0. to additive uniform noise of zero mean and Nml. to Normally distributed noise present in the system.

The plot in figure 4.8 gives the synchronization values against the coupling for the mutually coupled system for a typical case with feed forward coupling $g_1 = 0.1$. In this case, too, the uniform noise of finite mean causes the systems to synchronize even at weak coupling levels. A probable reason for this is that at high enough noise levels k , the coupling g gets added to the mean noise level to form a higher coupling in general, at which the systems are in synchrony in the noise free state. This is substantiated in figure 4.10, which shows the behaviour of the system in the presence of uniform noise of finite mean at different noise levels. It is clearly seen that the system

synchronizes sooner at higher noise levels as the coupling parameters are raised. Moreover if in the noise free case, the system was synchronizing faster (i.e. at lower couplings) then in the noisy state for the same coupling strengths, the noise level required to produce synchronization is lower.

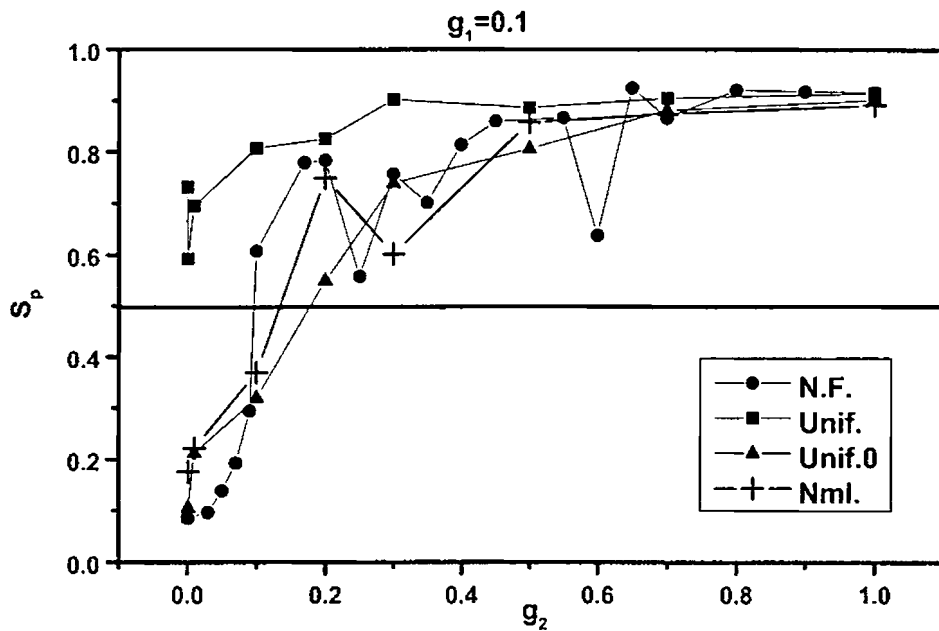


Figure 4.8. The effect of different types of noise at level $k = 70\%$ in a mutually coupled Rossler system on the synchronization as a function of the feedback coupling, g_2 for a typical case of forward coupling, $g_1 = 0.1$.

Nevertheless, the presence of phase synchronization by itself does not ensure that the dynamical parameters of the subsystems are coincident. This is still critically dependent on the coupling as evidenced in figure 4.9. Finally the effect of varying noise levels on the synchronization between systems with different feed forward coupling factors g_1 is shown. Figure 4.10(a) plots the

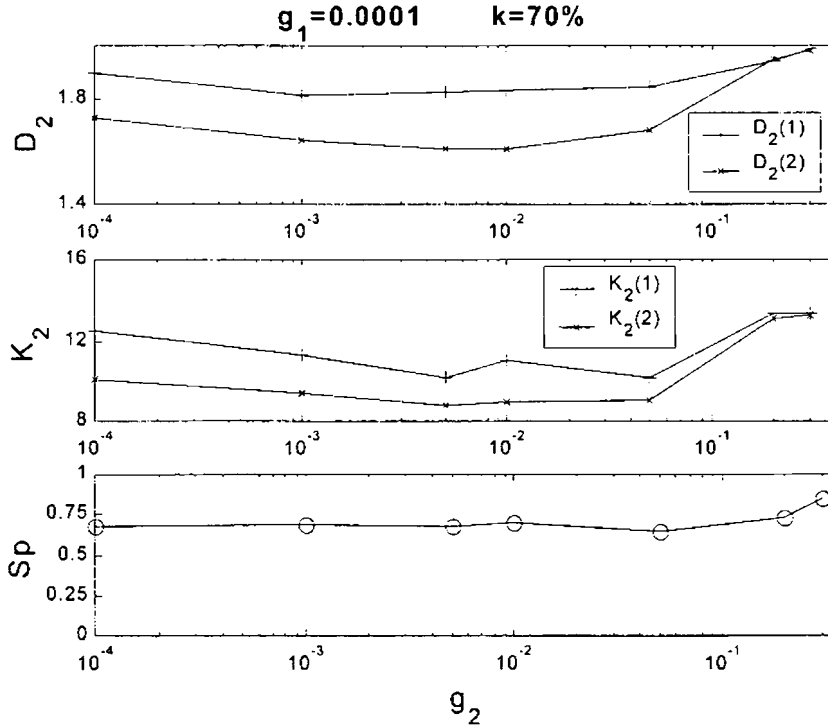


Figure 4.9. The variations in the parameters D_2 , K_2 and S_p for the coupled system with $g_1 = 0.0001$ and $g_2 = 0.001$ with additive noise at $k = 70\%$. The noise added is uniform with finite mean, Unif. The D_2 , K_2 coincidence occurs only beyond critical values of feedback coupling even though the synchronization is high at very weak coupling.

variation of synchronization for very weak forward coupling, to a moderately stronger coupling $g_1 = 0.01$. It is clear that in the latter case, since synchronization occurs sooner in the noise free state, a noise level of 30% is sufficient to induce synchronization in it as compared to the case with lower feed forward coupling.

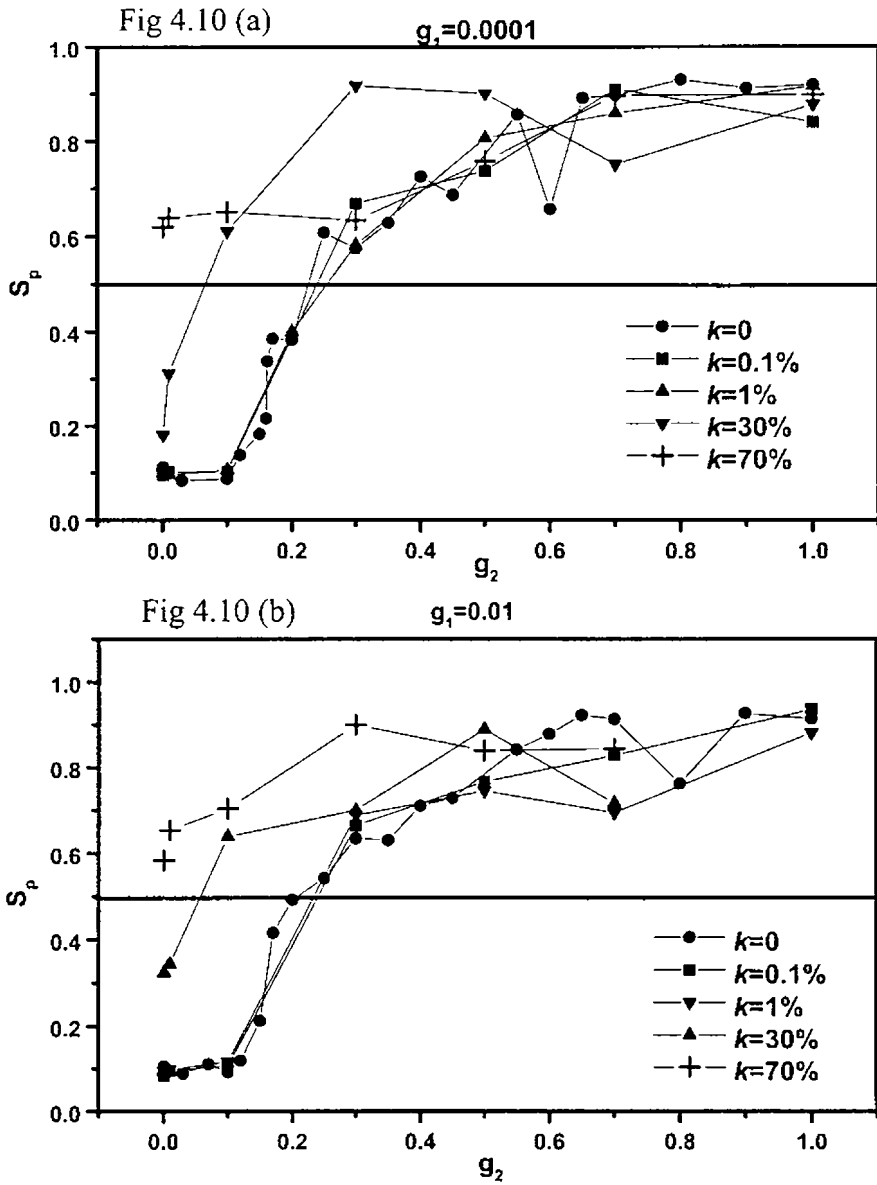


Figure 4.10. The dependence of phase synchronization on the coupling factor g_2 in the presence of various noise levels, k in the case of uniformly distributed noise with finite mean for the mutually coupled systems at two feed forward coupling values. (a) $g_1=0.0001$ and (b) $g_1=0.01$.

On the whole, the coupled Rossler system appears to be unaffected by noisy fluctuations in coupling. The normal and uniform noise with zero mean seem to produce no ill effects in the system with respect to the synchronization. Besides, uniformly distributed noise with finite mean apparently aids the system to synchronize at weak coupling.

4.6 Conclusion of the Model System Analysis

In this study, the effects of coupling on attractor dimension and coordination of a pair of coupled Rossler oscillators have been considered. Coupling two independent systems produces a variety of phenomena that throw light on the underlying dynamics of the system. The coupled systems are termed the drive and response and the connection between these is established through suitable factors. The correlation dimension (D_2) estimation reveals the variation of the corresponding parameter for the two systems in a random manner about the individual system D_2 value. Weak coupling in general lowers the computed correlation dimension, D_2 of the response and drive systems in a bi-directionally coupled scenario; thus minimizing the number of degrees of freedom required in specifying it. In the case of the neural system, millions of neurons interact in a complex manner at any instant to generate an output. In spite of there being innumerable variables in the system, a dimensional analysis reveals the dimensionality of the brain to be around 8-12 (Lutzenberger et. al., 1992; Lerner, 1996). This agrees with the result obtained in the present case of the coupled nonlinear oscillator that shows a lower dimensionality. This observation points to a possibility of modeling complex systems like the neural system as a network of coupled nonlinear oscillators.

The main interest is in the synchronization effect produced by the coupling. For a particular range of coupling parameters, we have identified a regime wherein the phases are entrained strongly. The strengths of coupling decide the point at which the systems lose their independent nature and synchronize. The onset of strong synchronization between the coupled units is translated into a coincidence of the invariant parameter D_2 of the individual systems. Once the systems synchronize, we may infer an overlap of the individual attractors with respect to the D_2 and K_2 parameters. The existence of a mathematical relation between the topological invariant D_2 of the subsystems and the phase synchronization index, S_p , that represents the coordination of the global systems suggests the underlying interdependence of these seemingly different aspects of the coupled systems. The system behaviour in the presence of noise suggests that the system is robust against the randomness that may be produced by most types of noise with a flat spectrum. However the system responds favourably to uniform noise with a finite mean in the sense that the noise induces the coupled systems to synchronize even with weak coupling. This does not mean a total coincidence of the topological parameters of the individual systems at very weak coupling. The coupled sub-systems essentially act as two independent systems albeit with a phase entrainment.

The time series data is only a manifestation of a multitude of interdependent factors giving rise to it. It has been proposed that interaction in the human brain generates a large number of attractors specified by various characteristic parameter such as embedding dimension ε_i , attractor basin B_i , generalized metric dimension D_{iq} , generalized entropy K_{iq} and Lyapunov constant λ_{iq} / Lyapunov function where i is the attractor index and q the generalization index. This is a pointer to the fact that the

interconnections between the neurons may be likened to a set of coupled nonlinear oscillators and the behaviour may be modeled based on these. The modeling of the neuronal function by using coupled Hodgkin-Huxley equations (Yoshinaga et. al., 1999) is a prime example of this idea in practice. Other attempts have been in simulating the observed characteristics of human EEG using neural network models in which the interacting units are nonlinear in nature with time delayed interactions built into the system (Bondarenko, 1994). Considerable success has also been achieved by the Freeman group (Kay et. al., 1995) in their modeling of the rat olfactory cortex using coupled oscillators. The present system has the advantage of being continuous in nature thus being capable of mapping characteristics of a real system. Moreover the presence of many parameters for fine tuning and incorporating multiple couplings makes it flexible for use in modeling complex systems in which innumerable variables may be operative at a given time making it high dimensional in nature.

The present model analysis was undertaken as an exercise in which tools of nonlinear time series may be applied to explore the dynamics of a coupled system. It throws up many interesting and significant results concerning the system attractor as well as coordination induced by coupling in noisy as well as noise-free cases. These can be used in suitably designing models for complex dynamical systems. This analysis also exhibits the emergence of collective behaviour when we consider two or more oscillators coupled together with feedback-feed forward mechanisms operative. The lowering of the coupling factor, g_2 for synchronization to occur in the closed case at higher feed forward factors may be thought of as a threshold lowering for the synchronization phenomenon. This fact has a far-reaching implication in designing artificial neural networks (ANN). Feed back in the design makes

the ANN a recurrent one. The ANN can be trained starting with low feedback coupling strengths and as the number of layers in the network is increased the observation will help in optimizing the connection strength.

The possibility of noise-induced coherence in complex systems has already been discovered in some systems. Work presented in this chapter also reveals such a possibility of noise-induced patterns in coupled nonlinear systems. One has to look into this for more details to check the possibility of occurrence of stochastic resonance in such a complex system.

Time Scales and the Unfolding of Neural Attractors

Time is one of the principal forms of the Supreme, Immortal, Unembodied Brahman. He who worships Time as Brahman, from him Time withdraws afar.

--- Maitrayani Upanishad IV, 6

The human brain is a nonlinear, non-equilibrium, stochastic and thermodynamically open system in which feedback - feed forward processes are operative. This conclusion was arrived at after a lot of meticulous research in this field. Hence to understand the collective dynamics of such a system, it is essential to know the timescales involved at the various stages of the multifold complicated process. The understanding of the brain dynamics has been of interest over the past several years by application of tools from the linear as well as nonlinear dynamics. But often enough the analysis has glossed over the time scales concept characteristic of each sub process activated in the generation of the composite complex process. Prigogine (1962) was probably the pioneer in introducing the concept of time

scales in the dynamics of a system in developing a theory of non-equilibrium statistical mechanics, which was given a stronger mathematical formulation by Balescu (1975). Pratap (1999) has carried out such a formulation for the synaptic transduction process by taking into consideration the relevant time scales of the system. The brain being a nonlinear thermodynamically open system, a meaningful theoretical analysis of its dynamics can be carried out only in the framework of non-equilibrium statistical mechanics.

5.1 Time Scales in the Neural System

The objective of the thesis is the investigation of brain dynamics during various mental states by analyzing the time varying electroencephalogram (EEG) signals using tools adopted from nonlinear dynamics and deterministic chaos paradigm. It is however imperative to have an understanding of the processes that go into the generation of electrical signals within the cerebral cortex by the action of a large number of neurons. The action potentials generated by the neurons are integrated at various stages of propagation from the sensory unit to the central nervous system (CNS) and back to the action muscle. These generate collective modes that get recorded as EEG on the scalp. A simple addition of the individual amplitudes of neuronal firings cannot reproduce the observed characteristics of EEG. Hence the integration process should be an involved mechanism. Further it has been found that the electrical characteristics of the action potential are quite different from those of EEG. While the characteristic time scale of the EEG is of the order of 0.1 sec., that of the action potential is ~ 1 msec. The difference of a factor of 100 between the two time scales implies the presence of a wide range of time scales in the dynamics. Hence the construction of a general time scale starts with identifying different characteristic parameters in neuron dynamics. A way

§

to derive the time scales based on the relevant parameters involved in the dynamics (Indic et. al., 1999) is portrayed below.

The collective effects in the cortex are studied by considering the dynamics of the individual neuron. The most significant feature in the neuron dynamics is the firing potential ϕ , which is the basic unit of information transmitted along the nerve fibre. In the neural firings a potential change is generated due to variations in Sodium and Potassium ion permeabilities of the membrane of an axon. It is known that there exists a resting potential of -80 mV and a threshold potential -50 mV. If the stimulus induces a potential difference across the membrane less than the threshold, there is no firing. Once the stimulus strength is sufficient to exceed the threshold, an action potential of about 40 mV is generated. The peculiarity of such a firing is that the amplitude of the potential remains constant while the firing frequency (ν) varies depending on the strength of the stimulus. The fact that the signal is not attenuated as it travels from one point to another both spatial and temporal indicates the nonlinear, non-equilibrium nature of the process generating it. Also there are two distinctly different classes of neurons namely inhibitory and excitatory ones. While the former class inhibits the firing process, the latter ones are those that result in excitatory mechanisms. Thus the process is distinctly different from the usual electrical conduction in a cable. The firing in myelinated axons takes place at the various nodes of Ranvier in a sequential manner. The velocity of propagation (V) forms another important parameter in the neuron dynamics. The electrical signals propagated along the length of the axon has a finite measurable speed and is about 100 m/sec. Further the system has feedback feed forward processes operative adding to its complexity.

The firing frequency is yet another important parameter and is the inverse of the refractory period of the neuron, which is the interval between two consecutive firings. It is usually about 1000 Hz and is inversely dependent on the stimulus strength. If two successive stimuli separated by a certain time interval are applied to the nerve fiber, the behaviour of the fiber will depend on the refractory time. Immediately after a nerve impulse has been initiated, the given part of the fiber is in the absolute refractory state, i.e. it cannot be excited again. This is followed by a relative refractory state in which the threshold potential is somewhat increased. The same neuron can have different refractory times at different instants, but they all have a greatest lower bound. The duration of the entire refractory time varies from one to a few milliseconds.

The action potential is generated by the action of electrical species such as ions of sodium, potassium, calcium etc., and these are characterized by an electrical charge (e) and ion mass (m). A signal received by one nerve or a group of nerves will be communicated to a large number of nerves by a cascading process through the axonal tree, the branches of which end in synapses connecting them with other cell bodies and dendrites. This cascade process will however not connect all neurons in the systems but will end up with the distribution of regular tubes and stripes. Hence one can define a number density (n) that represents the number of neurons per unit volume. This can also be defined as the fraction of affected neurons to total neurons in a unit volume. The chemical processes play a significant role in signal transmission by changing the electrical conductivity of the medium. This is represented by a non-dimensional parameter, ϵ_0 , representing the conductivity. It may however be realized that this by no means completes the set of parameters that constitute the dynamics in the brain. There could still

be many more processes unknown at this point of time, due to interplay of various parameters. Hence the above set may be considered an incomplete set, which is currently known. The above parameters along with the numerical values that go into the construction of a general time scale are given in Table 5.1.

Using these parameters, a dimensional analysis following Balescu (1975) can be performed to obtain the general time scale of the process in the following manner.

$$T = \phi^i V^j q^k \nu^p m^r n^s$$

$$= (\text{MLT}^{-2})^{i/2} (\text{LT}^{-1})^j (\text{ML}^3 \text{T}^{-2})^{k/2} (\text{T}^{-p}) (\text{M}^r) (\text{L}^{-3s}) \quad (5.1)$$

Equating powers of M, L and T on both sides we have

$$\begin{aligned} \text{Power of M} \Rightarrow \quad & \frac{i}{2} + \frac{k}{2} + r = 0 \\ \text{Power of L} \Rightarrow \quad & \frac{i}{2} + j + \frac{3}{2}k - 3s = 0 \\ \text{Power of T} \Rightarrow \quad & -i - j - k - p = 1 \end{aligned} \quad (5.2)$$

There are only three equations with six unknowns. So expressing p, r and s in terms of i, j and k, we get,

$$\begin{aligned} p &= -i - j - k - 1 \\ r &= -\frac{i}{2} - \frac{k}{2} \\ s &= -\frac{3}{2}i + \frac{1}{3}j + \frac{1}{2}k \end{aligned} \quad (5.3)$$

Table 5.1: The relevant parameters in the neural system with typical numerical values for each.

Name	Symbol	Dimension	Order of magnitude
Action potential	ϕ	$(MLT^{-2})^{1/2}$	10^{-1} volts
Propagation speed	V	LT^{-1}	100 m/seconds
Firing frequency	ν	T^{-1}	1000 Hz
Ionic charge	q	$(ML^3 T^{-2})^{1/2}$	1.6×10^{-19} Coulomb
Ionic mass	m	M	10^{-27} Kg
Ionic density	n	L^{-3}	2mM
Medium effect	ϵ_0	-	-
Ion plasma frequency square	ω_p^2	T^{-2}	$10^3 z \mu^{-1/2} n^{1/2}$ rad /sec

Substituting Eqs. (5.3) in Eq. (5.1) a general time scale is obtained as

$$T = \Gamma \nu^{-1} \quad (5.4)$$

where Γ is a dimensionless quantity defined as

$$\Gamma = \left(\frac{\phi^2 n^{1/3}}{m \nu^2} \right)^{i/2} \left(\frac{V n^{1/3}}{\nu} \right)^j \left(\frac{\epsilon_0 q^2 n}{m \nu^2} \right)^{k/2} \quad (5.5)$$

Expressing $i/2 = x$, $j = y$ and $k/2 = z$, Eq. (5.5) takes the form,

$$\Gamma = \left(\frac{\phi^2 n^{1/3}}{m v^2} \right)^x \left(\frac{v n^{1/3}}{v} \right)^y \left(\frac{\epsilon_0 q^2 n}{m v^2} \right)^z \quad (5.6)$$

In Eq. (5.6), x , y , z can take real or complex values. There could exist complex frequencies since the system is nonlinear. But for linear systems, x , y and z are real, rational numbers.

A general time scale T can be constructed as

$$T = \Gamma v^{-1} = a^x b^y c^z v^{-1} \text{ (say)} \quad (5.7)$$

The dimensionless quantity, Γ consists of three parts, the first one depends on the electrodynamic variable ϕ besides the dynamic variable firing frequency. This is the resistance per unit length per unit time. The second term consists of only mechanical variables and is the ratio of the distance traveled by the signal during a refractory period to a characteristic length defined by $n^{1/3}$. This signifies the transport process in the nerve fibres that carry the signal from one portion to another. In the third term however one

can write $\left(\frac{\epsilon_0 q^2 n}{m v^2} \right)$ as $\left(\frac{\epsilon_0 \omega_p^2}{v^2} \right)$ with ω_p as the ion plasma frequency.

The third term is the ratio of the square of the plasma frequency to the firing frequency and this characterizes the collective behaviour. Since n represents the neuronal density, this is the collective activity in which a large number of neurons participate.

Thus Eq. (5.7) consists of three parts:

- a: ratio of electric frequency to firing frequency.
- b: ratio of mechanical frequency to firing frequency.
- c: ratio of plasma frequency to firing frequency.

The indices x , y and z are natural numbers. They can be real or complex, rational, irrational or integral. If they are complex, the process can have time dependent amplitude and phase. If they are rational, the frequencies are compatible while if the frequencies are irrational, they are incommensurate. From Eq.(5.7) it is very clear that there exist three fold infinite time scales in the system. This point is very important in the analysis of EEG signals. Further, this clearly shows that the electrical, mechanical and plasma frequencies can be independent. However they can also get coupled by the choice of x , y and z . By proper choice of variables x , y and z the relevant time scales corresponding to the three different known processes can be retrieved and they are derived below.

1. **Sodium Potassium pump:** The Sodium Potassium pump depends on the threshold potential and hence on ϕ . Since it is a chemical process depending on the number of sodium ions going in and potassium ions coming out during the depolarization phases, the time scale should depend on mass and number density, as well but not on the firing frequency. To get the relevant time scale corresponding to this process, one must choose $y = z = 0$ and $x = -1/2$. Thus relevant time scale for this process is with $\phi \sim$ millivolts and $n \sim 100$

$$T_p = \left(\frac{m}{\phi^2 n^{1/3}} \right)^{1/2} \quad (5.8)$$

2. **Synaptic transduction:** The synaptic transduction process depends on the dielectric characteristics of the synaptic cleft as also on the speed at which the signal arrives at the pre synapse as well as the threshold potential. However, there is no explicit dependence on the number density, since there

is randomness in the injection of neurotransmitters in the cleft due to the discharge of vesicles. A time scale is constructed by a proper choice of x, y, z viz. $x = -y = z = -1/2$. Thus the time scale is obtained as

$$T_s = \left(\frac{mVv}{\epsilon_0 \phi^2 \omega_p^2} \right)^{1/2} \quad (5.9)$$

3. **Collective modes:** At various stages in a neural system, there are integration processes operative. The threshold potential is a consequence of the integration process. In a single neuron or in the case of synaptic transduction the process is always collective in nature. Also in the case of EEG signals, the process is indeed a collective one, which does not exhibit all the apparent regularities seen in single neuron firing sequence or the signal transmission from a pre synapse to a post synapse. If we consider this as a self-consistent process, which is in general responsible for the collective modes, then the relevant time scale is the interaction time scale,

$$T_i = (\epsilon_0 \omega_p^2)^{-1/2} \quad (5.10)$$

and this is obtained by setting $x = y = 0$ and $z = -1/2$.

Thus different time scales suitable for different mechanisms can be derived from the general time scale. There may be other relevant parameters. However, in this formulation only some of the known ones are considered. In the absence of an understanding of neuronal activities one cannot stipulate the domain of x, y and z . Hence, by substituting values of x, y and z arbitrarily a few more time scales are derived and are presented in Table 5.2. It is evident from the table that there exists a large class of time scales with a wide range of magnitude. The different values of ionic density would give

different values of x , y and z . However, in this construction the ionic density is taken as 10^6 m^{-3} .

Many authors in studying the dynamics of human brain have ignored the role of time scales. Parikh and Pratap (1984) developed an evolutionary equation in the framework of nonequilibrium statistical mechanics developed by Prigogine and his Brussels School in which the significance of time scales has been stressed. Further Pratap (1999) formulated a theory of sensory transduction considering the interaction time scale.

Table 5.2: Some typical time scales in the system for specific values of x , y , z .

Name	x	y	z	Time scale	Order of magnitude
Mechanical	0	-1	0	$\left(Vn^{1/3}\right)^{1/3}$	10^{-4}
Refractory	0	0	0	v^{-1}	10^{-3}
Electromechanical	1/4	-1/2	-1/4	$\left(\frac{\phi}{Vqvn^{2/3}}\right)^{1/2}$	10^7
Electromagnetic	1/2	0	-1/2	$\left(\frac{\phi}{qVn^{1/3}}\right)$	10^{19}

is randomness in the injection of neurotransmitters in the cleft due to the discharge of vesicles. A time scale is constructed by a proper choice of x , y , z viz. $x = -y = z = -1/2$. Thus the time scale is obtained as

$$T_s = \left(\frac{mVv}{\epsilon_0 \phi^2 \omega_p^2} \right)^{1/2} \quad (5.9)$$

3. Collective modes: At various stages in a neural system, there are integration processes operative. The threshold potential is a consequence of the integration process. In a single neuron or in the case of synaptic transduction the process is always collective in nature. Also in the case of EEG signals, the process is indeed a collective one, which does not exhibit all the apparent regularities seen in single neuron firing sequence or the signal transmission from a pre synapse to a post synapse. If we consider this as a self-consistent process, which is in general responsible for the collective modes, then the relevant time scale is the interaction time scale,

$$T_i = (\epsilon_0 \omega_p^2)^{-1/2} \quad (5.10)$$

and this is obtained by setting $x = y = 0$ and $z = -1/2$.

Thus different time scales suitable for different mechanisms can be derived from the general time scale. There may be other relevant parameters. However, in this formulation only some of the known ones are considered. In the absence of an understanding of neuronal activities one cannot stipulate the domain of x , y and z . Hence, by substituting values of x , y and z arbitrarily a few more time scales are derived and are presented in Table 5.2. It is evident from the table that there exists a large class of time scales with a wide range of magnitude. The different values of ionic density would give

different values of x , y and z . However, in this construction the ionic density is taken as 10^6 m^{-3} .

Many authors in studying the dynamics of human brain have ignored the role of time scales. Parikh and Pratap (1984) developed an evolutionary equation in the framework of nonequilibrium statistical mechanics developed by Prigogine and his Brussels School in which the significance of time scales has been stressed. Further Pratap (1999) formulated a theory of sensory transduction considering the interaction time scale.

Table 5.2: Some typical time scales in the system for specific values of x , y , z

Name	x	y	z	Time scale	Order of magnitude
Mechanical	0	-1	0	$\left(Vn^{1/3}\right)^{1/3}$	10^{-4}
Refractory	0	0	0	v^{-1}	10^{-3}
Electromechanical	1/4	-1/2	-1/4	$\left(\frac{\phi}{Vqvn^{2/3}}\right)^{1/2}$	10^7
Electromagnetic	1/2	0	-1/2	$\left(\frac{\phi}{qVn^{1/3}}\right)$	10^{19}

The concept of time scales is crucial to the development of the theory nonequilibrium statistical mechanics of brain. Practically, a direct consequence of the presence of such innumerable time scales in human brain dynamics is the nonstationarity of the signal, which affects the computation of invariant parameters characterizing the attractor of the dissipative nonlinear system under study.

5.2 Unfolding of Neural Attractors - A Time Scales Viewpoint

Knowledge that the brain dynamics is complex, combining various sub-processes depending on the various time scales, makes imperative the identification of relevant time scales as well as understanding the effect of different time scales on the estimation of various parameters representing the system (Indic et. al., 1999). The presence of different time scales and the major role they play on the information content of EEG analyses has been stressed in a recent communication (Indic, 1999). It was shown that the presence of multiple time scales in the dynamics is probably the reason for the computed parameters such as D_2 and K_2 being slowly varying functions of time. Hence, the study of these parameters must always be conducted by keeping in mind the idea of numerous, probably overlapping time scales in the dynamics of the brain.

In nonlinear time series analysis, the correlation dimension, D_2 which is one of the ergodic parameters commonly used to characterize a brain state is found to saturate to a stable value at high enough embedding dimensions. The evaluation of a stable value for this parameter is beset with a large number of practical problems such as finite data size, noise etc. (Rapp 1993, Abarbanel et. al., 1993) and these have been discussed in some detail in an earlier chapter. Notwithstanding this, the efficacy of the parameter as a

characterizing one for EEG segments from various mental states is more or less established and widely accepted. The most popular time series method for D_2 evaluation follows the Grassberger–Procaccia (G-P) algorithm or a variant of it. This is based on the Taken’s delay embedding method and depends crucially on the embedding dimension as well as the time lag chosen in constructing the vectors of the pseudo phase space of the system.

A short coming of the G-P approach of evaluating D_2 lies in using the information for sufficiently large embedding dimension m while discarding any information for low m . Schmid and Dunkii (1996) introduced the concept of the unfolding dimension by considering bi-parametrization of the curve of D_2 as a function of the embedding dimension, m . In their study, the bi-parametric analysis displayed results in support of the idea that it is possible to relate human EEG to the individual from whom it is obtained and this relation remains stable over time. Also this analysis exhibited a difference between different functional states of the brain. The parameters satisfied the pre-requisites of intra-individual stability as diagnostic markers on a per individual basis.

In the present case, we make use of the fact that the unfolding of the system attractor at each embedding dimension leading to saturation in D_2 depends crucially on the time scale chosen in the delay embedding. The study undertaken here looks into the effect of varying time lags in the embedding on the unfolding behaviour of the neural attractors in different mental states. The time lag in the delay embedding is an estimate of the time scale of the signal arising from the complex interactions taking place within the system. Thus such an analysis is actually a design to investigate the variations in the unfolding nature of the neural attractors resulting from the different dynamics following each mental state.

5.2.1 Method of Analysis

The correlation dimension provides information about the degrees of freedom of the attractor in the phase space of the complex system and for neuroscientists it is a measure of potential *clinical* importance. In the pseudo phase space of the system, the EEG signal is subjected to time delay embedding (Abarbanel et. al., 1993). If $v(t)$ is the EEG signal sampled regularly at the rate τ_s , we can reconstruct an m -dimensional space as

$$V(t) = [v(t), v(t + \tau_d), v(t + 2\tau_d), \dots, v(t + (m - 1)\tau_d)] \quad (5.11)$$

wherein τ_d is the chosen time delay. N is the total number of data points used for the embedding and m is called the embedding dimension. In order to evaluate the correlation dimension in this m -dimensional space, the Grassberger–Procaccia (G-P) algorithm (Grassberger & Procaccia, 1983) modified for finite length of the data set (Havstad & Ehlers, 1989) is employed.

Evaluation of correlation dimension, D_2

One of the popular methods for choosing an appropriate embedding dimension, m is that of false nearest neighbours (Abarbanel, et. al., 1993). Such methods are increasingly used in this line of work to avoid the tedious computation involved in repeatedly estimating D_2 at successively increasing embedding dimensions. For sufficiently large values of m , $D_2(m)$ saturates. The value of m at which the saturation sets-in is the embedding dimension of the system and the saturated value give the correct estimate of D_2 . However, the estimation depends also on the time lag τ_d involved in the reconstruction.

The method to arrive at the correct value of time lag is to repeatedly estimate the measure at successively higher lags and choose the optimum value at which the value of the parameter saturates. However the method based on the linear technique of auto correlation function (ACF) and its nonlinear counterpart, average mutual information (AMI) (Fraser & Swinney, 1986, Martinerie, et. al., 1992) have been used to decide on a suitable time lag. In the case of ACF, the time at which the function e-folds to its initial value or the first zero crossing point is chosen as the time lag. On the other hand, for mutual information, the criterion of choice is the time point of the first minimum of the function. If such a choice (τ_d) is made; the time scales lying in the interval (0- τ_d) are not taken into account and this may affect the evaluation of dynamical parameters.

The unfolding dimension parameter

The correlation dimension evaluated at successively increasing embedding dimension at a certain time delay gives a curve $D_2(m)$ and a bi-parametric fit has been proposed for this curve (Schmid & Dunkii, 1996). This fit is given as,

$$D_2(m) = b_0 \left[1 - \exp\left(-\frac{m}{m^*}\right) \right] \quad (5.12)$$

where m^* is a parameter known as the unfolding dimension and b_0 is the asymptotic value of $D_2(m)$. The unfolding dimension is a measure of the rate at which an attractor unfolds with increasing m . In usual practice, m^* is evaluated by fitting the curve of $D_2(m)$ against increasing embedding dimension at some optimal value of the time lag (Dunkii & Schmid, 1998). The question of how the numerous timescales existing in the brain contribute

to the attractor unfolding is yet to be addressed. As a case study we determine the correlation dimension $D_2(m)$ of the EEG data for progressively increasing embedding dimensions as also for varying values of time delay τ_d . In each case, a bi-parametric fit is made to $D_2(m)$ and the unfolding dimension parameter m^* is determined. The analysis leads to an insight into the behaviour of the unfolding dimension, m^* as a function of time. The study also throws light on the effect of active time scales in the system on the dynamics of the brain characterized by the correlation dimension.

5.2.2 Data Specifications

In this study we have analyzed the EEG data collected from (a) normal persons in eyes closed condition (EC) and (b) an epileptic patient during a period of non-epileptic discharge (NED) as well as during an epileptic discharge (seizure) (DED). In each case, 5 patients are studied and the results presented are representative of the whole group. During the recording, the EEG machine was coupled to a PC using an analog to digital converter (DT- 2841) and an array processor (DT-7020). The acquired data is sampled at a rate of 512 samples/s/channel and filtered using a FIR digital filter of order 150 with a bandwidth of 0.1-32 Hz. Visual screening of data is carried out to identify artifacts.

The EEG data under epileptic condition were collected from subjects who volunteered who were known epileptics with uncontrolled seizures in the age group of 20-25 years. Despite anticonvulsant medication, the subjects showed seizure discharges in their EEGs. The raw EEG signals were filtered through a band pass (0.05-32 Hz) fourth order Butter worth filter twice cascaded. The filtered data was found to be suitable for visual analysis by the neurologist. The records were scored as definite epileptic discharge (DED),

probable (PED) and non-epileptic discharge (NED) independently by two experts who differed in their scorings by less than 5%. The differences were resolved by discussion and a consensus rating was assigned to the discrepantly rated epochs.

5.3 Analysis of the Time Scale Effect

The EEG data is subjected to time delay embedding by choosing a low value of the embedding dimension m . The time delay, τ_d is initially chosen at a low value. The correlation dimension is determined at each choice of τ_d increasing m from 2 to 16. In each case the bi-parametric fit leads to a value of the unfolding dimension, m^* . The value of τ_d is then varied to a slightly higher value and the process repeated. The behaviour of m^* with time lag is studied.

5.3.1 Normal Eyes Closed Condition

It is observed that for the eyes closed condition; the unfolding rate increases with increasing time delay and finally reaching saturation. The analysis is carried out for the EEG data obtained from the left frontal (Fp1) region. For a sample data set of 1024 points, the ACF evaluation gives the time corresponding to $(1/e)^{\text{th}}$ of the initial value is found to be $\tau_{(ac)} = 10$ while characteristic time scale calculated from AMI is $\tau_{(am)} = 14$. This particular state is characterized by a $D_2 = 6.018$ evaluated at the AMI time lag and embedding dimension 15. The correlation dimension $D_2(m)$ is evaluated for τ_d varying 1 to 30, chosen randomly and in each case, m^* and b_0 are evaluated from the exponential fit to $D_2(m)$. Figure 1 shows a few $D_2(m)$ curves corresponding to certain typical time delays.

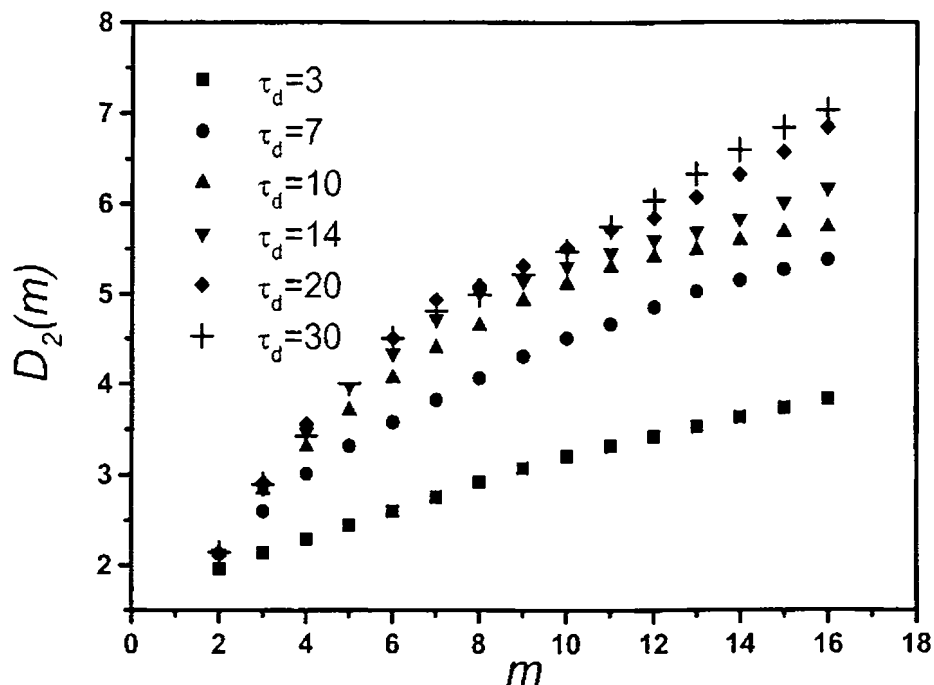


Figure 5.1 A set of curves of the correlation dimension, $D_2(m)$ as a function of the embedding dimension, m for various values of the lag time evaluated for FpI region under eyes closed condition.

The bi-parametric fit is made to each of the curves for varying values of time lag and the fit parameters b_0 and m^* are tabulated in table 5.3. It is seen that as time lag increases beyond 30, the vectors get projected onto totally uncorrelated directions giving very high and slightly erratic values of D_2 . For this reason, the highest chosen time lag is about 30. Also the maximum embedding dimension is restricted to about 18.

Table 5.3: A typical set of fit parameters b_0 and m^ obtained for the various time lags for region Fp1.*

Time lag τ_d	b_0	m^*
1	2.37283	2.545
3	3.6993	4.186
7	5.46546	5.28
10	5.93792	4.982
11	6.00821	4.85
14	6.22736	4.974
16	6.89269	5.725
20	7.35259	6.56
30	6.71074	6.22

The nature of unfolding with increasing time lag can be studied from figure 5.2 which depicts the variation of m^* with the varying time scale. It is obvious from the curve for the varying τ_d , that while there exists a tendency for saturation of D_2 at $\tau_d = 10$, this is lost at $\tau_d = 7$ as also at $\tau_d = 14$. There seems to be a critical value of τ_d where a perfect saturation is achieved and this may be chosen as the lag time for the evaluation of parameters like D_2 and K_2 . A fine scan of the curve for a closer grid of τ_d between $\tau_d = 7$ and $\tau_d = 14$ would probably give this critical value of τ_d . This region is also indicated in

figure 5.2, corresponding to region C3 between $\tau_d = 7$ and 14. We observe a plateau in C3 and a slightly different region in Fp1. This implies that different attractors exist at different points on the skull space and hence in the whole skull space one could expect a distribution of attractors. The unfolding dimension remains within certain bounds and beyond a critical time scale shows no further rise.

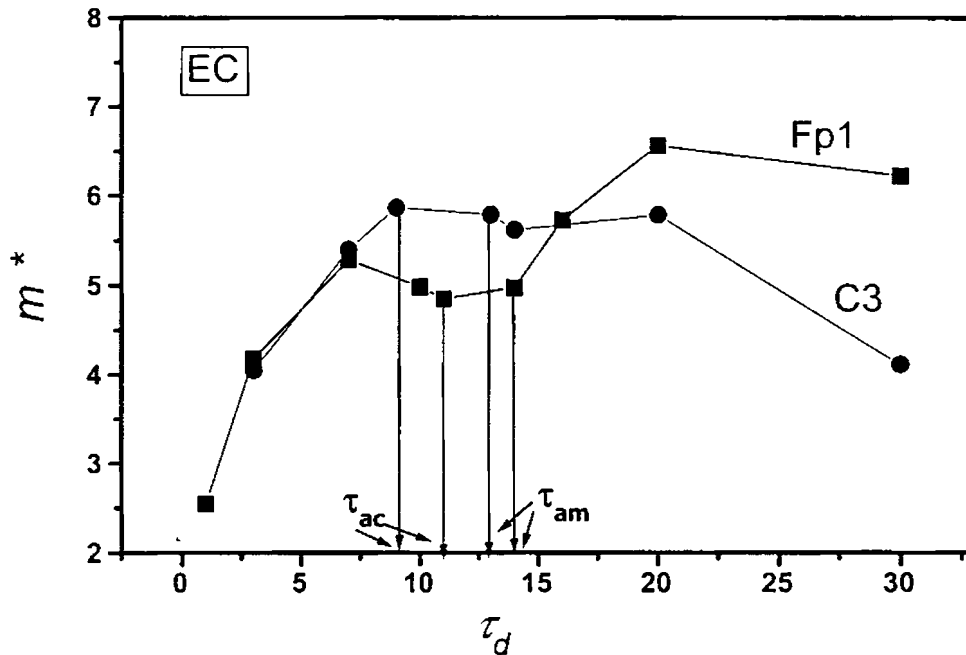


Figure 5.2. A plot showing the behaviour of the unfolding dimension parameter, m^* with varying time scale for the two brain regions Fp1 and C3 in eyes closed state. The time lags corresponding to AMI and ACF for each region are also indicated

While it is indeed true that the time scale determined from ACF or AMI is adequate for reconstruction purposes, those cases are not rare in which the attractor has not unfolded fully. This becomes all the more crucial if we look

into the time scales involved in pathological cases. It has been pointed out earlier that during pathological conditions, the different time scales in the system may be interacting with each other, thus affecting the estimation of the system parameters in a complex fashion.

5.3.2 Pathological Condition of Epilepsy

Epilepsy is a common pathological brain disorder resulting from seizures that temporarily impair brain function afflicting about 50 million people worldwide in some form. Research on this malady continues at a vigorous pace, with investigations ranging from how microscopic particles in the cell trigger seizures, to the development of new antiepileptic drugs as well as in epileptic seizure prediction. On an extracellular level, epilepsy phenomenon is characterized by the abnormal hyper synchronous activity of neuronal networks. These and the paroxysmally bursting units cause the steep high amplitude field potentials observed during epileptic condition.

In the present analysis, we consider the EEG of a subject during a definitive epileptic discharge (DED) and also during a non-epileptic discharge (NED) state. For the data from the Fp1 region, the autocorrelation, ACF criterion yields a time scale of $\tau_{(ac)} = 16$ and average mutual information, AMI gives a time scale of $\tau_{(am)} = 25$ during DED and for NED, $\tau_{(ac)} = 8$ and $\tau_{(am)} = 13$. The DED state at $m=15$ and $\tau_d = \tau_{(am)}$ gives a $D_2 = 4.804$ while for the same parameters, NED state has $D_2 = 6.889$. The unfolding analysis during DED yields an unfolding dimension m^* that increases with τ_d . Even beyond the $\tau_{(am)}$, m^* continues to increase implying an unfolding at a higher rate at higher time lags. Figure 5.3 shows the m^* behaviour with increasing time lags during DED and NED for Fp1 region. Interestingly, in spite of the low time scales as in $\tau_{(ac)}$ and $\tau_{(am)}$ estimates of NED, the unfolding dimension shows a

growth with increasing time lags. Despite the NED state having a relatively higher value of D_2 as compared to DED, m^* behaves in a similar manner for both.

The time scales are thus found to influence the rate of unfolding of the attractor in the DED as well as NED state and play a major role in deciding the course of the system evolution. This non-saturation of m^* in the NED case seems to point to the presence of higher time scales hidden in the dynamics, which are not directly visible from a linear (ACF) or nonlinear (AMI) viewpoint which are quite low as compared to the state of DED. This could be taken to mean that the time scales in the epileptic state are *latently* present in the system and that they affect the attractor unfolding and consequently the system dynamics as contained in the evolution of the parameters describing the system. The underlying time scales may not be fundamental in nature but arise as a result of interactions between different time scales during a complex brain experience such as epilepsy.

The same analysis carried out for region T4 gives slightly different results. In this region, the DED state is characterized by a $\tau_{(ac)} = \tau_{(am)} = 19$ and a D_2 value of 4.41 and NED is characterized by $\tau_{(ac)} = 10$ and $\tau_{(am)} = 13$ with $D_2 = 8.145$. The DED signal shows a behaviour of growth in unfolding dimension with increasing time lag which points to higher time scales underlying the dynamics. In contrast, the unfolding dimension in the NED case, seems to grow with time, reach a maximum and then saturate. This suggests a region in the brain that seems not too affected by the underlying epileptic discharge since it seems to have recovered the normal activity as evidenced by the lowering of time scales. The analysis of unfolding of attractors as a function of the time scales provides an insight into the behaviour of different brain regions to the same conditions of DED and NED.

This result seems to promise a great deal of clinical application when considering the regions that are apparently strongly affected by an epileptic discharge in contrast to weakly affected ones.

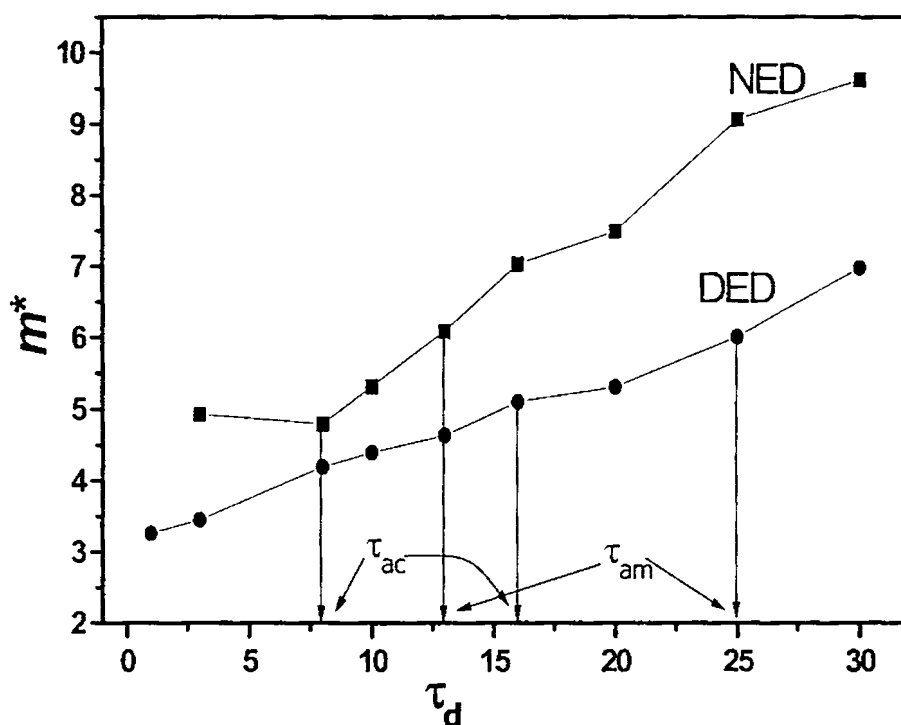


Figure 5.3: The behaviour of the unfolding parameter, m^* with time lag for the DED and NED portions of epileptic EEG recorded from the Fp1 region.

5.4 Conclusion

The human brain consists of a multitude of processes for which some of the relevant parameters are yet to be identified. This causes a wide spread in the time scales of the interacting processes from which the complex dynamics

emerge. An attempt is made to construct a general time scale for the dynamics by taking into account the many variables of the system. Some of the important processes such as Na-K pump, synaptic transduction etc. are characterized by particular choices of the indices in the general time scale relation. This also points to the probable existence of three fold infinite time scales in the system (Indic et. al., 1999) some of which may be overlapping as well. An optimization procedure to estimate the bounds on the x,y,z seems to be a quite interesting possibility and this in turn can provide relative contributions of the three processes towards the production of the existing complex state. The parametric domain of x,y,z can however be expanded by taking more variables than those in Eq. 5.1 and this in turn would reveal more significant processes that we can look for in brain dynamics.

In the study undertaken here, a nonlinear time series analysis is applied to the EEG signal recorded under normal relaxed state and during a pathological state to deduce the effect time scales may have on the unfolding of neural attractors. This has been done by analyzing the variation of the correlation dimension as a function of both the embedding dimension as well as the time delay. A bi-parametric fit is applied to this function which yields a parameter known as the unfolding dimension that is a measure of the unfolding rate of the system attractor at a given time scale. The behaviour of this unfolding rate with time is monitored in the case of normal subjects in eyes closed condition as well as for the pathological case of epilepsy when the subject is undergoing a seizure as well as during a non-epileptic discharge period. This method is proposed to be extended for the study of less understood conditions such as mental depression and slight mental derangement.

A few interesting observations are explained here. The ability of the unfolding dimension as a distinguishing parameter of different brain conditions makes it a good functional marker as discussed by Schmid & Dunki (1996). A direct D_2 evaluation fails to throw light on all the time scales inherent in the system. It has also been already proved that the evaluation of the information capacity, contained in the Kolmogorov entropy is affected by the choice of time delay (Indic, 1999). However, we have observed that the lag time controls the saturation feature in the determination of D_2 / K_2 as in the G-P algorithm. This further brings out the arbitrariness of the currently used methods of AMI or ACF. The close connection between the unfolding parameter variation features with the plot of D_2 against lag time has shown that an unfolding parameter analysis is more robust and reliable to choose the lag time. The possibility of determining the various overlapping time parameters in the complex system is also revealed.

In the case of normal eyes closed condition, a saturation of the unfolding dimension sets in at moderately low time lags. This seems to point to the presence of a critical time lag at which the system attractor unfolds completely. In contrast to the normal eyes closed state, for a definite epileptic seizure no saturation of m^* sets in suggesting a completing unfolding of the neural attractors only at higher time scales. Also, the distinct behaviour shown by the non-epileptic EEG segments of different brain regions is also of significant importance. It seems to suggest that the effects of the seizure activity may be concentrated in certain brain regions and as such, this is probably of high clinical importance. The present analysis also reveals the fact that there is distinctness in the behaviour of attractors at different brain regions. Thus considering the skull space as a geometric one, it contains a large variety of attractors of varying parameters and hence a study of the

system as constituted by a collection of attractors is more realistic. On the basis of this a nonequilibrium statistical dynamics for the brain was recently developed (Pratap, 2000).

Time scale analysis thus seems to be an important factor in the evaluation of parameters used to characterize the brain. Some work in this direction has been carried out in the study of signal transduction (Pratap, 1999) in which a nonlinear process was formulated for the phenomenon by taking into consideration the relevant time scales of the system. While the evaluation of invariant parameters is indeed important when studying a complex system as the brain, of more significance is the development of a comprehensive model that considers the brain as a dynamical system and leads to the estimation of the various characterizing measures and possesses predictive capability as well. Quite a few efforts have been made in this direction (Amit, 1989; McCulloch & Pitts, 1993; Parikh & Pratap, 1984) but as yet, since all the factors that underlie the dynamics have not been fully identified, a realistic model is still the researcher's dream.

EEG Complexity as a Tool to Probe Neural Dynamics

Clouds are not spheres, mountains are not cones, coastlines are not circles, and bark is not smooth, nor does lightning travel in a straight line.

--- Benoit Mandelbrot

In recent times, the application of nonlinear methods to the analysis of data obtained as output from complex systems in nature has been of interest to the scientific world. As discussed in previous chapters, in cases where the governing equations of motion or even the number of dynamical variables involved are unknown, the tools of nonlinear time series analysis have gained greater importance. The study of the Electroencephalogram (EEG) signal generated by the human brain is one of those complex signals, which is being strongly pursued with the techniques based on nonlinear dynamics and deterministic chaos (Elbert, Ray et. al., 1994). This line of approach includes the computation of invariant parameters such as generalized dimensions, entropies, Lyapunov exponents etc. from the EEG signal by considering it as a

time series to characterize the dynamics of particular brain states (Pezard et. al., 1996; Pritchard & Duke, 1992).

The studies based on the above mentioned characterizing parameters have been applied in many cases to distinguish normal subjects from those suffering from pathological conditions such as epilepsy (Martinerie et. al., 1998; Lehnertz & Elger, 1995). Of the generalized dimensions, the correlation dimension that estimates the active degrees of freedom and among entropies, the Kolmogorov–Sinai (K-S) entropy that gives information regarding the dynamics; have been the subjects of much research (Pezard et. al., 1996). However, the computation of these based on the Grassberger-Procaccia algorithm (Grassberger & Procaccia, 1983a,b) and its variants make the assumption of infinite length, stationary and noise-free data. But many authors have proved the nonstationarity of EEG signals arising probably from the presence of a number of time scales in the underlying dynamics. A direct consequence of such nonstationarity is the slow variation of the computed 'invariants' with time (Indic, 1999). Yet another parameter, the Lyapunov exponent, which estimates the long-term average rate of exponential growth of small perturbations to initial conditions, is very sensitive to noise (Wolf et. al., 1985; Kantz & Schreiber, 1997). Also the numerical computation of the Lyapunov spectrum is tedious and cumbersome.

Nevertheless, the computational studies have practical use in distinguishing between various functional as well as pathological brain states and have even been found to be suitable functional markers with intra-individual stability (Schmid & Dünki, 1996). The application of these methods in the prediction of the onset of epileptic seizures (Le Van Queyan et. al., 1999; Martinerie et. al., 1998) and in gaining insight into the co-ordination of cortical regions under different conditions cannot be undermined (Varela et.

al., 2001). Hence, while the utmost care has to be exercised in accepting the quantitative results of the time series analysis of the EEG signal; the validity of such parameters with statistical significance as comparative measures across varying mental states has been more or less widely established.

Complexity measures are another class of statistics characterizing a time series that have arrived recently on the scene. Measures characterizing the relative 'randomness' in data sets have been thought of as useful markers discriminating between the conditions generating them in each case. Though other measures of complexity exist (Wackerbauer et. al., 1994; Radhakrishnan & Gangadhar, 1998), the use of entropy measures that quantify the rate of information generation in the system has been observed to be more widely useful in practical applications. The Approximate Entropy (ApEn) introduced by Pincus (1991) is one such measure that explores the time ordering of data points in a finite set by measuring the logarithmic likelihood that runs of patterns that are close remain close on next incremental comparisons. This statistic can compute a complexity measure for systems ranging from the purely deterministic to totally random realms and was applied to many clinically relevant studies in biological systems. Lately, a new and related measure, the Sample Entropy (SampEn) was devised by Richman and Moorman (2000) as a measure that rectifies some of the in-built drawbacks of the ApEn such as bias and inconsistency in results. This novel measure has been demonstrated to be useful in the discriminatory study of cardio-vascular data (Richman & Moorman, 2000), which is typical of short, noisy data occurring in biological systems. As mentioned above, the discrimination between various mental states using invariants characterizing the EEG signal is now largely accepted. The computation of complexity measures such as SampEn scores above the more popular D_2 estimation etc.

due to the fact that these are algorithmically simpler to implement and hence easier to compute. Also the effect of nonstationarity of the time series, as in the EEG is also dealt with effectively since they are designed to suit short data segments. These and other attractive features have made these measures popular in physiological data analysis.

6.1 Complexity Measures for Time Series Data

The categorization of many complexity measures for dynamical systems is built upon the antinomies of structural versus dynamical properties of point sets and of homogeneous versus generating partitions. The two types of support usually considered are phase space and position space.

1. **Homogeneous Partitions** (P^H) are partitions into cells of identical volume with respect to the Lebesgue measure. This kind of partition corresponds to a homogeneous concept of space making it easier to handle. Moreover, this implies universality since each measure derived within a corresponding partition is independent of any specific properties of the system concerned.
2. **Generating Partitions** (P^G) are partitions into cells whose boundaries are generated by the properties of the system under investigation. The most important feature of this type of partition is that boundaries between cells are always mapped onto themselves during the evolution of the system.
3. **Structural measures** (S^M) of a system are measures of properties of the system, which do not explicitly contain information about its dynamics. The formal basis of a measure for such properties is the probabilities p_i to find a point in a given cell (state) of the chosen

partition. The mathematical 'measure' of a point set i.e. a probability distribution is a prototype of such a structural measure.

4. **Dynamical measures** (D^M) on the other hand are measures of properties, which contain information regarding the dynamics. Their basis is given by the transition probability $p_{i \rightarrow j}$ between cells for successive time steps. They consider the dynamical behaviour of a system in terms of its temporal evolution.

Combining these four separate criteria, four different classes of complexity can be obtained. These are the structural measures based on a homogeneous partition ($S^M P^H$), structural measures based on generating partitions ($S^M P^G$), dynamical measures based on homogeneous partition ($D^M P^H$) and dynamical measures based on generating partitions ($D^M P^G$).

We consider a one-dimensional system in discrete time given by the map F from a closed interval A onto itself.

$$F : A \rightarrow A, \quad x \rightarrow F_r(x) \tag{6.1}$$

$x \in A$ is called a state of the system, the range $r \in R$ represents the parameter space of the system. From a temporally discrete, spatially continuous map, a *symbolic dynamical system* can be generated by an additional discretization of the state space A . If the state space A of the dynamical system is divided into N cells A_i that are non-empty then the collection of all cells is called a partition, $P = \{A_i\}_{i=1}^N$ if the A_i are mutually disjoint and the union of A_i produces the state space: $\bigcup_{i=1}^N A_i = A$.

By labeling each element of the partition P with a symbol a_i , the time evolution of the dynamical system can be expressed by a symbol sequence

$S=s_0s_1s_2\dots$. This sequence is constructed such that after each step i the state of the system x_i is assigned to the corresponding symbol s_i . This symbol is determined by the cell A_i that is met by the trajectory at time i . The set of all symbols $s_i \in \{a_0, a_1, a_2, \dots, a_{N-1}\}$ is called an *alphabet* of cardinality N . The resulting symbolic dynamical system is defined as:

$$\Sigma_F \rightarrow \Sigma_F, \quad S \rightarrow \hat{\sigma}_F(S) = S' \quad (6.2)$$

such that each symbol in the sequence S satisfies the condition, $s_{i+1} = s_i' = \sigma_F(s_i)$. Σ_F is the space of all admissible symbol sequences. Admissible sequences are those that are induced by the dynamics of the system F for all initial states $x_0 \in A$ at time step $i=0$. The operator σ_F is called shift operator on Σ_F and it describes the dynamics generated by F in the space Σ_F of symbol dynamics. The length L of a symbol sequence S is defined by $S = \{s_i\}_{i=0}^{L-1}$. In principle, the theory of symbolic dynamical systems deals with sequences of infinite length ($L=\infty$). The symbolic dynamical system is constructed in a way that leaves it topologically equivalent to the original definition in Eq. (6.1). This implies a well-defined assignment of trajectories to symbol sequences that represent topological properties of the underlying dynamical system faithfully.

Based on the framework of the formalism of symbolic dynamical systems a number of measures may be described that characterize the complexity of the system in terms of its structural properties. The Algorithmic complexity is defined as the number of bits of the shortest algorithm, which is capable of reproducing a given symbol sequence. This is a concept aimed specifically at the problem of distinguishing between the random and the nonrandom. The problem lies in determining a computable measure of

complexity. No absolute measure is possible because minimal programs by definition correspond to random numbers and it is not possible to define a measure of complexity. A practical realization of this theoretical approach was proposed by Ziv and Lempel popularly known as the LZ complexity, which measures the number of distinct patterns that must be copied to reproduce a given string. Briefly described, a string $S=a_0a_1\dots a_{N-1}$ is scanned from left to right and a complexity counter $c(S)$ is increased every time a new substring of consecutive digits is encountered in the scanning process. The resultant number $c(S)$ is the complexity measure of the string S . Clearly any procedure such as this will overestimate complexity of strings; nevertheless the comparisons will be meaningful. For a random string of length N , the LZ complexity is given by,

$$b(N) = \frac{hN}{\log_K(N)} \tag{6.3}$$

where K denotes the number of elements in the alphabet and h , the normalized source entropy. This is the information obtained when each state is equally probable.

i.e.

$$h = \frac{-\sum_{i=1}^N p_i \ln p_i}{\ln N}$$

The procedure for comparing the LZ complexity of a given string to that of random strings of the same length is as outlined below. The normalized entropy h is evaluated by determining the probability p_i for each state. This probability is obtained by counting the occurrences of each symbol in the alphabet and then dividing by the total number of symbols in the string. A common occurrence is that each state or symbol from the alphabet is equally probable in which case, $p_i = 1/N$ and $h=1$. Comparing with the complexity for

a random number string, $\lim_{N \rightarrow \infty} \left[\frac{c(S)}{b(N)} \right]$ is evaluated for a non-random string with N elements. If this ratio is less than 1, then we can conclude that this is due to a pattern formation in the string S. (Wackerbauer et. al., 1994; Rasband, 1997)

6.2 Approximate Entropy as a Complexity Measure

A highly informative statistic of the genre of nonlinear measures of complexity is the Approximate Entropy (ApEn) introduced by Pincus in the early nineties (Pincus, 1991). Based on a mathematical approach to calibrate an ensemble extent of sequential interrelationships, the ApEn family of parameters provides a quantification of 'regularity' of the data under study. Algorithmically easy to implement and hence computationally viable, ApEn is well suited for the analysis of typically short, noisy time series like the EEG. The K-S entropy, which is usually used to quantify time series 'randomness', suffers from the drawback of being affected by the presence of low magnitude noise in the data. Hence, to ensure convergence of this measure, very long data sets that tend to make the computation tedious and time consuming will be required. The ApEn measures were suggested as an alternative applicable to short, noisy experimental data especially from in-vivo biological experiments.

A measure of the regularity of a time series will be informative about the underlying complexities in the processes giving rise to it. The Approximate entropy measure gives such an estimate depending on the ordering of elements in a time series of data, which is quite effective in the classification of complex systems from the realm of deterministic chaotic as well as stochastic processes. The capability of ApEn algorithm to quantify the

regularity aspect with a limited amount of data makes it a powerful measure for use in myriad situations (Pincus, 1991). This entropy measure assigns a nonnegative number to a time series with larger values corresponding to greater apparent randomness of the process giving rise to the data while smaller values point to regular features in the data.

In order to evaluate the ApEn for a given time series of N points, the following method is adopted. Suppose the time series is represented by $\{x(i)\}$ where $i = 1, 2, \dots, N$; then for a fixed window length m , vector sequences of the form

$$y(i) = [x(i), x(i+1), \dots, x(i+(m-1))] \quad (6.4)$$

are created. On the basis of this embedding in the \mathcal{R}^m space, we define the separation between two vectors $y(i)$ and $y(j)$ as

$$d[y(i), y(j)] = \max(|x(i+k-1) - x(j+k-1)|) \quad (6.5)$$

where $k = 1, 2, \dots, m$ and for each i , $1 \leq i \leq N - m + 1$.

We define,

$$C_i^m(r) = \frac{1}{N - m + 1} (\text{Number of } j \text{ such that } d[y(i), y(j)] \leq r) \quad (6.6)$$

where r is a small fixed parameter. Usually, r is set to be 15% or 20% of the standard deviation of the data. The $C_i^m(r)$'s measure within a tolerance level r , the regularity of patterns in the data similar to a given pattern of window length m .

Next we define,

$$\Phi^m(r) = \frac{1}{N - m + 1} \sum_{i=1}^{N-m+1} \ln C_i^m(r) \quad (6.7)$$

and the Approximate Entropy is given for a data set of N points as

$$ApEn(m, r, N) = \Phi^m(r) - \Phi^{m+1}(r) \quad (6.8)$$

The $ApEn(m, r, N)$ is a 'family' of statistics in the sense that for a given application, comparison of the measure between different systems holds only for fixed values of m and r . The window length m specifies the length over which the regularity in data patterns is evaluated and r , the filter level that sets the tolerance in the $C_i^m(r)$ calculation. The ApEn measure is a sensitive parameter that detects changes in underlying episodic behaviour that may not be reflected in amplitudes (Pincus & Keefe, 1992). Since ApEn usually varies in direct correlation with changing background noise characteristics, it is suited for comparison of data sets from a common experimental protocol. This makes it a useful tool in the analysis of multichannel EEG recordings pertaining to different mental states.

The choice of N , m and r usually depends on the specific application of the measure. Since the length of the data set, N is limited by the experimental paradigm, for appropriate comparisons between data sets, the same number of points is preferred. It has been reported that for numerous applications to distinguish the data on the basis of regularity for both deterministic and random processes, with $m=1$ and $m=2$ for N varying from 50 to 5000 points, values of r between 10% to 25% of the standard deviation (S.D) of the data $x(i)$ are seen to produce good statistical validity of ApEn (Pincus, 1991 and references therein). For the analysis of most physiological signals, a normalized version of ApEn is adopted with $m = 1$ or $m = 2$ and $r = 20\%$ of S.D of the time series. Table 6.1 is a comparison of the evaluated ApEn parameter with the reported values for model data sets for differing values of filter factor r and number of data points, N .

6.3 Gender Difference Reflected in EEG Complexity Analysis

The study of gender differences that surface in mental, psychological and social reasoning has been a fascinating area of research for some time now. Various reports of the differences in the size, shape and connectivity of the male and female brains have poured in from different quarters (Gur et. al., 1999; Allen & Gorski, 1991) in neuroanatomy as also survey studies from the social sciences that point to the distinct ways in which the brain works depending on the gender (Meyers-Levy & Maheswaran, 1991; Meyers-Levy and Sternthal, 1991). The importance of such studies lies in the fact that once the fundamental differences are established, neurophysicians as also psychologists can make treatment of maladies more gender specific and hence more effective. Moreover the differences may also be useful in learning about the variations in the evolution of the male and female neural systems.

The major cognitive gender differences have been declining including the traditional ones of stronger verbal abilities of women and efficient mathematical skill of men (Linn and Petersen, 1985; Caplan et. al., 1985). One reason for this has been attributed to the theory that children are no longer segregated on the basis of gender based activities and that behavioural development interacts with hormones and the development of cognitive skills and brain structures might help develop better spatial abilities in women (Geary, 1989). While a lot of conflicting and contradictory literature exists on the gender based differences (Corsi-Cabrera et. al., 1989; Byne et.al., 1988) there has also been evidence showing male brains are more lateralized than females at structural (Kulynych et. al., 1994) as well as functional levels (Wood et. al., 1991; Shaywitz et. al., 1995; Sadato et. al., 2000). The actual state of affairs is probably somewhere in between and a way to delve into the subtle differences may be beneficial in understanding

the underlying reason for the gender differences in decision making and other social behaviour.

In this maze of conflicting opinions regarding the existence of the difference in gender in the brain as well as its actions, an attempt is made here to look into the complexity nature of the EEG signal from a dense array recording. The aim is to detect changes in the neuronal signal from male and female subjects taking part in the study. The signal complexity is characterized with global linear measures (Wackermann, 1999) and the nonlinear family of complexity statistic, the Approximate Entropy (ApEn) (Pincus, 1991).

6.3.1 Experimental Details

In recent times, the limited spatial resolution of the conventional EEG technology has been tackled by introducing high resolution EEG (HR- EEG) (Babiloni et.al, 1997; Wang & He, 1998; Edlinger et. al., 1998). A prerequisite for such methods is adequate sampling of the potential distribution on the scalp surface. The point-spread function of conduction of potential from brain surface to the scalp averages about 2.5 cm (Gevins, 1990). Thus to adequately cover the surface of the scalp with electrodes having inter-electrode distance in this range, EEG equipment supporting at least 128-channels is required (Sreenivasan et.al., 1998). Hence in this study, we resort to the use of data recorded using a 128-channel Electrical Geodesic™ system, with a sampling frequency of 200Hz referenced to a vertex electrode. The electrode configuration of the recording system is shown in figure 6.1. The schematic also gives an arbitrary classification of electrodes into groups I-IV representative of the major cortical regions - the prefrontal, frontal-temporal, parietal and occipital. An online band pass filter from 0.1 to 70 Hz was used

and impedances were kept below 25kΩ. Vertical and horizontal eye movements were monitored with a subset of 128 electrodes.

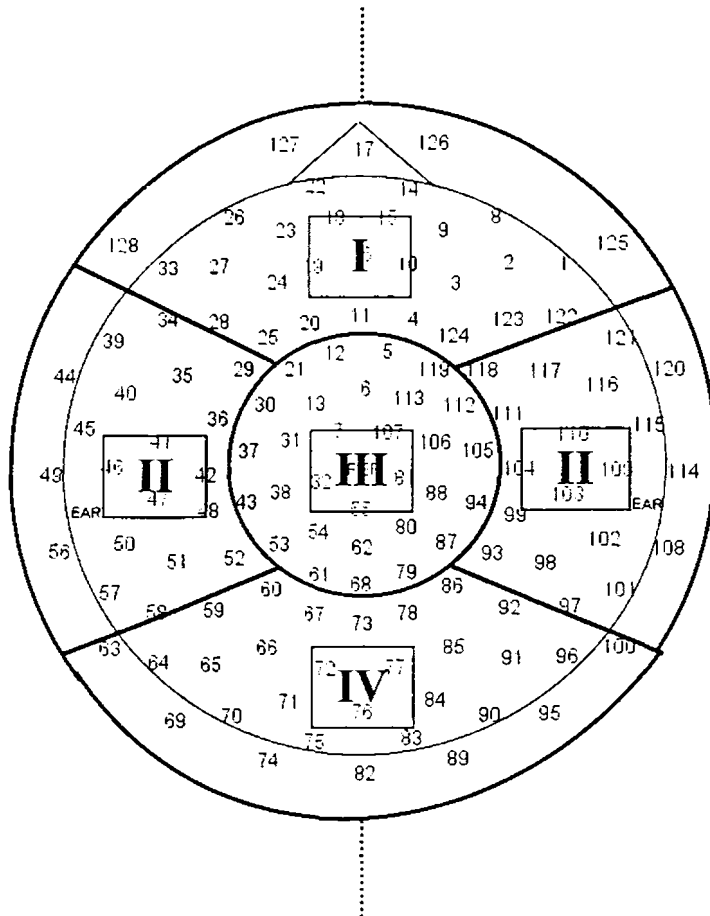


Figure 6.1. The schematic illustrating the electrode placement in the 128-channel dense electrode array. The electrodes are divided into 4 sets representative of the major cortical regions such as frontal, temporal, central and occipital. The dotted line indicates the direction across which the electrodes are to be considered as symmetrically placed.

The EEG was recorded from 10 female (mean age=28.7) and 10 male subjects (mean age=28.8). The complexity variations under two different conditions are studied: (a) passive, eyes closed (no task) (b) passive, eyes open and (c) mental task state of serial subtraction in the eyes closed condition. In the mental arithmetic task, subjects were instructed to subtract 7's from 1000 continuously with eyes closed for a period of 2 minutes. The resultant EEG records were transferred from the Net Station acquisition system for further off-line analysis on a personal computer.

6.3.2 Complexity Analysis

The EEG signal is a serial recording of electric potential generated on the cortical scalp and measured at regular intervals at a specific number of electrodes. A measure of the regularity of a time series will be informative about the underlying complexities in the processes giving rise to it. The study of the EEG signal from the perspective of complexity is hence useful in gaining knowledge regarding the processes that may be operating within the brain in a cooperative manner to produce it. The 128-channel recording used here has the added advantage over the conventional International 10-20 electrode configuration system in that it provides a much better spatial resolution of the cortical surface to reveal characteristics that had remained unseen due to the limited number of recording channels. A schematic of the dense array electrode configuration is given in figure 6.1 with an arbitrary classification of electrodes into groups representative of the major cortical regions - the prefrontal, frontal-temporal, parietal and occipital.

In this study, two slightly different techniques- one based on linear measures and the other on the nonlinear statistic of Approximate Entropy-are employed to analyze the measure of hidden regularity in the apparently

random EEG signal to infer the difference if any in the measured signal due to a gender difference. The various measures are computed on equal length segments of EEG data divided into sliding windows to account for the nonstationary behaviour of the neural signal (Indic et. al., 1999). Moreover equal data sets facilitate the easy comparison of the computed measures from the different techniques adopted.

(i) Linear complexity measures to quantify complexity

The first method adopted is that of the family of linear global complexities that are found to be robust markers of brain functional states during sleep as well as sensory and motor processes and even in the study of various pharmacological effects (Wackermann, 1999 and references therein). The instantaneous time EEG signal is considered as a vector representing the system state in a space whose maximal dimension is given by the number of electrodes in a global representation of the spatially distributed system. The linear characterization is carried out using three measures (a) Σ : measure of the global field strength (μV), (b) Φ : measure of global frequency of field changes (Hz) and (c) Ω : measure of spatial complexity. While Σ and Φ are related to the Hjorth complexities originally proposed for single channel EEGs, Ω follows from the analysis of the covariance matrix formed from the global data recorded at each instant. On the basis of such a global description of the measured signal, each brain 'macro' state can be represented by a point in the three dimensional state spanned by the Σ , Φ and Ω axes. The three descriptors may be defined in the following manner.

The recorded signal from K electrodes ($K=128$ in our case) is stacked column wise ($\{x_1(t)\}, \{x_2(t), \dots, \{x_K(t)\}$) to form an EEG data matrix of dimension ($N \times K$) where N is the data length (Wackermann 1996). Each vector $u_n = (x_1(t), x_2(t), \dots, x_K(t))$ represents the system trajectory at a given

instant in the global description of the system. The data is assumed to be centered to zero mean value in all channels ($\sum_n u_n = 0$) and also transformed to the average reference ($\sum_n u_n^i = 0$). From this data matrix, the three measures are evaluated as,

$$\Sigma = \frac{1}{N} \sqrt{\frac{\sum_n \|u_n\|^2}{NK}} \quad (6.9)$$

and

$$\Phi = \frac{1}{2\pi} \sqrt{\frac{\sum_n \left\| \left(\frac{u_n - u_{n-1}}{\Delta t} \right) \right\|^2}{\sum_n \|u_n\|^2}} \quad (6.10)$$

where Δt is the sampling time of the recording.

The covariance matrix of the EEG data matrix is given by

$$C = \frac{1}{N} \sum_n u_n u_n^T \quad (6.11)$$

$\lambda_1, \lambda_2, \dots, \lambda_K$ the eigen values of this matrix are estimated and normalized as: $\lambda'_i = \lambda_i / \sum_i \lambda_i$. The spatial complexity Ω is then computed as,

$$\log \Omega = - \sum_{i=1}^K \lambda'_i \log \lambda'_i \quad (6.12)$$

(Σ, Φ, Ω) represent a set of three quantities representing the global spatio-temporal dynamics of the electrical field of the brain in the instantaneous state. Wackermann (1999) adopts a representation in two different

dimensions; I and E defined by a transformation of the logarithmized Σ and Φ coordinates as

$$\begin{aligned}\log E &= \log \Sigma + \log \Phi \\ \log I &= \log \Sigma - \log \Phi\end{aligned}\tag{6.13}$$

In this work, we look at the representations of the quantifiers in the $(\log E, \log \Omega)$ and $(\log E, \log I)$ planes to study if the complexity variations due to gender differences during particular mental states are reflected in these.

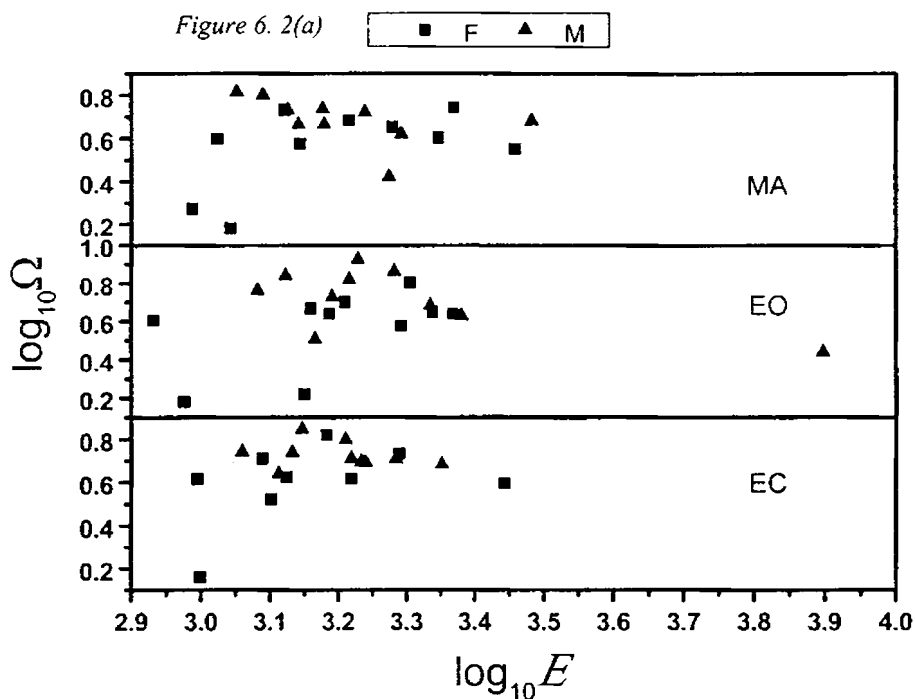
The global representation of the 'functional state' of the brain is adopted which assesses the entire topographies of the measured electric fields by collapsing the dynamics into the three linear complexity quantifiers (Σ, Φ, Ω) . Following equation (6.9) – (6.12), the three measures are computed and an analysis of variance (ANOVA) is performed to compare the statistical outcome of the complexity measures of each gender group in each of the three brain conditions of eyes closed, eyes open and mental arithmetic. The probability of $P < 0.05$ is chosen as the significant level. Table 6.2 depicts these statistical results for the linear quantifiers in the three mental states.

While the first two measures do not significantly reflect differences in gender under the passive states, the global complexity measure Ω varies between the two sets ($P < 0.05$). From this initial evaluation, we may infer a subtle difference in the dynamics during the passive state of no-task, eyes closed. This effect is not evident during the eyes open case though. However, once the subjects are made to do the identical mental task of serial subtraction the subsequent dynamics follows the same complexity pattern between genders. Figure 6.2 (a,b) are plots of the linear complexity measures represented in the planes $(\log E, \log \Omega)$ and $(\log I, \log E)$ planes as in

equation (6.13). A concise view of the nature of linear complexity variations between different gender groups may be obtained from these plots. It is observed that there is no distinctive region in the planes occupied by each gender group for any of the three conditions. One reason for this could be the limited number of subjects in this study. Nevertheless, the complexity values of the two genders overlap finely indicating that no much difference is to be expected even in larger samples.

Table 6.2. A descriptive table of the P values for the linear complexity measures corresponding to the three cases- passive eyes closed, eyes open and performing mental arithmetic.

Linear complexity measures	P value for the eyes closed state (E.C.)	P value for the eyes open state (E.O.)	P value for the mental task state (M. A.)
Σ	0.789	0.896	0.997
Φ	0.685	0.543	0.981
Ω	0.032	0.058	0.078



Only in the case of male subjects does there appear to be a rise in Ω -complexity during eyes open case as compared during the eyes closed state. This effect seems to be absent in the case of the female volunteers. The lack of distinctive behaviour during mental arithmetic between genders seems to concur with the presently accepted idea of no gender predominance in cortical activity of mental or cognitive tasks (Geary, 1989).

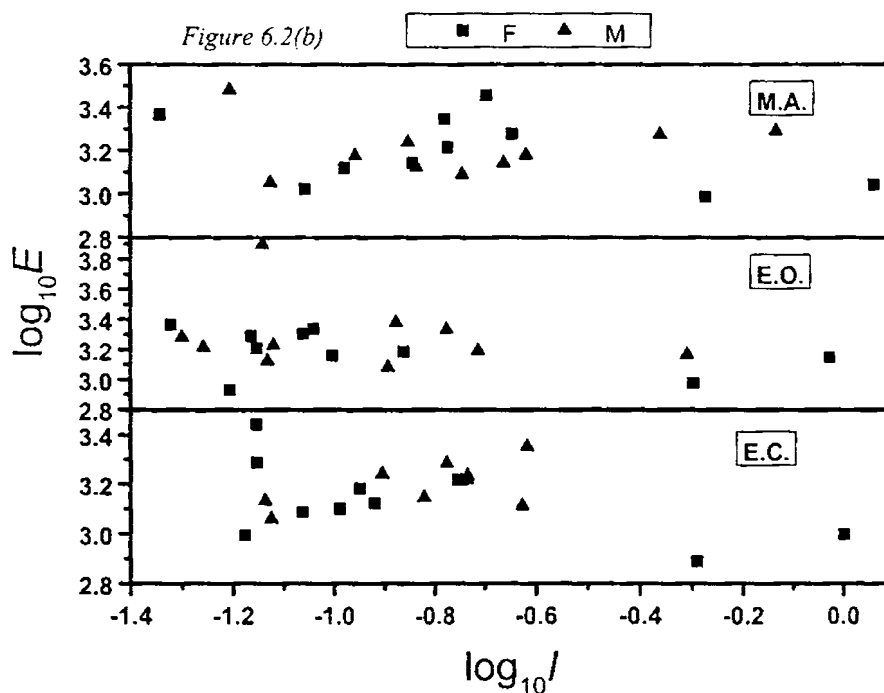


Figure 6.2. The representation of linear complexity measures for individual subjects from the two gender groups during the three conditions of eyes closed (E.C), eyes open (E.O) and mental arithmetic (M.A.) in the (a) $\log E$ - $\log \Omega$ plane and (b) $\log I$ - $\log E$ plane.

(ii) Approximate Entropy (ApEn) measure to quantify complexity

The analysis based on the nonlinear complexity statistic is carried out according to the procedure discussed in section 6.2. In the passive relaxed eyes closed case, the ApEn measure was computed for the individual subjects in both the gender groups and the results were compared. The standard statistical tests were carried out using the SPSS Ver. 10 software package.

The Kolmogorov –Smirnov test confirmed application of normality of the distributions of the computed statistic. The Wilcoxon rank sum test was conducted at a significance level, $P = 0.001$. Figure 6.3 is a plot of the complexity statistic for the two gender categories during the eyes closed

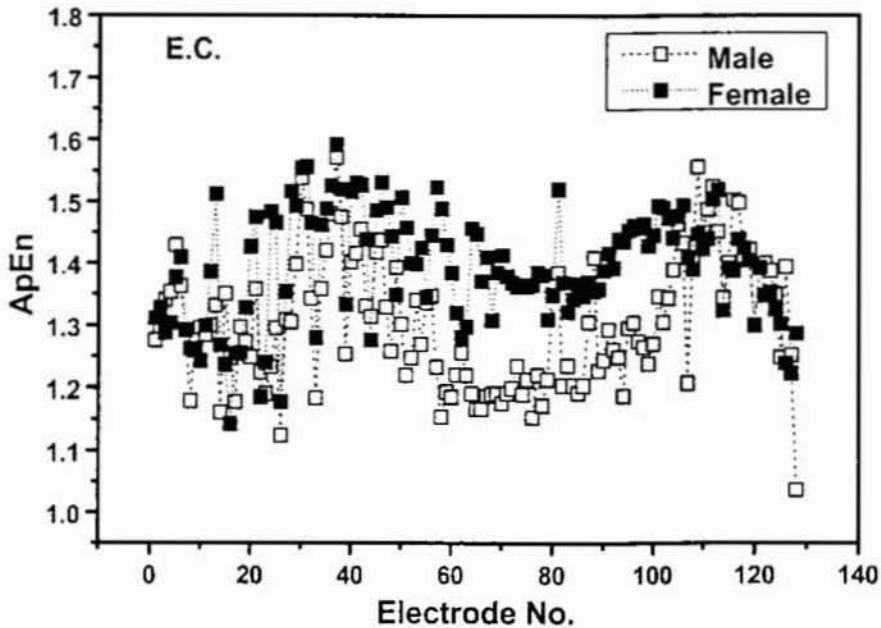


Figure 6.3. The ApEn statistic for each of the two genders- males (M) and females (F) – in the eyes closed (E.C.) state.

state. It is apparent that the ApEn measure is higher for most of the channels of the female group in comparison to the male category. The significant difference in the regularity statistic confirms the subtle differences in the way in which female and male brains process information. For a closer inspection of the complexities manifested through the ApEn values, the dense array EEG

channels were grouped into 4 categories representative of the four major brain regions viz. the prefrontal, frontal-temporal, central-parietal and occipital. Most of the prefrontal, frontal-temporal and centro-parietal electrodes have higher ApEn values for the female group than for the males. The advantage of the nonlinear statistic over the global complexity measures is in the fact that ApEn is computed for the signal ensuing from each electrode site on the scalp rather than averaging over the whole dynamics. This is useful in detecting localized effects that may be grossed over in the global approach.

In the case of the subjects in the eyes open state; the ApEn measure gave significant changes between the two gender groups in the Wilcoxon test with $P < 0.001$. The nonlinear statistic thus appears to detect the complexity difference between genders during the eyes open case as well, which was absent in the computed global complexity measures. This seems to support the idea of a complexity difference existing between males and females during no-task states rather than during a mental arithmetic task with specific functional processes such as perception, association, memory, retrieval etc., which are coordinated in a complex manner to perform the task. The higher ApEn measure maybe taken to imply more independent, parallel processes active in females as compared to their male counterparts during no task conditions. The apparent change in the two no-task conditions is an increase in the complexity statistic over most of the central, temporal, occipital regions. On the other hand, during the mental arithmetic case, the ApEn again provides non-significant variation between the complexities of the two gender groups. Figures 6.4 and 6.5 correspond to the ApEn variations in the eyes open and mental arithmetic conditions for the two gender groups.

In this study the subjects who take part in the three experiments are kept the same so that spurious variations do not result consequent to the within subject effect in each test group. Hence even though the subject number in each group is limited, the similarity in the complexity exhibited by the two groups during the mental task may therefore be taken as a genuinely embedded phenomenon in the electric field variations.

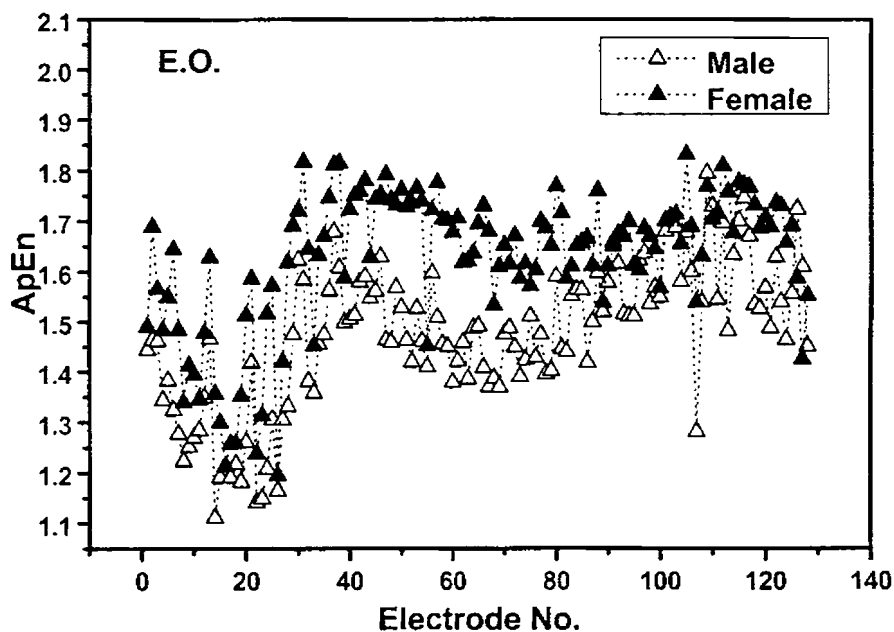


Figure 6.4. The ApEn statistic plotted for each of the two genders- males (M) and females (F) – for the eyes open case (E. O.)

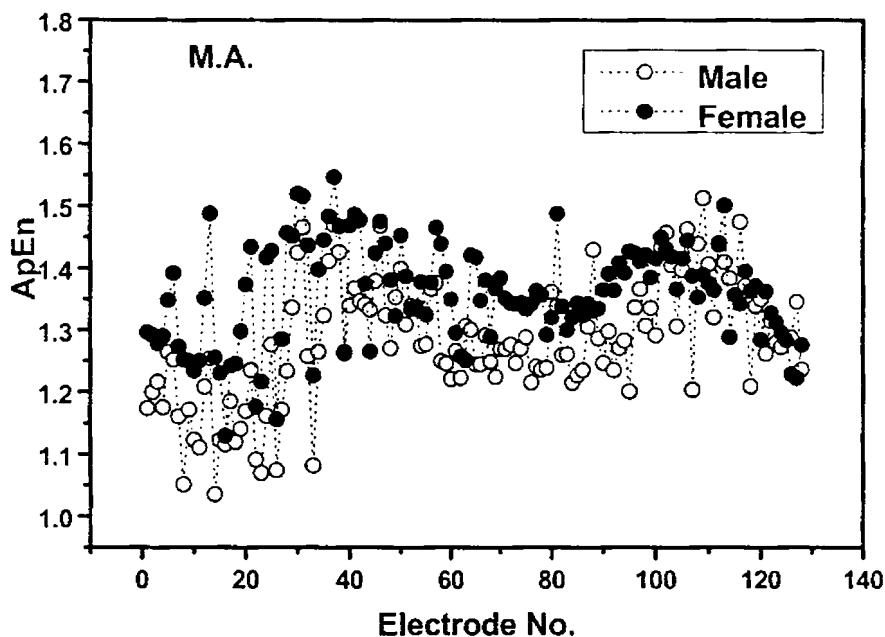


Figure 6.5. The ApEn statistic plotted for each of the two genders- males (M) and females (F) – for the mental arithmetic (M. A.) task condition.

6.3.3 Discussion on the Observations of the Gender-based Study

The work presented here attempts a characterization of the difference in male and female brain processing by studying the complexity aspect of the nonstationary EEG signal by application of principles of global linear as well as nonlinear time series analysis. While it is observed that the global linear quantifiers may work well as a first option in inspection of complex physiological signals, complexity information is supplemented by analyzing the variation in the nonlinear ApEn statistic analysis of EEG time series emanating from individual electrodes. This statistic has been recently applied

to distinguish variation in complexity of EEG recorded from a control group and groups suffering from epilepsy and mania (Bhattacharya, 2000; Radhakrishnan & Gangadhar, 1998). In the work undertaken here, even from a limited set of subjects, both the methods detect complexity differences in the EEG from the two gender groups during passive eyes closed state. Moreover this analysis is based on a dense array recording that provides much better spatial resolution of the analyzed signal. Approximate entropy appears to be an efficient statistic in that it not only reveals complexity variations if any, but since it is based on single time series, also presents a detailed picture of the complexity spread on the cortical surface. Accordingly in this study while only one of the global complexity measures Ω , shows significant variation between males and females during eyes closed state the ApEn statistic detects subtle differences in complexity levels of spontaneous EEG from the male and female groups during the passive no-task states of both eyes closed and eyes open conditions. It also implies that the presence of visual stimulus alone is not sufficient to bring the complexity levels into coincidence between the two sexes. Rather, such a coincidence occurs only in the case of a task dominated mental state, which requires a number of functions such as perception, association, memorization etc. to take place in a systematic manner to effect its performance.

This analysis can be taken as a first step towards more such detailed experiments with measures looking into subtle gender based differences in neuronal dynamics. A bigger sample of subjects belonging to distinct age groups may be analyzed. It has been pointed out recently that the process of neuronal aging and changes in sex-hormone levels during aging seem to be instrumental in a number of structural gender differences (Swaab et. al., 2001). Age based gender differences in Alzheimer's disease related

neocortical pathology that has been reported, is a strong pointer to the need for inclusion of subjects in various age groups for such studies.

6.4 Complexity Analysis of Various Brain States

In contrast to the relatively simple method used to infer the gender difference reflected in the complexity analysis of EEG signal during some brain states, the study undertaken now is an in-depth and systematic attempt to study the variations in the complexity as the brain state varies. This analysis applies a new and related statistic to the ApEn measure, known as the sample entropy (SampEn) statistic, to human EEG data for a complexity characterization of three different states (a) passive, eyes closed state (E.C.), (b) a mental task state (M. A.) and (c) epileptic spike condition (Ep. Sp.). The EEG recording of the first two cases is from normal subjects who are at first in a relaxed eyes closed state and then made to do a mental arithmetic task. The epileptic spike data is acquired from subjects who are known epileptics under medication as part of treatment. The motivation in undertaking this analysis lies in assessing the variations in complexity exhibited by the scalp- recorded EEG due to the underlying neuronal dynamics in these totally distinct conditions. A recent study reports the use of ApEn statistic in distinguishing between different levels of human consciousness ranging from the relaxed eyes closed to the deep sleep stage (Gu, Meng & Shen, 2003). We go a step further in attempting to detect complexity changes in similar looking EEG records pertaining to relaxed, eyes closed state and a task state of mental arithmetic.

The next interest lies in the complexity analysis of the spike condition exhibited by epileptic subjects. Epilepsy is a pathological condition characterized by spiky pattern in continuous EEG and seizure at times. A

complexity analysis of EEG of such a spike condition is carried out and compared against the normal, eyes closed state. As expected, the SampEn analysis shows more regular structure in the spike data than in the normal state (Radhakrishnan & Gangadhar, 1998) as reported earlier in other measures such as D_2 etc. (Lehnertz & Elger, 1995). Yet the clinical interest that this statistic may hold as a computationally simpler tool as compared to other quantities cannot be undermined. Moreover its ability to distinguish the pathological epileptic state even from data recorded in the absence of a seizure in clinical terms makes it a potential tool in automated diagnosis. The question of temporal fluctuations in complexity of normal series in comparison with pathological cases is addressed in the subsequent section. This analysis draws on the idea of multiscale entropy analysis (Costa et. al., 2002) that looks into the effect of computation of the measure at multiple scales than at a single scale of the time series. The single scale computation may mask the structure due to the long-range correlations in the data that may be revealed by a multiscaling process. The time scales of a process however are not the same as those referred to as the scale factors in the multiscale analysis. Indic et. al. (1999) have evaluated the typical time scales of the neuronal processes such as the Na-K pump, synaptic transduction etc. by considering the relevant parameters involved in these mechanisms. It has been found that the time scales range over various orders of magnitude pointing to the presence of innumerable probably overlapping time scales in the human brain dynamics. The scaling adopted in this study points to the coarse-graining level at which the time-correlations in the original data are revealed and are not directly related to the time scales in the underlying dynamics. The coarse graining at various levels followed by entropy evaluation facilitates the investigation of the possibility of variation of SampEn with the scaling as was

observed in the case of heart rate data by Costa et. al. (2002). A multiscale analysis along similar lines is attempted here for the normal EEG in contrast to the pathological time series.

6.4.1 Sample Entropy: Quantification of Regularity of Experimental Data

A measure of the regularity of a time series will be informative about the underlying complexities in the processes giving rise to it. However the problem encountered in developing such a meaningful quantity in experimental situations is the short and noisy data generated in complex systems especially in biology. Pincus (1991) developed a regularity measure related to the Kolmogorov entropy known as the Approximate Entropy (ApEn), which was found to be effective in the classification of complex systems from the deterministic chaotic as well as stochastic realms. The measure found widespread application in model systems as well as actual data from experimental situations especially from biology (Pincus & Viscarello, 1992; Ryan et. al., 1994). This entropy measure assigns a nonnegative number to a time series with larger values corresponding to greater apparent randomness of the process underlying the data while smaller values point to regular features in the data. Despite the many features that make it a popular complexity measure, the ApEn suffers from the drawback of being a biased statistic. This leads to the measure being heavily dependent on the length of the data set under consideration as well as failing to produce consistent results (Richman & Moorman, 2000). This and other discrepancies are rectified in the newly developed Sample entropy algorithm, which is related to the ApEn measure. A detailed description of the drawbacks in the ApEn algorithm and the better results accorded by the sample entropy statistic in

the case of model data as well as clinical data is available in Richman and Moorman (2000).

In order to evaluate the SampEn statistic for a given time series of N points, the following method is adopted (Richman and Moorman 2000). Suppose the time series is represented by $\{x(i)\}$ where $i = 1, 2, \dots, N$; then for a fixed window length m , vector sequences of the form

$$\bar{y}_m(i) = [x(i), x(i+1), \dots, x(i+(m-1))] \quad (6.14)$$

are created. On the basis of this embedding in the \mathbb{R}^m space, we define the separation between two vectors $\bar{y}_m(i)$ and $\bar{y}_m(j)$ as

$$d[\bar{y}_m(i), \bar{y}_m(j)] = \max(|x(i+k-1) - x(j+k-1)|) \quad (6.15)$$

where $k = 1, 2, \dots, m$ and for each i , $1 \leq i \leq N - m + 1$.

Let $B_i^m(r)$ be $(N - m - 1)^{-1}$ times the number of vectors $\bar{y}_m(i)$ within r of $\bar{y}_m(j)$ with j ranging from 1 to $(N - m)$ and $i \neq j$. The latter condition is in keeping with the idea of eliminating self-matches between templates $\bar{y}_m(i)$ and $\bar{y}_m(j)$ whenever $i = j$, which were the main sources of bias in the ApEn statistic.

Define the function,

$$B^m(r) = \frac{\sum_{i=1}^{N-m} B_i^m(r)}{N - m} \quad (6.16a)$$

In a like manner, $A_i^m(r)$ is defined as $(N - m - 1)^{-1}$ times the number of vectors $\bar{y}_{m+1}(i)$ are within r of $\bar{y}_{m+1}(j)$; again with j ranging from 1 to $(N - m)$ and $i \neq j$ and the function $A^m(r)$ as,

$$A^m(r) = \frac{\sum_{i=1}^{N-m} A_i^m(r)}{N-m} \quad (6.16b)$$

Hence while $B^m(r)$ gives the probability that the two sequences match for m points; $A^m(r)$ is the probability that the match is for $m + 1$ points. The Sample entropy is defined as,

$$SampEn(m, r) = \lim_{N \rightarrow \infty} \left[-\ln \left(\frac{A^m}{B^m} \right) \right] \quad (6.17)$$

which is estimated by the statistic $SampEn(m, r, N)$ defined as,

$$SampEn(m, r, N) = \left[-\ln \left(\frac{A^m}{B^m} \right) \right] \quad (6.18)$$

The $SampEn(m, r, N)$ is a 'family' of statistics in the sense that for a given application, comparison of the measure between different systems holds only for fixed values of m and r . Since $SampEn$ varies in direct correlation with changing background noise characteristics, it is suited for comparison of data sets from a common experimental protocol. This makes it a useful tool in the analysis of multichannel EEG recordings pertaining to different mental states. The choice of N , m and r usually depends on the specific application of the measure just as in the ApEn case. It has been reported that for numerous applications to distinguish the data on the basis of regularity for $m=1$ and $m=2$ for N varying from 50 to 5000 points, values of r between 10% to 25% of the standard deviation (S.D) of the data $x(i)$ are seen to produce good statistical validity of ApEn (Pincus, 1991 and references therein). All these conditions appear to hold good for SampEn as well, which is a measure related to ApEn. Figure 6.6 is a comparison of the complexity

values given by the ApEn and SampEn measures for a random signal of mean 0 and standard deviation 1 at various filter levels as well as number of points, N . It can be observed at higher values of r and also at high N , the measures agree. But at lower values of the parameters, the self-biasing nature of ApEn leads to lower estimates of complexity.

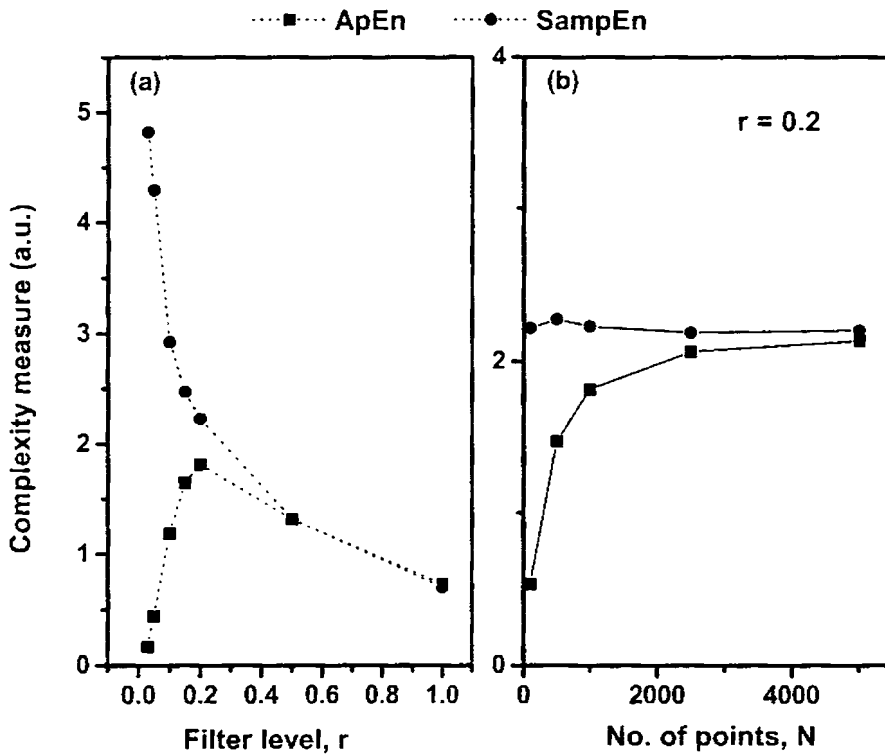


Figure 6.6 The comparison between the ApEn and SampEn measures for a random data set at varying parameter values (a) filter level (r) at fixed number of data points, $N=1000$ and (b) N at fixed value of $r=0.2$.

This single scale complexity analysis that is usually adopted may result in a masking of the effects of long range order in the physiological time series from healthy subjects as reported in a recent study of Costa et. al. (2002). They study the effects of coarse graining the heart inter-beat interval data at various scaling levels and carry out the sample entropy analysis on each of the coarse grained sets to reveal the effects of temporal fluctuations in the data. In a similar vein, we evaluate the multiscale entropy measure for the normal subject data as well as the spike data from pathological subjects. The analysis is carried out according to the following sequence. A coarse graining of the one dimensional time series that forms the data set is effected at a particular scale factor to generate a different time series and the complexity measure is evaluated for this newly formed time series. In the present case, the EEG time trace emanating from each electrode location is subjected to the scaling and subsequently, the SampEn measure is evaluated for this modified time sequence each time. From a one-dimensional discrete time series, $\{x_i\}$; $i = 1, 2 \dots N$, we construct the time series $\{y^\tau\}$ scaled by a factor τ . The new series is constructed as,

$$y_j^\tau = \frac{1}{\tau} \sum_{i=(j-1)\tau+1}^{j\tau} x_i, \quad 1 \leq j \leq N/\tau \quad (6.19)$$

When $\tau = 1$, the new data set y is same as the original time series x . In the single scale case, we divide the data set into windows of fixed length and estimate the statistic by averaging over a number of such windows. In the multiscale case, SampEn is evaluated on the new sets run over the whole data length with a scaling τ and the behaviour of the complexity measure with the scaling factor is studied.

6.4.2 Classification of Data

The main thrust in this work is the analysis of the complexity variation in the human cortical space in from the EEGs recorded from two different groups: (I) normal subjects and (II) subjects suffering from the pathological ailment of epilepsy. The normal group was studied to bring out the differences among a passive state as against a task state of mental arithmetic. From the former group, recording was carried out from 12 subjects with mean age 29 under two conditions (a) Passive relaxed eyes closed (E.C.) (2) mental arithmetic with eyes closed (M.A.), where subjects were instructed to silently serially subtract 7's from 1000 for 2 minutes.

The importance of the study of the pathological cases especially of epilepsy has been stressed at various occasions in this work. In this particular case, the epileptic spike activity (Ep. Sp.) was recorded under eyes closed state from a group of 5 subjects (mean age = 14) suffering from the pathological condition of epilepsy. These records were studied and compared with the similar eyes closed state of normal subjects.

The data recording system and the details of electrode classification are as explained in section 6.3.2.

6.4.3 Complexity Analysis using SampEn

The objective underlying this analysis is to look at the variations in the complexity exhibited by a global EEG recording as a result of the varying dynamics of the system with the change in brain state. The complexity of the EEG time trace emerging from each of the recording channels is quantified by the statistic of Sample Entropy (SampEn). EEG signals have been revealed to be nonstationary in nature leading to a drift of the system invariants with time. A prescription to handle such data is the division of time series into

short time windows (Pradhan & Dutt, 1993) and in keeping with this principle, the data is divided into non-overlapping windows of 1000 data points and the SampEn measure evaluated for each of these.

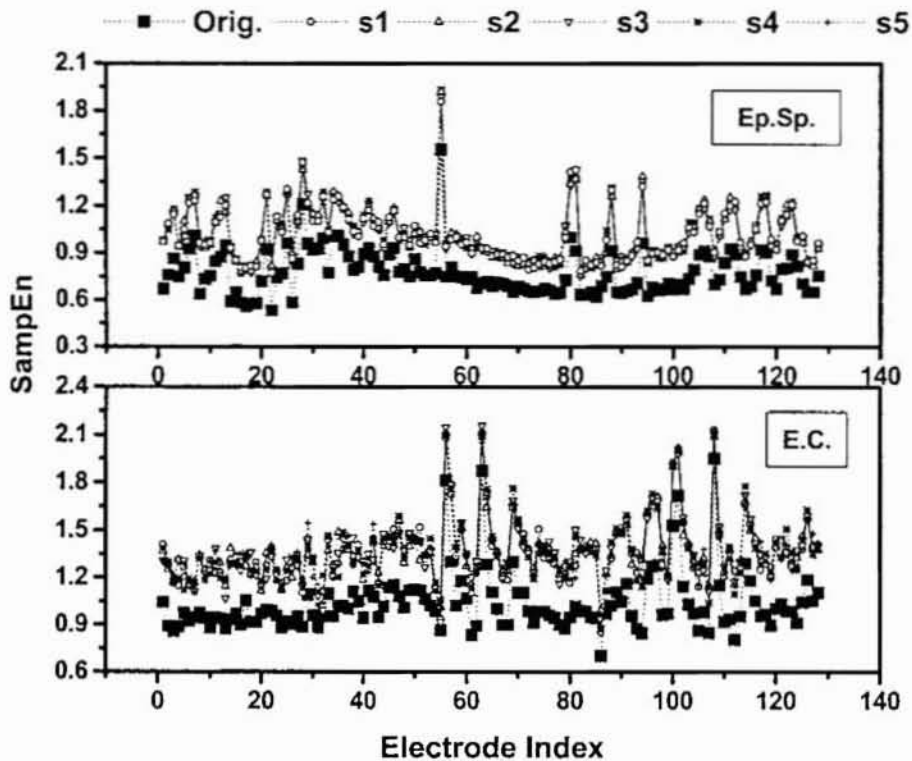


Figure 6.7. The plots for the SampEn statistic in the case of the normal EEG (only E. C. state presented here; though similar results were obtained for M. A. as well) and the pathological case represented by the spike condition (Ep. Sp.) and five of the surrogate data sets generated in each case.

Prior to the complexity analysis, surrogate data testing is carried out to check the validity of application of nonlinear measures on the recorded EEG data. The detailed procedure for the generation as well as testing of the null hypothesis of surrogate data testing was elaborated in chapter III. Accordingly, ten surrogate data sets were generated by the Fourier shuffling method and SampEn statistic evaluated for each of these in the three cases of E. C., M. A. and Ep. Sp. The computed statistics in each of the original and surrogate sets were compared by applying the Mann-Whitney U test following Theiler et. al. (1992). Significant difference of the P-value, $P < 0.005$ in all the three cases gave reasonable ground for assuming the presence of nonlinearity in the data and this is also obvious in the plots in figure 6.7 that present the variation of SampEn for the surrogate data sets along with the original EEG data. The surrogate sets lead to complexity values that form a cluster and as expected, the stronger randomness inherent in these data is reflected in the higher values of sample entropy in comparison with that for the EEG data.

(i) Normal case: Passive, relaxed state Vs. Mental task state

The SampEn measure evaluated for the passive state of eyes closed condition when compared with task state of mental arithmetic shows that the complexity was lowered in the mental task state. Figure 6.8 shows the plot for the evaluated complexity measure for the two conditions for the 128 channel data. Since on visual inspection most of the channels exhibit almost similar complexity values, the channels are grouped into 4 major regions, named I – IV covering the channels pertaining to the prefrontal, frontal-temporal, central-parietal and occipital regions and these are more closely examined. The classification of the dense array electrodes into these 4 groups is depicted in figure 6.1.

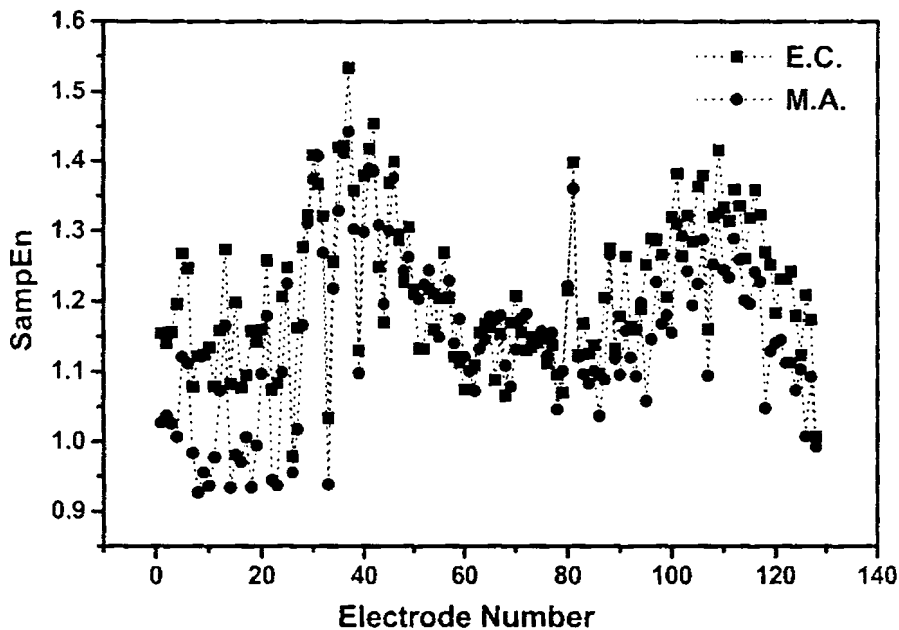


Figure 6.8. Variation in the Sample Entropy (SampEn) for the normal eyes closed state (E.C.) and during a mental calculation (M. A.) task for the 128 channel data set.

The statistical analysis of the computed measures is determined in the following manner. After confirming the validity of equal variances for the test populations, two-way repeated measures analysis of variance (ANOVA) is carried out for examining the effect of mental arithmetic on the mental state as characterized by the complexity statistic. Two-within subject factors were used: state (2 levels- eyes closed and mental arithmetic state) and electrode (n levels). The analysis was carried out individually over the set of electrodes based on the classification mentioned earlier. In each of these groups i.e.

regions I to IV as in figure 6.1, there are about 30 electrodes and the number of electrodes in each of the regions is the number of levels (n) in the electrode factor specified in the repeated measures analysis. It was observed that the main effects due to state (all four regions) and electrode (in regions I, II and III) were significant for the sample entropy (SampEn) measure. The electrode effect is non-significant in the region IV comprising most of the channels over the occipito-parietal region. The variation in SampEn with state at the electrodes is characterized by the (state*locus interaction) which is

Table 6.2. A brief description of the two- way repeated analysis ANOVA used for the statistical analysis of the complexity variation as the mental state changes from a passive state (E.C.) to a mental task state (M. A.)

Effect	Region I		Region II		Region III		Region IV	
	F value	P value	F value	P value	F value	P value	F value	P value
State	37.044	<0.001	36.245	<0.001	35.102	<0.001	30.587	<0.001
Electrodes	2.673	<0.001	2.744	<0.001	3.27	<0.001	0.659	0.908
State * electrode interaction	1.033	0.423	1.36	0.085	1.061	0.385	1.746	<0.05

found to be insignificant in regions I, II and III. However, region IV shows a significant interaction between the state and electrodes. Hence we may infer that apart from the electrodes in the occipito-parietal regions the effect on

SampEn statistic due to mental arithmetic is almost the same at the other sites. A brief description of the statistical analysis is depicted in Table 6.2.

A major advantage of using a dense array recording is the better spatial resolution provided when compared to the conventional recording making use of the limited 16 to 19 channels. The statistical analysis outlined above was conducted again by considering only 19 channels in approximate correspondence with the 19 electrode sites in the International 10-20 convention. The chosen electrodes were 23, 9, 11, 28, 123, 39, 121, 42, 104, 49, 114, 60, 86, 62, 64, 96, 73, 71 and 84. A comparison of these sites with the schematic shows that these are broadly representative of the major cortical regions of the brain. Two-way, repeated measures ANOVA carried out for the complexity statistic with the factors – state (2 levels) and electrodes (19 levels) led to the following results. The main effects of state and electrode were significant at $P < 0.001$ with F-values 36.883 and 4.159 respectively but the state*electrode interaction in this case was non-significant with F-value=0.685 and $P = 0.823$. However, the analysis of region IV as explained above, had prompted us to believe otherwise and hence it is seen that detailed structure may be lost due to the limited number of channels that are conventionally used. The gross analysis failed to reveal the significant difference in the effect caused by the mental arithmetic state on the electrode sites in the occipito-parietal regions. This result also brings to the fore the better information carrying capacity of dense array recording.

Figure 6.9 plots the SampEn measures over these four major brain regions where the complexity drop during mental arithmetic as compared to the eyes closed state is seen in regions I and IV. Over the rest of the brain, there is not much complexity difference in the two states. The reduction in SampEn for the prefrontal region may be looked upon as the reduced

neuronal complexity of this region during mental arithmetic as compared with the others. While small yet statistically insignificant rise in Kolmogorov entropy, K_2 during arithmetic task over rest state has been reported (Micheloyannis et. al., 1998), SampEn clearly illustrates the decrease in complexity for the frontal regions. Moreover the decrease in complexity in the parieto-occipital regions points to the involvement of this region in the subtraction task. Mental arithmetic is a complex task that requires integration of multiple processes carried out by a large-scale network of distributed yet interconnected local networks (McCloskey, 1992). The complexity analysis supports this idea and is also in accordance with imaging evidence that suggests the participation of parietal areas in addition to the prefrontal areas in mental calculation (Kazui, Kitagaki & Mori, 2000). The lowered complexity in the occipito-parietal channels suggests the activation of visuo-verbal regions while the frontal activation has always been linked with working memory and attention (Harmony et. al., 1999). The task here being serial subtraction, the processes can be comprehended as the sequential procedure of recognizing the numerals, forming a mental picture of the operations before the actual processing, storage of the current data in the working memory before going on to the next subtraction. The ease with which the areas participating in the task can be identified is a point in favour of the use of this complexity measure as a marker of activity of brain regions under specific conditions.

The temporal variation in complexity of some channels belonging to the right and left hemispheres is shown in figure 6.10. It is indicative of stronger sequential regularity in the EEG signal from the prefrontal regions during eyes closed than during mental arithmetic task.

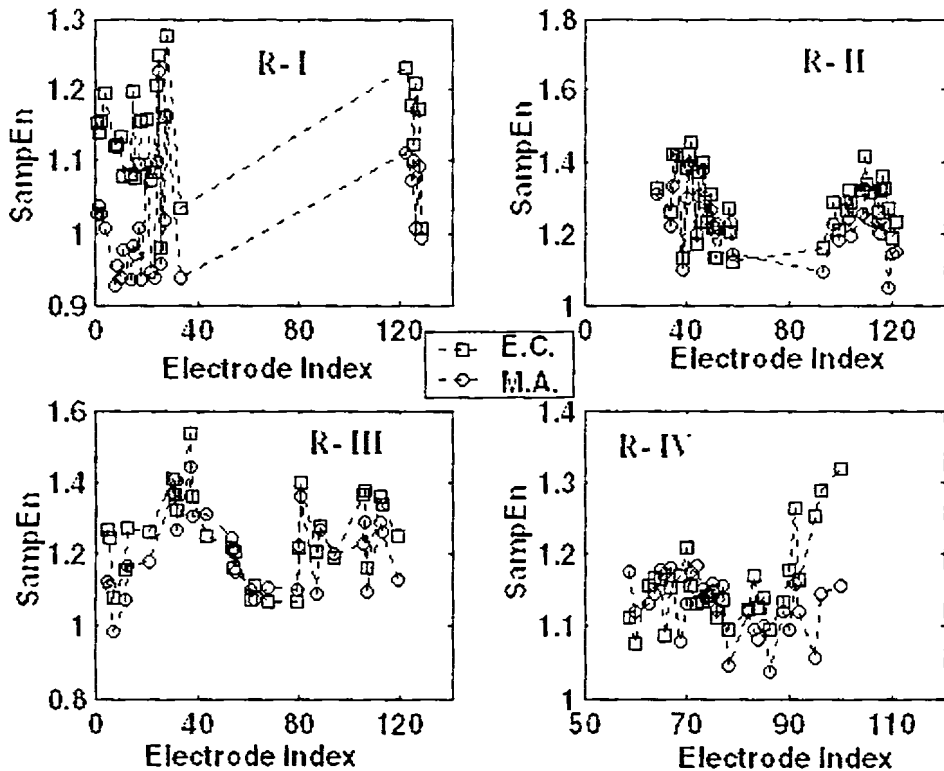


Figure 6.9. A detailed comparison of SampEn measure for the mental arithmetic (M.A.) state with that of eyes closed (E.C.) case for each of the four groups numbered I to IV.

No significant inter-lobe complexity differences are discernible between symmetrically placed electrodes indicating homogeneity in the system complexity over the scalp. The electrodes have been chosen on the basis of their relative positions across the dotted line in figure 6.1 which may be thought of passing through the midline of the brain. The bilateral activation

suggested in the fMRI study of mental arithmetic (Rickard et. al., 2000) also supports such a finding. The advantage of non-invasive techniques like the EEG, in comparison with relatively expensive imaging methods as the first tool in studying the human brain under myriad conditions is brought to the fore by such studies.

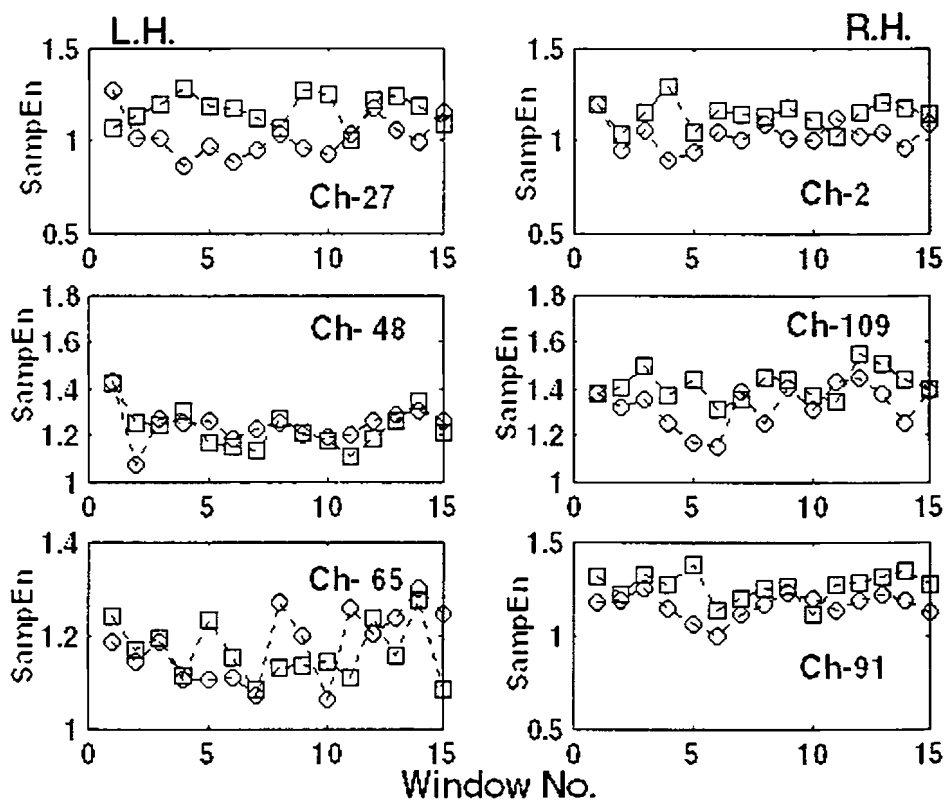


Figure 6.10. The plots comparing SampEn statistic in the case of symmetrical channels in each brain lobe. The channels are chosen at random to be representative of a particular region.

(ii) Healthy condition Vs. Pathological condition

The data recorded from epileptic subjects in the eyes closed case was found to exhibit spiky character, which is often found in epileptics. This data when analyzed showed much lowered complexity when compared with the eyes closed state of a normal healthy person. Figure 6.11 shows that the SampEn measure during the epileptic spike is smaller than the corresponding values over all the channels distributed over the cortex. Bhattacharya (2000) recently reported that there is indeed a lowering of ApEn measure for a 16-channel data set for epileptic subjects.

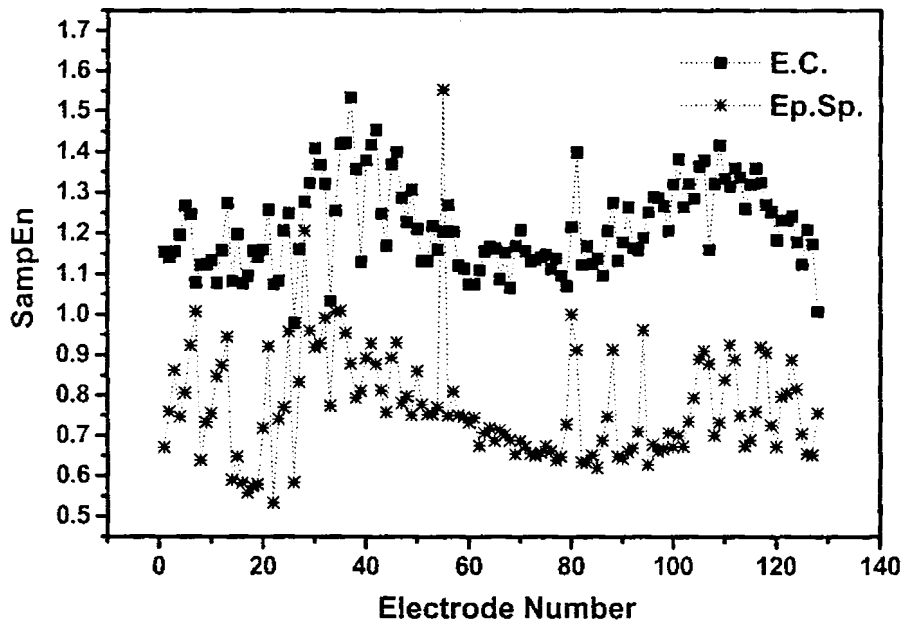


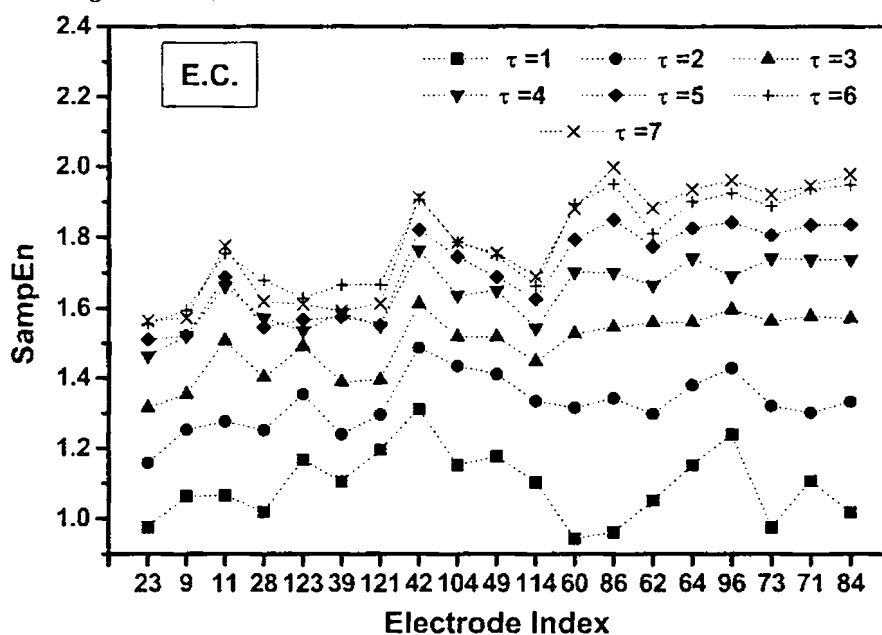
Figure 6.11. The complexity analysis for the epileptic spike data (Ep. Sp.) in comparison with the relaxed eyes closed (E.C.) case is presented.

However, we can say that the dense array EEG gives a closer view of the generalized statement made in that paper. This complexity reduction is also in

accordance with the lower values of various nonlinear parameters such as the correlation dimension, Taken's estimator and so on during an epileptic discharge (Lehnertz & Elger, 1995; Lerner, 1996; Radhakrishnan & Gangadhar, 1998). From a mechanistic point of view, the strong reduction in the SampEn measure points to the greater component or subsystem autonomy. Thus for normal subjects in comparison with the subjects suffering from a pathological illness, there are more independent, parallel, functional processes active.

In the multiscale (MS) analysis undertaken to observe the effects due to long range correlations that are usually present in normal physiological time series, the method introduced by Costa et. al. (2002) is adopted.

Figure 6.12(a)



A data set of length $N = 7370$ is chosen for the spike as well as normal eyes closed data and accordingly, new data sets are made to evaluate the MS SampEn with scaling factor τ from 1 to 7. In this case the maximum scaling factor is set to 7 so that the resultant data set will be ~ 1000 data points suitable for the SampEn algorithm. Figures 6.12(a) and (b) plot the SampEn measure over the various scaled data sets corresponding to the healthy and the epileptic groups for the particular set of 19 channels of the electrode

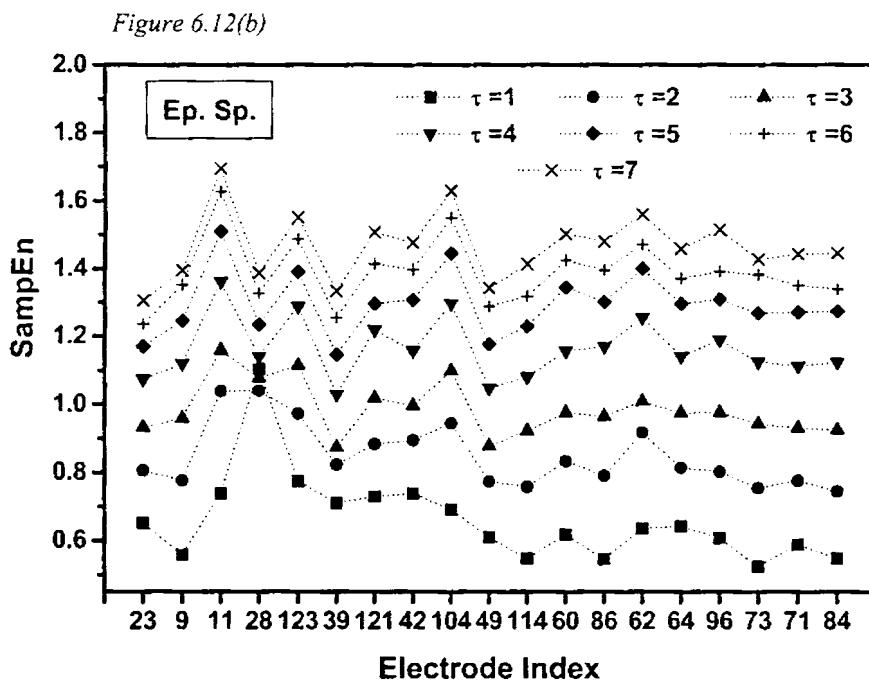


Figure 6.12. The sample entropy for some selected channels from the dense array EEG of the normal eyes closed condition, E C. (a) and the spike data, Ep. Sp. (b) in the multiscale analysis at varying levels of scaling, τ is plotted. The 19 channels represented here roughly correspond to the 19 channels of the International 10-20 system.

array, indicated in a preceding section that approximately correspond with the channels in the International 10-20 convention.

In the case of the eyes closed state, as the scaling increases the SampEn also increases for most channels and as $\tau \rightarrow 7$, the entropy value tends to saturate. Hence even for longer data sets, we may conclude that the saturation nature will set in around $\tau = 6$ or 7. The behaviour of the entropy measure for the pathologic group is the same as the normal state data set with an increase of the measure with scale factor, τ . However, saturation in the evaluated SampEn values does not occur even at τ value of 7.

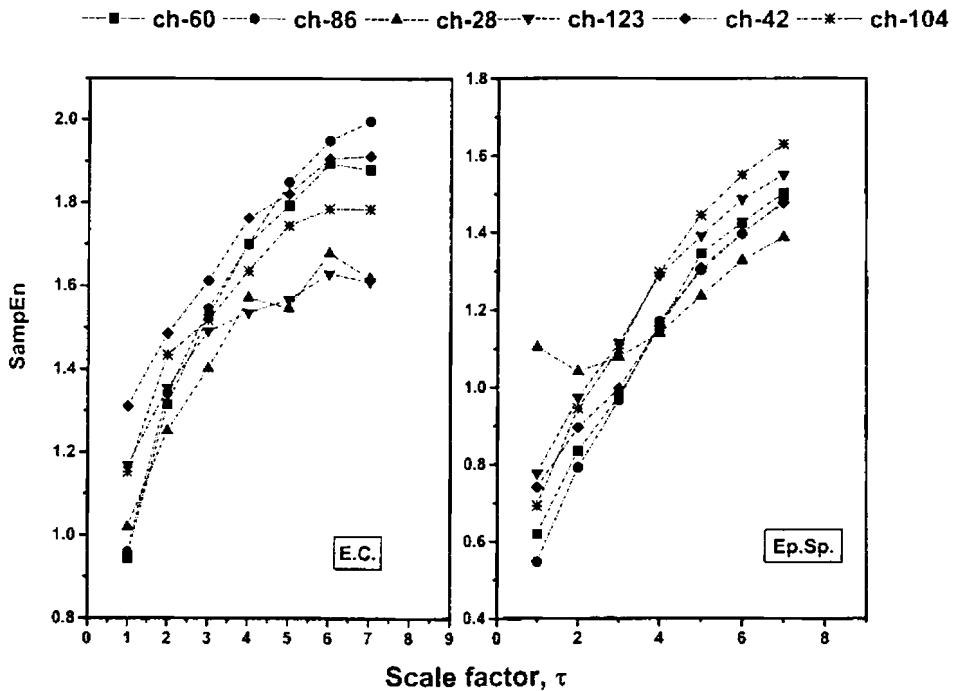


Figure 6.13. The SampEn in multiscale analysis is plotted for some symmetrical channels chosen from the four major regions in the eyes closed (E.C) and epileptic (Ep.Sp.) conditions for varying τ .

Despite the fact that higher values of τ could not be analyzed due to the limited length of the available spike data; we may infer that the nature of time fluctuations in the pathological data set does not lead to a saturation in the complexity of the data set at any scale. Figure 6.13 is a comparison of the multiscale entropy measure for the two subject groups – normal and pathological- for a random selection of channels with increasing scale factor τ .

6.5 Conclusions of the Complexity Approach to EEG Analysis

In this final section we take stock of the various observations made regarding the varying neuronal dynamics from the perspective of complexity measures. While the initial effort was concentrated on establishing the technique as a useful tool for evaluation, the subsequent work established the viability and feasibility of the use of this measure to gain insight into the dynamics of the brain as the condition changes.

The Approximate Entropy measure was chosen as a nonlinear complexity probe and compared against the class of linear measures in delving into the changes in complexity if any that are exhibited by the genders in undergoing simultaneous actions. It was established that in comparison with the linear quantifiers; ApEn is sensitive to changes in complexity and the genders do vary in complexity in some passive states such as eyes closed and eyes open when no tasks are carried out. Such studies are relevant in the context of learning more about the organization of behaviour in males and females according to which their mental, emotional and social character is built. Moreover such studies are constructive in devising alternative therapy measures in case of psychiatric illnesses in the different sexes.

In the section 6.4, the complexity aspect of EEG data recorded during the three conditions of (a) normal eyes closed, (b) mental arithmetic and (c) epileptic spike activity was analyzed. The dense array configuration provides simultaneous records of the EEG signal from a large number of channels that is useful to gain a more complete picture of the activity distributed over the cortex. The normal eyes closed state is considered as a base line state and the complexity during the other two states are compared with this. It is found that even during a cognitive task such as mental arithmetic that consists of a series of processes such as perception of information, processing of arithmetical signs, retrieval and memorization mechanisms; the complexity in most of the brain regions remains the same as that during the relaxed, passive state. The prefrontal region and some parts of the occipito-parietal region exhibit lowered complexity during serial subtraction task in comparison with the corresponding regions during the passive eyes closed condition. Moreover, the dynamical complexity pattern of symmetrical regions over time also remains largely identical indicating both the brain lobes exhibit synchronous behaviour in complexity variations.

The sharp reduction in the SampEn measure for the epileptic spike data over the whole skull space is in agreement with the finding that epileptic behaviour in general, is reflected in the lowering of various parameters such as correlation dimension. The multiscale entropy is evaluated for the data from the eyes closed (normal) as well as the spike data to explore the effect of coarse graining the data at various scaling levels, τ . The scaling factor τ , may be thought of as a sampling time step and the multiscale analysis is carried out on such sampled data sets. τ effectively acts as a filter and as τ increases, the lower frequency components in the data dominate. There is a systematic rise in SampEn values with τ for all the channels; until saturation

sets in at the higher scaling for the normal eyes closed state. On the other hand, for the spike data, complexity variations between brain regions exist even at higher τ or correspondingly lower frequency components. We may summarize that the saturation nature of MS SampEn holds for the healthy case at reasonable values of scaling factor while in the pathological case saturation fails to occur at the scaling factors considered in this study. This implies a slow saturation effect setting in at probably higher values of the scaling. Though confined by the limited data length available in this case, it may nevertheless be surmised that spike data from pathological subjects significantly manifests different saturation effects in multiscale analysis in comparison with data from normal subjects. An analysis with longer data is imperative to validate these observations, which are presented here as a preliminary result.

The complexity analysis can be considered as a first tool to classify mental processes especially with regard to abnormal conditions such as schizophrenia, mental depression and so on. In such cases, the effect of the multiple time scales on the dynamical complexity will be more crucial and hence a multiscale entropy analysis in such contexts will be more appropriate and useful for diagnostic as well as research purposes.

Synchronization Phenomenon in Cognitive Processes

*When all at once I saw a crowd,
A host, of golden daffodils;*

*Ten thousand saw I at a glance,
Tossing their heads in sprightly dance.*

--- William Wordsworth in The Daffodils

The functional and anatomical specializations of the brain that are brought to the fore by physiological, neurophysiological and neuroimaging studies pose a unique problem. How does the brain orchestrate the many emotions, perceptions, thoughts and actions that are brought into play effortlessly from neural processes that are distributed across the brain? Secondly what are the neural mechanisms that select and coordinate this distributed brain activity to produce a flow of adapted and unified cognitive moments? The answers to these fundamental problems are provided by the large-scale integration phenomenon existing in the brain.

It is the neural assemblies that provide a framework for the integration of the distributed neural activity. Neural assemblies may be defined as distributed local networks of neurons transiently linked by dynamic connections. In the brain, the emergence of a specific neuronal assembly by selective interaction of a given group with others is thought to underlie every cognitive act. The linking is mediated via direct or indirect connections that are typically reciprocal. Also two types of connectivity may exist: one within the same cortical area or between regions at the same level of network and the second between different levels of network in different brain regions (Varela et. al., 2001). Connections of the latter type have been traditionally described as feedback-feedforward. In this context, 'local' and 'large' scale integration may be distinguished between. While local integration refers to a common resonance mode exhibited on a spatial scale less than 2mm; large scale integration concerns neural assemblies which are farther apart in the brain typically > 1cm and with transmission delays over 8-10 ms. This could mean that assemblies between occipital and frontal lobes or across hemispheres are separated by dozens of milliseconds in transmission time. It may however be noted that synchrony may also exist between regions whose separation falls in an intermediate range. While local field potentials (LFP) and synchrony between single units can be checked in the case of the local spatial integration studies, large scale coordination analyses rely on intracortical electroencephalography (iEEG) or surface electroencephalography (EEG) or magnetoencephalography (MEG) itself.

Any mechanism for neural coordination must involve interactions between the participating local networks but the specific nature of such interactions is still being debated. It is widely accepted though that networks of reciprocal interactions mediated through phase synchrony are the key for

integration. The study of integration through synchronization can be achieved by focusing on the temporal dynamics of the neural networks in the millisecond range. Direct evidence in support of phase synchrony has been provided by extensive studies on visual binding (Roelfsema et. al., 1997; Munk et. al., 2000). It has also been recently reported that intracranial EEGs from human rhinal cortex and hippocampus tend to demonstrate greater synchrony in subjects learning words and later remembered than words later forgotten. The brain behaviour correlation suggests that these interactions may contribute to effective memory formation (Wagner, 2001).

The means that have been employed to look at the coordination were traditionally linear ones of which the cross power spectrum, coherence (Makeig & Inlow, 1993), the mutual dimension (Stam et. al., 1996) etc. are the most popular. Power spectrum is able to show the energy distribution among the harmonical components of the signal; cross-spectrum and coherence reveal and quantify the linear relationship between processes recorded on different channels of the recording. The time evolution of these analyses illustrates the time-frequency dynamics of the biological signal. The application of the cross correlation measures takes place mostly for the analysis of Local Field Potentials (LFP) like in the case of Baker et. al. (2001), who studied long spike trains (mean about 33,000 spikes) simultaneously from multiple single neurons in the primary motor cortex (M1) of two conscious macaque monkeys performing a precision grip task. When applied to non-invasively obtained signals, the measures that depend on the amplitudes are restricted in application and hence the methods that deal directly with the phase of signals are resorted to. The data obtained from physiological systems are nonstationary as has been stressed at various points throughout this report. This is the main cause for the limitations

inherent in the application of the linear techniques. In this context was introduced the phase method which is based on the premise that the time series data are the outputs of two coupled oscillators and their phase difference may be measured to quantify the strength of interaction between them.

Recently many attempts to study the coupling between brain regions have been carried out in contexts related to the performance of cognitive tasks by utilizing the noninvasively obtained electrophysiological signals from the brain (Mormann et. al., 2000; Bhattacharya et. al, 2001; Bhattacharya & Petsche, 2001; Jaušovec & Jaušovec, 2000; Lachaux et. al., 1999). Most of these tasks have been on mathematical (Zago & Tzourio-Mazoyer, 2002) and verbal activities (Schack et. al., 2000). Some others are also concentrated on the brain state during neurophysiological disorders (Tononi & Edelman, 2000). These studies are mainly based on the EEG and MEG signals in one form or the other. These and many others have established the prominence of phase synchrony studies in learning about hemispheric dominance, long distance coupling and other effects during performance of complex cognitive tasks. Other than behavioural effects studies have also been carried out in understanding the neural mechanisms underlying specific brain tasks.

The techniques that were developed theoretically in studying the dynamical behaviour of coupled oscillators have been successfully adapted to look for coupling based on an analysis of time series data from physical, chemical and biological systems as well. Most extensive in the case of bio-signals has been the application of the phase synchronization ideas to systems like the cardio-respiratory process (Schäfer et. al, 1999), human postural control data (Rosenblum et. al, 1998) and to the signals from the brain. Since the data at hand is from a complex system for which the

equations of motion or for that matter even the full set of variables are not identified, the usefulness of such methods are remarkable and the results there from are far reaching. Before proceeding with the analysis of the EEG signals undertaken as part of this work, the theoretical development of the ideas of phase synchronization as applied to bio-signals may be reviewed.

7.1 Theoretical Background on Synchronization

The history of synchronization goes back to the 17th century when the famous Dutch scientist, Christian Huygens (1673) reported on the observation of synchronization of two pendulum clocks. The systematic study of this phenomenon both theoretically and experimentally were initiated amongst others by Sir Edward Appleton (1922) and Balthasar van der Pol (1927). They showed that the frequency of a triode generator could be entrained or synchronized by a weak, external signal with slightly different frequency. These studies were of high practical importance because such generators became basic elements of radio communication systems. The mathematical theory of synchronization was developed later on and the review of this with regard to classical periodic oscillators under external forcing and in the general case of noisy and lastly chaotic oscillators is considered in the sequel.

7.1.1 Entrainment of a Periodic Oscillator

Stable periodic self-sustained oscillations of an autonomous dissipative dynamical system are represented by a stable limit cycle in its phase space. If the oscillator is forced externally, this simple dynamics is destroyed. The first step towards the description of the system dynamics is by perturbing the system by applying a small force and the analysis is carried out by introducing new variables such as phase and amplitude to the unperturbed

system. The phase is a variable that corresponds to the motion along the limit cycle, i.e. along the direction where neither contraction nor expansion of the phase volume occurs. Hence this direction in phase space and thereby *the phase of oscillations corresponds to zero Lyapunov exponent*.

A natural way to define phase is to take it proportional to time and increase by 2π during one period of oscillation T_0 , the unperturbed period. Then the dynamics of the phase on the cycle can be described as,

$$\frac{d\phi}{dt} = \omega_0 \quad (7.1)$$

where $\omega_0 = \frac{2\pi}{T_0}$. Amplitudes are the other variables of the dynamical system that are locally transversal to the cycle; they correspond to the *negative* Lyapunov exponents.

The description in terms of Lyapunov exponents clearly explains why the phase is an exceptional variable of a dynamical system. Since it corresponds to the sole neutrally stable direction, the phase in contrast to the amplitudes can be controlled by a weak external action. A weakly perturbed amplitude will relax to its stable value, whereas a small perturbation of the phase neither grows nor decays. Thus even very small phase perturbations can be easily accumulated. So far the phase is defined on the limit cycle and not in its vicinity. One way to extend this definition is to demand that Eq.(7.1) is valid not only on the cycle but also in its neighbourhood as well; this phase is also denoted by ϕ . Such a definition implies that the transversal hypersurfaces of constant phase are the isochrones, i.e. they are invariant if the dynamics is observed stroboscopically with the period of oscillations T_0 . Because hypersurfaces form a foliation of a neighbourhood of the cycle, the correct phase ϕ can be obtained from any other cyclic (phase-like) variable θ

via some transformation, $\phi = \phi(\theta, A)$, where A denotes the amplitude variables. Sometimes to characterize the synchronization of a particular system, it is advantageous to use θ : this variable can be estimated from data and the mean observed frequencies of forced or coupled oscillators obtained by means of ϕ or θ coincide:

$$\Omega = \langle \dot{\phi} \rangle = \langle \dot{\theta} \rangle$$

The difference in the relaxation time scales of perturbations of the amplitudes and phase allows one to describe the effect of small periodic external force with a single phase equation. Making a perturbation expansion, it can be seen that owing to the stability property, deviations of the amplitudes are small while deviations of the phase can be large (albeit slow). Hence the phase equation can be derived as (Kuramoto, 1984)

$$\frac{d\phi}{dt} = \omega_0 + \varepsilon Q(\phi, \varphi) \quad (7.2)$$

where ε is a small parameter proportional to the amplitude of the force, φ its phase obeying $\dot{\varphi} = \frac{2\pi}{T}$ and Q is 2π periodic in ϕ and φ functions. Eq.(7.2)

describes dynamics on a torus $0 \leq \phi \leq 2\pi$, $0 \leq \varphi \leq 2\pi$.

Taking the Poincaré map at $\varphi = 0$, Eq. (2) can be reduced to a circle map as:

$$\phi_{n+1} = \phi_n + F(\phi_n) \quad (7.3)$$

with a 2π periodic function F . The dynamics of this map can be characterized by the rotation number (Ott, 1993)

$$\rho = \lim_{N \rightarrow \infty} \frac{\phi_N - \phi_0}{2\pi N}$$

This number is the ratio between the observed frequency of oscillations Ω and the frequency of the external force ω :

$$\rho = \frac{\Omega}{\omega} \quad \text{where } \Omega = \langle \dot{\phi} \rangle$$

If ρ is rational, the observed frequency is in rational relation with the frequency of the external force

$$\Omega = \frac{m}{n} \omega$$

and this regime is called $m:n$ synchronization.

Consider a detailed understanding of the above definition by taking for simplicity the case of 1:1 synchronization. Usually this phenomenon is understood as the appearance of a certain relation between phases or as phase locking. In literature, this notion is used in differing senses. In the most restrictive sense, phase locking is said to exist if the phases of two or more oscillators coincide exactly. In this case, it would mean $\phi = \varphi$. This is a special case of the phases having a constant shift, $\phi = \varphi + \text{constant}$. Both these mean that the phase of the oscillator rotates uniformly with the frequency of the external force. From Eq. (7.2), however it follows that we cannot expect these properties to be valid even for small forcing. Indeed, Eq.(7.2) admits the solution $\frac{d\phi}{dt} = \omega$ only in a particular case when the coupling function Q depends on the phase difference only, i.e. $Q(\phi, \varphi) = Q(\phi - \varphi)$. Let us introduce the phase difference $\Phi = \phi - \varphi$ and rewrite Eq. (7.2) as

$$\frac{d\Phi}{dt} = \omega_0 - \omega + \varepsilon Q(\Phi) \quad (7.4)$$

in the synchronous state, this equation should have (at least one) stable point. This happens if the frequency mismatch (detuning) is small enough, i.e.

$\varepsilon Q_{\min} < (\omega - \omega_0) < \varepsilon Q_{\max}$ and this condition determines the synchronization (phase-locking, mode-locking) region on the (ω, ε) plane. Within this regions, the phase difference remains constant, $\Phi = \delta$, and the value of this constant depends on the detuning, $\delta = Q^{-1}\left(\frac{(\omega - \omega_0)}{\varepsilon}\right)$.

But in the general case, the coupling function $Q(\phi, \varphi)$ cannot be reduced to a function of the phase difference Φ . Then even in a synchronous regime Φ is not constant but fluctuates, although these fluctuations are bounded. Thus, we can define phase locking according to relation,

$$|\phi - \varphi - \delta| < \text{const.} \quad (7.5)$$

from which the condition of frequency locking,

$$\Omega = \langle \dot{\phi} \rangle = \omega$$

naturally follows. This definition is made use of in periodic regimes when the forced oscillations are not close to the original limit cycle. A detailed description of the synchronization transition in a periodically forced weakly nonlinear oscillator with the amplitude of the external force is given in Pikovsky et. al. (2000).

7.1.2 Noisy Oscillators

Let us now consider the effect of noise on phase synchronization (Stratonovich, 1963). The simplest way to model a noisy environment is to add a noise to Eq. (7.2), or for the simplest possible solution add to Eq. (7.4).

$$\frac{d\Phi}{dt} = \omega_0 - \omega + \varepsilon Q(\Phi) + \xi(t) \quad (7.6)$$

The dynamics of the phase can be treated as the dynamics of an overdamped particle in a potential.

$$V(\phi) = (\omega - \omega_0)\phi - \varepsilon \int_0^\phi Q(x) dx$$

The average slope of the potential is determined by the mismatch of frequencies of the autonomous oscillator and external force; the depth of the minima (if they exist) is determined by the amplitude of the forcing. Consider the case of a particle representative of phase as depicted in Figure 7.1. Without noise, the particle would either rest in a minimum or slide downwards along the potential, if there are no local minima; this corresponds to synchronous and nonsynchronous states resp.

Suppose the noise is small and bounded then its influence results in fluctuations of the particle around a stable equilibrium, i.e. in fluctuations of the phase difference around some constant value. Contrary to this if the noise is unbounded, there is always a probability for the particle to overcome a potential barrier ΔV and hop to a neighbouring minimum of the potential. The time series looks

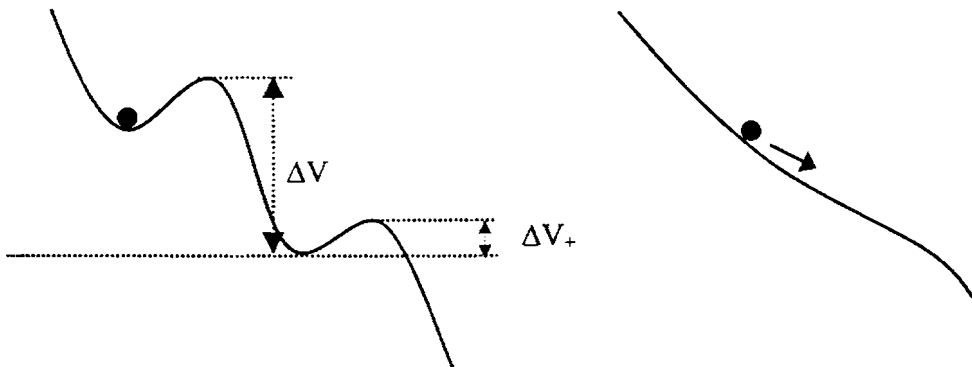


Figure 7.1. *The phase represented as a particle in an inclined potential within and outside the synchronization regime.*

like a sequence of these phase slips and relation (7.5) does not hold. Nevertheless for small noise, the phase locking is detectable although it is not perfect. We can observe epochs of phase entrainment between the phase slips. Averaged locally over such an epoch, the frequency of the oscillator coincides with that of the external force. The observed frequency that is computed via averaging over a long period of time differs from that of the external force though this difference is small if the slips are rare.

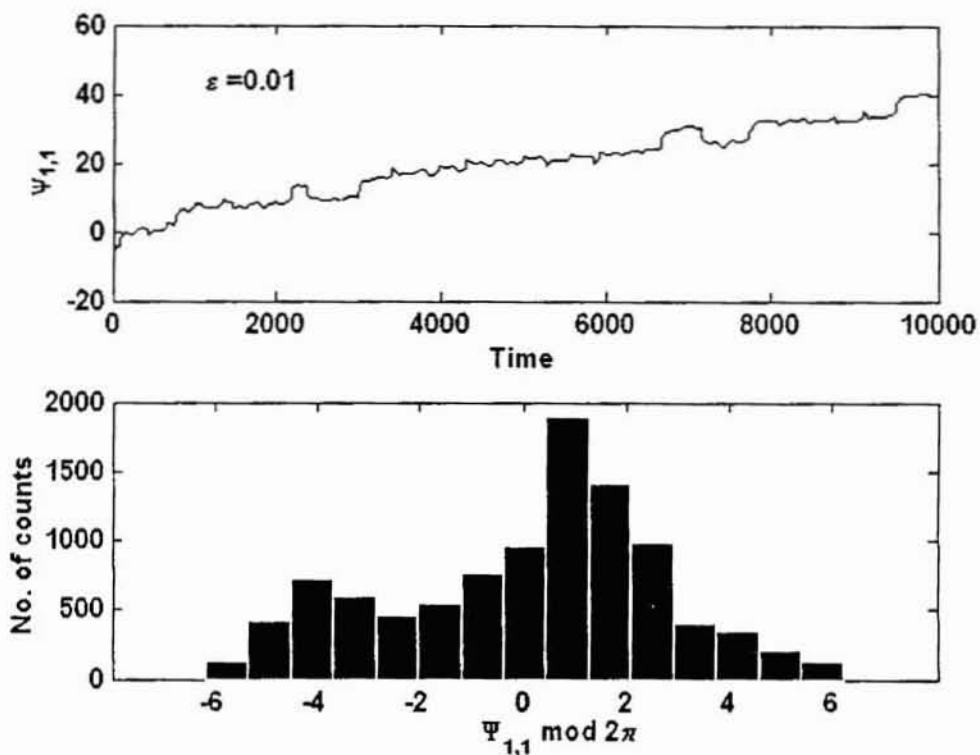


Figure 7.2(a)

Phase locking in noisy systems can be also understood in a statistical sense, as the existence of a preferred value of the phase difference $\Psi \bmod 2\pi$. Indeed the particle spends most of the time around a stable equilibrium then rather quickly jumps to a neighbouring equilibrium where the phase difference differs by a multiple of 2π . This can be reflected by the distribution of $\Psi \bmod 2\pi$.

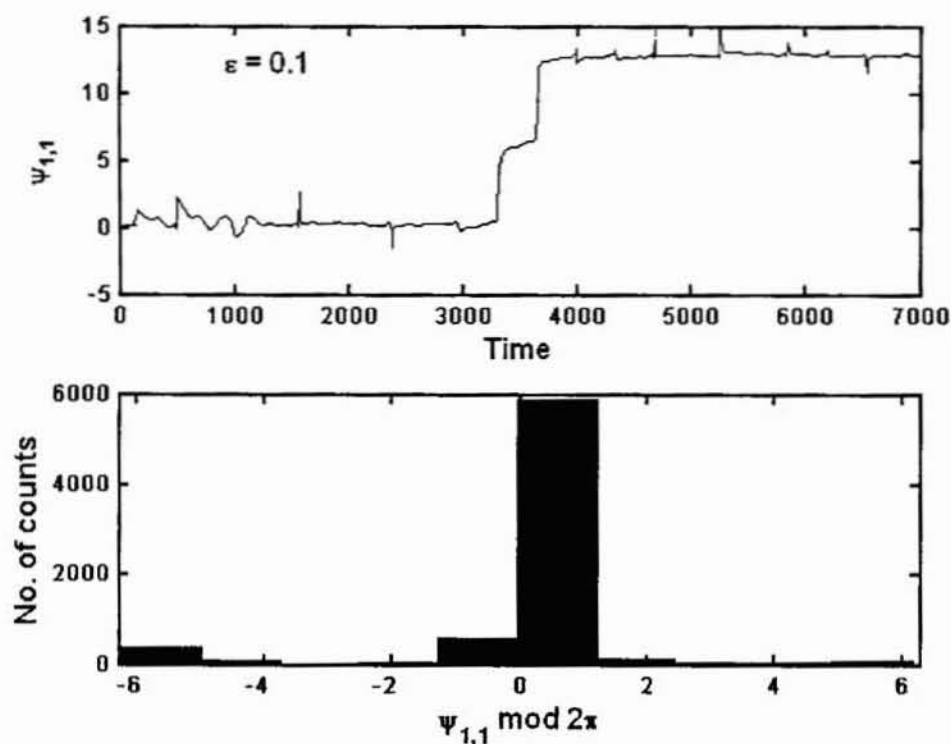


Figure 7.2(b)

Figure 7.2. The relative phase distribution in a coupled pair of Rossler oscillators. There is no phase locking in the weak coupling of $\epsilon=0.01$ (a) while at higher values of coupling $\epsilon=0.1$, phase locking sets in as indicated by the peak in the histogram (b).

A nonsynchronous state would have a broad distribution whereas synchronization would correspond to a unimodal distribution. Figure (7.2) is a graphical representation of this in the case of two chaotic oscillators with no coupling as compared to the coupled case.

7.1.3 Chaotic Oscillators

Any autonomous continuous-time dynamical system with chaotic behaviour possesses one zero Lyapunov exponent that corresponds to the shifts along the flow. So phase can be introduced for this case as well. There are many ways in which the phase for a system may be defined. Three approaches may in general be followed for the phase (Pikovsky et. al., 1997).

(a) Suppose we define a Poincaré secant surface for a chaotic system. Then for each piece of a trajectory between two cross sections with this surface, the phase can be defined as a linear function of time, so that the phase increment is 2π at each rotation:

$$\phi_M(t) = 2\pi \frac{t - t_n}{t_{n+1} - t_n} + 2\pi n, t_n \leq t \leq t_{n+1} \quad (7.7)$$

Here t_n is the time of the n^{th} crossing of the secant surface. This definition is ambiguous because it depends on the choice of the Poincaré surface. Nevertheless defined in this manner the phase has an important property: its perturbations neither grow nor decay in time, so it corresponds to the direction with the zero Lyapunov exponent in the phase space.

(b) The phase can also be introduced as an angle between the projection of the phase point on the Poincaré plane and a given direction in the plane

$$\phi_p(t) = \arctan\left(\frac{y}{x}\right) \quad (7.8)$$

The two phases ϕ_M and ϕ_p defined above do not coincide over time scales less than the average period of oscillation, however, they have equal average growth rates. In other words, the mean frequency defined as the average of $\left(\frac{d\phi_p}{dt}\right)$ over large periods of time coincides with the usual definition of the mean frequency via the average number of crossings of a Poincaré surface per unit time.

(c) An alternative definition of phase is known as the analytic signal concept prevalent in the signal processing. This general approach based on the Hilbert transform and introduced by Gabor back in the late '40s (Gabor, 1946). The analytic signal is a complex function of time defined as

$$\xi(t) = s(t) + i\tilde{s}(t) = A(t)e^{i\phi_H(t)} \quad (7.9)$$

where $\tilde{s}(t)$ is the Hilbert transform of $s(t)$

$$\tilde{s}(t) = \frac{1}{\pi} P.V. \int_{-\infty}^{\infty} \frac{s(\tau)}{t - \tau} d\tau \quad (7.10)$$

where *P.V.* is the Cauchy principal value of the integral. The instantaneous amplitude $A(t)$ and phase ϕ_H of the signal are thus uniquely defined.

The Hilbert transform can be considered as the convolution of the functions $s(t)$ and $(1/\pi t)$. Hence the Fourier transform $\tilde{S}(\omega)$ of $\tilde{s}(t)$ is the product of Fourier transforms of $s(t)$ and $(1/\pi t)$. For physically relevant positive frequencies, $\tilde{S}(\omega) = -iS(\omega)$ i.e. ideally $\tilde{s}(t)$ can be obtained

from $s(t)$ by the filter whose amplitude response is unity and whose phase response has a constant ($\pi/2$) lag at all frequencies.

Although the analytic signal approach provides a unique definition of phase of a signal, ambiguity still exists for the phase definition of a dynamical system as the result depends on the choice of the variable. But the advantage of the analytic signal is that the phase can be easily obtained from experimentally measured time series or in some other situation in which Poincaré section construction is difficult.

In contrast to the case of periodic oscillators, the growth of the phase of a chaotic system is in general non-uniform. The Poincaré return times, which may be considered as instantaneous periods themselves depend on the coordinates of the intersection with the Poincaré surface, i.e. on the irregular amplitude. This dependence may be taken as arising due to some effective 'noise' although in this case the irregularity has a purely 'deterministic' origin. Thus the synchronization phenomena for a chaotic system are similar to those in noisy periodic oscillators (Rosenblum et. al., 1996; Pikovsky et. al., 1997).

7.2 Towards Data Analysis: Quantifying Strength of Synchronization

In this section we see how the concept of phase synchronization can be used in order to reveal the presence of interaction between systems from experimental data. We have already summarized that synchronization of weakly coupled oscillators appears as some relation between their phases and frequencies. In the context of data analysis we exploit this fact to tackle the inverse problem i.e., inference of the presence of synchronization from data. To this end, we have to estimate from the signals the phases and frequencies and look for relations between them.

The problem being assessed may be put in the following manner: Suppose we observe a system with a complex structure that is not known exactly, and measure two time series at its outputs. The goal is not only to find out whether these signals have dependence or not, which can be done using the traditional statistical techniques, but to extract additional information on the interaction of some subsystems within the system. However, some additional knowledge is needed regarding the observed objects to conclude that they are self-sustained oscillators having their own rhythms, which may be adjusted due to interaction. The advantage of the phase synchronization method is that it enables the study of rather weak interactions between the two oscillatory systems as well. The notion of phase synchronization implies only some interdependence of the phases, whereas the irregular amplitudes may remain uncorrelated. The irregularity of amplitudes can mask the phase locking but the signals may be less sensitive in the detection of the systems' interrelation.

Indeed the coherence technique, which has been used extensively to study interdependence of signals, in the case of EEG signals too, is a measure of the linear covariance of between two spectra. These spectra can be estimated from finite data sets by first subdividing the whole data set into segments and then computing using the discrete Fourier transform (DFT) the approximate spectra and finally averaging these sub spectra over all the segments. Segments here refer to successive time intervals defined by a window sliding in time over the whole recording. Hence a single measure of coherence typically depends on several seconds of data, which limits the temporal resolution of the method. But the method also requires that each data segment correspond to the same process with the same spectral properties. Since this assumption of stationarity can rarely be validated either

in time or across trials, a measure that does not require stationarity is much preferred. Besides this, coherence also varies with amplitude covariance and since phase locking is sufficient to conclude that two subsystems (such as in the brain) interact, methods for sole detection of *phase coherence* gain significance. Moreover, the classic statistical analysis of coherence is based on a comparison with independent white noise signals (Lachaux et. al., 1999).

We follow the phase synchronization techniques therefore to delve into the nature of regional coupling in the brain during various tasks in this study. Of the three phase determination methods listed in an earlier section, the method of Gabor’s analytic signal lends itself as most suited in cases wherein neither the full set of variables nor the determining equations of the system underlying the signal are known. The phase synchrony method is based on the well established fact that weak coupling first affects the phases of oscillators while their amplitudes remain largely uncorrelated in time (Rosenblum et. al., 1996). Reiterating some of the aforementioned points, the key to detecting the synchronization between two systems is in the relation between their phases. Consider two signals with phases ψ_i and ψ_j at any instant evaluated by application of Eq. (7.9) - Eq. (7.10). A phase locking of $m:n$ between the two signals is defined (Tass et. al., 1998) as,

$$\left| \psi_{m,n} \right| = \left| m\psi_i - n\psi_j \right| < \varepsilon \tag{7.11}$$

where ε is an arbitrarily small constant. Since real data has characteristics of noisy oscillators the relative phase which performs a random-walk-like motion has a well-expressed peak in the distribution of the relative phase ($\psi_{m,n} \bmod 2\pi$) if the two systems weakly interact.

In order to characterize the strength of the synchronization the actual deviation of the actual distribution of the relative phase from the uniform one

has to be determined. Tass et. al. (1998) introduced an index based on the Shannon entropy defined as

$$\rho = \frac{(S_{\max} - S)}{S_{\max}} \quad (7.12)$$

where S is the Shannon entropy as obtained from information theory given as,

$$S = -\sum_{i=1}^N p_i \ln p_i \quad (7.13)$$

Here p_i is the relative probability of occurrence and S_{\max} , the normalizing constant is $\ln N$ where N is the number of bins. Normalized in this manner, $0 \leq \rho \leq 1$, where $\rho = 0$ corresponds to a uniform distribution or no synchronization while $\rho = 1$ corresponds to a Dirac delta function-like distribution or perfect synchronization.

7.3 Application of Phase Synchronization to Normal and Pathological EEG Signals

7.3.1 No-task Passive States

The present study is an application of the method of phase synchronization to look into the interactions between cortical areas during no-task conditions, which are the eyes closed and eyes open. An attempt is also made to study the temporal variation of the synchronization that may exist between brain regions. The temporal analysis is relevant in the context of the nonstationary nature of the EEG signals consequent to the existence of a number of time scales in human brain dynamics, which is known to affect the computation of the invariant parameters as discussed in an earlier section. A novel technique has been introduced to arrive at a mean synchronization index for each

channel under study representing the strength of coordination of that channel with respect to all other channels involved in the study.

The data analyzed in this study is collected from normal subjects with electrodes arranged on the scalp in the International 10-20 system with an EEG machine coupled to a PC using an analog to digital converter (DT- 2841) and an array processor (DT-7020). For the eyes closed and eyes open conditions, the electrode locations are Fp1, Fp2, F3, F4, F7, F8, C3, C4, T3, T4, P3, P4, T5, T6, O1 and O2. This schematic is illustrated in chapter 3. The acquired data is sampled at a rate of 512 samples/s/channel and filtered using a FIR digital filter of order 150 with a bandwidth of 0.1-32 Hz.

The Weighted Averaging Technique: The phase synchronization analysis is extended over each of the 16 channels taken two at a time. When studying the coordination between any two cortical regions, the EEG signal from each location forms the signal ψ_i so that the phase synchronization index between these can be evaluated by using Eq.(7.11) - Eq.(7.13) for non-overlapping sliding windows of fixed time duration. This enables the analysis of temporal variation in phase synchronization as contained in the index ρ . In order to study the variation in ρ for each of the cortical regions in time, we carry out the aforementioned analysis and then subject the indices to a method of weighted average to obtain the mean phase synchronization over a certain time period.

If we consider a particular cortical region or location say, Fp1 the phase synchronization relative to this channel is evaluated for all the other locations. If we have a 16 channel input data, there will be 15 phase synchronization indices since the self-synchronization index is 1 and is trivial. In order to determine a mean synchronization for the channel Fp1 an

averaging is to be carried out in such a way that the synchronization index contributions are weighted according to their relative separation from the channel. This method is resorted to because the interactions between neighbouring regions will obviously be stronger, generating a higher ρ value as compared to regions farther away. Hence when an average over all the channels is carried out, the stronger contributions of the neighbouring regions will dominate and mask the effect of weaker yet significant contributions from farther regions of the brain. To circumvent this undesired effect, a modified averaging method is adopted in this study. We start with a set of ρ values for the given channel with respect to all other channels for a continuous time period of say T seconds divided into n windows of fixed time duration. Hence for a location i , for each window the set of synchronization indices is denoted by $\{\rho_{ij}\}$ with j varying from 1 to 16 and $j \neq i$. For each of these time windows, a histogram of the ρ values is determined. Since with respect to each channel there are more number of farther lying regions than neighbouring regions, the frequency will be higher for lower values of ρ . The maximum frequency of occurrence, ρ_{max} is noted and the deviation of a given synchronization index value from the minimum phase synchronization index, $(\rho_{ij})_{min}$ is determined. If it is found to be lesser than a threshold value - chosen here to be a quarter of the range i.e. the difference between the maximum and minimum of the ρ values - the contribution from that synchronization index is scaled by an index $(\rho_{max}/3)$. The values to be scaled are chosen according as,

$$(\rho_{ij} - (\rho_{ij})_{min}) < R_{th} \quad (7.14)$$

and the scaling is carried out as

$$\rho'_{ij} \equiv w\rho_{ij} \quad (7.15)$$

where $R_{th} = \frac{1}{4}[(\rho_{ij})_{\max} - (\rho_{ij})_{\min}]$ and $w = P_{\max}/3$.

The average synchronization index of that particular window for the channel i is a mean of these scaled set of ρ values i.e. $\{\rho'_{ij}\}$ and the net average phase synchronization index for the particular channel the average of the mean ρ value in each window. The reason for the particular threshold, R_{th} and weight value w is that the choice of these ensures a smooth scaling of the ρ_{ij} without changing the distribution that existed before the scaling. The advantage of such a weighted averaging technique is that it retains the effect of higher synchronization between regions arising from their neighbourliness as well as contains the effect of lesser but significant synchronization that may exist between farther regions. In figure 7.3, a plot of the actual as well as scaled phase synchronization index values for frontal region Fp1 relative to all the other channels for the eyes closed state in a particular time segment is given. It can be seen that only those values that are much lower than the highest values get scaled and the others remain unaffected.

Hence the net phase synchronization index for a given channel i averaged over sliding windows of a fixed time duration is,

$$\rho = \frac{1}{N_t} \sum_{k=1}^{N_t} \left(\frac{1}{n} \sum_{\substack{j=1 \\ j \neq i}}^n \rho'_{ij} \right)_k \quad (7.16)$$

where N_t is the total number of time windows over which the time average of ρ is considered and n the number of channels to which the coordination of each channel is considered. n will be one less than the number of channels in the study. Based on this index, the temporal variation is considered over the passive states.

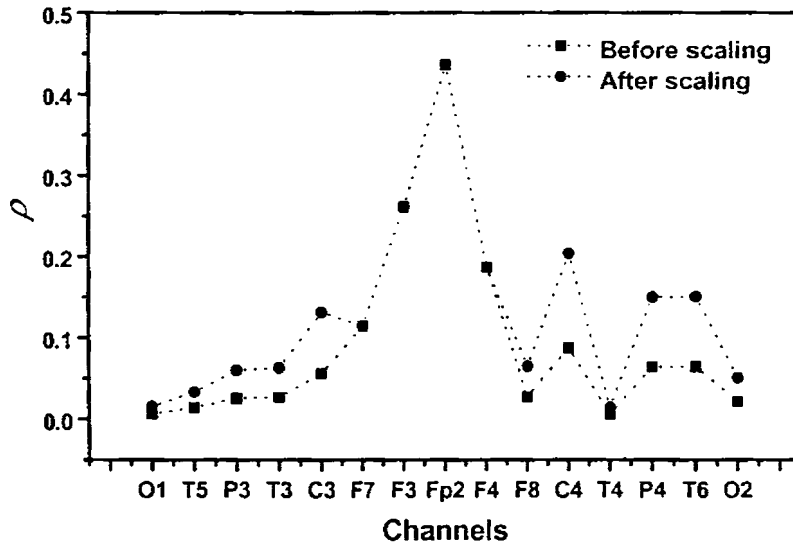


Figure 7.3. The set of phase synchronization index, ρ values corresponding to a typical window for the Fp1 region relative to all the other channels in the E.C. case. The actual values as well as those after carrying out the scaling are indicated. The dotted lines are merely for guiding the eye.

In this study, the EEG signal from the no-task eyes closed and eyes open conditions is divided into non-overlapping windows of duration 2 seconds each. The phase synchronization index for each of the 16 channels is determined with respect to the other 15 channels for continuous windows for a time of 140 seconds. The scaling for the indices between neighbouring regions is provided by employing the technique weighted averaging described above, and the scaled set of indices are averaged for each of the windows. A further averaging is carried out over intervals of 10 seconds, 20 seconds, 28 seconds and 70 seconds to get a general picture of the behaviour of the

synchronization phenomenon exhibited by the cortical regions under the two different conditions.

One of the initial observations is that synchronization is observed to be stronger for the eyes closed (E.C) condition as compared with the eyes open (E.O) state. The evaluated synchronization indices are relatively higher all over the cortex in the E.C case against the values computed during the E.O condition. Figure 4 is a plot of the synchronization index ρ evaluated using the weighted scaling method as in Eq. (7.14). - Eq. (7.16) for each channel for both these conditions. Each ρ value comprises the effect of the net coordination of that channel with the rest of the brain during the time under consideration.

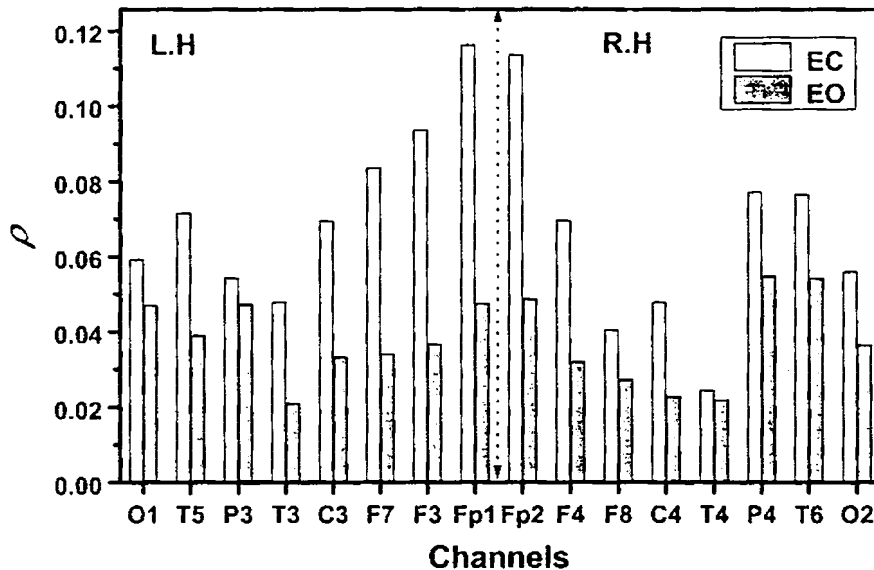


Figure 7.4 A comparison of the net synchronization index, ρ for the various cortical regions during the eyes closed (E.C.) and eyes open conditions (E.O.)

This observation could be interpreted as the dependence of the synchronization index with the organization in the brain. In the E.C. state, the ocular inputs are absent and hence to that extent the degree of randomness is widespread. Hence the synchronization present in the system dominates over the background.

Yet another striking observation seems to be the stronger level of interaction of the left hemisphere as compared to the right one in the E.C case. In the E.O case on the other hand, the symmetrical regions of the brain show almost similar tendencies of interaction with the rest of the brain. Apart from the frontal regions, for the E.C condition the regions such as (C3, C4) and (P3, P4) which are situated on and near the midline of the brain, are in higher states of synchronization. This points towards a higher amount of information transfer between the brain lobes during the eyes closed condition. In contrast to the temporal-parietal regions, the occipital-temporal regions are in higher state of synchrony. In general, the brain regions interact strongly within themselves leading to higher coherence of the brain state during the eyes closed condition as compared to the visually stimulated E.O case.

The temporal variation of the phase synchronization index reflecting the strength of interaction was studied by evaluating it for sliding windows of 2s duration. The synchronization index was first averaged over 10 second intervals (5 windows) each to look for a variation over the 14 such intervals that occur for the total 140seconds record of the no-task state. Then the averaging is considered over 20seconds (10 windows) intervals, 28seconds (14 windows) intervals and finally 70seconds (35 windows) intervals. These particular time slots were chosen for the averaging process since these being factors of the total time (~140seconds); give equal averaging intervals. In

the colour coded illustrations 7.5(a)–(c) for eyes closed case, synchronization index for the channels averaged over each of 10s, 20s, 28s and finally in figure 5(d) the average ρ value over 70s is given. It is clearly seen that for short time intervals, it is quite difficult to perceive strong changes, if any, in the coordination exhibited by cortical regions. This is because in the passive state no sudden changes take place to get reflected in the synchronization index. However, a general trend can be observed for the channels that for the frontal regions Fp1, Fp2 and occipital regions O1 and O2, the net synchronization index ρ is almost uniformly distributed in the whole time span though with a decrease towards the final intervals as compared to the initial and central time slots. This decrease in synchrony with time effect is more pronounced for regions surrounding the central- parietal-temporal regions (C3 & C4), (T3 & T4), P4 and T6 and more clearly observable in figure 5(c) for the 28s interval. In the final plot for 70s interval, the general synchronization trend exhibited by the cortical regions when the whole of the observation time is divided exactly into two halves is shown. From here we observe that there is an enhanced coordination for most of the frontal regions especially in the left hemisphere during the second half of the observation period. Had the synchrony been decreasing steadily with time, such a behaviour would not have occurred. This could only mean an increase in synchrony some time after the beginning of the recording towards the central time slot. In the smaller time interval averaging with 10s and 20s (Figures 7.5(a-b)) the initial slots had exhibited higher synchrony than the final ones. In figure 7.5(c) where time sections of 28s were averaged, there was evidence in atleast six to seven channels of higher synchrony in the central slots than in the ones just preceding these. This implies that while initially there is high synchronicity in the brain; as time progresses there is a lowering of the

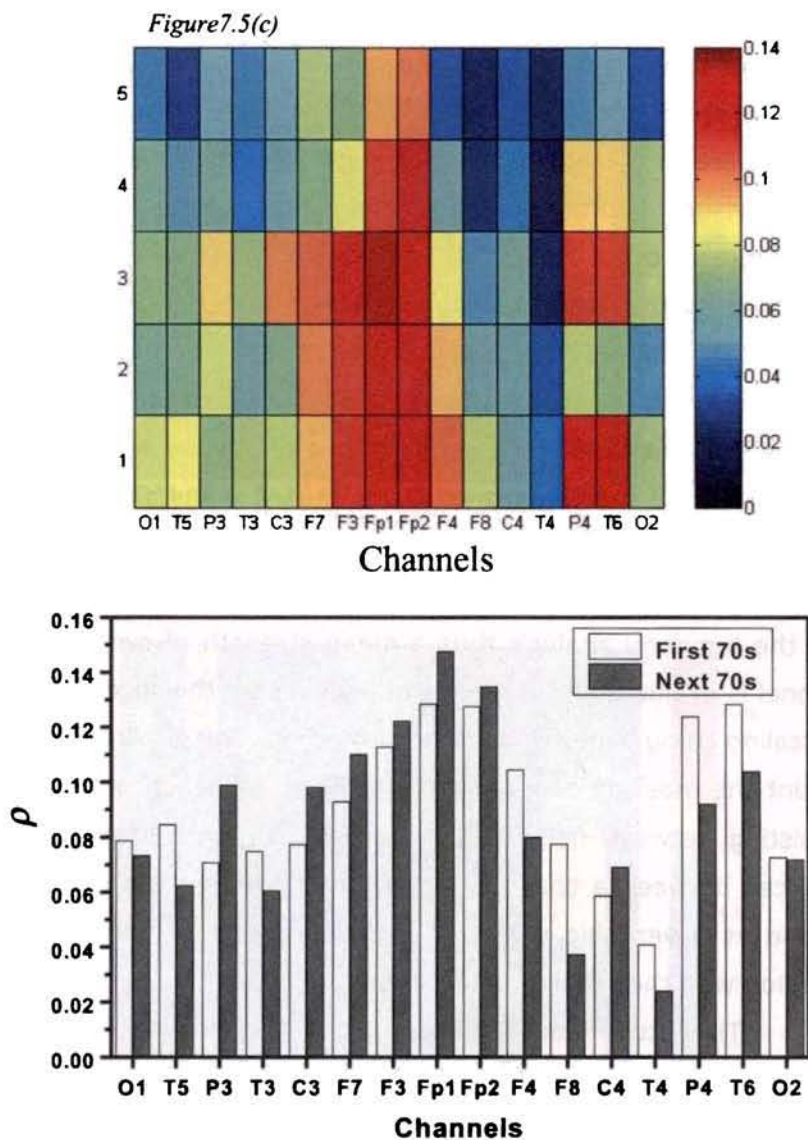


Figure 7.5(d)

Figure 7.5. Temporal variation in the phase synchrony index, ρ during the eyes closed state over time intervals of $T= 10s$ (a), $20s$ (b), $28s$ (c) and $70s$ (d).

interactions between various brain regions.

A similar line of analysis adopted for the E.O case gives results shown in figures 7.6(a)-(c). In this case, under the effect of visual stimulus, all cortical areas are in a state of lowered synchronization since the processes involved in visual information processing lead to a higher dynamical complexity spread over the cortex. Hence we consider here the overall temporal effect on the synchronization effect of the brain regions for longer time slots of 20s, 28s and 70s. It is observed that most of the cortical regions have almost equal yet lowered (In comparison to E.C) strength of coordination over all the time intervals starting from the beginning to the end of the recording period. We may deduce that this means a sustained complexity in the dynamics of the visually stimulated state causes a loss in coordination between the individual cortical regions.

In the temporal analysis thus a mean strength of synchronization for each channel is evaluated from the set of ρ values for the specified channel by suitably scaling using a newly introduced method. This scaling method takes into account the masking of lower yet significant values of ρ by the higher ρ values existing between neighbouring regions. Hence the averaging of the scaled indices between a channel and the rest of the brain regions may be looked upon as a veritable measure of the strength of coordination of that cortical region with the other cortical areas.

The study reveals apart from the known fact of lowered complexity for the eyes closed state, the time dependence of cooperative behaviour of the brain regions. While there is a reduction in the strength of synchronization as time passes for the eyes closed condition, the lowered

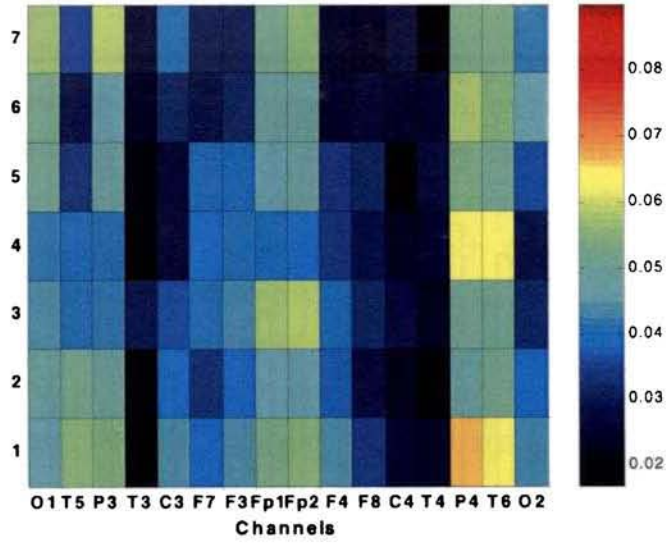


Figure 7.6(a)

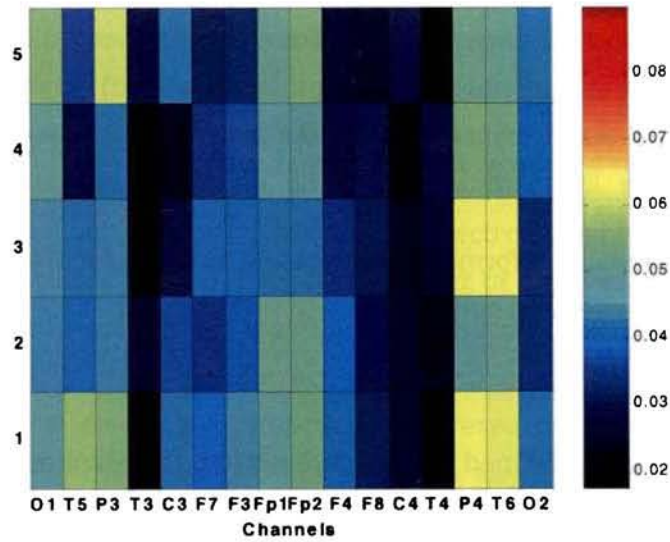


Figure 7.6(b)

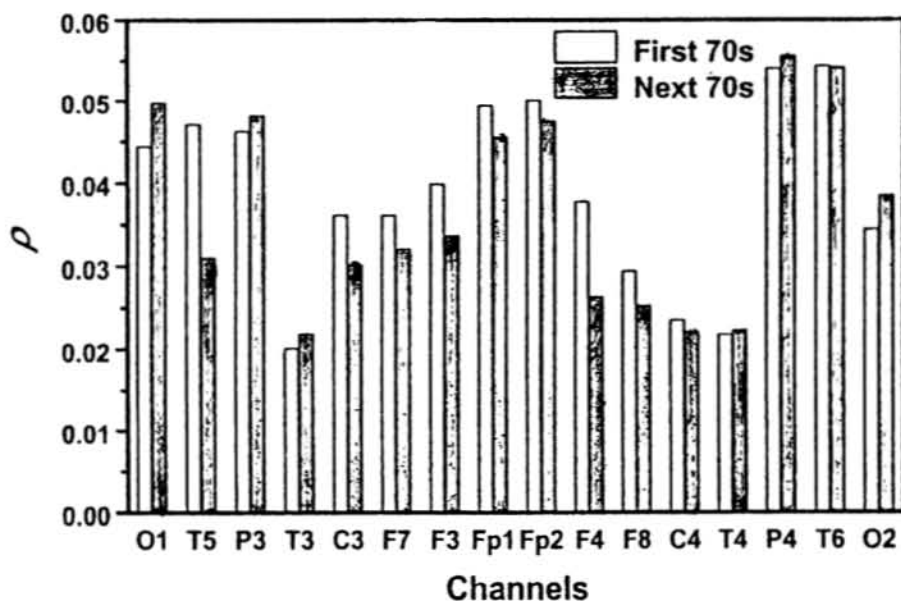


Figure 7.6(c)

Figure 7.6. Temporal variation in the phase synchrony index, ρ during the eyes open state over time intervals of $T=10s$ (a), $28s$ (b) and $70s$ (c).

coordination during visual information processing persists for the whole time interval in which the eyes are open.

7.3.2 Epileptic Condition

An epileptic seizure is defined as a paroxysmal, self-limited change in behaviour associated with excessive electrical discharge from the central nervous system. The term seizure actually refers to a transient alteration of behavior due to abnormal synchronized and repetitive bursts of firing of

neurons in the central nervous system. Epilepsy is a syndrome of episodic brain dysfunction characterized by recurrent unpredictable spontaneous seizures. The diagnosis of epilepsy is not a simple one. Currently there are more than twenty documented types of seizures, and no two people who have the same disorder are affected in precisely the same manner. For instance, Partial seizures begin in a localized brain region, whereas Generalized seizures show widespread involvement of both hemispheres. Examples of generalized seizures are absences (petit mal), myoclonic, or tonic-clonic (grand mal) seizures. A complex partial seizure is associated with impairment of consciousness while a simple partial seizure is not. Most complex partial seizures originate from the temporal lobe and are also called temporal lobe seizures. Epileptics frequently have more than one type of seizure. When simple partial seizure precedes a complex partial seizure, it is referred to as an aura. More recent classifications of epileptic syndromes incorporate such features as etiology, age of onset, and the different combinations of seizures that an epileptic has. Other commonly used terms include ictal (of seizure itself) and interictal (between seizures). Convulsion implies ictal behavior with vigorous motor activities. Status epilepticus denotes a very prolonged seizure or series of seizures occurring so frequently that full recovery of brain function does not occur interictally. Electroencephalographic (EEG) investigation remains the most important aspect of the presurgical evaluation of this abnormal condition. Analysis of unselected EEG activity between events (interictal) or of specific activity during events (ictal) can provide evidence of focal electrical dysfunction. The research in epilepsy is a full-fledged branch in the Neurosciences since the key to prevent the onset of spontaneous neuronal firing etc. is not yet clearly known.

The phase synchrony analysis when extended to study the interactions in the brain during epilepsy throws light on the marked variations in the brain interaction state during the non-epileptic periods and epileptic discharge. The synchronization index was evaluated for each channel of the 8-channel data set with respect to each of the other channels for sliding windows of 2second duration each. The mean synchronization index over each such 2s period was then determined to learn about the variations in the cooperative behaviour of each brain region.

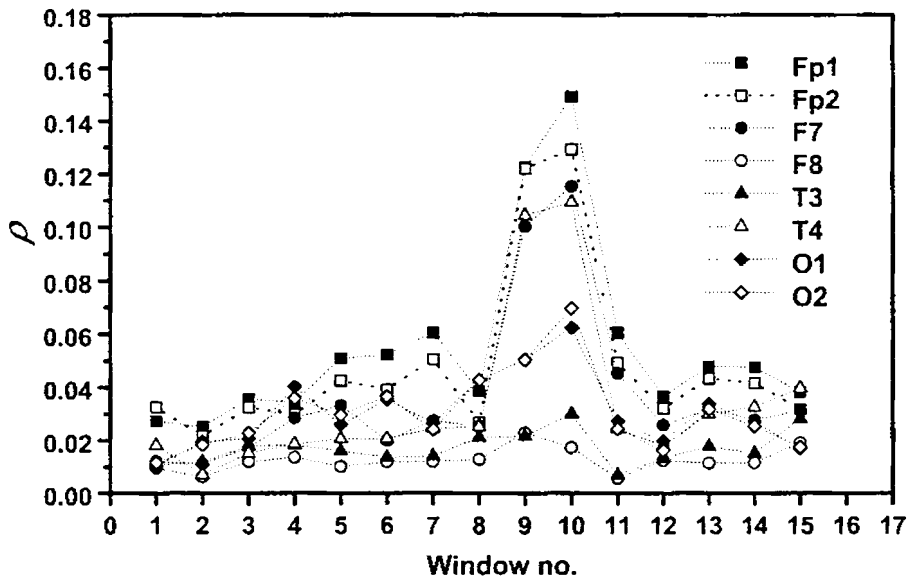


Figure 7.7

The mean phase synchronization index evaluated for an epileptic subject, ρ for each location is plotted against the window number. Each window is of 2s duration and the time encompasses both NED and DED periods.

The study reveals that as shown in figure 7.7, the synchronization is largely the same ~ 0.02 over regions distributed in skull space from windows 1 to 7. But immediately afterwards the synchronization strength is enhanced to much higher values ~ 0.12 , implying some major change in the brain state. It is found that these windows 8-11 correspond to the definite epileptic discharge (DED) period and the time preceding the seizure i.e. windows 1-7 to the non-epileptic discharge (NED) period. Another noteworthy point is that not all regions exhibit the same amount of increase in the synchronization index. For instance, while regions Fp1, Fp2, F7 and T4 show considerable increase of interaction, O1 and O2 appear to be only partially affected while F8 and T3 do not seem to be affected at all. Lehnertz and Elger (1995) showed that during an epileptic seizure the neuronal complexity is lowered and hence the interactions are probably enhanced. The significant fact brought out by this line of investigation is that the synchronization is indeed higher during intervals of strong discharge as compared to that of non-epileptic discharge.

There is evidence that the onset of an epileptic discharge causes a decrease in the degrees of freedom as contained in the correlation dimension D_2 (Lehnertz & Elger, 1995) of the attractors. This compactness could also be a further cause for the stronger interactions amongst the attractors thus resulting in a higher synchronization index. Hence there is an apparent cross correlation existing between D_2 and ρ . Figure 7.8 gives the synchronization index, ρ with respect to location F7 for typical windows corresponding to DED and NED. This region was undertaken for the study because it was the one that showed a marked difference in D_2 during the DED and NED periods. Hence it is to be assumed that this region is strongly affected by the seizure episode. Further while the strong interaction between neighbouring regions such as (F7-Fp1) is to be expected for both the NED and DED conditions, the

high amount of synchronization between regions farther away in the lobe opposite to F7 such as Fp2 and T4 show that there is a functional cooperativity between distant regions under a complex brain experience such as epilepsy. In the work on the unfolding of the neural attractors, it was shown that the rate at which the attractors unfold depends critically on time scales. In the case of epileptic seizures the presence of high time scales in the dynamics was detected not only during DED period but also in the NED windows. The present study corroborates the finding in that analysis that the seizure activity is probably confined to certain brain regions - those that have a marked rise in neural co-operativity - signified by the large ρ values (Pravitha et. al., 2001). Moreover this analysis sharply brings to focus the distant connectivity between neural regions that accompany abnormal brain conditions like epilepsy.

The study reveals in the case of the pathological condition of epilepsy, there is selective increase of phase synchronization index between certain brain regions during the seizure period and the regions involved may be lying far apart and even in opposite brain lobes. The study reveals the sharp increase in coordination and loss of complexity in the cortical areas of the normally functioning brain disrupted by an abnormal seizure state.

The present analysis has produced some corroborative results to those already known regarding no task conditions. However the new parameter comprising all the interactions of a given cortical region with the rest of the brain may be applied to the study of other mental activities such as word processing and mental arithmetic as well as to pathological conditions such as Alzheimer's disease etc. to gain better understanding of the mechanism of the neural cooperativity. As the next step, we apply techniques to arrive at the

direction of the actual coupling that may be taking place between the neural oscillators.

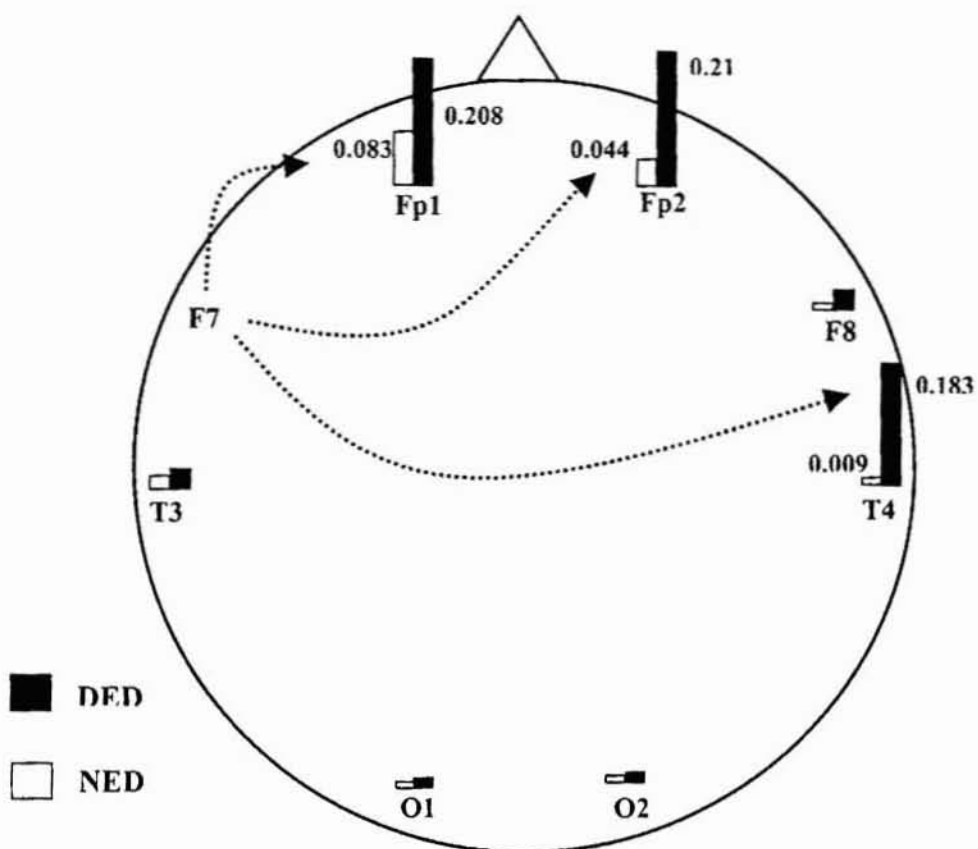


Figure 7. 8. The distribution of the ρ values over the skull space for the F3 region for two typical windows corresponding to the NED and DED periods. The long distance synchrony enhanced during the DED period is clearly observable

7.4 Phase synchrony to Study Effect of Fatigue on Mental Tasks

Having looked into the cases of no-task conditions as well as a pathological state the idea of extending the phase synchrony to delve the directionality of the coupling between cortical regions during a specific mental task state is undertaken in this section. The phase coherent nature of brain dynamics with reference to a certain cognitive state involving many processes such as association and memory is studied and the effect that a fatigue causing exercise may have on the synchronous nature is examined. The mental task state is that of arithmetic carried out mentally and there exist reports that the performance of arithmetic is obviously a complex task, involving several subcomponents (Ashcraft, 1992; McCloskey *et al.*, 1985) such as separate mechanisms for the retrieval of arithmetic facts and the performance of calculation procedures which may be controlled by a distributed network. Imaging studies have confirmed the role of posterior parietal cortex in arithmetic calculation and implicate other regions, including prefrontal cortex (Rueckert *et. al.*, 1996) during this task while noninvasive methods such as the phase synchrony techniques have not exactly delved into this problem. In this study, we deal not directly with the mental calculation task but explore the effect that exertion may have on the synchrony pattern in the brain with reference to a specific mental task carried out before and after the onset of fatigue.

Perception of exertion during exercise is a topic of great interest to sport physicians and sportsmen worldwide. The idea of effort during exercise and its relationship to fatigue is still not well understood (Hampson *et. al.*, 2001). Moreover, the effect of fatigue on the brain state during performance of mental tasks is yet to be addressed. Once the relationship among fatigue, intensity of effort and pacing strategies during exercise get established; this

knowledge will benefit groups engaged in activities requiring exertion in daily life such as sprinters, athletes, weightlifters and so on. Three models of fatigue consequent to exertion have been proposed. The first is the peripheral model in which muscle metabolic factors control or dictate the onset of fatigue and the reduction or termination of exercise. In the central teleoanticipatory model, subconscious brain centres or functional activities set predetermined exercise activity whereas in the cognitive discussion model, the sensation of fatigue itself controls exercise intensity, using prior experience as a comparator or regulator of exercise intensity (Hampson et. al., 2001). The second and third models point to the presence of brain activity in the perception and regulation of fatigue consequent to physical exercise. Hence an analysis of how fatigue changes the neural connectivity during specific tasks will enable an understanding of the effect of fatigue on the co-operate nature of the sub cortical networks.

In this pilot study, we use the mental calculation task which has been suggested as a complex task integrating multiple processes sub served by a large network of widely separated and interconnected local networks (McCarthy & Warrington, 1990; McCloskey, 1992). The effect of fatigue inducing exercise is studied on a mental arithmetic task by analyzing the synchronization behaviour of cortical regions before and after the onset of fatigue. Further, the nature of coupling between various regions is looked into by making use of the directionality index that has been successfully applied to probe the synchrony behaviour of heart rate and respiration cycles in infants (Rosenblum et. al., 2002).

7.4.1. Detecting the Directionality of Coupling from Phase

In identifying the interdependencies between coupled (sub) systems from multivariate data two problems can be formulated. The first is to reveal whether the systems under investigation are coupled and to quantify the intensity of interaction while the second is to characterize the causal or driver-response relationships. The first is solved by the introduction of a phase synchronization index based on the phase derived from the data and the second by introducing an index which will contain information on the directionality of coupling (Rosenblum et. al., 2002).

The main idea involved in detecting the coupling direction is that weak coupling affects the phases of interacting oscillators, whereas amplitudes remain largely unperturbed. Hence the dynamics could be reduced to those of phases $\phi_{1,2}$ and the equation of temporal evolution can be written as,

$$\dot{\phi}_{1,2} = \omega_{1,2} + \varepsilon_{1,2} f_{1,2}(\phi_{2,1}, \phi_{1,2}) + \xi_{1,2}(t)$$

Here $\xi_{1,2}$ are random terms describing noisy perturbations that are always present in real world systems; small parameters $\varepsilon_{1,2} \ll \omega_{1,2}$ characterize the strength of coupling. The regular component of the phase dynamics being two-dimensional, the detection of the asymmetry in interaction becomes simplified. If the coupling is bi-directional, f_1 and f_2 , which are 2π periodic in both arguments depend on both ϕ_1 and ϕ_2 . In case of unidirectional coupling, say from system 1 to system 2, $f_1 = f_1(\phi_1)$ where as $f_2 = f_2(\phi_1, \phi_2)$ is the function of both arguments.

As discussed in an earlier section, the phase may be evaluated and a synchronization index determined from the EEG signal by following the Eq. (7.11) –(7.13). Once the synchrony patterns are established, the question of directionality in the coupling can be addressed. This is important in revealing

whether the interaction is bi- or uni- directional and also to quantify the degree of asymmetry in the coupling (Rosenblum & Pikovsky, 2001). From the time series of the phases, for each time point increments of the form

$$\Delta_{1,2}(k) = \phi_{1,2}(t_k + \tau) - \phi_{1,2}(t_k) \quad (7.17)$$

are computed wherein τ can be some fixed constant. These increments can be considered as generated by some unknown two-dimensional noisy map,

$$\Delta_{1,2}(k) = \mathfrak{T}_{1,2}(\phi_{1,2}(k), \phi_{2,1}(k)) + \eta_{1,2}(k) \quad (7.18)$$

The dependencies of Δ on ϕ_1 and ϕ_2 are fit using a finite Fourier series as the probe function in the following manner,

$$F_{1,2} = \sum_{m,l} \Delta_{m,l} e^{im\phi_1 + il\phi_2} \quad (7.19)$$

with $|l| \leq 3, |m| \leq 3$ and $|m| = |l| = 1$. From this the cross-dependencies of phase dynamics are quantified by means of coefficients $c_{1,2}$ defined as,

$$c_{1,2}^2 = \int_0^{2\pi} \int_0^{2\pi} \left(\frac{\partial F_{1,2}}{\partial \phi_{2,1}} \right)^2 d\phi_1 d\phi_2 \quad (7.20)$$

The directionality index is finally calculated as,

$$d^{(1,2)} = \frac{c_2 - c_1}{c_2 + c_1} \quad (7.21)$$

This normalized index varies from 1 in the case of unidirectional coupling (1→2) to -1 in the opposite case (2→1). Vanishing index $d^{(1,2)} = 0$ corresponds to symmetric bi-directional coupling. This method has been successfully applied to analyze the nature of coupling in oscillator systems (Rosenblum & Pikovsky, 2001) as also in the case of cardio respiratory interaction (Rosenblum et. al., 2002). The application of this

concept to the phase interaction derived from the EEG data leads to insights regarding how the cortical regions interact during specific mental states. In this case, the effect of fatigue inducing exercise on the arithmetic task is investigated to study how variations in neuronal network coupling occur.

7.4.2 Data Acquisition and Classification

In recent times, the limited spatial resolution of the conventional EEG technology has been tackled by introducing high resolution EEG (HR- EEG) (Babiloni et. al., 1997; Edlinger et. al., 1998). A pre-requisite for such methods is adequate sampling of the potential distribution on the scalp surface. The point-spread function of conduction of potential from brain surface to the scalp averages to about 2.5 cm (Gevins, 1990). Thus to adequately cover the surface of the scalp with electrodes having inter-electrode distance in this range, EEG equipment supporting at least 128 channels is required (Srinivasan et. al., 1998). Hence in this study, we resort to the use of data recorded using a 128 channel Electrical Geodesic™ system, with a sampling frequency of 200Hz referenced to a vertex electrode. The electrode configuration of the recording system is shown in figure 7.9. An online band pass filter from 0.1 to 70 Hz was used and impedances were kept below 25k Ω . Vertical and horizontal eye movements were monitored with a subset of 128 electrodes.

Fifteen healthy subjects participated in the study of which 9 were males and 6 females. Their mean age was 27.6 for males and 28.2 for females and they were under no medication for neuro- psychotic illnesses. EEGs were recorded under two different conditions. At first, the subjects were made to do a mental arithmetic task with their eyes closed. This was serial

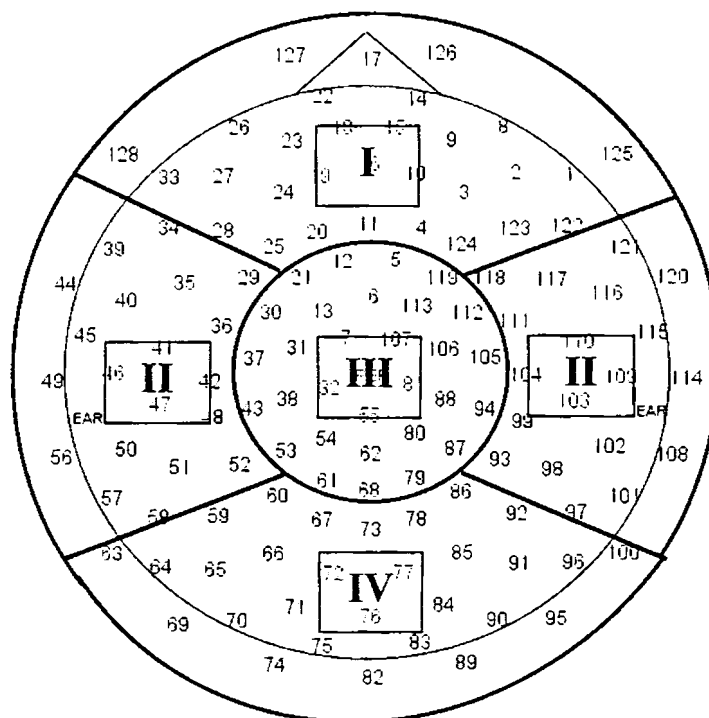


Figure 7.9. The schematic of the dense array electrode placement scheme for EEG recording along with the classification of the channels into 4 groups based on their cortical locations.

subtraction in which the subjects serially subtracted 7s' from 2000 for a duration of 2 minutes. Subsequent to this, each subject underwent a fatigue test. This test required the subject to perform an isometric leg extension at 20% of their maximum voluntary contraction (MVC) until the subject became fatigued and could no longer achieve the desired level of power output. At the end of this, subjects repeated the same mental arithmetic task during which

EEG was again recorded. The resultant data records were transferred from the Net Station acquisition system for further offline analysis.

7.4.3 Phase Synchrony and Directional Coupling Analysis

The analysis of the phase synchrony is carried out by classifying the electrodes on the basis of their relative positions on the cortex so that there is almost equal number of electrodes representative of each brain region in each subgroup. This is depicted in figure 7.9 along with the schematic for the electrode placement in the dense array system. The mean value of the phase synchronization index, ρ evaluated as in equations (7.11)-(7.13). Figure 7.10 is a comparative look at this index for the two states mental arithmetic before (M.A.) and after the fatigue inducing exercise (M.A.F.). It is obvious that in all the 4 brain regions, there is a rise in phase synchrony for most of the channels following the physical exercise. This could mean that there is greater coupling induced among the brain regions following fatigue in the system. While it has been proved that mental arithmetic by itself leads to desynchronization in various brain regions (Inouye et. al., 1993), following the fatigue there is a rise in synchrony during the same process and this seems to be quite a global effect since there are only a few electrodes that seem to be at lower synchrony as compared to the state before the onset of fatigue.

In order to look at the temporal variation in the synchrony effect or whether there is a change in the synchrony pattern with time after fatigue in comparison to the same task state prior to the fatigue onset the following path is chosen. The analysis of synchronization is done over non-overlapping windows of 5s each, satisfying the nonstationary condition and in each window the synchronization index is evaluated. Then in the mental task state prior to the exertion, the number of connections for each channel with

moderately high values of ρ is determined. The limiting values of synchrony index that limit the moderately high synchrony regime are chosen as 0.3 and 0.7. Hence those pair-wise connections with $\rho < 0.3$ or $\rho > 0.7$ which exhibit very low synchrony between virtually uncoupled regions in the former case

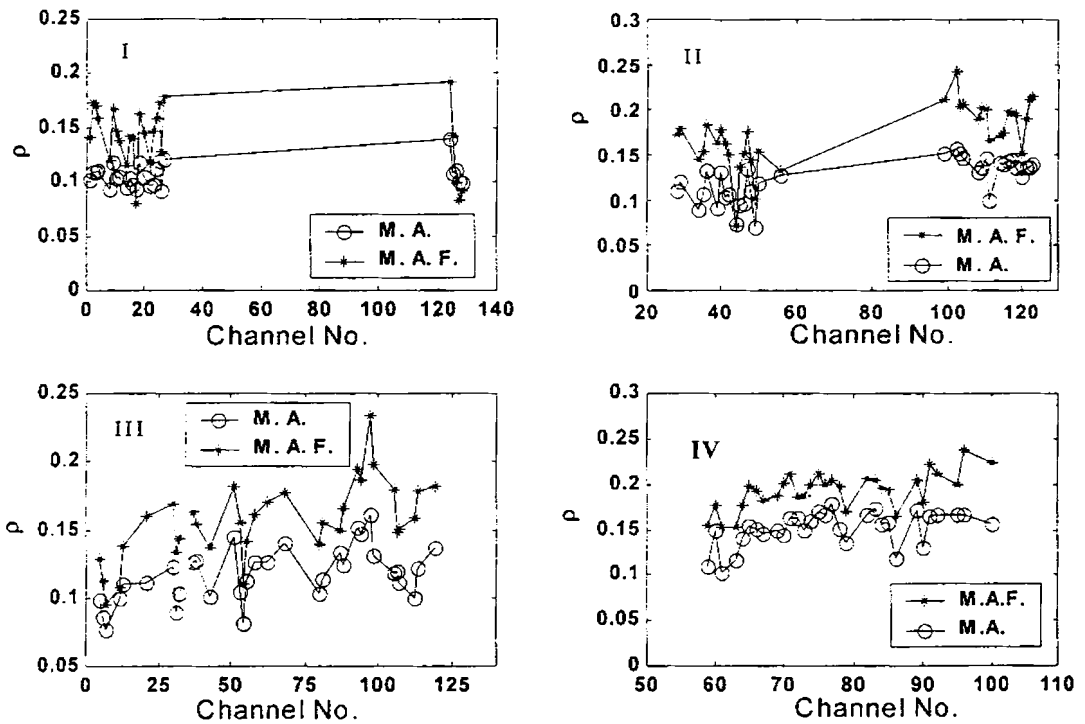


Figure 7.10. The computed phase synchrony index ρ for the two cases of M.A. and M. A. F. for the four representative cortical regions I to IV

and very high synchrony arising due to near neighbourliness of electrodes in the latter are neglected. We take into account the moderately strong

couplings between farther lying regions that point to task related coupling between neuronal sub cortical networks. The same is determined for the corresponding time segments in the case of the mental task performed after the fatigue inducing exercise.

It is observed from figure 7.11 that on an average over time as well, the number of connections for each channel with moderately strong coupling rises after the exercise. The number of strong connections emanating from each channel is more in the mental arithmetic state after fatigue onset for a time of 50 s (10 windows) after starting the calculation task. This could mean that fatigue causes not only a rise in the magnitude of synchrony in the system but the various regions exhibit greater number of couplings during an identical task done after the onset of fatigue. The overall coherence effect of the system may thus be said to have risen following the fatigue inducing exercise. This is yet another evidence in favour of the teleoanticipatory model that supposes a change in the brain activity following exercise and the possibility of the brain playing a central part in the perception and regulation of fatigue induced by physical exertion. However it may be noted in figure 7.10 that the variations in the synchrony indices during both states are almost similar for most of the electrodes since the control task is the same and hence the same complex functional subtasks such as perception of numbers and mathematical operators, calculation of the difference operation and memorization take place during the mental arithmetic task. The plausible reason for the rise in synchrony in M.A.F. can be explained in the following manner. During an exercise, the brain in general is more organized due to concentration and this state persists into the next state, which in this case is the mental arithmetic task. The higher synchrony during fatigue state takes up a longer time to relax to the normal state. Yet another conjecture is that

the exercise having caused fatigue, the subject has to concentrate more strongly in an effort to conduct the assigned mental arithmetic task. This is manifested as a stronger synchronization between the brain regions.

Addressing the question of the nature of coupling, the directional indices are computed for the various channels relative to each other by applying Eq. (7.17) - (7.21). $d^{(1,2)} \sim 0$ implies bi-directional coupling provided the corresponding $\rho^{(1,2)}$ is moderately strong ensuring that the two channels are indeed phase coupled. The low $d^{(1,2)}$ (almost 0) arises due to bi-directionality and not because of the absence of phase synchrony between the two regions. From the computed directionality factors, those connections are determined that are uni-directionally coupled in one direction with positive $d(1,2)$ with connection from 1→2 as also those with high negative values implying unidirectional coupling from 2→1.

We have illustrated in figure 7.12 the electrodes in the two states of mental arithmetic prior and after onset of fatigue which are mutually coupled ($d(1,2) \sim 0$) and also those with coupling existing in one direction. Since clear cut cases of unidirectional coupling do not exist, we have chosen those electrodes with $d(1,2)$ within 75% of the maximum (positive) computed value as having forward coupling alone and the channels with $d(1,2)$ within 75% of the minimum (negative) computed index are marked as exhibiting coupling in the reverse direction only. In the case of mental arithmetic carried out before the exercise, most of the mutual connections exist in the prefrontal cortex and a few among the occipital sites. The role of the prefrontal cortex in calculation has been stressed in many previous reports (Stam et. al., 1996; Inouye et. al., 1993) and the presence of fatigue leads to a breakdown

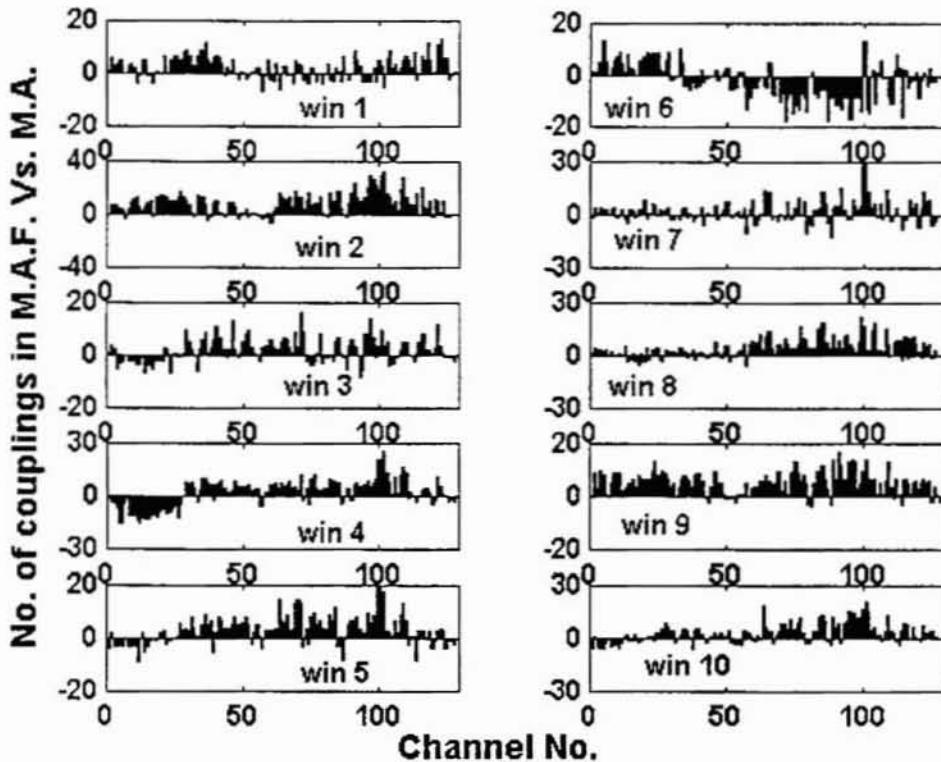


Figure 7.11. The difference in number of couplings (N) of ρ bet 0.3 and 0.7 for the two states MA and MAF. If at a given electrode the number of couplings is >0 , it implies more connections of that electrode relative to all other channels in the MAF state than in MA

of some of these symmetrical connections with new ones forming in the right temporo-parietal electrodes as well the occipital regions. There are also unidirectional long-distance connections established in the fatigued state (M. A. F.) that were absent in the state prior to physical exertion. However some connections between the right temporo-parietal regions (II in right hemisphere) and the left temporal region (II in left hemisphere) that recur in

both states point to the possibility of these regions interacting with each other specific to the task at hand, i.e. mental arithmetic. But the symmetrical connections in both states exist only between close lying electrodes though there are more in the M.A.F. state in which there is an enhancement in the global synchrony pattern as well compared to the M.A. state in the absence of fatigue. This scheme of connectivity appears to be associated with the task of mental arithmetic though this has to be established with more supportive evidence.

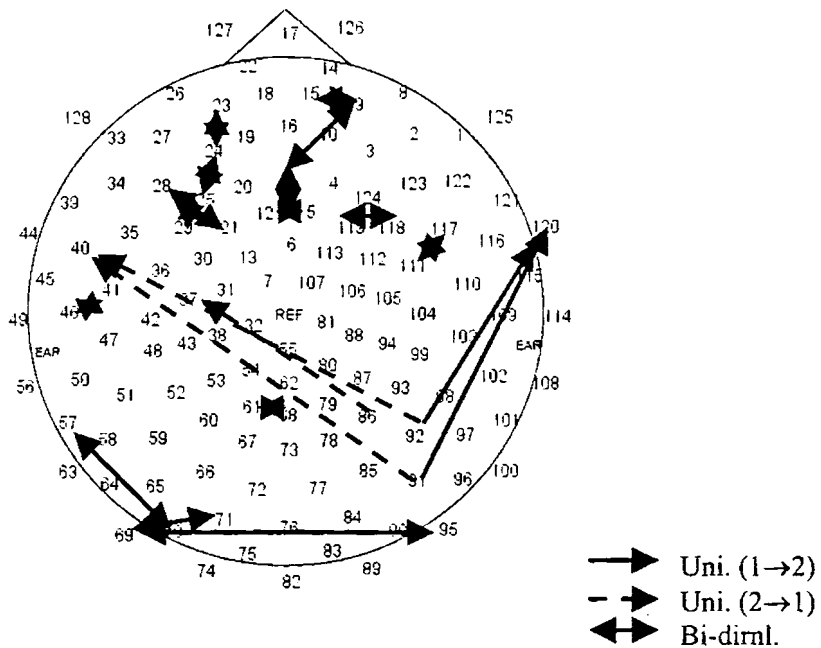


Figure 7.12(a)

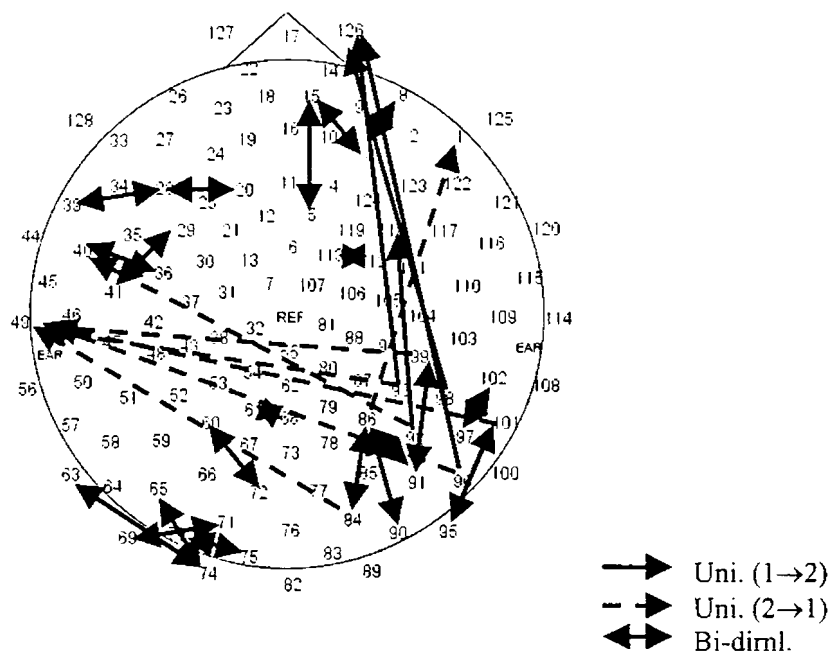


Figure 7.12 (b)

Figure 7.12. The directional connections between electrodes during M.A. (a) and M.A.F. (b). The enhancement in symmetrical connections after onset of fatigue is clearly visible

Thus fatigue seems to raise the coherence level in the system and this is reflected not only in the higher synchrony indices but also in the number of stronger couplings exhibited by each channel. Moreover the response of the system to the fatigue seems to be an enhancement in the number of long

distance connections and a shift of the symmetrical couplings to regions in the parietal-occipital regions of the right lobe.

It has been observed in many cases that there is long distance synchrony among cortical regions in the performance of cognitive tasks. This pilot study aimed at studying the coherence nature of sub cortical neuronal networks during the task of serial arithmetic subtraction and the effect of fatigue on the cognitive task reveals that the phase synchrony in the system is enhanced following the onset of fatigue during performance of the task than in the normal unfatigued state. Moreover, the number of such strong connections with respect to the individual electrodes also increases on the average in the fatigued state. This could mean that the system as a whole moves toward a more coherent state following the fatigue inducing exercise. Mental arithmetic was chosen as the specific task since being a complex functional task it has been revealed to activate particular brain regions as well as the coupling between widely separated regions such as the prefrontal and motor areas. The advantage of such non-invasive phase synchrony methods lies in the ability to gain knowledge regarding brain function in the presence of lesser known phenomena such as perceived exhaustion related to a particular task, in this case, mental arithmetic.

It has been recently reported (Nybo & Nielsen, 2001) that cerebral electrical activity rather than muscle activity is altered significantly by exertion following prolonged exercise and studies such as ours gain relevance in understanding how fatigue affects brain activity during performance of specific tasks. Moreover we also observe variations in the nature of coupling between the cortical regions in the fatigued state. While in the state prior to the exercise, there were more symmetrically connected electrodes in the prefrontal-frontal regions, the fatigue state is marked by lesser number of

such bi-directional couplings and a shift of such connections towards the parieto-occipital regions. The long distance connectivity between the temporo-parietal regions with some electrodes in the prefrontal cortex seems to be a signature of the induced fatigue. On the whole the fatigue in the system induces more connectivity and moves the system towards higher coherence.

7.5 Concluding Remarks

Cooperative behaviour of chaotic dynamical systems and in particular, synchronization phenomena have received much attention lately. The theory of synchronization is a rapidly growing branch of nonlinear science and occurs in areas such as laser dynamics (Roy & Thornburg, 1994), secure communications (Parlitz et. al., 1996) and biological systems (Blasius & Stone, 2000; *Nonlinear Analysis of Physiological Data*, 1998). Synchronization is a very general term that encompasses a number of definitions such as generalized, partial, practical, lag etc. (Rulkov et. al., 1995; Rosenblum et. al., 1997) phase synchronization is found to occur in many complex interacting systems in which despite the amplitudes being uncorrelated, the phases show entrainment. The Hilbert transform method is one of the popular methods to derive the phase from observed signals. It has recently been established that an alternative technique to arrive at a phase locking statistic using wavelets exhibits only minor differences with the Hilbert method and that too the differences manifest only for small windows of observation. This implies that all such techniques offer a common framework for use in the detection of synchronization at different spatial levels from the single cell level to the level of EEG recordings (Le Van Queyan et. al., 2001).

The work described in the above sections encompasses the application of the ideas of phase synchrony to the EEG signal recorded during different brain conditions and the discussion of the relevant results. The temporal variation in the phase synchrony of normal relaxed states is conducted that shows the reduced synchrony state of the brain in the presence of visual stimulus in the eyes open state. Of greater clinical interest is the detection of enhanced synchrony during the pathological condition of epileptic seizure discharge. This analysis can also bring to light the synchronization between distant cortical regions during the seizure state. In the subsequent section, the effect that fatigue induced by physical exercise on the performance of mental arithmetic task is analyzed in detail. It is observed that as compared to the task performance before exercise, that after fatigue has set in, is characterized by a marked increase of synchrony. Moreover the directional coupling is determined pointing to a rise in the long distance couplings as well as symmetric interactions mainly in the occipito-parietal regions.

Phase synchrony studies have reached a stage where the variations in coupling patterns in the brain may be directly related to the changes in behaviour. Moreover research is now concentrated to the parallel phase synchrony over different frequency bands. Such studies may be integral to the precipitation of a characteristic spectrum of frequencies that are instrumental in carrying information regarding various stages of integration occurring during specific conditions. At the heart of these analyses lies the need to understand the collective nature of mechanisms and regions in the brain and identify the abnormal patterns of neuronal integration that are causative of different abnormalities in brain functioning and on the basis of this knowledge, seek remedial measures.

Neural Models 8

However, if we do discover a complete theory, it should in time be understandable in broad principle by everyone, not just a few scientists. Then we shall all, philosophers, scientists, and just ordinary people, be able to take part in the discussion of the question of why it is that we and the universe exist.

--- Stephen Hawking

The human brain that consists of over 10^{11} neurons in the cortex domain has taken a billion years to evolve into a highly organized structure in the known universe. It not only controls and monitors all bodily functions but is also the seat of knowledge, emotions and thought and in the typical lifetime of a person carries out innumerable functions and tasks that are beyond description. A scientific theory of the brain would be able to explain the known facts about the brain starting from a few fundamental principles. From this perspective, there has not yet been a theory for the brain and its functions.

Currently, there are numerous experimental observations on the brain structure and behaviour as also a few theories and models that pertain to certain specific aspects of the brain function such as vision or motor co-

ordination. The search that began around fifty years ago with the modeling of the cellular structure in the brain led to the development of the interesting computational structure known as Artificial Neural Network that has been found to be useful in modeling many real life-complex data. This chapter briefly reviews the main concerns in the development and partial answers provided by the existing neural models. The final sections explain a preliminary attempt to arrive at a map for the brain based on the EEG output.

8.1 Modeling the Brain

The neuron is the basic unit of information processing in the brain. Identified by Cajal in 1908 as the cellular constituents of the brain specialized for rapid inter communication, the main property of nerve cells is supra threshold excitability. It was discovered that application of a strong enough stimulus caused these to effect current pulses that came to be known as 'Action Potentials'. The neural circuitry was recognized as highly complex by Cajal and his associates and studies in neuroanatomy point to an interconnectivity that far surpasses all imagination. For instance the Purkinje cells are estimated to possess about 2×10^5 synapses and there are about 250 morphological types of neurons in a small single patch of brain cortex. In addition to dendrites, each neuron has an axon whose specific property is to carry action potential. At the end of each axon are usually dendritic arbors so that each neuron can transmit its pulse to neurons of the order of up to several hundreds. The resulting neural net is hence very complex. Besides these are the various types of neurotransmitters. Depending upon the type of receptor proteins embedded in the neural membrane, neurotransmitters and currents either depolarize the membrane so that the neuron is excited or hyperpolarise it so that the neuron is inhibited. Other molecules that affect

the neurons include monoamines, which modify the excitability thresholds. All these tempt one to the idea of modeling the brain as a random net of neurons swimming in a bio-chemical soup. Yet this is far from true and there is high degree of specificity in the pattern of inter-neural connectivity.

In developing a model for the brain, there are various levels of neural organization to be addressed from individual neurons through local neural circuits to large aggregates of neurons acting collectively. Hodgkin and Huxley proposed a model to study the generation of action potentials in single neurons (Hodgkin & Huxley, 1952). Based on experiments in the giant axons of the squid, the set of equations, though complicated, provided a fairly accurate representation of generation and propagation of action potential. By the mid 50s' the action potentials and synaptic transmission were understood in at least phenomenological terms. The presence of nonlinear dynamics following the nonlinearity in behaviour of cellular structures also has more or less been established. The behaviour of the irregular pulsations of a synaptically isolated lateral pyloric (LP) neuron in the pyloric central pattern generator (CPG) of the lobster is an example of this. This time recorded series was found to possess a positive Lyapunov exponent exhibiting chaotic nature (Abarbanel et. al., 1996a). A three dimensional model proposed by Hindmarsh and Rose (1994) and later modified and analyzed thoroughly reproduced the behaviour exhibited by single neurons. A review of the role of chaos in neural systems holds the view that chaotic dynamics is made inevitable by nature in neural assemblies. Due to this, neurons possess adaptability, reliability as well as the ability for rapid response to changing external stimuli required for efficient information processing and response. Moreover the instability in the phase space is made use of to rapidly achieve a selected target state.

In general, noise may also be considered a candidate in neuronal complexity. But the temporal information coding by the time intervals between action potentials needs a stable mechanism such as chaos to be implemented. Also since the incoming signals through synapses and dendrites being highly irregular, the neurons are able to recognize the message using synchronization, which is impossible to achieve with inputs from truly noisy neurons. Only chaotic neurons are capable of generating such large-scale synchronization and desynchronization. Hence chaos in neural assemblies at the cortical level appears to be inherent rather than a befitting mechanism to the manifested phenomena (Rabinovich & Abarbanel, 1998).

8.2 Artificial Neural Networks and Models of Neocortex

Even before the Hodgkin-Huxley equation was formulated, McCulloch and Pitts (1943) proposed a network that could perform all processes described by a finite number of symbolic expressions such as simple arithmetic, classifying, storing and retrieving data, recursive application of logic rules etc. The neural model consists of a set of binary elements, which are neurons that are either on or off representing the threshold in the neural firing and the output of each neuron depends upon the input in which weights are fixed. These were the first examples of model neural nets designed to perform specific tasks. The question of what would happen if such a net malfunctions prompted von Neumann, the leading mathematician who is a pioneer in the development of the digital computer, to introduce the idea of redundancy into the net with which more reliability was found to be achieved by the McCulloch-Pitts (M-P) neuron. Subsequent work by Winograd & Cowan (1963) constructed a redundant neural network in which they utilized a distributed representation

of information. This provides an insight into the functioning of neural networks in the brain even if some of the units are damaged.

The idea of distributed representation of information is supported by Hebb's theory (1964), which proposed that as an organism learns different tasks, its brain connectivity continually changes so that these create cell assemblies. Hebb postulated that repeated activation of one neuron by another, across a particular synapse, increased its conductance to that group of weakly connected cells, if synchronously activated. Hebb's ideas gave rise to Neurodynamics as the study of the generation and propagation of synchronized neural activity. Rashevsky and co-workers (1938) began work on the activation and propagation by applying principles of calculus rather than logic and this was followed up by Wiener. Cragg and Temperly in 1954 pointed out the remarkable similarity between the properties of neurons in a densely connected net and those of spinning atoms in a lattice, which were later supported by the work of Little in the mid-seventies. The first detailed analysis of the triggering and propagation of large-scale brain activity was by Beurle in 1956 who focused on the proportion of neurons becoming activated per unit time in a given volume element of a slice of model brain tissue consisting of randomly connected neurons (Cowan & Sharp, 1988).

The synaptic modification proposed by Hebb paved way for the development of adaptive nets which could learn to perform specific tasks. Pattern recognition and classification were taken as specific problems in this direction. The Perceptron model introduced by Rosenblatt (1958) was a definite improvement over the McCulloch Pitts neural model and could be trained to classify certain sets of patterns as similar or distinct. The perceptron consists of sensory units interconnected to the motor units by modifiable weights. These weights are adjusted depending on the response

and it is found that these weights converge only for a finite number of representations of stimulus-response patterns. The Adaline structure is a variant of the perceptron models differing only in the training procedure. Despite their many advantageous features, perceptrons failed to classify some simple patterns such as T and C. This was attributed mainly to the nature of the M-P neurons which made even the implementation of the simple NOT operation require several units. This limitation is overcome with the introduction of modified architecture with 'hidden units'. Though Perceptron or Adaline models with only single layer units are not computationally universal, the problem of assigning credits to the hidden units in multilayer perceptron models is unsolvable. The limitation of single Perceptrons and Adaline models can be overcome with a more complex architecture incorporating hidden units with modifiable connections.

The most notable feature of the perceptron is that its memory of the learnt task is distributed over the modified connections and hence it is less likely to be disrupted by damage. Yet the associative nature of human memory remains unaddressed. The study of neural nets with associative memories began on an extensive scale around 30 years ago (Taylor, 1964). The net similar in structure to the perceptron has no hidden units nor does it rely on M-P neurons. Applying the Hebbian principle, the net learns to associate differing sensory patterns to motor responses by repeated presentation of pairs of patterns. This and later models proposed by Taylor contained the association areas of the cerebral cortex and cerebellum. About the same time, Steinbuch introduced a planar net of switches interposed between arrays of sensory receptors and motor effectors known as the Learning Matrix which also had associative memory incorporated in it. These attempts were followed by theories of Marr put forth in the early seventies for

the functioning of the cerebellum, the hippocampus and in a more elaborate sense of the neocortex. These theories have not been fully tested; yet there have been some observations consistent with theory.

Of the many models of memory, the Anderson and Cooper (1978) model holds a place of prominence. While the functions of individual neurons in many parts of the brain have been fairly well understood, the collective process in which large bodies of interconnected neurons give rise to specific mental activity is much less known. This is the case when the activity of single cells is considered in a higher cortical function or in the localization of a region in the nervous system in which storage of memory takes place. The fundamental problem arising in understanding the organization of memory in a biological system is the involvement of the vast information storage and retrieval mechanism of a system composed of vulnerable and relatively unreliable elements. The neural models introduced by Anderson and Cooper account for the acquisition and storage of distributed memories that display features such as recognition, association, generalization and some of the features of mental behaviour associated with animal memory. It has been suggested that much of the learning and resulting organization of the central nervous system occurs through some kind of modification of the efficacy or strength of at least some of the synapses, thus altering the relation between presynaptic and post synaptic potentials. Distributed memories result from a small but coherent modification of a large number of synaptic junctions. The neurons of the primary sensory areas display various forms of stimulus selectivity, i.e. they may respond preferentially to a tone of a given frequency, a light spot of a given color, a light bar of certain orientations etc. Thus, stimulus selectivity is considered as the general property of sensory neurons and it is conjectured that development of such selectivity obeys some

general rule. Distributed memory considers the simultaneous or near simultaneous activities of many different neurons. A large spatially distributed pattern of neuron discharges, each of which might not be very far from spontaneous activity, could remain important even if this is hard to detect.

The model of Anderson and Cooper consists of N neurons $1, 2, \dots, N$ each of which has some spontaneous firing rate r_j^0 . Then a vector is defined whose components are the difference between the actual firing rate r_j of the j^{th} neuron and the spontaneous firing rate r_j^0 . Hence, we may write,

$$f_j = r_j - r_j^0 \quad (8.1)$$

Two groups of neurons are connected to one another by replacing the multiplicity of synapses between axons and dendrites by a single ideal junction. This summarizes logically the effect of all the synaptic contacts between the incoming axon branches from neuron j say in the F bank and the dendrites of the outgoing neuron i in the G bank neurons. While F is concerned with incoming signals, G is associated with responses. Even though the firing rate of a neuron depends in a complex and nonlinear fashion on the presynaptic potentials, there is usually a reasonably well-defined linear region. The firing rate g_i of neuron i in G is mapped from the firing rates of all the neurons f_j in F by

$$g_i = \sum_{j=1}^N A_{ij} f_j \quad (8.2)$$

where A_{ij} is a mapping matrix depending on g_i and f_j .

The neural activity f in the F space is mapped into the neural activity g in the G space and this can be written in a compact form as

$$g = Af \quad (8.3)$$

where A is a matrix with elements, A_{ij} .

Thus memory is stored in the modifiable mapping of the type A. In contrast to machine memory, which is local, the animal memory is likely to be distributed and addressable by content or by association. It is convenient to write the mapping A as

$$A = \sum_{\mu\nu} C_{\mu\nu} g^\mu \times f^\nu \quad (8.4)$$

Based on the Anderson and Cooper model, Parikh and Pratap (1984) developed a generalized evolutionary model in the framework of nonequilibrium statistical mechanics as developed by Brussel School to simulate the memory effects. Consider again a network of N neurons that are all linked to each other. In the absence of input, the neurons have a certain amount of spontaneous activity, which is described by the firing frequencies r_j^0 . The firing frequency is random in time and r_j^0 is considered as random variable having a distribution around the time-averaged mean. The difference between the actual firing rate r_j and the spontaneous firing rates r_j^0 is represented as

$$h_j^0 = r_j - r_j^0 \quad (8.5)$$

The same stimulus can lead to firing patterns that vary from trial to trial, but the average of the firing rates is roughly constant. Therefore, the frequencies h_j^0 are also random variables distributed about appropriate mean values. In

order to simulate the memory effects consider that in the time interval $-\infty$ to 0 (at instants $\beta_1, \beta_2, \dots, \beta_K$) there have been K experiences and associated correlations, defined by certain input and output firing rates. Denoting input and output firing rates as f_j^ν and g_i^μ respectively, where ν and μ take values from 1 to K and $i, j=1, \dots, N$ neurons for all the past K events. Here f_j^ν are the afferent frequencies of the ν^{th} species at the instant j and g_i^μ are the efferent ones.

The state of the neural network at $t=0$ may be defined by a distribution function $\rho(\{g_i^\mu\}, \{f_j^\nu\}, \{h_j^0\}, t=0)$. The problem is to obtain the distribution function $\rho(\{g_i\}, t)$. If a transition probability, $G(\{g_\alpha\} | \{g_i^\mu\}, \{f_j^\nu\}, \{h_j^0\}, t-\tau)$ is defined, which takes the state at $t-\tau$ to t , then one can obtain $\rho(\{g_i\}, t)$ by writing an evolution equation as

$$\rho(\{g_\alpha\}, t) = \int_0^t \int d\{g_i^\mu\} \int d\{f_j^\nu\} \int d\{h_j^0\} G(\{g_\alpha\} | \{g_i^\mu\}, \{f_j^\nu\}, \{h_j^0\}, t-\tau) \times \rho(\{g_i^\mu\}, \{f_j^\nu\}, \{h_j^0\}, \tau) d\tau \quad (8.6)$$

In the equation, integrations are effected over all the variables except the g_α i.e. all the variables on the right of the vertical bar appearing in the definition of G . It may be noted that time appears in the transition probability as $t-\tau$ which implies that Eq. (8.6) is non-Markovian in nature. In this equation, G is the kernel in the integral equation. This kernel G maps the input stimulus at $t=0$ into the output signal at t after subjecting to the interactions in the medium which is heterogeneous. Different hypothesis about the synaptic changes would lead to different forms for G . This model is

a general evolutionary model of a distributed memory with the "Kernel" in the equation simulating the changes in the synaptic behaviour produced by external stimuli (Parikh & Pratap, 1984).

The analysis of the collective modes in the brain has been undertaken by various groups as well. In a subsequent work to the one described above, Kulkarni et. al. (1997) analyzed the actual EEG records in accordance with the idea of the signal being generated by the cooperative activity of a large number of neurons. The parametric map approach for the modeling of time series with broadband spectra was demonstrated by Abarbanel et. al., (1990). Many models for the analysis of the observed EEG signal are broadly based on such maps of which a prominent one could prove the predictability in EEG patterns that was limited to a few steps (Parikh & Pratap, 1991). In recent times, the use of nonlinear autoregressive structures for the modeling of the output from continuous time dynamical systems with special implication for EEG modeling have been suggested (Ozaki et. al., 1999). Neural modeling continues to exist as a challenging field to researchers and the search for a model that encompasses the system complexity on the whole is ongoing.

8.3 Maps in the Brain

The most astounding discovery in neuroscience in this century is that there is a constant generation of neuronal cells in adult primates in basal ganglia (Gould et. al., 1999) and that they migrate tangentially and dorsally from a lateral region (Kaas & Reiner, 1999). It was almost axiomatic for medical scientists that while all body tissue are regenerated during life, brain cells are formed during a short period after birth, and that their number only decrease in time and not increase. The implication of this assumption is that the various neuronal connections can be made only from amongst this given

number of cells and that as they degenerate due to ageing, the number of connections also get decreased in time which manifests itself in an altered metabolic condition amongst other effects. The above discovery is significant in this context that the existing connections can be maintained and even fresh ones can be formed with the help of these newly generated neurons by giving constant stimuli.

It is well established by now that when a sensory terminal receives a stimulus (stimuli) it is transmitted to the cortex and the neuronal firings establish patterns in the brain. These patterns are distinctly different for different kinds of signals received by the same individual and they also differ from person to person; i.e. different persons will not have the same map established in the brain for the same input signal or identical signal inputs. This implies that the acquired characteristics as well as psychological make up play a significant role in the formation of brain maps.

There have been various attempts in the study of map formation both invasive and noninvasive (Law & Paton, 1981). In the invasive case, an amino acid (proline) labeled with radioactive tritium is injected into one of the optic nerves. The animal brain is then sliced after a fortnight to determine the distribution of radioactivity. It was found that the neuronal cells affected by the radioactivity form patterns consisting of stripes in the cerebral cortex. This method however has a limitation for it does not convey any insight regarding dynamic activity in the brain. Recently noninvasive processes have been developed to study the dynamical process in synapses (Colicos et. al., 2001; Pratap 1999) both experimentally and theoretically. Since intra cellular electrode stimulation (invasive) as in the voltage clamp method result in a psychological perturbation of the system, the recent method based on a noninvasive stimulation by changing the photoconductivity of the membrane

of the system is an improvement. This again may result in a perturbation since conductivity changes play a significant role in the synaptic transduction (Pratap, 1999). The above-mentioned impasse may be avoided by studying the electrical activity of the brain as obtained from the electroencephalogram (EEG).

In the recent past, there have been a series of noninvasive attempts to locate and determine the distribution of activity sources in the cortex, which generate electric/magnetic activity, which are measured at the scalp surface (Wang & He, 1998). In this method, EEG/MEG potential measured is assumed to be generated by a current function satisfying a two dimensional Laplace equation. Having obtained the function and applying Maxwell's equation with homogeneous conductivity the authors have located the source distribution. In this the assumption made is that the sources are of internal origin (Chapman & Bartels, 1940). In geomagnetism this method has been used extensively, but did not give any information regarding the internal structure, since the conductivity distribution is heterogeneous and complex. This is exactly the condition even in the cerebral cortex. Further, in the general problem of signal propagation along the nerve while there is no amplitude modulation, frequency modulation is found to be directly proportional to the stimulus strength. These features are not exhibited by any electrical system to which Maxwell's equation are applied. Hence the validity of Maxwell's equation in such a complex system is to be further examined especially when the conductance is a complex function of the fields. It should be realized that in the cortex in particular and in the nervous system in general there are a wide variety of amino acids, enzymes and also different kinds of cells and hence such a procedure does not give any insight into the dynamics of the system. An attempt was made in the last decade to

formulate a quantum theory for a more realistic brain (Donald, 1990) model with limited success. It should further be realized that a nonlinear, complex, non-Marcovian system such as human brain is dynamically a non-Hamiltonian system. This implies that there does not exist a *potential* in the usual sense. If however we define a Motion Generating Function (MGF) it would be a complicated function of space-time. The system is thermodynamically open and hence there is no equilibrium state even in the asymptotic sense and therefore use of a two-dimensional or three-dimensional Laplace's equation is inadequate to the problem in hand. However there can be steady states (Glansdorff & Prigogine, 1971) and the dynamics is dominated by nonlinearity and feedback-feed forward mechanisms.

In view of the above, a different approach has been adopted in this study. From the analysis of the EEG signal, it is largely accepted that system is nonlinear and complex; but there are invariants such as the correlation dimension (D_i), Kolmogorov entropy (K_i), Lyapunov exponents (λ_i) etc. which are distinctly different at different points pointing to the presence of more than one attractor in the scalp area. Hence the system may be assumed to consist of a *collection of attractors* instead of a single global attractor. The system is represented in an attractor space equivalent to the gamma space (or Γ space) in non-equilibrium statistical mechanics. This space is spanned by the known invariant parameters such as D_i , K_i , λ_i etc. A multi-species representation is obtained which is dynamic in nature. Since at a given scalp point attractors appear and then disappear in time, the global state of the system in the attractor space is ever changing as it evolves in time. Thus neither the neuronal number nor the number of connections or the number of attractors in the attractor space is conserved. Under these circumstances, the

formulation of a nonequilibrium statistical mechanics has to be done in an entirely new format.

8.4 Formulation of Nonequilibrium Statistical Mechanics

Equilibrium of a dynamical system, by definition, is that the system remains in that state for all times to come. The assumption made under this condition is that if the system is perturbed and then left alone, it attains the equilibrium state asymptotically. This asymptotic nature implies that as the system is perturbed, it relaxes exponentially i.e. the time behaviour is of the form $\exp(-t/\tau)$ and as $t \rightarrow \tau$, the perturbation attains an e-folded value and hence is negligible. Such assumptions are probably satisfied when the system is linear. However in the case where the interactions in the system are nonlinear, instabilities can set in and ultimately take the system over to an explosive state. It could also lead to a generation of synergic frequencies, which lead the system to a new state of equilibrium different from the equilibrium state at which the perturbation was done. This scenario necessitates the development of a statistical mechanics for the system far removed from equilibrium that traces its evolution in time.

Interactions in the human brain generate a large number of attractors specified by various characteristic parameters such as embedding dimension ε_i , attractor basin B_i , generalized metric dimension D_{iq} , generalized entropy K_{iq} and Lyapunov exponent λ_{iq} /Lyapunov function. Here, i is the attractor index and q are integers $0 \leq q \leq \infty$ for any specified i . The value $q=0$ for the i^{th} attractor is known as *Hausdorff* dimension. The dimension at $q=1$ is called the *information* dimension while $q=2$ case corresponds to the

two body *correlation* dimension. D_{iq} for $q > 2$ are the higher order dimensions and all these are geometric parameters specifying the shape of the attractor in a suitably chosen phase space. Similarly K_{iq} are the Shannon entropy and K_{i2} is known as Kolmogorov entropy of the i^{th} attractor which is the measure of the information capacity of the system. $\lambda_{iq} = 0$ for any q implies that Lyapunov exponents do not indicate the stability/ instability of the system. In such a case one has to resort to Lyapunov functions. It should be emphasized here that the above parameters are only a *certain* set of 'invariant' parameters and that this set is not closed by any means.

The collection of attractors as has been mentioned before is considered in this section. If at a given point on the scalp space, an attractor specified by the invariant characteristic parameters disappears at a given instant t_1 , and reappears at a different scalp point at t_2 we say that a scattering process is complete in the interval $(t_2 - t_1)$. If this attractor does not appear at all, we consider this as a case of loss from the system. It could also happen that the same attractor can appear at the same scalp point at t_2 . This we denote as a temporal scattering.

In the present case, the measured data, the EEG, indicates the end result of all interactions in the system at the space-time point from which it is collected. Hence the effort must be to infer the plausible interactions in the system, which result in the final state indicated by the data set. This is a particular case of doing an inverse analysis of the data set to get an insight into the interactions in the system. Hence one necessarily has to assume a model in which an interaction is postulated and examine whether the assumed model reproduces the output data. To study such a system, the first

step is to perform a singular value decomposition (SVD) of the digitized EEG output.

8.4.1 Schematics of SVD

The digitized output data from a 16 channel EEG machine is now analyzed channel wise. The data from a single channel is divided into 10 windows, each containing 2 second data (1024 data points). The data is then arranged in the form of a delayed matrix (Broomhead & King, 1986) in an embedding space of dimension (15) giving a rectangular matrix F . We now obtain from this a (15x15) symmetric square matrix $F^T F$ and determine the eigen values λ_{ijk} and the corresponding eigen functions ϕ_{ijk} where i denotes the index specifying the location of the electrode or channel index (1-16) and j is the window number (1-10). k denotes the order of the eigen value having a range of 1- ∞ . This procedure is known as the singular value decomposition

The most significant feature in SVD is that the eigen values fall into two distinctly different groups; one having significant eigen values denoting the deterministic component while for the other group, the eigen values are very small and hence insignificant giving the noise contribution. The eigen values are arranged in descending order of importance and all the lower ones which are less than or equal to the e -folded value of the most significant value are neglected. If now the original time series is projected onto the space spanned by these basis functions, a noise free series is obtained. It should however be realized that in this process only a very insignificant residue of the noise is filtered out and that a significant part of the random component has contributed to the eigen functions. Contrary to the case of linear systems, nonlinearity does not permit a stochastic series as being written as an addition of harmonic component and a random factor. This fact

is reflected in the small eigen values neglected in the analysis. It should also be mentioned that it is safer to choose an embedding dimension, which is larger than the attractor dimension. The most remarkable feature of this decomposition is that these eigen functions would include all the main features of the system such as nonlinearity and non-Marcoffian nature. This becomes obvious, in the representation of the orthogonal functions in a different orthogonal basis function sets.

8.4.2 Eigen Function Representation

It is well known that one can represent a given set of orthogonal functions in a different set of orthogonal basis functions. Hence we can write

$$\phi_{ijk}^{\nu} = \sum_l a_{ijkl} \zeta_l^{\nu}$$

where ζ_l^{ν} are Gegenbauer polynomials. For the value $\nu = 1/2$ the above reduces to Legendre polynomials. Thus

$$\phi_{ijk}^{1/2} = \phi_{ijk} = \sum_l a_{ijkl} P_l \quad (8.7)$$

where now the coefficients a_{ijkl} are functions of space time variables and thereby account for the nonlinearity and complexity of the system. P_l s are independent of the space-time variables. The coefficients a_{ijkl} could be determined using the usual orthogonality property of the Legendre polynomials.

Equation (8.1) can be considered as a numerical fit as

$$a_{ijk,m} = \int \phi_{ijkl} P_m dx \quad (8.8)$$

Since ϕ_{ijk} are known, the above integration can be effected numerically and the coefficients are determined. This is tantamount to fitting the curve depicting ϕ with analytical functions P_m . We shall however make this transformation at a later stage.

8.4.3 Inverse Scattering Calculation

An inverse scattering calculation can be performed using these orthogonal eigen functions and eigen values (Toda, 1975). This procedure is distinctly different from the inverse problem discussed in earlier attempts. We consider here an attractor collection in an attractor space and not the actual brain in the configuration space. This collection is characterized by the eigen functions and eigen values and the evolution equation in general can be written as

$$\phi_{ijk}'' + V(\Phi, t)\phi_{ijk} = \lambda_{ijk}\phi_{ijk} \quad (8.9)$$

The double primes indicate double differentiation with respect to the argument of the function. Φ is the set of all eigen functions for the entire scalp domain. Thus

$$\Phi = \{ \phi_{ijk} \} \quad (8.10)$$

and the set includes all location points i , all windows in each channel (i, j) and all the functions in each channel and in each window (i, j, k) . V represents the MGF in a global sense.

The MGF is a nonlinear function of its argument and at any specific point, the interaction with all other points in the skull space is taken care of by taking Eq. (8.10) for all channels, for all windows and all the functions in

the same window. Since the ϕ_k s are orthogonal, one can expand V in terms of Φ s as

$$V(\Phi, t) = \sum_{n=0}^{\infty} A_n(t) \Phi^n \quad (8.11)$$

where A_n are to be determined from the equation (8.9) written as

$$V(\Phi, t) = \frac{\sum_{ijk} [\lambda_{ijk} \phi_{ijk} - \phi_{ijk}^n]}{\phi_{ijk}} \quad (8.12)$$

In this preliminary investigation equation (8.12) is rewritten as

$$V(\Phi, t) = -\frac{[\Phi^n - \lambda\Phi]}{\Phi} \quad (8.13)$$

where Φ is given in (8.10). To simplify this further, we have taken Φ as

$$\Phi = \sum_{k=1}^5 \phi_{ijk} \quad (8.14)$$

as the number of significant eigen functions in each channel and in each window are only about 5 in number. Since all the elements on the right hand side of Eq. (8.13) are known numerically, this equation is evaluated at each scalp point, each window and used in the map construction.

8.5 Map Construction

In drawing the maps, a 16 channel digitized EEG output is used for the two cases- eyes closed and eyes open. We evaluated the MGF given by Eq. (8.13) and plotted the isocontours for this function.

It has been shown (Indic et. al., 1999; Indic, 1999) that the EEG generated time series are in general nonstationary, and hence this effect can be kept a minimum by taking shorter windows. However too short a window length would introduce spurious correlations. Hence a choice of two second windows, each containing 1024 data points is made. Also the attractors in the various windows have dimensions of the order of 5-7. Hence in carrying out

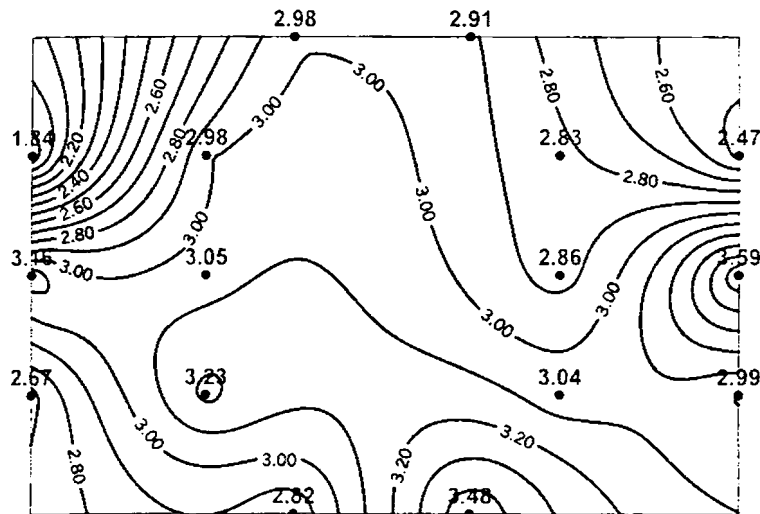


Figure 8.1(a) The iso contours of MGF evaluated at 16 location points in the skull space for the eyes closed condition. The curves represent the intersection contours with the topological manifold.

the SVD we arranged the data in a delayed matrix F in an embedding dimension 15. This gives the total number of rows as 1010 using $N_T = N + m - 1$ where N_T is the total number of data points, N is the total number of rows and m the embedding space.

From this, the 15×15 matrix $F^T F$ is formed and the eigen values and eigen functions λ_{ijk} and ϕ_{ijk} where i runs from 1-16, j from 1-10 and k , $1-\infty$ are evaluated. As has already been pointed out by Broomhead & King (1986),

8.5.1 Topological Manifolds

A topological space by definition is a set of arbitrary elements (or points) based on a certain relation in a R^n (real, n dimensional) space. If these elements are confined to a certain subspace, we call this subspace a manifold. The most commonly understood and familiar to physicists is the double cone with the apex at the point 'event' situated on the space coordinate (x-axis) and the cone having its axis along the time axis normal to the space coordinate (y-axis). The x-axis divides the space into two viz. past and future and the cones divide the space into time like and space like. These cones open out to $\pm\infty$ and this is known as an open manifold. However if the relation generating these surfaces is bounded, we call it as a closed manifold.

In the present case we do not have a metric as in the previous one. We therefore define the MGF as the relation defining the manifold. Thus the relation can be defined as

$$V(\Phi, t) = C \quad (8.15)$$

where we evaluate $V(\Phi, t)$ from the relation given by Eq. (8.13). We have estimated the above quantity at the various scalp points (16 in number) for the adjacent instants of time t_0 and t_0+2 seconds and plotted the iso-contours at (a,b). These iso-contours for the eyes closed state are given in figure 8.1(a,b) and 8.2(a,b) represent similar contours for the eyes open state. If we now stack one above the other the two figures 8.1(a,b) (b above a); we can construct the surfaces by joining the contours of any specified value. The stacked arrangement is given in figure 8.3. Similar plot for eyes open case is given in figure 8.4.

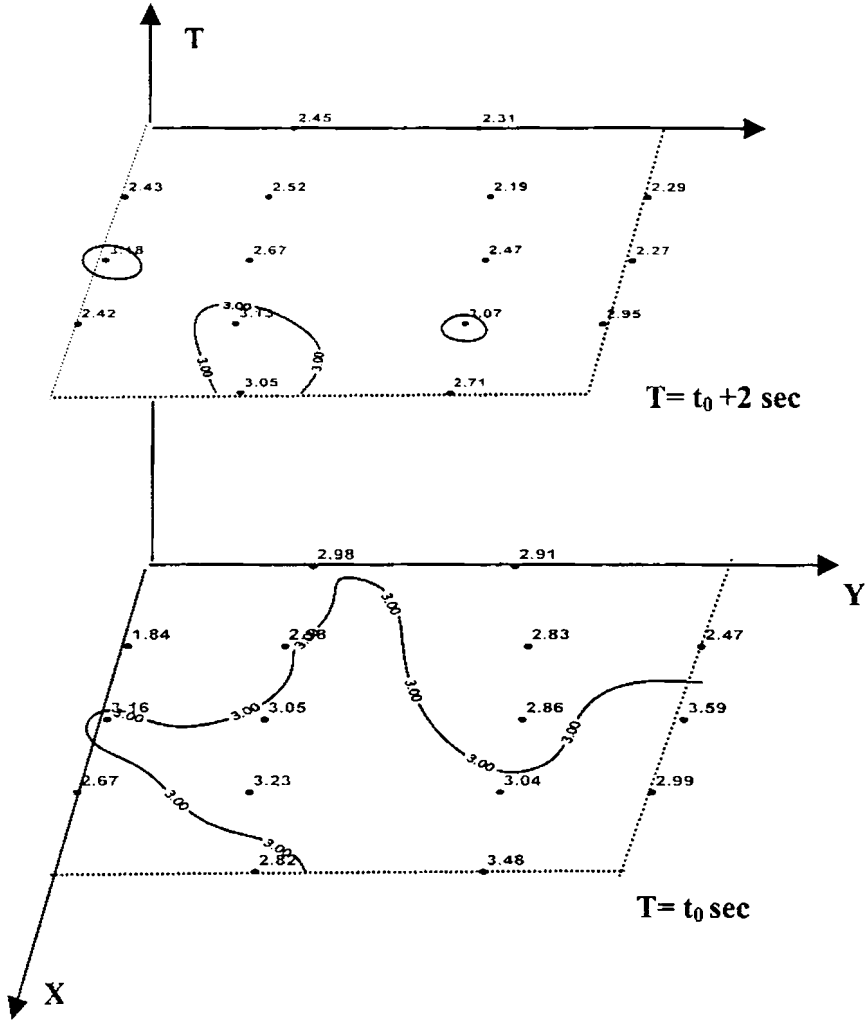


Figure 8.3. The two diagrams 8.1 (a & b) drawn in a perspective scheme. It becomes evident that the simply connected region splits up into multiply connected domains as time progresses. To avoid confusion we have selected only $V=3$ (in arbitrary units).

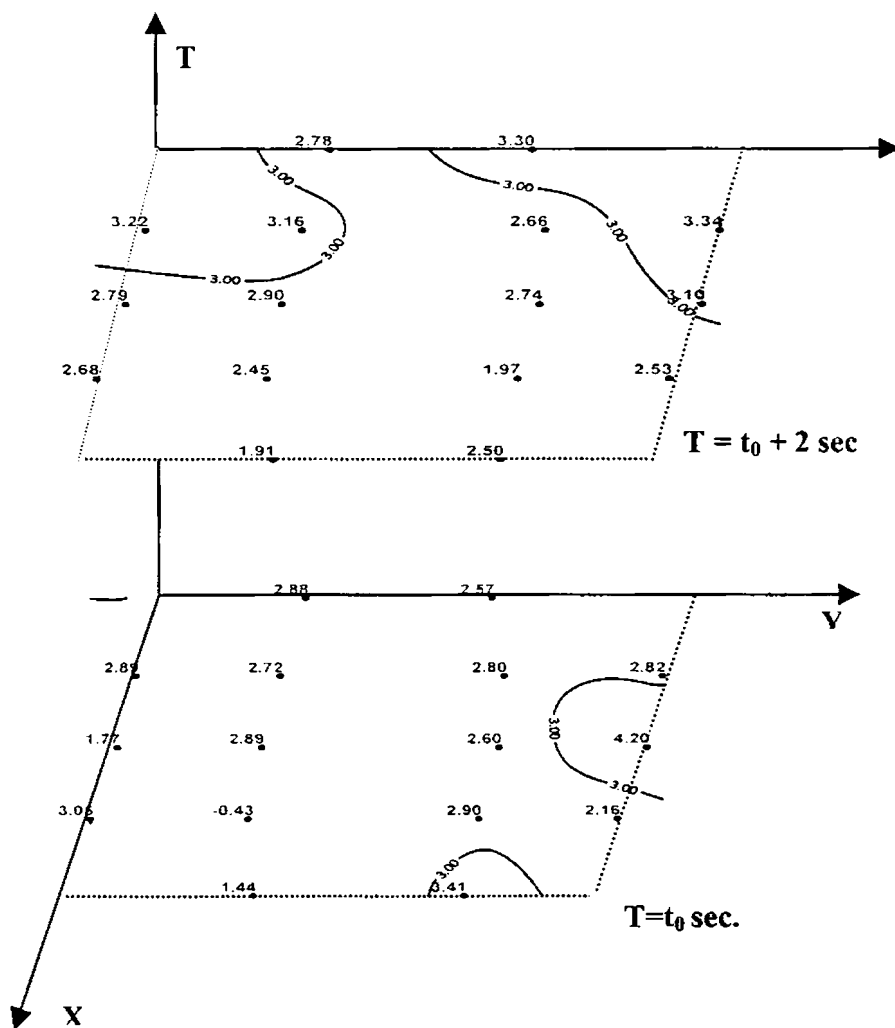


Figure 8.4. The two diagrams 8.2 (a & b) drawn in a perspective scheme. Here the disjointed tubular structures coalesce into one simply connected domain in the adjacent window. To avoid only $V=3$ (in arbitrary units) is presented.

In the resulting diagrams, we can visualize that there are protruding finger /tongue like structures some of which get closed, (because one does not see a closed contour with the same values in the next higher diagram in the stack) while the others are open and that they spin different patterns in the space-time continuum. It becomes quite obvious that these manifolds spin different structures revealing the high degree of complexity inherent in the system. It is indeed a major task to identify such a structural behaviour with any given thought process looking at the amount of computational complexities. Nevertheless, if we can develop this into an online system, it can reveal the brain dynamics.

The results are presented for the two cases of eyes closed figure 8.1 (a, b) and eyes open figure 8.2(a, b). Figure 8.1(a, b) are the two separated frames at the instants t_0 and $(t_0 + 2)$ sec. This could be considered as a curve generated by the intersection of the topological surface with the planes at t_0 and $t_1 = (t_0 + 2 \text{ sec})$. In figure 8.1(a) the isocontours are not closed, since we have only 16 channels and that is not enough for the complete map. The contours would have been closed if we had 64 or 128 or more location points. In the $(t_0 + 2)$ sec. frame, the composite surface of 8.1(a) has separated itself into three islands and this could be visualized as three finger-like structures starting from the composite surface. While the surface 8.1(a) is simply connected, in 8.1(b) frame they are multiply connected. One can construct the composite picture by stacking these two as shown in figure 8.3. Incidentally we have not drawn the explicit surface but the structure is obvious.

The opposite feature is seen in the case when eyes are open- figure 8.2(a, b). Here at t_0 , we have two tube intersections with the plane but they coalesce into one in 8.2(b). A perspective view of this can be comprehended

from figure 8.4. Thus while in figure 8.1, the mono structure evolves into tubular structures, in the second case we get disjointed structures coalescing to form a cogent structure. Thus the complexity is evident from a wide variety of surface structures and that they go from simply connected to multiply connected and back to simply connected spaces.

The merits of this method are that we obtain a visual representation of the evolution of thought processes in the brain by taking various time frames in the interval $(i, i+1)$. We there by achieve from an online system a moving representation of the brain activity in time. This may possibly be used to classify different thought processes or the same thought process under diverse emotional states. Secondly by writing the equations for tangent, normal and bi-normal for these surfaces one can explicitly represent the dynamics of this complex system. This we are pursuing at present. These three vector equations however will be in the space-time continuum but will be functions of the various invariants of the systems such as D_i , K_i , λ_i etc. It should however be realized that as stated above these invariants do not form a complete closed set. Probably one can embark into the search for new invariants. This may also reveal aspects of dynamics which are yet unknown. The dynamics of these surfaces from a clinician's point of view will be helpful to understand the emotional stresses a patient is undergoing during conditions such as those induced by Parkinson's or Alzheimer's disease or even mental depression. In this sense, this opens up a new and wide field for investigation.

On the demerit side, there are a few limitations in this analysis. In the present analysis, windows of two seconds data length are chosen. If we reduce this to one second, the number of data points may become insufficient to give consistent and coherent results. Thus we get in 2second windows only

broader time scales. Since the data is of millisecond interval, we miss a large amount of information in the dynamics, which is very significant since the natural time scale in the system is small and the system is nonlinear, complex and thermodynamically open. Probably a more sensitive data collection process may give a closer scan. This has to be investigated further.

8.6 Conclusion

The method of arriving at conclusions based on maps is only in the preliminary investigation stage and hence the conclusions that can be drawn from it are plausible rather than unique. A remarkable feature revealed here is that the study of complexity can be undertaken by increasing the space dimension. At present a simple case as defined in Eq. (8.8) is undertaken. A higher degree of complexity can be brought into the analysis by taking higher powers of Φ in the definition of V and this results in higher space-time dimension.

A serious difficulty in the study is to obtain what is called a 'baseline'. Towards this end, a large number of cognitive and other task states should be analyzed. The investigation of the manifold dynamics during different pathological conditions such as seizures, depression etc. is expected to turn up results that will go a long way towards the comprehension of the functioning of the brain useful from a clinical point of view.

Conclusions and Themes for Future Research

God has put a secret art into the forces of nature so as to enable it to fashion itself out of chaos into a perfect world system.

--- Immanuel Kant

A technique usually adopted in physiological system examination involves the nonlinear analysis of the time series signal generated from it and subsequent interpretation of results. The frustration that was experienced earlier in failing to detect patterns within biological time series by using the usual statistical techniques was obliterated by the entry of the newer paradigm of nonlinear theory and deterministic chaos. The work presented in this contribution is a compilation of the relevant findings in the attempted deciphering of the brain dynamics by application of these principles.

While nonlinearity was long accepted as ubiquitous in nature the application of its methods and techniques to infer the dynamics of bio-systems was introduced only in the early eighties. As with any new research

field this multidisciplinary approach directed at studying the neural dynamics with principles from physics and mathematics had its fair share of triumphs and setbacks that have been discussed in various contexts in this thesis. At this juncture, the field has come of age and rather than wrangle over many disputable questions such as the chaotic nature of the brain, researchers are concentrating on more meaningful objectives. These are questions regarding what new information pertaining to the brain functioning can be gained by applying novel, nonlinear methods and how these can be made useful in diagnosis or treatment of abnormal brain conditions.

In this work, the electroencephalogram signal recorded on the scalp forms the time series data, which is subjected to the repertoire of techniques developed within the framework of nonlinear theory of oscillations and deterministic chaos. The implications of the results obtained are judiciously accepted on the background of known facts regarding the brain function. The possibility of modeling the brain as a system of coupled nonlinear units has been greatly worked upon. A similar line of approach undertaken by us investigated the static and dynamical aspects of a coupled set of nonlinear oscillators. Besides this, the cooperative nature between the subunits was looked into. This analysis was then extended to include the more natural noisy coupling schemes that may be expected in biological environments. It was observed that while the dynamics of the subsystems evolved in an individual manner, noise was found to catalyze the onset of synchronization or cooperative nature between the coupled units. This finding against the context of stochastic resonance in living systems holds potential for further investigation.

The idea of processes in the neural system occurring at vastly varied timescales has gained significance in the recent past. This phenomenon is

looked upon as a natural cause of the inherent nonstationarity of the recorded EEG signal which has led to modifications and caution in examining results from application of algorithms originally devised for infinitely long, noise-free, stationary data as obtained from model nonlinear systems. In this work, we have attempted a study of the unfolding of the neural attractors with varying time scales for normal and the abnormal epileptic brain conditions. The rate of unfolding quantified by a parameter known as the unfolding dimension was observed to have saturation behaviour for attractors reconstructed from normal EEG signals. The epileptic subject EEGs on the other hand exhibited an unfolding behaviour that failed to attain saturation with increasing time scales. Moreover this behaviour was observed even during the no-seizure or the 'normal' state of the epileptic subjects. The unfolding dimension may thus be looked upon as a marker of brain malfunctioning and may be developed into a monitor with predictive capability. The subsequent section addressed the question of signal complexity using Approximate entropy (ApEn) and its variant Sample entropy (SampEn) as quantifiers to study the data. Examining a dense array EEG data, SampEn measure was able to identify variations in complexity exhibited by various brain regions during a mental arithmetic task of serial subtraction. The activation of multiple brain regions was detected by this technique, which is relatively simple as compared to sophisticated imaging methods such as PET and MRI; yet equally effective.

The gender-based study produced interesting findings of a subtle complexity variation existing during passive conditions of eyes closed and eyes open state. The onset of a common task scenario of mental arithmetic was found to smear out such differences pointing to a common mode of operation in both genders. This is probably a result of the common type of learning or training process that the subjects had undergone in childhood

irrespective of the gender. This finding supports the idea of such analyses being able to emphasize commonalities among people in the use of brain areas. This is not withstanding the fact that human brain anatomy differs considerably from person to person and individuals differ in the strategies they use to accomplish simple mental tasks like reading or remembering words.

The collective nature of cell assemblies in the brain during task performance has been stressed in much of the recent research literature. How the brain regions interact so that information necessary for the performance of a task flows in the brain is significant in learning about the patterns that may be associated with particular tasks and how these are orchestrated in carrying out complex operations. The EEG may be utilized to look for phase entrainment in the signals emanating from multiple brain locations and the strength of interaction between the regions quantified with a parameter known as the synchronization index. It is seen that despite the signal traces being uncorrelated and highly irregular looking in amplitude, their phases do exhibit an entrainment specific of certain states. We have investigated the temporal evolution of the synchrony exhibited by cortical regions during passive conditions and this has been extended to include the analysis of the epileptic condition. The phase synchrony method reliably points out the rise in synchronization in the brain during a seizure state as well as the long distance interactions that are a hallmark of abnormal brain discharges. This technique was applied to the study of effect of fatigue on the performance of a mental task. In this case, mental arithmetic was chosen as the specific task state on which the effect that fatigue induced by physical exertion was monitored. A rise in synchrony during the mental task under fatigued state was observed and a directional coupling analysis indicated an increase in the number of

connections in the parietal –occipital regions of the brain when compared to the task performance under unfatigued conditions. The technique is thus quite effective in giving information regarding the brain coordination due to intangible effects such as mental fatigue. Once the relationship among fatigue, intensity of effort and pacing strategies during exercise get established; this knowledge will benefit groups engaged in activities requiring exertion in daily life such as sprinters, athletes, weightlifters and so on.

The *ultimate* brain model is yet to be realized. The efforts in this direction were initiated as early as 1943 by Hebb and today there exist individual mathematical models for the many specific brain functions such as the olfactory bulb and so on. The emergence of the field of neural networks based on the learning strategy in the brain utilizing distributive networks and its success in modeling many complex real world phenomena has provided a boost to the field of data based prediction and modeling. In modeling the highly complex brain state which is nonlinear and in which feedback and feedforward mechanisms are operative, we have adopted an approach within the realm of nonequilibrium statistical dynamics to formulate an inverse value problem and determined numerically an effective Motion Generating Function using the EEG data. This is a function encompassing all the interactions in the system that has been captured by the EEG signal. The isocontours of this function evaluated over successive time intervals stacked one over the other may be thought of as giving spatio-temporal evolution of the system. Such EEG based brain maps may be considered a preliminary effort in accounting for the system behaviour by including all the system complexities. Yet these are expected to yield important information about the brain functioning for pathological conditions such as seizures, depression, derangement etc. useful from a clinical point of view.

Research in cognitive neuroscience is an attempt to unravel the mysteries of the most complex living structure, the brain, using all the known theories and techniques from various fields of science. The general objective remains a basic understanding of brain functioning during performance of cognitive tasks as well as the abnormalities that may creep up to disrupt its normal functioning causing conditions that are to be treated clinically. A few of themes for future research may be listed as follows.

- ❖ Investigation of the dynamic functional coupling between the rhythmic activity of different cortical regions during motor behaviour, verbal cognitive tasks, auditory stimulation tasks.
- ❖ Bridging the gap between the various brain imaging techniques and establishing more composite means of study involving the temporal resolution of the EEG with the better spatial resolution of the techniques such as fMRI and the latest diffuse optical imaging methods.
- ❖ A greater impetus may be given to the study of pathological brain conditions such as prediction of seizures, motor dysfunction as in Parkinson's disorder, Alzheimer's disease and the lesser-known abnormalities such as depression and derangement.
- ❖ The development of an online diagnostic system, which computes the nonlinear quantifiers even as the recording is carried out to provide the clinician with additional information regarding the brain state that is not directly perceptible from the EEG record.
- ❖ A search for new, computationally viable quantifiers better suited to deal with nonstationary biological data that contain relevant dynamical information pertaining to the underlying system.

- ❖ A more wholesome development of the skeletal theory for the brain function evolution that has been proposed in the framework of nonequilibrium statistical mechanics.

The process of understanding and learning how the brain operates is a tedious yet highly exciting field. It has implications in the development of new fields, for instance those based on emergent complex behaviour such as cellular automata, learning methods as in artificial neural networks, genetic algorithms and synergetics. Nonlinear dynamics paradigm is a suitable ideology when trying to make sense of the morass of data available from the highly nonlinear and complex brain. We have attempted to review as well as present some new findings in the examination of brain dynamics using the nonlinear time series analysis technique. It must however be realized that there exist limitations in the characterization and prediction of cortical activity and neither is it suggested that nonlinear dynamics would answer all our questions. But it provides neurophysicists with a revolutionary approach to formulate old questions and rearticulate new ones bettering our knowledge of the brain in the process.

Bibliography

- Abarbanel, H.D.I., Brown, R. & Kadtke, J.B. (1990) Prediction in chaotic nonlinear systems: Methods for time series with broadband Fourier spectra, *Physical Review A*, **41**: 4, 1782-1807.
- Abarbanel, H.D.I., Brown, R., Sidorowich, J.J. & Tsimiring, L.Sh. (1993) Analysis of observed chaotic data in physical systems, *Reviews of Modern Physics*, **65**, 1331-1392.
- Abarbanel, H.D.I. (1996) *Analysis of observed chaotic data*, Springer-Verlag, New York, Inc.
- Abarbanel, H.D.I., Huerta, R., Rabinovich, M.I., Rowat, P.F., Rul'kov, N.F. & Selverston, A.I. (1996a) Synchronized action of synaptically coupled chaotic single neurons, *Neural Comput.*, **8**, 1567-1602.
- Albano, A.M & Rapp, P.E. (1992) On the reliability of dynamical measures of EEG signals. In: *Nonlinear Analysis of EEG*, Ed. B.H. Jansen & M.E. Brandt, World Scientific, Singapore, 117-139.
- Allen, L.S. & Gorski R.A. (1991) Sexual dimorphism of the anterior commissure and massa intermedia of the human brain, *J. Comp. Neurol.*, **312**, 97-104.
- Amit, D.J. (1989) *Modeling the Brain Function: The World of Attractor Neural Networks*. Cambridge University Press.
- Anderson, J.A & Cooper, L.N. (1978) Biological organization of memory, *Pluriscience Encyclopedia Universals France S.A.*
- Anischenko, V., Vadivasova, T., Postnov, D. & Safanova, M. (1992) Synchronization of chaos, *International Journal of Bifurcation and Chaos*, **2**:3, 633-644.
- Aronson, I.S. & Rulkov, N. (1989) Nontrivial structure of synchronization zones in multidimensional systems, *Physics Letters*, **138(A)**, 375.
- Ashcraft, M. H. (1992) Cognitive arithmetic: A review of data and theory, *Cognition*, **44**, 75-106.
- Babiloni, F., Babiloni, C., Carducci, F., Gaudio, M.D., Onorati, P. & Urbano, A. (1997) A high resolution EEG method based on the correction of the surface Laplacian estimate for the subjects variable scalp thickness, *Electroencephalography & Clinical Neurophysiology*, **103**, 486-492.

- Babloyantz, A., Salazar, J.M. & Nicolis, C (1985) Evidence of chaotic dynamics of brain activity during sleep cycle, *Physics Letters*, **3**, 152-156.
- Baker, S. N., Spinks, R., Jackson, A. & Lemon, R.N.(2001) Synchronization in monkey motor cortex during a precision grip task. I. Task-dependent modulation in single-unit synchrony, *J. Neurophysiology*, **85**, 869-885.
- Balescu, R. (1975) *Equilibrium and Nonequilibrium Statistical Mechanics*, John Wiley & Sons, New York.
- Bhattacharya, J.(2000) Complexity analysis of spontaneous EEG, *Acta Neurobiologiae Experimentalis*, **60**, 495-501.
- Bhattacharya, J. & Petsche, H. (2001) Enhanced phase synchrony in the electroencephalograph γ band for musicians while listening to music, *Physical Review E*, **64**, 012902.
- Bhattacharya, J., Petsche, H., Feldmann, U. & Rescher, B. (2001). EEG gamma-band phase synchronization between posterior and frontal cortex during mental rotation in humans, *Neuroscience Letters*, **311**, 29-32
- Birbaumer, N., Lutzenberger, W., Ray, H., Braun, C. & Mayer-Kress, G. (1996) Perception of music and dimensional complexity of brain activity, *International Journal of Bifurcation and Chaos*, **6:2**, 267-278.
- Bizas, E., Simos, P.G., Stam, C.J., Arvanitis, S., Terzakis, D. & Micheloyannis, S. (1999) EEG correlates of cerebral engagement in reading tasks, *Brain Topography*, **12:2**, 99-105.
- Blasius, B. & Stone, L. (2000) Chaos and phase synchronization in ecological systems, *International Journal of Bifurcations and Chaos*, **10:10**, 2361-2380.
- Bondarenko, V.E. (1994) A simple neural network model produces chaos similar to the human EEG, *Physics Letters A*, **196**, 195-200.
- Broomhead, D.S. & King, G.P. (1986) Extracting qualitative dynamics from experimental data, *Physica D*, **20**, 217 - 236
- Bryant, P. & Jeffries, C. (1987) The dynamics of phase locking and points of resonance in a forced magnetic oscillator, *Physica D*, **25**, 196-232.
- Buzug, Th. & G. Pfister (1992) Optimal delay time and embedding dimension for delay-time coordinates by analysis of the global static and local dynamical behavior of strange attractors, *Physical Review A*, **45**, 7073-7084.

- Byne, W., Bleier, R. & Houston L. (1988) Variations in human corpus callosum do not predict gender, *Behavioural Neuroscience*, **102**:2, 222-227.
- Caplan, P.J., McPherson, G.M. & Tobin, P. (1985) Do sex-related differences in spatial abilities exist? *American Psychologist*, **40**, 786-799.
- Casdagli, M., Eubank, S., Farmer, J.D. & Gibson, J. (1991) State space reconstruction in the presence of noise, *Physica D*, **51**, 52-98.
- Casdagli, M.S., Iasemidis, L.D., Savit, R.S., Gilmore, R.L., Roper, S.N. & Sackellares, J.C. (1997) Nonlinearity in invasive EEG recordings from patients with temporal lobe epilepsy, *Electroencephalography & Clinical Neurophysiology*, **102**, 98-105.
- Chaos and Society* (1995) Ed. Albert, A., Burke, VA, IOS Press.
- Chaos Theory in the Social Sciences: Foundations and Applications*, (1995) Ed. L.D. Kiel & Elliott, E., Ann Arbor, The University of Michigan Press.
- Chapman, S. & Bartels, J. (1940) *Geomagnetism*, I and II, Oxford, Clarendon, UK.
- Coffman, K., McCormick, W.D. & Swinney, H.L. (1986) Multiplicity in a chemical reaction with one-dimensional dynamics, *Physical Review Letters*, **56**, 999-1002.
- Cohen, D. (1972) Magnetoencephalography: Detection of the brain's electrical activity with a superconducting magnetometer, *Science*, **175**, 664-666.
- Colicos, M. A., Collins, B.E., Sailor, M. J. & Gada, Y. (2001) Hippocampal synapse remodeling induced by photoconductive silicon stimulation, *Cell*, **107**, 605-618.
- Corsi-Cabrera, M., Herrera, P. & Malvido, M. (1989) Correlation between EEG and cognitive abilities: sex differences, *International Journal of Neuroscience*, **45**, 133-141.
- Costa, M., Goldberger, A.L. & Peng, C.-K. (2002) Multiscale analysis of complex physiologic time series, *Physical Review Letters*, **89**:6,068102.
- Cowan, J.D. and Sharp, D.H. (1988) Neural Nets. *Quart. Rev. Biophys*, **21**, 365-427.
- D'Humieres, D., Beasley, M.R., Huberman, B., Libchaber, A. (1982) Chaotic states and Routes to chaos in the forced pendulum, *Physical Review A*, **26**, 3483-3496.
- Donald, M. J.(1990) Quantum theory and the brain, *Proc. Roy. Soc. London A.*, **427**, 43-93.
- Dunki, R. M. & Schmid, G. B.(1998). Unfolding dimension and the search for functional markers in human electroencephalogram, *Physical Review E*, **57**, 2115-2122.
- Eckmann, J.-P. & Ruelle, D. (1985) Ergodic theory of chaos and strange attractors, *Reviews of Modern Physics*, **57**, 617-656.

- Eckmann, J. -P., Kamphorst, S.O., Ruelle, D. & Ciliberto, S.(1986) Lyapunov exponents from a time series, *Physical Review A*, **34**, 4971-4979.
- Eckmann, J. P., Kamphorst, S. O. & Ruelle, D.(1987) Recurrence plots of dynamical systems, *Europhysics Letters*, **4**, 973-979.
- Edlinger G., Wach P. & Pfurtscheller, G. (1998) On the realization of an analytic high resolution EEG, *IEEE Transactions on Biomedical Engineering*, **45**:6, 736-745.
- Elbert, T., Ray W. J., Kowalik Z. J., Skinner J. E. & Birbaumer, N. (1994) Chaos and Physiology: Deterministic chaos in excitable cell assemblies, *Physiological Reviews*, **74**:1, 1-97.
- Eschweiler, G. W., Wegerer, C., Schlotter, W., Spandl, C., Stevens, A. & Bartels, M. (2000) Left prefrontal activation predicts therapeutic effects of repetitive transcranial magnetic stimulation (rTMS) in major depression, *Psychiatry Research*, **99**,161-172.
- Farmer, J. D., Ott, E. & Yorke, J. A. (1983) The dimension of chaotic attractors, *Physica*, **7**, 153-180.
- Feigenbaum, M.J. (1978) Quantitative universality for a class of nonlinear transformations, *J. Stat. Phys.*, **19**, 25-52.
- Ferri, R., Pettinalo, S., Alicata, F., Gracco, S.D., Elia, M. & Musumeci, S.A. (1998) Correlation dimension of EEG slow wave activity during sleep in children and young adults, *Electroencephalography & Clinical Neurophysiology*, **106**, 124-128.
- Fraser, A.M. & Swinney, H.L.(1986) Independent coordinates for strange attractors from mutual information, *Physical Review A*, **33**, 1134-1140.
- Freeman, W. J., (1986) Petit mal seizures spikes in olfactory bulb and cortex caused by runaway inhibition after exhaustion of excitation, *Brain Res. Rev.*, **396**, 259-284.
- Freeman, W. J., Yao, Y. & Burke, B. (1988) Central pattern generating and recognizing in olfactory bulb: a correlation learning rule, *Neural Networks*, **1**, 277-288.
- Freeman, W. J. (1995) The physiology of perception, *Scientific American*, **264**,78-85.
- Freiwald, W.A., Valdes, P., Bosch, J., Biscay, R., Jimenez, J.C., Rodriguez, L. M., Rodriguez, V., Kreiter, A.K. & Singer, W. (1999) Testing nonlinearity and directedness of interactions between neural groups in the macaque inferotemporal cortex, *Journal of Neuroscience Methods*, **94**, 105-119.
- Gabor, D. (1946) Theory of communication, *J. IEE London*, **93**:26, 457-492.
- Galka, A. & Ozaki, T. (2001), Testing for nonlinearity in high-dimensional time series from continuous dynamics, *Physica D*, **158**, 32 - 44

- Gallez, D. & Babloyantz, A. (1991) Predictability of human EEG: A dynamical approach, *Biological Cybernetics*, **64**, 381-391.
- Gammaitoni, L., Hanggi, P., Jung, P. & Marchesoni, F. (1998) Stochastic Resonance, *Reviews of Modern Physics*, **70**:1, 223-287.
- Geary, D.C. (1989) A model for representing gender differences in the pattern of cognitive abilities, *American Psychologist*, **44**, 1155-1156.
- Gevens, A. (1990) Dynamic patterns in multiple lead data. In: *Event-related Brain Potentials: Basic Issues and Applications*, Ed. J. Rohrbaugh, R. Johnson, T. Parasraman, Oxford University Press, New York, 44-56.
- Gibson, J.F., Farmer, J.D., Casdagli, M. & Eubank, S. (1992) An analytic approach to practical state space reconstruction, *Physica D*, **57**, 1-30.
- Glansdorff, P. & Prigogine, I. (1971) *Thermodynamic Theory of Structure, Stability and Fluctuations*, Wiley and Sons, London.
- Glass, L. & Mackey, M.C. (1988) *From Clocks to Chaos*, Princeton University Press, Princeton, New Jersey.
- Glass, L., Kaplan D. T. & Lewis J. E. (1992) Test for deterministic dynamics in real and model neural networks, In *Nonlinear Analysis of EEG*, Ed. B. H. Jansen & M. E. Brandt, World Scientific, Singapore, 233-249.
- Gould, E., Reeves, A. J., Graziano, M.S.A. & Gross, C.G. (1999) Neurogenesis in the Neocortex of Adult Primates, *Science*, **286**, 548-552.
- Grassberger, P. & Procaccia, I. (1983a) Characterisation of strange attractors, *Physical Review Letters*, **50**, 346-349.
- Grassberger, P. & Procaccia, I. (1983b) Measuring the strangeness of strange attractors. *Physica D*, **9**, 189-208.
- Grassberger, P. & Procaccia, I. (1983c) Estimation of the Kolmogorov entropy from a chaotic signal, *Physical Review A*, **28**, 2591-2593.
- Gu, F., Meng, X. & Shen, E. (2003) Can we measure consciousness with EEG complexities? *International Journal of Bifurcation and Chaos*, **13**:3, 733-742.
- Guastello, S.J. (1995). *Chaos, Catastrophe, and Human Affairs: Applications of Nonlinear Dynamics to Work, Organizations, and Social Evolution*. Hillsdale, NJ: Lawrence Erlbaum.

- Gur, R. C., Turetsky, B. I., Matsui, M., Yan, M., Bilker, W., Hughett, P. & Gur, R. E. (1999) Sex differences in brain gray and white matter in healthy young adults: correlations with cognitive performance, *Journal of Neuroscience*, **19**:10, 4065-4072.
- Hampson, D. B., Gibson, A. S., Lambert, M. I., Noakes, T. D. (2001). The influence of sensory cues on the perception of exertion during exercise and central regulation of exercise performance, *Sports Medicine*, **31**:13, 935-952.
- Harmony, T., Fernández, T., Silva, J., Bosch, J., Valdés, P., Bouzas, A. F., Galán, L., Aubert, E. & Rodríguez, D. (1999) Do specific EEG frequencies indicate different processes during mental calculation? *Neuroscience Letters*, **268**, 25-28.
- Havstad, J. & Ehlers, C. L. (1989) Attractor dimension of nonstationary dynamical system from small data sets, *Physical Review A*, **15**, 845-853.
- Hayashi, H. & Ishiyuka, S. (1987) *Chaos in molluscan neuron: chaos in biological systems*. Ed: H. Degn, A.V. Holden, LE Olsen, NY Plenum, 157-166.
- Hayashi, H., Nakao, M. & Hirakawa, K. (1982) Chaos in the self sustained oscillations of an excitable biological membrane under sinusoidal oscillation, *Physics Letters*, **88**, 265-266.
- Hebb, D.O. (1964) *The organization of behaviour*, Wiley NY.
- Hidaka, I., Nozaki, D. & Yamamoto, Y. (2000) Functional stochastic resonance in the human brain: Noise induced sensitization of baroreflex system, *Physical Review Letters*, **85**:17, 3740-3743.
- Hilborn, R. C. (1994) *Chaos and Nonlinear Dynamics*, Oxford University Press.
- Hindmarsh, J.L. & Rose, R. M. (1994) A model of neuronal bursting using three coupled first order differential equations, *Proc. R. Soc. London B*, **221**, 87-102.
- Hock, C., Villringer, K, Muller-Spahn, F., Wenzel, R., Heekeren, H. & Schuh-Hofer, S. (1997) Decrease in parietal cerebral hemoglobin oxygenation during performance of a verbal fluency task in patients with Alzheimer's disease monitored by means of near-infrared spectroscopy (NIRS)—correlation with simultaneous rCBF-PET measurements, *Brain Research*, **755**, 293–303.
- Hodgkin, A.L. & Huxley, A.F.(1952) Quantitative description of membrane current and its application to conduction and excitation in nerve. *J. Physiol.*, **117**, 500-544.
- Indic, P., Pratap, R., Nampoore, V. P. N. & Pradhan, N. (1999) Significance of time scales in nonlinear dynamical analysis of electroencephalogram signals, *International Journal of Neuroscience*, **99**, 181-194.

- Indic, P. (1999) Time scale dependence of human brain dynamics, *International Journal of Neuroscience*, **99**,195-199.
- Inouye, T., Shinosaki, K., Iyama, A. & Matsumoto, Y. (1993) Localization of activated areas and directional EEG patterns during mental arithmetic, *Electroencephalography & Clinical Neurophysiology*, **86**, 224-230.
- Jaušovec, N. & Jaušovec, K. (2000) EEG activity during the performance of complex mental problems, *International Journal of Psychophysiology*, **36**, 73-88.
- Jeong, J., Kim, S.Y. & Han, S. H. (1998) Nonlinear dynamical analysis of the EEG in Alzheimer's disease with optimal embedding dimension, *Electroencephalography & Clinical Neurophysiology*, **106**, 220-228.
- Jeong, J., Gore, J.C. & Peterson, B. S. (2001) Mutual information analysis of the EEG in patients with Alzheimer's disease, *Clinical Neurophysiology*, **112**, 827-835.
- Jiang, Y. (2000) Globally coupled maps with time delay interactions, *Physics Letters A*, **267**,342-349.
- Jobsis, F. F. (1977) Noninvasive infrared monitoring of cerebral and myocardial sufficiency and circulatory parameters, *Science*, **198**,1264-1267.
- Kaas, J. H. & Reiner, A. (1999) The neocortex comes together, *Nature*, **399**, 418-419.
- Kantz, H. & Schreiber, T. (1997) *Nonlinear Time Series Analysis*, Cambridge University Press.
- Kantz, H. (1994) A robust method to estimate the maximal Lyapunov exponent of a time series, *Physics Letters A*, **185**, 77-87.
- Kaplan, D.T. & Glass, L. (1992) Direct test for determinism in a time series, *Physical Review Letters*, **68**, 427-430.
- Kay, L., Shimoide, K & Freeman W. J. (1995). Comparison of EEG time series from rat olfactory system with model composed of nonlinear coupled oscillators, *International Journal of Bifurcation and Chaos*, **5**:3, 849-858.
- Kazui, H., Kitagaki, H. & Mori, E. (2000) Cortical activation during retrieval of arithmetic facts and actual calculation: a functional magnetic imaging study, *Psychiat. Clin. Neurosci.*, **54**, 479-485.
- Kennel, M.B, Brown, R. & Abarbanel, H.D.I. (1992) Determining the embedding dimension for phase space reconstruction using a geometrical construction, *Physical Review A*, **15**, 3403-3411.

- Kevrekidis, J.G., Aris, R. & Schmidt, L.D. (1986) Forcing an entire bifurcation diagram: Case studies in chemical oscillators, *Physica D*, **23**, 391-395.
- Koukkou, M., Lehmann, D., Wackermann, J. Dvorak, I. & Henggeler, B. (1993) Dimensional complexity of EEG brain mechanism in untreated schizophrenia, *Biol. Psychiatry*, **33**, 397-407.
- Kowalik, Z. J. & Elbert, T. (1995) A practical method for the measurements of the chaoticity of electric and magnetic brain activity, *International Journal of Bifurcation and Chaos*, **5**, 475-490.
- Kuffler, S.W., Nicholls, J.G. & Martin, A.R.(1984) *From Neuron to Brain: A Cellular Approach in the Functions of the Nervous System*, Sinauer Associates Inc., Sunderland, Mass.
- Kulkarni, D.R., Parikh, J.C. & Pratap, R. (1997) Simulation of characteristics and artificial neural network modeling of electroencephalograph time series, *Physical Review E*, **55**, 4508-4512.
- Kulynych, J.J., Vladar, K., Jones, D.W. & Weinberger, D.R. (1994) Gender differences in the normal lateralization of the supra-temporal cortex: MRI surface-rendering morphometry of Heschl's gyrus and the planum temporal, *Cerebral cortex*, **4**, 107-118.
- Kuramoto, Y. (1984) *Chemical Oscillations, Waves and Turbulence*, Springer, Berlin.
- Lachaux J.-P., Rodríguez, E., Martinerie, J. & Varela, F.J. (1999) Measuring phase synchronization in brain signals, *Brain Mapping*, **8**, 194-208.
- Lalaja, V, Nampoori, V. P. N & Pratap, R.(1987) Nonlinear analysis of an EEG during epileptic seizure, *Current Science*, **56**, 1039.
- Law, M.I. & Constantine-Paton, M.(1981) Anatomy and physiology of experimentally produced striped tecta, *Journal of Neuroscience*, **1**: 741-759
- Le Van Queyan, M., Martinerie, J., Baulac, M. & Varela, F. (1999) Anticipating epileptic seizures in real time by a nonlinear analysis of similarity between EEG recordings. *Computational Neuroscience, Neuroreport*, **10**, 2149-2155.
- Le Van Queyan, M., Foucher, J., Lachaux J.-P., Rodríguez, E., Lutz, A., Martinerie, J. & Varela, F.J. (2001) Comparison of Hilbert transform and wavelet methods for the analysis of neuronal synchrony, *Journal of Neuroscience Methods*, **111**, 83-98.
- Lehnertz, K. & Elger, C.E. (1995) Spatiotemporal dynamics of the primary epileptogenic area in temporal lobe epilepsy characterized by neuronal complexity loss, *Electroencephalography and Clinical Neurophysiology*, **95**, 108-117.

- Lerner, D.E. (1996) Monitoring changing dynamics with correlation integrals: Case study of an epileptic seizure, *Physica D*, **97**, 563-576.
- Liebert, W. & Schuster, H.G. (1989) Proper choice of time delays for the analysis of chaotic time series, *Physical Letters A*, **142**, 107-111.
- Linn M.C. & Petersen, A. C. (1985) Emergence and characterization of sex differences in spatial ability: A Meta Analysis, *Child Development*, **56**, 1479-1498.
- Longtin, A., Bulsara, A. & Moss, F. (1991) Time interval sequences in bistable systems and the noise induced transmission of information by sensory neuron, *Physical Review Letters*, **67**, 656-659.
- Lorenz, E.N. (1963) Deterministic nonperiodic flow, *Journal of the Atmospheric Sciences*, **20**,130-41.
- Lutzenberger, W., Birbaumer, N., Elbert, T., Rosckstroh, B. & Flor, H. (1992) Dimensional analysis of the human EEG and intelligence, *Neuroscience Letters*, **143**, 10-14
- Makeig, S. & Inlow, M. (1993) Lapses in alertness: coherence of fluctuations in performance and EEG spectrum, *Electroencephalography and Clinical Neurophysiology*, **86**, 23-35.
- Mandelbrot, B.B. (1985) *The Fractal Geometry of Nature*, Freeman, SanFrancisco.
- Martinerie, J., Adam, C., LeVan Queyen, M., Baulac, M., Clemenceau, S., Renault, B. & Varela, F. (1998) Epileptic seizures can be anticipated by nonlinear analysis, *Nature Medicine*, **4**:10, 1173-1176.
- Martinerie, J.M., Albano, A.M., Mees, A.I. & Rapp, P. E. (1992) Mutual Information, strange attractors and the optimal estimation of dimension, *Physical Review A*, **45**, 7058-7064.
- Matsumoto, T., Chua, L. O. & Komoro, M. (1987a) Birth and death of the double scroll, *Physica D*, **24**, 97-124.
- Matsumoto, G., Aihara, K., Takahashi, N., Yoshizawa, S. & Nagumo J (1987b) Chaos and phase locking in normal squid axons, *Physics Letters*, **123**, 162-166.
- May, R.M. (1976) Simple mathematical models with very complicated dynamics, *Nature*, **261**, 459-467.
- McCarthy, R.A. & Warrington, E.K. (1990) *Cognitive Neuropsychology: A Clinical Introduction*, Academic Press, SanDiego, LA.

- McCloskey, M., Caramazza, A. & Basili, A.G. (1985) Cognitive mechanisms in number processing and calculation: Evidence from dyscalculia, *Brain and Cognition*, **4**, 171–196.
- McCloskey, M. (1992) Cognitive mechanisms in numerical processing: evidence from acquired Dyscalculia, *Cognition*, **44**, 107-157.
- McCulloch, W.S. & Pitts, W. (1943) A logical calculus of the ideas immanent in nervous activity, *Bulletin of Mathematical Biophysics*, **5**, 115-133.
- Meyers-Levy J. & Maheswaran D. (1991) Exploring differences in males' and females' processing strategies, *Journal of Consumer Research*, **18**, 63-70.
- Meyers-Levy J. & Sternthal, B. (1991) Gender differences in the use of message cues and judgments, *Journal of Marketing Research*, **28**, 84-96.
- Micheloyannis, S., Flitzanis, N., Papanikolaou, E., Bourkas, M., Terzakis, D., Arvanitis, S. & Stam, C.J. (1998) Usefulness of nonlinear EEG analysis, *Acta Neurologica Scandinavica*, **97**, 13-19.
- Minorsky, N. (1969) *Nonlinear Oscillations*, D. van Nostrand Company Inc., Princeton, USA.
- Mitra, M. & Skinner, J. E. (1993) Low dimensional chaos maps learning in a model neuropil (rabbit olfactory bulb), *Integrative Physiological and Behavioral Science*, **27:4**, 304-322.
- Molle, M., Marshall, L., Wolf, B., Fehm, H.L. & Born, J.(1999) EEG complexity and performance measures of creative thinking, *Psychophysiology*, **36:1**,95-104.
- Mori, T. & Kai, S. (2002) Noise-induced entrainment and stochastic resonance in human brain waves, *Physical Review Letters*, **88:21**, 218101.
- Mormann, F., Lehnertz, K., David P. & Elger, C.E. (2000) Mean phase coherence as a measure for phase synchronization and its application to the EEG of epilepsy patients, *Physica D*, **144**, 358-369.
- Mpitsos, G. J., Burton Jr., R. M., Creech, C. & Soinila, S. O. (1988) Evidence for chaos in spike trains of neurons that generate rhythmic motor patterns, *Brain Res. Bull.*, **21**, 529-538.
- Munk, M., Roelfsema, P., Fries, P., Kreiter, A. & Singer, W. (2000) Rapidly changing synchronization of gamma-frequency oscillations across visual, parietal, and motor areas of the macaque monkeys performing a visuo-motor task, *Soc. Neurosci. Abstr.*, **777**, 6.
- Newhouse, S., Ruelle, D. & Takens, F. (1978) Occurrence of strange axiom Attractors near quasiperiodic flows on T^m ($m=3$ or more), *Comm. Math. Phys.*, **64**, 35-40.

- Nonlinear Analysis of Physiological Data* (1998) Eds. H. Kantz, J. Kurths & G. Mayer-Kress, Springer-Verlag, Berlin.
- Nybo, L. & Nielsen, B. (2001) Perceived exertion is associated with an altered brain activity during exercise with progressive hyperthermia, *J. Appl. Physiol.*, **91**, 2017-2023.
- Osborne, A. R. & Provenzale, A. (1989) A finite correlation dimension for stochastic systems with power law spectra, *Physica D*, **35**, 357-381.
- Osipov, G.V., Pikovsky, A.S., Rosenblum, M.G. & Kurths, J. (1997). Phase synchronization effects in a lattice of nonidentical Rossler oscillators, *Physical Review E*, **55**, 2353-2361.
- Ott, E. (1993) *Chaos in Dynamical systems*, Cambridge University Press, Cambridge.
- Ozaki, T., Jimenez, J.C., Biscay, R. & Valdes, P. (1999). Nonlinear time series models and neural dynamical systems, In: *Nonlinear dynamics and Brain Functioning*, Ed. N. Pradhan, P. E. Rapp & R. Sreenivasan, Nova Science Publishers Inc., New York, 155-200.
- Packard, N.H., Crutchfield, J.P., Farmer, J.D. & Shaw, R. S. (1980) Geometry from a time series, *Physical Review Letters*, **45**, 712-715.
- Palus, M. (1996) Nonlinearity in normal human EEG: Cycles, temporal asymmetry, nonstationarity and randomness, not chaos, *Biological Cybernetics*, **75**, 389-396.
- Palus, M. (1999) Nonlinear dynamics in EEG analysis: Disappointments and perspectives. In: *Nonlinear Dynamics and Brain Functioning*. Eds. N. Pradhan, P.E. Rapp, R. Sreenivasan, Nova Science Publishers, 201-216.
- Parikh, J.C. & Pratap, R. (1984). An evolutionary model of a neural network, *Journal of Theoretical Biology*, **108**, 31-38.
- Parikh, J.C. & Pratap, R. (1991) A map describing the EEG activity of brain, *Pramana J Phys.*, **36**, L347-352.
- Parker, T.S. & Chua L.O. (1987) Chaos: A tutorial for engineers, *Proc. of the IEEE*, **75**:8, 982-1008.
- Parlitz, U., Junge, L., Lauterborn, W. & Kocarev, L. (1996a) Experimental observation of phase synchronization, *Physical Review E*, **54**:2, 2115-2117.
- Parlitz, U., Kocarev, L., Stojanovski, T. & Preckel, H. (1996b) Encoding messages using chaotic synchronization, *Physical Review E*, **53**, 4351-4361.

- Pereda, E., Gamundi, A., Rial, R. & González, J. (1998) Nonlinear behaviour of EEG: Fractal exponent versus correlation dimension in awake and sleep stages, *Neuroscience Letters*, **250**, 91-94.
- Petracchi, D., Pellegrini, M., Pellegrino, M., Barbi, M. & Moss, F. (1994) Periodic forcing of a K⁺channel at various temperatures, *Biophys. J.*, **66**, 1844.
- Pezard, L., Martinerie, J., Müller-Gerking, J, Varela, F. J. (1996) Entropy quantification of human brain spatio-temporal dynamics, *Physica D*, **96**, 344-354.
- Pikovsky, A.S. (1984) On the interaction of strange attractors, *Z. Phys B.*, **55**, 149-154.
- Pikovsky, A.S., Rosenblum, M.G., Osipov, G.V. & Kurths, J. (1997) Phase synchronization of chaotic oscillators by external driving, *Physica D*, **104**, 219-238.
- Pikovsky, A., Rosenblum, M. & Kurths, J. (2000) Phase synchronization in regular and chaotic systems, *International Journal of Bifurcation and Chaos*, **10**:10, 2291-2305.
- Pincus, S.M. (1991) Approximate entropy as a measure of system complexity. *Proc. Natl. Acad. (USA)*, **88**, 2297-2301.
- Pincus, S.M. & Keefe, D.L. (1992) Quantification of hormone pulsatility via an approximate entropy algorithm, *American Journal of Physiology*, **262** (5 Pt 1), E741-54.
- Pincus, S.M. & Viscarello, R.R. (1992) Approximate entropy: a regularity measure for fetal heart rate dynamics, *Obstet. Gynecol.*, **79**, 249-255.
- Poincaré, J.H. (1892) *Les méthodes nouvelles de la mécanique céleste*, Gautier-Villars, Paris.
- Posner, M.I. & Raichle, M.E. (1994) *Images of Mind*, Scientific American Library, NY.
- Pradhan, N. & Narayan Dutt, D. (1993) Use of running fractal dimension for the analysis of changing patterns in electroencephalograms, *Computations in Biology and Medicine*, **23**:5, 381-388.
- Pradhan, N., Sadasivan, P. K., Chatterji, S. & Dutt, D. N. (1995) Patterns of attractor dimensions of sleep EEG, *Computations in Biology and Medicine*, **25**:5, 455-462.
- Pradhan, N. & Sadasivan, P. K. (1996) The nature of dominant Lyapunov exponent and attractor dimension curves of EEG in sleep, *Computations in Biology and Medicine*, **26**:5, 419-428.
- Pradhan, N. & Sadasivan, P. K. (1997) Validity of dimensional complexity measures of EEG signals, *International Journal of Bifurcation and Chaos*, **7**:1, 173-186.

- Pratap, R. (1999). An analytic theory of sensory transduction. In: *Nonlinear Dynamics and Brain Functioning*, Eds. N. Pradhan, P.E. Rapp, R. Sreenivasan, Nova Science Publishers, 87-11.
- Pratap, R.(2000) Nonequilibrium statistical mechanics of brain function. In: *Nonlinear Phenomena*, Ed. S.K. Malik, M.K. Chandrasekharan, and N. Pradhan, Indian National Science Academy, New Delhi, 343-361.
- Pravitha, R., Indic, P., Nampoori, V.P.N., Pratap, R. (2001) Effect of time scales on the unfolding of neural attractors, *International Journal of Neuroscience*, **111**:3-4, 175-186.
- Prigogine, I. (1962) *Non equilibrium Statistical Mechanics*, John Wiley & Sons, Inc.
- Pritchard, W.S. & Duke, D. W. (1992) Dimensional analysis of no-task human EEG using Grassberger-Procaccia method, *Psychophysiology*, **29**, 182-192.
- Pritchard, D. & Theiler, J. (1994) Generating surrogate data for time series with several simultaneously measured variables, *Physical Review Letters*, **73**:7, 951-954.
- Pritchard, W.S., Duke, D.W., Coburn, K.L., Moore, N.C., Tucker, K.A., Jann, M.W. & Hostetler, R.M. (1994) EEG based, neural net predictive classification of Alzheimer's disease versus control subjects is augmented by nonlinear EEG measures, *Electroencephalography & Clinical Neurophysiology*, **91**,118-130.
- Pritchard, W.S., Duke, D.W. & Kriehle, K.K. (1995) Dimensional analysis of resting human EEG II: Surrogate data testing indicate nonlinearity but not low dimensional chaos, *Psychophysiology*, **32**, 486-491.
- Provenzale, A., Smith, L.A, Vio, R. & Murante, G. (1992) Distinguishing between low dimensional dynamics and randomness in measured time series, *Physica D*, **58**, 31-49.
- Rabinovich, M.I. & Abarbanel, H.D.I. (1998) The role of chaos in neural systems, *Neuroscience*, **87**:1,5-14.
- Radhakrishnan, N. & Gangadhar, B.N. (May/June1998) Estimating regularity in epileptic seizure time-series' data, *IEEE Engineering in Medicine and Biology*, 89-94.
- Rambouts, S.A.R.B., Keunen, R.W.M., Stam, C.J. (1995) Investigation of nonlinear structure in multichannel EEG, *Physics Letters A*, **202**, 352-358.
- Rapp, P.E., Zimmerman, I.D., Albano, A.M. , Degeezman, C. & Greenbaum N.N. (1985) Dynamics of spontaneous neural activity in the simian motor cortex : the dimension of chaotic neuron, *Physics Letters*, **6**, 335-338.
- Rapp, P.E. (1990) A guide to dynamical analysis. (Personal communication).

- Rapp, P.E. (1993) Chaos in the neurosciences - Cautionary tales from the frontier, *Biologist*, **40**, 89-94.
- Rapp, P. E. (1999) Nonlinear dynamical analysis and the investigation of the human central nervous system. In: *Nonlinear Dynamics and Brain Functioning*, Eds. N. Pradhan, P.E. Rapp, R. Sreenivasan, Nova Science Publishers, 1-5.
- Rasband, S. N. (1997) *Chaotic Dynamics of Nonlinear Systems*, Wiley Interscience.
- Rashevsky, N. (1938) *Mathematical biophysics*, University of Chicago press.
- Richetti, P., DeKepper, P., Roux, J.C. & Swinney, H.L. (1987) A crisis in the Belousov-Zhabotinskii reaction: experiment and simulation, *J. Stat. Phys.*, **48**, 977-990.
- Richman, J. S. & Moorman, J. R. (2000) Physiological time-series analysis using approximate entropy and sample entropy, *Am. J. Physiol Hear Circ Physiol.*, **278**, H2039-H2049
- Rickard, T.C., Romero, S.G., Basso, W.C., Flitman, S. & Grafman, J. (2000) The calculating brain: an fMRI study, *Neuropsychologia*, **38**, 325-335.
- Roelfsema, P. R., Engel, A. K., Konig, P. & Singer, W. (1997) Visuomotor integration is associated with zero time-lag synchronization among cortical areas, *Nature*, **385**, 157-161.
- Roschke J & Basar, E. (1988) The EEG is not a simple noise: strange attractors in the intra cranial structures. In: *Dynamics of Sensory and Cognitive Processing in the Brain*, Ed. E. Basar, NY Springer, 203-216.
- Röschke, J. & Aldenhoff, J. B. (1992) A nonlinear approach to brain function: Deterministic chaos and sleep EEG, *Sleep*, **15**:2. 95-101.
- Röschke, J., Fell, J. & Beckmann, P. (1993) The calculation of the first positive Lyapunov exponent in sleep EEG data, *Electroencephalography & Clinical Neurophysiology*, **86**, 348-352.
- Rosenblatt, F. (1958) The perceptron: A probabilistic model for information storage and organization in the brain, *Psychological Review*, **65**, 386-408.
- Rosenblum, M.G., Pikovsky, A. & Kurths, J. (1996) Phase synchronization of chaotic oscillators, *Physical Review Letters*, **76**:11, 1804-1807.
- Rosenblum, M.G., Pikovsky, A. & Kurths, J. (1997). From phase to lag synchronization in coupled chaotic oscillators, *Physical Review Letters*, **78**:22, 4193-4196.

- Rosenblum, M.G., Kurths, J., Pikovsky, A.S., Schafer, C., Tass, P. & Abel, H.H. (1998). Synchronization in noisy systems and cardio respiratory interaction, *IEEE Engineering in Medicine and Biology*, **17**, 46-53.
- Rosenblum, M. G. & Pikovsky, A. S. (2001) Detecting direction of coupling in interacting oscillators, *Physical Review E*, **64**, 045202 (R).
- Rosenblum, M. G., Cimponeriu, L., Bezerianos, A., Patzak, A. & Mrowska, R. (2002) Identification of coupling direction: Application to cardio-respiratory interaction. *Physical Review E*, **65**, 041909.
- Rosenstein, M.T., Collins J.J & De Luca, C. J. (1993) A practical method for calculating largest Lyapunov exponents from small data sets, *Physica D*, **65**, 117-134.
- Rosenstein, M. T., Collins, J.J. & De Luca, C. J. (1994) Reconstruction expansion as a geometry based framework for choosing proper delay times, *Physica D*, **73**, 82-98.
- Rossler, O. E. (1976) An equation for continuous chaos, *Physics Letters*, **57**, 397-504.
- Roy, R. & Thornburg Jr., K. S. (1994) Experimental synchronization of chaotic lasers, *Physical Review Letters*, **72**, 2009-2012.
- Rueckert, L., Lange, N., Partiot, A., Appollonio, I., Litvan, I., Le Bihan, D. & Grafman, J. (1996) Visualizing cortical activation during mental calculation with Functional MRI, *Neuroimage*, **3**, 97-103.
- Ruelle, D. & Takens, F. (1971) On the nature of turbulence, *Comm. Math. Phys*, **20**, 167-192.
- Ruelle, D. (1989) Chaotic evolution and strange attractors, Cambridge University Press.
- Rulkov, N.F., Sushchik, M.M., Tsimring L.S. & Abarbanel, H.D.I.(1995) Generalized synchronization of chaos in directionally coupled chaotic systems, *Physical Review E*, **51**, 980-994.
- Russell, D.F., Wilkens, L.A. & Moss, F. (1999) Use of behavioural stochastic resonance by paddlefish for feeding, *Nature*, **402**, 291-294.
- Ryan, S.M., Goldberger, A.L., Pincus, S.M., Mietus, J. & Lipsitz, L.A. (1994) Gender- and age-related differences in heart rate dynamics: are women more complex than men? *J. Am. Coll Cardiol.*, **24**, 1700-1707.
- Sadato, N., Ibañez, V., Deiber, M.-P. & Hallett, M. (2000) Gender difference in premotor activity during active tactile discrimination, *NeuroImage*, **11**, 532-540.
- Sakatani, K., Katayama, Y., Yamamoto, T., Suzuki, S. (1999) Changes in cerebral blood oxygenation of the frontal lobe induced by direct electrical stimulation of thalamus and

globus pallidus: a near infrared spectroscopy study, *J Neurol Neurosurg Psychiatry*, **67**, 769–773.

Sanchez-Diaz, A., Mirasso, C. R., Colet, P. & Garcia-Fernandez, P. (1999) Encoded Gbit/s digital communications with synchronized chaotic semiconductor lasers, *IEEE Journal of Quantum Electronics*, **35**, 292-297.

Sano, M. & Sawada, Y. (1985) Measurement of the Lyapunov spectrum from a chaotic time series, *Physical Review Letters*, **55**, 1082-1085.

Sauer, T., Yorke, J. A. & Casdagli, M. (1991) Embedology, *J. Stat. Phys.*, **65**, 579-616.

Schack, B., Rappelsberger, P., Anders, C., Weiss, S. & Möller, E. (2000). Quantification of synchronization processes by coherence and phase and its application in analysis of electrophysiological signals, *International Journal of Bifurcation and Chaos*, **10**:11, 2565-2586.

Schmid, G. B. & Dunki, R. M. (1996) Indications of nonlinearity, intraindividual specificity and stability of human EEG: The unfolding dimension, *Physica D*, **93**, 165-190.

Schrieber, T. & Schmitz, A. (1996) Improved surrogate data for nonlinearity tests, *Physical Review Letters*, **77**:4, 635-638.

Schrieber, T. (1997) Detecting and analyzing nonstationarity in a time series using nonlinear cross predictions, *Physical Review Letters*, **78**:5, 843-846.

Schuster, H.-G. (1988) *Deterministic Chaos* (2nd edition), VCH, New York.

Shafer, C., Rosenblum, M. G., Abel, H. H., & Kurths, J. (1999) Synchronization in the human cardiorespiratory system, *Physical Review E*, **60**, 857-870.

Shaywitz, B.A., Shaywitz, S.E., Pugh, K.R., Constable, R.T., Skudlarski, P., Fulbright, R.K., Bronen, R.A., Fletcher, J.M., Shankweiler, D.P., Katz, L. & Gore, J.C. (1995) Sex differences in the functional organization of the brain for language, *Nature*, **373**, 607-609.

Sherman, A., Rinzel, J. & Keizer, J. (1988) Emergence of organized bursting in clusters of pancreatic β -cells by channel sharing, *Journal of Biophysics*, **54**, 411-425.

Skinner, J. E., Martin, J. L., Landisman, C. E., Mommer, M. M., Fulton, K., Mitra, M., Burton, W. D. & Saltzberg, B. (1990) Chaotic attractors in a model of neocortex: Dimensionalities of olfactory bulb surface potentials are spatially uniform and event related. In: *Brain Dynamics Progress & Perspectives*, Ed. E. Basar & T. H. Bullock, Springer-Verlag, Berlin, 119-134.

Sosnovtseva, O. V., Balanov, A. G., Vadivasova, T. E., Astakhov, V. V. & Mosekilde, E. (1999). Loss of lag synchronization in coupled chaotic systems, *Physical Review E*, **60**:6, 6560-6565.

Spehlmann, R.(1986) *EEG Primer*, Elsevier Biomedical Press, NY,

Srinivasan, R., Tucker, D. M. & Murias, M.(1998) Estimating the spatial Nyquist of the human EEG, *Behaviour Research Methods, Instruments and Computers*, **30**:1, 8-19.

Stam, K.J, Tavy, D.L., Jelles, B., Achtereekte, H.A., Slaets, J.P. & Keunen, R.W.(1994) Non-linear dynamical analysis of multichannel EEG: clinical applications in dementia and Parkinson's disease, *Brain Topography*, **7**:2,141-150.

Stam, C.J., van Woerkom, T.C.A.M. & Pritchard, W. S. (1996) Use of nonlinear EEG measures to characterize EEG changes during mental activity, *Electrencephalography and Clinical Neurophysiology*, **99**, 214-224.

Strangman, G., Boas, D.A. & Sutton, J.P. (2002) Non-invasive neuroimaging using near-infrared light, *Biol Psychiatry*, **52**, 679-693

Stratonovich, R.L.(1963) *Topics in the Theory of Random Noise*, Gordon and Breach, NY.

Swaab D.F., Chung W.C.J., Kruijver F.P.M., Hofman & M.A., Ishunina T. A.(2001) Structural and functional sex differences in the human hypothalamus, *Hormones and Behavior*, **40**, 93-98.

Takens, F. (1980) Detecting strange attractors in turbulence, in *Dynamical Systems and Turbulence* (Springer Lecture Notes in Mathematics), **898**, 365-381.

Takens, F. (1981) Detecting strange attractors in turbulence, In: *Dynamical Systems and Turbulence*, Eds. D. Rand and L.-S. Young, Lecture Notes in Mathematics, **898**, Springer-Verlag, Berlin. 366-381.

Tass, P., Rosenblum, M. G., Weule, J., Kurths, J., Pikovsky, A., Volkmann, J., Schnitzler, A. & Freund, H.-J. (1998). Detection of n:m phase locking from noisy data: Application to magnetoencephalography, *Physical Review Letters*, **81**:15, 3291-3294.

Taylor, W.K. (1964) Cortico-thalamic organization and memory, *Proc. Roy. Soc. London*, **B159**, 466-478.

Theiler, J (1986) Spurious dimension from correlation algorithms applied to limited time series data, *Physical Review A*, **34**, 2427-2432.

Theiler, J. (1987) Efficient algorithm for estimating the correlation dimension from a set of discrete points, *Physical Review A*, **36**, 4456-4462.

- Theiler, J. (1990) Statistical precision of dimensional estimates, *Physical Review A*, **41**, 3038-3051.
- Theiler, J. (1991) Some comments on the correlation dimension of $1/f^\alpha$ noise, *Physics Letters A*, **155**, 480-493.
- Theiler, J., Eubank, S., Longtin, A., Galdrikian, B., & Farmer, J.D. (1992) Testing for nonlinearity in time series: The method of surrogate data, *Physica D*, **58**, 77-94.
- Toda, M., (1975) Studies of a non-linear lattice *Physics Reports*, **18c**:1, 1-123.
- Tononi, G. & Edelman, G.M. (2000) Schizophrenia and the mechanisms of conscious integration, *Brain Research Review*, **31**, 391-400.
- Vadivasova, T. E., Balanov, A.G., Sosnovtseva, O.V., Postnov, D.E., & Mosekilde, E. (1999) Synchronization in driven chaotic systems: Diagnostics and Bifurcations, *Physics Letters A*, **253**, 66-74.
- Varela F., Lachaux J.-P., Rodriguez E. & Martinerie, J. (2001) The brain web: Phase synchronization and large scale integration, *Nature Neuroscience Reviews*, **2**, 229-239.
- Wackerbauer, R., Witt, A., Atmanspacher, H., Kurths, J. & Scheingraber, H. (1994) A comparative classification of complexity measures, *Chaos, Solitons & Fractals*, **4**:1, 133-173.
- Wackermann, J. (1996) Beyond mapping: estimating complexity of multichannel EEG recordings, *Acta Neurobiologiae Experimentalis*, **56**, 197-208.
- Wackermann, J. (1999) Towards a quantitative characterization of functional states of the brain: from the nonlinear methodology to the global linear description, *International Journal of Psychophysiology*, **34**, 65-80.
- Wagner, A. D. (2001) Synchronicity: when you're gone I am lost without a trace? *Nature Neuroscience*, **4**:12, 1159-1160.
- Wang, J. & He, B. (1998) A computer simulation study of cortical imaging from scalp potentials, *IEEE Transactions on Biomedical Engineering*, **45**, 724-735.
- Watanabe, E., Maki, A., Kawaguchi, F., Yamashita, Y., Koizumi, H. & Mayanagi, Y. (2000) Noninvasive cerebral blood volume measurement during seizures using multichannel near infrared spectroscopic topography, *J Biomed Optics*, **5**, 287-290.
- Watters, P.A. (1998) Fractal Structure in Electroencephalogram, *Complexity International*, <http://www.csu.edu.au/ci/vol5/watters>
- Whitney, H. (1936) Differentiable manifolds, *Ann. Math.*, **37**, 645.

- Wiesenfeld, K., Bracikowski, C., James, G. & Roy, R. (1990) Observation of antiphase states in a multimode laser, *Physical Review Letters*, **65**, 1749-1752.
- Winograd, S. & Cowan, J.D. (1963) *Reliable computation in the presence of noise*, Cambridge, Mass: MIT press.
- Witt, A., Kurths, J. & Pikovsky, A. (1998) Testing stationarity in time series, *Physical review E*, **58**:2, 1800-1810.
- Wolf, A., Swift, J.B., Swinney, H.L. & Vastano, J.A. (1985) Determining Lyapunov exponent from a time series, *Physica D*, **16**, 285-317.
- Wood, F.B., Flowers, D.L. & Neylor, C.E. (1991) Cerebral laterality in functional neuroimaging, In: *Cerebral laterality: Theory and Research*, Ed. F. L. Ketterle, Lawrence Erlbaum associates, Hillsdale, New Jersey. P., 103-116.
- Yoshinaga, T., Sano, Y. & Kawakami, H. (1999) A method to calculate bifurcations in synaptically coupled Hodgkin-Huxley equations, *International Journal of Bifurcation and Chaos*, **9**,1451-1458.
- Yu, D., Lu, W., Harrison, R. G. (1999) Detecting dynamical nonstationarity in time series data, *Chaos*, **9**:4, 865-870.
- Zago, L. & Tzourio-Mazoyer, N. (2002) Distinguishing visuospatial working memory and complex mental calculation areas within the parietal lobes, *Neuroscience Letters*, **331**:1, 45-49.

Material on EEG waves: <http://www.crossroadsinstitute.org/eeg.html>
<http://www.arts.uwaterloo.ca/~sreinis/eeg.html>

PET information: <http://www.nucmed.buffalo.edu/positron.htm>

Errata to the thesis

1. Pg. 24 Lines after Eq. 2.1 – x and F are vectors

This is a dynamical system since for any initial state of the system, $x(0)$ the equations can be solved to obtain the state $x(t)$ at a later time $t > 0$. $F = (F_1, \dots, F_N)$ is a vector field in the state space, i.e. F_i are functions of $x^{(i)}$ and $p^{(i)}$ are the corresponding vectors of control parameters (if any).

2. Page 25, following eq. 2.2 x is a vector.

x_n has N components, $x_n = (x_n^{(1)}, x_n^{(2)}, K, x_n^{(N)})$.

3. Page 25: In the repeated operation of F on the initial state x_0 a misprint has occurred and is rectified as:

$$x_1 = F(x_0), \quad x_2 = F(x_1) = F(F(x_0)), \quad K, \quad x_n = F^n(x_0)$$

4. Page 26, line 12

Hence the application of this theorem to a single differential equation of order N involves solving the differential equation for the highest derivative, which is written as,

$$x^{(N)} \equiv \frac{d^N x}{dt^N} = f\left(t, x, \frac{dx}{dt}, \frac{d^2 x}{dt^2}, K, \frac{d^{N-1} x}{dt^{N-1}}\right)$$

5. Page 30, Eq. 2.6

$$F(x_0 + \eta(t)) = F(x_0) + DF(x_0) \cdot \eta + O(\eta^2)$$

6. Pg 215 line 8. Replace word 'locus' by 'electrode'

The variation in SampEn with state at the electrodes is characterized by the (state*electrode interaction) which is....

7. Page 243 line 7

We follow the phase synchronization techniques, therefore, to delve into....

In the bibliography section

1. Page (ii) Ref. No. 1, The journal is Physics Letters A.
2. Page (ix) Ref. no. 12 The journal is Physics Letters A
3. Page (xiii) Ref. no. 13 The journal is Physics Letters A
4. Page (xv) Ref. no. 6 The journal is Physics Letters A

G 8575

"The search for what is meaningful and what is true by opposition to noise is a tentative step that appears to be intrinsically related to the coming into consciousness of man facing the nature of which he is a part."

Ilya Prigogine.

